Final Report

October 25, 2012

Generation of Comprehensive Surrogate Kinetic Models and Validation Databases for Simulating Large Molecular Weight Hydrocarbon Fuels

2007 MURI Topic: Science-Based Design of Fuel-Flexible Chemical Propulsion/Energy Conversion Systems
Contract/Grant No. FA9550-07-1-0515
July 1, 2007 – June 30, 2012

Prof. Frederick L. Dryer, Principal Investigator
Princeton University
Mechanical and Aerospace Engineering
School of Engineering and Applied Sciences
D-329D Engineering Quadrangle
Princeton University
Princeton, NJ 08544-5263

Phone: 609-258-5206
FAX: 609-258-6109
Email: fldryer@Princeton.EDU

Co-Investigators and Institutions:

Prof. Yiguang Ju	Princeton University (PU)
Prof. Chih-Jen Sung	University of Connecticut (UCONN)
Prof. Kenneth Brezinsky	University of Illinois at Chicago (UIC)
Prof. Robert J. Santoro	Penn State University (PSU)
Prof. Thomas A. Litzinger	Penn State University (PSU)

Visiting Researchers:

Prof. Henry J. Curran (NUI Galway) Princeton University (PU)

October 25, 2012

REPORT DOCUMENTATION PAGE

Form Approved
OMB No. 0704-0188

1. REPORT DATE *(DD-MM-YYYY)*	**2. REPORT TYPE**	**3. DATES COVERED** *(From - To)*
10/01/2012	Final Report	7/02/2007 – 6/30/2012

4. TITLE AND SUBTITLE

Science-Based Design of Fuel-Flexible Chemical Propulsion/Energy:
Generation of Comprehensive Surrogate Kinetic Models and Validation Databases for Simulating Large Molecular Weight Hydrocarbon Fuels

5a. CONTRACT NUMBER

5b. GRANT NUMBER
FA9550-07-1-0515

5c. PROGRAM ELEMENT NUMBER

6. AUTHOR(S)
Frederick L. Dryer (PI) and Yiguang Ju (Co-I), Princeton University
Kenneth Brezinsky (Co-I), University of Illinois at Chicago
Robert J Santoro (Co-I) and Thomas A. Litzinger (Co-I), The Pennsylvania State University
Chih-Jen Sung (Co-I), University of Connecticut

5d. PROJECT NUMBER

5e. TASK NUMBER

5f. WORK UNIT NUMBER

7. PERFORMING ORGANIZATION NAME(S) AND ADDRESS(ES)

Princeton University	4 New South Bldg, Princeton, NJ 08544
University of Illinois, Chicago	842 W. Taylor St. M/C 251, Chicago, IL 60608
The Pennsylvania State University	110 Tech Center Bldg, University Park, PA 16802
University of Connecticut	438 Whitney Rd Ext., Unit 1133, Storrs, CT 06269-1133

8. PERFORMING ORGANIZATION REPORT NUMBER

9. SPONSORING / MONITORING AGENCY NAME(S) AND ADDRESS(ES)

USAF, AFRL DUNS 143574726
AF Office of Scientific Research
875 N. Randolph St. Rm 3112
Arlington VA 22203
(703) 696-9729

Grant Monitor:
Dr. Julian Tishkoff
Dr. Chiping Li
AFOSR/NA
(703) 696-8574

10. SPONSOR/MONITOR'S ACRONYM(S)
AFOSR/PKR2

11. SPONSOR/MONITOR'S REPORT NUMBER(S)
AFRL-OSR-VA-TR-2012-1159

12. DISTRIBUTION / AVAILABILITY STATEMENT
Distribution A: Approved for Public Release

13. SUPPLEMENTARY NOTES The views and conclusions contained herein are those of the author and should not be interpreted as necessarily representing the official policies or endorsements, either expressed or implied, of the Air Force Office of Scientific Research, or the U.S. Government.

14. ABSTRACT
This multi university research initiative investigated "surrogate fuel" mixture methodology for representing fully prevaporized chemical kinetic/transport global combustion properties of real fuels. Concepts by which surrogate mixtures of a small number of molecular class components would emulate the global combustion properties of each specific real fuel were developed and tested experimentally by comparing surrogate mixture and real fuel behavior in a wide variety of fundamental combustion venues, including: high pressure reflected shock tube ignition delay, rapid compression machine ignition, variable pressure flow reactor reactivity/species time history, high pressure pulsed shock tube speciation, laminar premixed burning rate and strained extinction, laminar counter-flow, strained-extinction configurations, and laminar annular diffusive soot extinction configurations. Matching the "real fuel combustion property targets" of hydrogen/carbon molar ratio (H/C), derived cetane number (DCN), threshold sooting index (TSI), and average mean molecular weight (MW_{ave}) of mixtures with those of the real fuel was shown to result in nearly identical global combustion behavior of the real fuel and the surrogate. Mixtures of surrogate components which had nearly identical combustion property targets were also shown to have nearly the same distribution of key (CH2, CH3, benzyl) chemical functional groups. Methodologies for determining combustion property targets and creating matching surrogate mixtures were demonstrated. Experimental data for surrogate components were collected from each venue, and vapor phase transport data for components and reaction intermediates were determined created. Surrogate mixture models were constructed and tested against surrogate mixture data. Assimilation of physical property considerations within the context of emulating chemical properties was considered. Finally, the implications of this research to furthering understanding multi-phase combustion in applied venues research were considered. Multiphase combustion sooting of a real jet fuel and matched surrogate mixtures were also compared in a high pressure model combustor.

15. SUBJECT TERMS
Real fuel properties, Real fuel modeling, Surrogate fuels, Surrogate components, Combustion property targets, Chemical kinetic experimental data, Kinetic modeling, Real fuel physical properties, Alkanes, Iso-alkanes, Cycloalkanes, Alkyl- aromatics.

16. SECURITY CLASSIFICATION OF:			**17. LIMITATION OF ABSTRACT**	**18. NUMBER OF PAGES**	**19a. NAME OF RESPONSIBLE PERSON**
a. REPORT	**b. ABSTRACT**	**c. THIS PAGE**			Frederick L. Dryer
Unclassified	Unclassified	Unclassified			**19b. TELEPHONE NUMBER** *(include area code)* 609-258-5206

Standard Form 298 (Rev. 8-98)
Prescribed by ANSI Std. Z39.18

Abstract

This multi-university research initiative investigated "surrogate fuel" mixture methodology detailed kinetic models for representing fully prevaporized chemical kinetic/transport global combustion properties of real fuels. Concepts by which surrogate mixtures of a small number of molecular class components would emulate the global combustion properties of each specific real fuel were developed and tested experimentally by comparing surrogate mixture and real fuel behavior in a wide variety of fundamental combustion venues, including: high pressure reflected shock tube ignition delay, rapid compression machine ignition, variable pressure flow reactor reactivity/species time history, high pressure pulsed shock tube speciation, laminar premixed burning rate and strained extinction, laminar counter-flow, strained-extinction configurations, and laminar co-annular diffusive soot extinction configurations. Matching the "real fuel combustion property targets" of hydrogen/carbon molar ratio (H/C), derived cetane number (DCN), threshold sooting index (TSI), and average mean molecular weight (MW_{ave}) of mixtures with those of the real fuel was shown to result in nearly identical global combustion behavior of the real fuel and the surrogate. Methodologies for determining combustion property targets and creating matching surrogate mixtures were demonstrated. Mixtures of surrogate components that had nearly identical combustion property targets were found to have nearly the same distribution of key (CH_2, CH_3, benzyl) chemical functional groups. Experimental data for surrogate components were collected from each venue, and vapor phase transport data for components and reaction intermediates were determined created. Data were utilized to test and construct detailed and reduced kinetic models for surrogate components and their mixtures. Models taken from the literature (n-decane and n-dodecane, and iso-octane) were further modified and new models were produced for toluene, n-propyl benzene, and 1,3,5 trimethyl benzene. Model reduction techniques were developed and applied to permit comparisons of predictions with flame data for burning rate and extinction. Approaches that would improve the efficiency of numerical computations were also investigated. Assimilation of physical property considerations within the context of simultaneously emulating chemical properties was also considered.

Finally, the implications of this research to furthering understanding of multi-phase combustion in applied venues were discussed. Multiphase combustion sooting of a real jet fuel and matched surrogate mixtures were compared in a high pressure model combustor by demonstrating that surrogate mixtures that emulate real fuels can be produced using combinations of several n-alkane, iso-alkane, and alkyl-mono-aromatic hydrocarbon fluids, each containing primarily only one type of molecular class components.

Executive Summary

The projected evolution of petroleum-derived and petroleum/alternative-derived blended jet fuels and emerging propulsion technologies point to an increasing need to understand physical and chemical kinetic fuel property effects on multiphase, gas turbine combustion performance and emissions. Surrogate fuel concepts provide a pragmatic approach for modeling physical and chemical properties of real fuels that vary geographically, seasonally, and historically and that contain hundreds of individual species. Provided that surrogate fuel formulations can replicate real fuel properties, the models derived for such mixtures can be utilized in engineering design tools to predict fuel effects on new combustion technologies, as well as for screening the compatibility of candidate non-petroleum derived alternative fuels with legacy equipment.

To first order, molecular weight principally dominates physical property emulation, while chemical structure dominates chemical kinetic emulation. Thus, significant complexity exists in terms of defining the number of surrogate components and their mixture composition needed to simultaneously model both physical and chemical kinetic properties. While researchers continue to debate the relative importance of physical or chemical kinetic fuel properties, the relative accuracies to which physical and chemical behaviors need to be replicated remain unclear. Coupling of the two issues results if the combustion event affects fuel viscosity or surface tension at the atomizer (important atomization parameters) and/or preferential vaporization of the atomized droplets is significant. In the latter case, then the overall molecular class fractions as well as their distribution over the fuel distillation range must be considered as emulation targets. Notwithstanding these two issues, chemical kinetic property emulation appears to be the more limiting concern, since the complexity of describing chemical kinetics grows inordinately with the number of individual molecular classes that are required to model a real fuel. Today, jet fuels certified for use generally contain normal- and iso-alkanes, cyclo-alkanes, and alkyl aromatics in varying proportions, with very small amounts of multi-ring aromatics. Representing each of these general classes as well as their distributions over the distillation curve remains a daunting task not only in characterizing these parameters for the real fuel of interest, but in terms of developing the appropriate surrogate mixture and chemistry model.

This multi university research initiative (MURI) investigated a “surrogate fuel” mixture methodology for representing fully prevaporized, chemical kinetic/transport-controlled, global combustion properties of real fuels. Concepts by which surrogate mixtures of a small number of molecular class components would emulate the global combustion properties of each specific real fuel were developed and tested experimentally by comparing surrogate mixture and real fuel behavior in a wide variety of fundamental combustion venues, including: high pressure reflected shock tube ignition delay, rapid compression machine ignition delay, variable pressure flow reactor reactivity/species time history, high pressure pulsed shock tube speciation, laminar counter-flow flame premixed burning rate and strained extinction, and laminar counter-flow flame, strained-extinction configurations.

The key “combustion property targets” of the real fuel that should be replicated by any surrogate mixture were hypothesized, based upon a qualitative understanding of combustion kinetic properties affecting global combustion behaviors. It was found that matching the real fuel combustion property targets - hydrogen/carbon molar ratio (H/C), derived cetane number (DCN), threshold sooting index (TSI), and average mean molecular weight (MW_{ave}) - through proper choice of surrogate components and their mixtures resulted in nearly identical global combustion

behavior of the real and surrogate fuels. Small scale experimental methods and procedures for determining these property targets for real fuels, surrogate components, and their mixtures were developed and applied to experimentally evaluate the molecular classes and specific components needed for reproducing real fuel global combustion behavior. A novel method for experimentally determining the average molecular weight of a fuel was also developed, and a new function, the radical index (R_i), that characterizes the high temperature reactivity of fuels relative to alkanes under diffusive controlled conditions, was proposed. It was shown that the R_i, the transport weighted enthalpy (TWE), and MW_{ave} universally correlate the counter flow diffusive strained extinction of all fuels. Analysis of results using these parameters permitted ranking of chemical kinetic, energy density, and diffusive transport impacts on extinction.

Two mixtures of different surrogate components were investigated in depth to proof the proposed surrogate formulation concept: 1) a 1st generation surrogate of n-decane, iso-octane, and toluene) and 2) a 2nd generation surrogate of n-dodecane, iso-octane, n-propyl benzene, and 1,3,5 trimethylbenzene. While the property ranges of the 1st generation surrogate components could not encompass the average molecular weight and sooting property targets of real Jet A and JP-8 fuels, comparisons of premixed chemical kinetic behavior with real fuels was possible. In addition, use of the 1st generation components allowed use of existing kinetic model capabilities in order to analyze real fuel combustion behavior. Mixtures of the 2nd generation components were found to emulate all of the combustion property targets not only of Jet A and JP-8 fuels appearing in use over the period 2006-2009, but those of all non-petroleum derived alternative fuels (either as pure feed stocks or in up to 50% blends with petroleum derived fuels) that were under test by the Air Force. The notable exception was a high molecular weight, very low DCN alternative fuel composed of highly isomerized paraffinic kerosene (denoted IPK).

Comparisons of a 2nd generation surrogate formulated to match all four of the above property targets of Jet A POSF 4658 fuel were shown to closely exhibit the same global combustion properties of the fully prevaporized real fuel across all of the fundamental experimental configuration listed above. It was found that there was not a single unique mixture of 2nd generation components that emulated the real fuel, but that several mixtures of varying compositions shared the same property targets. Though the molecular compositions of the surrogate mixtures were different, each were found to have nearly the same distribution of key (CH_2, CH_3, benzyl) chemical functional groups. Other group distributions (C, CH) made up less than 10% of the mass of the surrogate mixtures and were of only secondary importance in determining the global combustion behavior of the mixture.

It was shown that no detailed chemical analysis of the real fuel is required to generate a suitable surrogate mixture. Furthermore, surrogate mixtures may not need to contain representative molecular structures for each molecular class found in the real fuel. Surrogate mixtures composed of ~30 molar percent methylcyclohexane in n-decane/iso-octane/toluene and having the same combustion property targets of H/C and DCN as the1st generation Jet A POSF 4658 surrogate mixture had the same global combustion properties as each other and the real fuel itself. Thus it appears that cycloalkanes are not required to reasonably emulate real fuels containing significant molecular class fractions of this molecular structure.

The synthetic fuel produced from natural gas, S-8 POSF 4734, that contains large fractions of weakly branched mono and di methyl alkanes was emulated using mixtures of n-dodecane and iso-octane that replicated its combustion property targets, demonstrating that weakly branched alkanes need not be treated as a unique structure in formulating surrogate mixtures. Finally, a

surrogate mixture of n-decane and iso-octane formulated to match the combustion property targets of 2-methyl heptane was shown to replicate the global combustion properties of the weakly branched isomer, further supporting that distinct functional group distributions represented by the molecular distribution, not the individual molecular makeup specifically, are key to replicating global combustion properties.

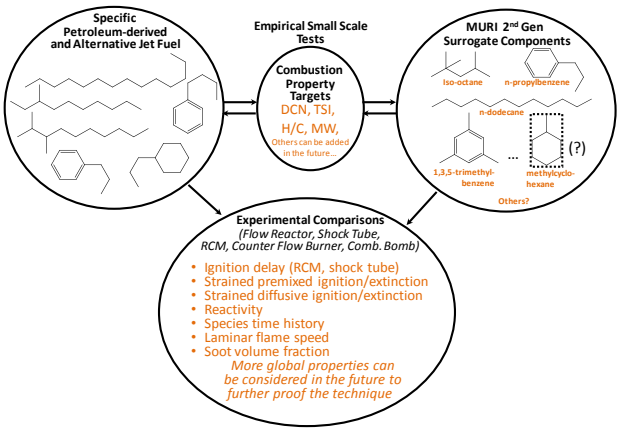

Figure 1. Schematic summary of the MURI surrogate formulation concept.

Figure 1 schematically summarizes the surrogate concept developed by the MURI. The combustion property targets of any real jet fuel composed of non-oxygenated species can be easily determined using small scale, small fuel sample experimental methods. The MURI created algorithms for identifying mixtures of the 2nd generation surrogate components, selected by assuring that the combustion property target ranges of real fuels can be emulated with sufficient independence by varying the mixture of the components. Mixtures are then identified that match the combustion property targets of the real fuel.

Emulation of the surrogate mixture by comparison of global combustion properties in a wide range of experimental venues and conditions are then used to test the veracity of the result. The method is entirely general and can be reformulated simply to consider additional property targets and surrogate components, for example mono and/or multi-ring cycloalkanes or multi ring aromatics. Though the MURI validation of the surrogate method experimentally is certainly one of the most comprehensive in terms of venues and conditions, it is not assured that these venues sufficiently encompass all of the fundamental properties relevant to applied combustion problems. For example, neither this program nor any other have considered the potential surrogate formulation requirements that might result from considering turbulent combustion time scales and turbulence/chemistry coupling associated with combustion instabilities. As additional targets might well evolve from such considerations, the present set provide a significant base to which others can be added. The above methods are entirely extendable directly to consideration of non-oxygenated gasolines and diesel fuels. Moreover by considering oxygenate functional groups, atom conservation that includes oxygen atoms, and modifications of appropriate methodologies to include oxygen effects on diffusive sooting, these methods can also be extended to consideration of real fuels containing oxygenated species.

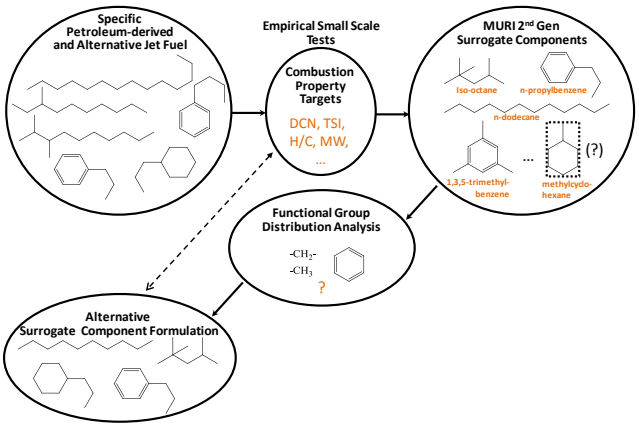

Figure 2. A summary schematic relating the surrogate mixture concept to distinct chemical functional group distribution determinations and the relationship of the 2nd generation

Figure 2 schematically represents the relationship of the MURI surrogate formulation method to functional group theory and to the inter-relationships of surrogate mixtures formulated using surrogate components that include species other than those composing the 2nd generation selection. The dashed arrow represents the process of producing surrogate mixtures utilizing components other than the 2nd generation selection, applying the identical concepts described above. The only constraint is that mixtures of the selected components can meet the criteria of matching the real fuel property targets. This constraint is a weak one, permitting one to consider the availability of and veracity established for kinetic/transport descriptions of the surrogate components and their mixtures. This constraint was applied in selecting the 2nd generation components, but other choices may be preferred and/or emerge as better choices in the future.

Finally, the distinct functional group distribution represented by the 2nd generation surrogate derived for the fuel of interest can itself be utilized to create surrogate mixtures with the same functional group distribution and hence, an equal ability to represent the fully prevaporized global combustion behavior of the real fuel.

A very important corollary of the above points is that if two real fuels have the same combustion property targets, then each should have the same distinct functional group distribution and will behave the same across all of the fundamental experimental venues and conditions noted in Fig. 1. This hypothesis was tested by producing two mixtures of different hydrocarbon fluids (commercially manufactured solvents), each formulated to have the same combustion property targets as a particular target Jet A and a JP-8 samples. As the Jet A and JP-8 samples each had nearly identical property targets, all of the fluid mixtures and the real fuels had nearly identical reactivity profiles when measured in the Princeton Variable Pressure Flow Reactor and the same global sooting behavior in laminar co-annular diffusion flames. Finally, sooting as a function of overall equivalence ratios for the hydrocarbon fluid mixtures formulated to represent the JP-8 sample and the sample itself were found to compare within 20% in high pressure, multi-phase, model combustor experiments. In summary of this result, surrogate mixtures can be formulated from different hydrocarbon fluid streams having defined molecular class structure and carbon number range to artificially produce "fuels" that have the same combustion property targets and fully prevaporized global combustion behavior as a real fuel. By applying this method, the physical properties of the hydrocarbon fluid "fuels" that have combustion property targets of jet fuels can be varied independently of their fully prevaporized global combustion behavior to assess the relative importance of physical and chemical properties in multiphase combustion venues at a scale relevant to applied combustion systems. This methodology has four advantages over utilizing characterized jet fuel samples for similar studies:

1) Hydrocarbon streams of singular molecular class and carbon number range are much better chemically defined by refining processes than are jet fuels.

2) Hydrocarbon fluid streams are much less costly in terms of materials to formulate surrogate mixtures than pure component streams.

3) Hydrocarbon fluid streams offer superior flexibility for the study of physical/chemical property integration.

4) As the combustion property targets of the real jet fuel of interest and each hydrocarbon fluid stream surrogate mixture would be the same, our findings suggest that a commonality of chemical functional groups may be assumed. Thus all can be modeled numerically in terms of

chemical kinetic and gas phase transport properties by the same 2nd generation surrogate mixture model.

Kinetic modeling of the components and their mixtures utilized in this MURI research has also been pursued. **Table 1** and **Table 2** (below) list the models developed at Princeton and at the University of Illinois at Chicago over this research. Brief summary information and where each model may be obtained are also provided.

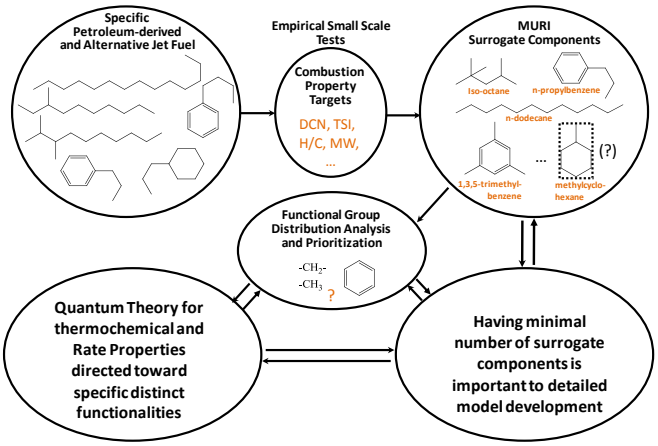

Figure 3. Relationship of the MURI surrogate fuel concepts to advancing kinetic representations of real fuels.

Finally, **Figure 3** relates the surrogate concept developed in this MURI to the advancement of modeling efforts. The functional group identifications produced by the MURI approach and the approach itself represents an empirically-based alternative to direct measurement of functional group distributions by, for example, nuclear magnetic resonance or other techniques. A most important difference is that for jet fuels, the relative significance of the respective functional groupings on global combustion properties have been defined as a result of the testing and surrogate formulation procedure. The prioritization can lead to a considerable simplification in the types and numbers of components needed to integrate physical and chemical kinetic fuel modeling in the future. Moreover, the functional groupings represent the collective significance of atomistic, quantum mechanical results to improving surrogate fuel modeling, as well as provide focus to defining surrogate components selections and where kinetic modeling efforts should be emphasized. However, an important aspect missing from Fig. 3 is that detailed models for surrogate mixtures that emulate both physical and chemical properties are most certain to be too complex for use in computational design of future propulsion systems. Model reduction methods presently available for application to detailed kinetic models are unlikely in themselves to address this problem and new methods for representing chemical kinetics at much more reduced dimensionality remain to be identified.

In closing this executive summary, the complexity of multiphase combustion requires simplifying approximations in models that are used to describe physical and chemical kinetic properties of real fuels, and their implementation on computational tools. From what is known presently, it is difficult for industry to define what predictive accuracy is desirable for improving gas turbine designs tools to advance engine performance for areas such as main combustor relight, lean premixed combustion stabilization, or augmenter ignition, flame stabilization, and operation. There is an equal difficulty presently to specify where simplifying assumptions in the models for physical and chemical kinetic properties of real fuels will result in least impact on predicting combustion system parameters of interest. Experimental studies targeting these particular issues will be essential in establishing directions and emphasis in targeting fundamental research to these needs and in engineering tool development and applications.

Publication Title	Authors	Link To Publication or Model	Notes on Kinetic Modelling Content
Comprehensive Detailed Chemical Kinetic Modelling Study of Toluene Oxidation	Metcalfe et al. [1]	http://dx.doi.org/10.1021/ef200900q	The literature data pertaining to toluene oxidation is reviewed and incorporated into a state of the art kinetic model.
Methyl butanoate Inhibition of n-heptane Diffusion Flames Through an Evaluation of Transport and Chemical Kinetics	Dooley et al. [2]	http://dx.doi.org/10.1016/j.combustflame.2011.09.016	Relationships for the estimation of Lennard-Jones collisional model parameters are presented on a molecular functional class basis. This transport model is used as input for all flame calculations presented below.
Kinetic Effects of Aromatic Molecular Structures on Diffusion Flame Extinction	Won et al. [3]	http://dx.doi.org/10.1016/j.proci.2010.05.082	A kinetic model for the oxidation of n-propyl benzene is described, based upon toluene [1], both are tested against diffusion flame extinction measurements.
A Jet Fuel Surrogate Formulated By Real Fuel Properties	Dooley et al. [4]	http://dx.doi.org/10.1016/j.combustflame.2011.11.002	A kinetic model to simulate mixtures of n-decane/iso-octane/toluene is assembled from the state of the art literature, utilising the toluene model as a base [1], and used to fundamentally interpret combustion measurements of the 1st generation surrogate.
Laminar Flame Speeds and Extinction Stretch Rates of Selected Aromatic Hydrocarbons	Hui et al. [5]	http://dx.doi.org/10.1016/j.fuel.2012.02.045	The models proposed in [1-3] are tested against measurement of a variety of premixed and diffusive flame properties exhibited by toluene and n-propyl benzene.
A Shock Tube and Kinetic Modelling Study of the Autoignition of n-Propylbenzene	Wang et al. [6]	7th United States Combustion Meeting Atlanta, Georgia (available from stephen.dooley@ul.ie)	The model presented in [3] is developed further, tested against, and used to interpret high and intermediate temperature ignition delays.
The Combustion Properties of 1,3,5-Trimethylbenzene and a Kinetic Model	Diévart et al. [7]	To appear in *Fuel* http://www.sciencedirect.com/science/journal/00162361	With the toluene model [1] used as a template a 1,3,5 trimethyl benzene model is constructed and tested against a range of global combustion properties.
The Combustion Kinetics of a Synthetic Paraffinic Jet Aviation Fuel and a Fundamentally Formulated, Experimentally Validated Surrogate Fuel	Dooley et al. [8]	http://dx.doi.org/10.1016/j.combustflame.2012.04.010	The model presented in [2] is augmented to include n-dodecane chemistry. The model others available in the literature are compared against measurements for n-dodecane/iso-octane combustion.
A Reduced Kinetic Model for the Combustion of Jet Propulsion Fuels	Dooley et al. [9]	To appear at The American Institute for Aeronautics and Astronautics, Aerospace Sciences Meeting, Dallas, Texas, USA, 7th January 2013 (available from stephen.dooley@ul.ie)	The performance of the iterative model construction presented above is comprehensively tested and reviewed versus other state of the art literature models for each individual surrogate fuel component. The predictability of the model is demonstrated versus each of the macro combustion measurements presented in [4,10] for the proposed Jet-A surrogate fuels. Several reduced models of different dimensional sizes are presented and their performance demonstrated versus same data, offering the user a choice between model fidelity and computational cost.

References

1) W.K. Metcalfe, S. Dooley, F.L. Dryer. "A Comprehensive Detailed Chemical Kinetic Modeling Study of Toluene Oxidation", *Energy and Fuels* (2011) 25:4915-4936.
2) S. Dooley, S.H. Won, F.L. Dryer, Y. Ju, "Methyl Butanoate Inhibition of n-Heptane Diffusion Flames through an Evaluation of Transport and Chemical Kinetics", *Combust Flame* (2012) 159:1371-1384.
3) S.H. Won, S. Dooley, F.L. Dryer, Y. Ju, "Kinetic Effect of Molecular Structure on Extinction Limit of Aromatic Diffusion Flames", *Proc. Combust Inst* (2011) 33:1163-1170.
4) S. Dooley, S.H. Won, M. Chaos, J. Heyne, Y. Ju, F.L. Dryer, K. Kumar, C.J. Sung, H. Wang, M. Oehlschlaeger, R.J. Santoro, T.A. Litzinger, "A Jet Fuel Surrogate Formulated By Real Fuel Properties", *Combust Flame* (2010) 157:2333-2339.
5) X. Hui, A.K. Das, K. Kumar, C.J. Sung, S. Dooley, F.L. Dryer, "Laminar Flame Speeds and Extinction Stretch Rates of Selected Aromatic Hydrocarbons", *Fuel* (2012) 97:695-702.
6) H. Wang, M.A. Oehlschlaeger, S. Dooley, F.L. Dryer, "A Shock Tube and Kinetic Modelling Study of the Autoignition of n-Propylbenzene", 7th United States Combustion Meeting, Georgia Institute of Technology, Atlanta, Georgia, USA, 20th-23rd March 2011.
7) P. Dievart, H.H. Kim, S.H. Won, Y. Ju, S. Dooley, F.L. Dryer, W. Wang, M.A. Oehlschlaeger, "The Combustion Phenomena of 1,3,5-trimethylbenzene and a Kinetic Model", *Fuel* under review (Sept. 2012).
8) S. Dooley, S.H. Won, S. Jahangirian, Y. Ju, F.L. Dryer, H. Wang, M.A. Oehlschlaeger "The Combustion Kinetics of A Synthetic Paraffinic Jet Aviation Fuel and A Fundamentally Formulated, Experimentally Validated Surrogate Fuel", *Combust Flame* (2012) 159:3014-3020.
9) S. Dooley, F.L. Dryer, T. Farouk, S.H. Won "Reduced Kinetic Models for the Combustion of Jet Propulsion Fuels", American Institute for Aeronautics and Astronautics, Aerospace Sciences Meeting, Dallas, Texas, USA, 7th January 2013.
10) S. Dooley, S.H. Won, J. Heyne, Y. Ju, F.L. Dryer, K. Kumar, C.J. Sung, H. Wang, M. Oehlschlaeger, R.J. Santoro, T.A. Litzinger, "The Experimental Evaluation of a Methodology for Surrogate Fuel Formulation to Emulate Gas Phase Combustion Kinetic Phenomena", Combust Flame (2012) 159:1444—1466

Table 1. Original combustion modeling contributions from Princeton supported by the MURI; all models and supporting texts are available from fldryer@princetron.edu.

Publication Title	Authors	Link To Publication or Model	Notes on Kinetic Modelling Content
High Pressure Study of n-Propylbenzene Oxidation	Gudiyella and Brezinsky [3]	http://dx.doi.org/10.1016/j.combustflame.2011.09.013	A detailed kinetic model for the oxidation of n-propylbenzene is described, using C_0-C_4 and toluene from [1], tested against shock tube, flow reactor, and jet stirred reactor speciation data.
The High Pressure Study of n-Propylbenzene Pyrolysis	Gudiyella and Brezinsky [4]	http://dx.doi.org/10.1016/j.proci.2012.05.007	A detailed kinetic model for the pyrolysis of n-propylbenzene is described, using the n-propylbenzene oxidation model from [3], tested against shock tube speciation data.
High Pressure Study of 1,3,5-Trimethylbenzene Oxidation	Gudiyella and Brezinsky [5]	http://dx.doi.org/10.1016/j.combustflame.2012.06.014	A detailed kinetic model for the oxidation of 1,3,5-trimethylbenzene is described, based upon m-xylene [2], and tested against shock tube speciation data.
Experimental and Modelling Study on the Pyrolysis and Oxidation of Iso-Octane	Malewicki et al. [6]	http://dx.doi.org/10.1016/j.proci.2012.06.137	The refinement and validation of the iso-octane sub-model in [1] is described, tested against shock tube speciation and ignition measurements, and flow reactor speciation data.
Experimental and Modelling Study on the Pyrolysis and Oxidation of n-Decane and n-Dodecane	Malewicki and Brezinsky [7]	http://dx.doi.org/10.1016/j.proci.2012.06.156	The refinement and validation of the n-decane sub-model in [6] and extended to n-dodecane is described, tested against shock tube speciation and ignition measurements, and flow reactor speciation data.
Experimental and Modelling Study on the Oxidation of Jet A and the n-Dodecane/iso-Octane/n-Propylbenzene/1,3,5-Trimethylbenzene Surrogate Fuel	Malewicki and Brezinsky [8]	To appear at Combustion and Flame http://www.sciencedirect.com/science/journal/00102180 (available from kenbrez@uic.edu)	A detailed kinetic model to simulate mixtures of n-dodecane/iso-octane/n-propylbenzene/1,3,5-trimethylbenzene is assembled from the state of the art literature, utilising the revised n-decane/iso-octane/toluene model as a base [7], and tested against shock tube speciation and ignition measurements, and flow reactor speciation data.

References

1) S. Dooley, S.H. Won, M. Chaos, J. Heyne, Y. Ju, F.L. Dryer, K. Kumar, C.J. Sung, H. Wang, M. Oehlschlaeger, R.J. Santoro, T.A. Litzinger, "A Jet Fuel Surrogate Formulated By Real Fuel Properties", Combustion and Flame 157 (12) (2010) 2333-2339
2) S. Gudiyella, T. Malewicki, A. Comandini, K. Brezinsky, "High Pressure Study of m-Xylene Oxidation", Combustion and Flame 158 (4) (2011) 687-704
3) S. Gudiyella, K. Brezinsky, "The High Pressure Study of n-Propylbenzene Pyrolysis", Proceedings of the Combustion Institute 34 (2012)
4) S. Gudiyella, K. Brezinsky, "High Pressure Study of n-Propylbenzene Oxidation", Combustion and Flame 159 (3) (2012) 940-958
5) S. Gudiyella, K. Brezinsky, "High Pressure Study of 1,3,5-Trimethylbenzene Oxidation", Combustion and Flame 159 (11) (2012) 3264-3285
6) T. Malewicki, A. Comandini, K. Brezinsky, "Experimental and Modeling Study on the Pyrolysis and Oxidation of Iso-Octane", Proceedings of the Combustion Institute 34 (2012)
7) T. Malewicki, K. Brezinsky "Experimental and Modeling Study on the Pyrolysis and Oxidation of n-Decane and n-Dodecane", Proceedings of the Combustion Institute 34 (2012)
8) T. Malewicki, S. Gudiyella, K. Brezinsky, "Experimental and Modeling Study on the Oxidation of Jet A and the n-Dodecane/iso-Octane/n-Propylbenzene/1,3,5-Trimethylbenzene Surrogate Fuel", Combustion and Flame (In Press)

Table 2. Original combustion modeling contributions supported by the MURI, all models and supporting texts are available from kenbrez@uic.edu

Archival Publications Resulting from this Research

G. Mittal, C. J. Sung. Homogeneous Charge Compression Ignition of Binary Fuel Blends. *Combust Flame* (2008) 155:431-439.

G. Mittal, M. Chaos, C. J. Sung, F. L. Dryer. Dimethyl Ether Autoignition in a Rapid Compression Machine: Experiments and Chemical Kinetic Modeling. *Fuel Processing Technology* (2008) 89(12):1244-1254.

Y. Ju, X. Gou, W. Sun, Z. Chen. An On-Grid Dynamic Multi-Timescale Method with Path Flux Analysis for Multi-Physics Detailed Modeling of Combustion (invited review paper), Journal of the Combustion Society of Japan, Vol.51, 2009.

K. Kumar, G. Mittal, C. J. Sung. Autoignition of n-Decane under Elevated Pressure and Low-to-Intermediate Temperature Conditions. *Combust Flame* (2009) 156:1278-1288.

G. Mittal, C. J. Sung. Autoignition of Methylcyclohexane at Elevated Pressures, *Combust Flame* (2009) 156:1852-1855.

S. Dooley, S.H. Won, M. Chaos, J. Heyne, Y. Ju, F. L. Dryer, K. Kumar, C-J. Sung, H. Wang, M. A. Oehlschlaeger, R.J., Santoro, T. A. Litzinger. A Jet Fuel Surrogate Formulated by Real Fuel Properties, *Combust Flame* (2010) 157:2333-2339.

X. Gou, W. Sun, Z. Chen, Y. Ju. A Dynamic Multi-Timescale Method for Combustion Modeling with Detailed and Reduced Chemical Kinetic Mechanisms, *Combust Flame* (2010) 157:1111-1121.

K. Kumar, C. J. Sung. An Experimental Study of the Autoignition Characteristics of Conventional Jet Fuel/Oxidizer Mixtures: Jet-A and JP-8, *Combust Flame* (2010) 157:676-685.

K. Kumar, C. J. Sung. Flame Propagation and Extinction Characteristics of Neat Surrogate Fuel Components, *Energy and Fuels* (2010) 24: 3840-3849.

K. Kumar, C. J. Sung. A Comparative Experimental Study of the Autoignition Characteristics of Alternative and Conventional Jet Fuel/Oxidizer Mixtures, *Fuel* (2010) 89:2853-2863.

A. Mensch, R. J. Santoro, T. A. Litzinger, S.-Y. Lee. Sooting Characteristics of Surrogates For Jet Fuels, *Combust Flame* (2010) 157:1097-1105.

W. Sun, Z. Chen, X. Gou, Y. Ju. A Path Flux Analysis Method for the Reduction of Detailed Chemical Kinetic Mechanisms, *Combust Flame* (2010) 157:1298-1307.

S.H. Won, W. Sun, and Y. Ju. Kinetic Effects of Toluene Blending on the Extinction Limit of n-Decane Diffusion Flames, *Combust Flame* (2010) 157:411-420.

Z. Chen, X. Gou, Y. Ju. Studies on the Outwardly and Inwardly Propagating Spherical Flames with Radiation Heat Loss, *Combust Sci Technol* (2010) 182: 124–142.

Z. Chen, M. P. Burke, Y. Ju. On the Critical Flame Radius and Minimum Ignition Energy for Spherical Flame Initiation, *Proc Combust Inst* (2011) 33, 1219–1226.

Y. Ju, W. Sun, M. P. Burke, X. Gou, Z. Chen. Multi-timescale Modeling of Ignition and Flame Regimes of n-Heptane-Air Mixtures near Spark Assisted Homogeneous Charge Compression Ignition Conditions, *Proc Combust Inst* (2011) 33:1245-1251.

K. Kumar, C. J. Sung, X. Hui. Laminar Flame Speeds and Extinction Limits of Conventional and Alternative Jet Fuels, *Fuel* (2011) 90: 1004-1011.

G. Mittal, M. P. Raju, C.J. Sung. Vortex Formation in a Rapid Compression Machine: Influence of Physical and Operating Parameters, *Fuel* (2011) 94: 409-417.

S.H. Won, S. S. Dooley, F.L. Dryer, Y. Ju. Kinetic Effect of Molecular Structure on Extinction Limit of Aromatic Diffusion Flames, *Proc Combust Inst* (2011) 33:1163–1170.

S.H. Won, S. Dooley, F. L. Dryer, and Y. Ju, A Radical Index for the Determination of the Chemical Kinetic Contribution to Diffusion Flame Extinction of Large Hydrocarbon Fuels, *Combust Flame* (2011) 159:541-551.

Zheng Chen, Michael P. Burke, Yiguang Ju, On the critical flame radius and minimum ignition energy for spherical flame initiation, *Proc Combust Inst* (2011) 33:1219-1226.

S. Dooley, S.H. Won, J. Heyne, T.I. Farouk, Y. Ju, F.L. Dryer, K. Kumar, X. Hui, C-J. Sung, H. Wang, M. A. Oehlschlaeger, T.A. Litzinger, R.J. Santoro, T. Malewecki, K. Brezinsky. The Experimental Evaluation of a Methodology for Surrogate Fuel Formulation to Emulate Gas Phase Combustion Kinetic Phenomena, *Combust Flame* (2012) 159:1444-4466.

S. Dooley, S.H. Won, Y. Ju, F.L. Dryer, H. Wang, M. A. Oehlschlaeger. The Combustion Kinetics of a Synthetic Paraffinic Jet Aviation Fuel and a Fundamentally Formulated, Experimentally Validated Surrogate Fuel, *Combust Flame* (2012) 159: 3014-3020.

S. Dooley, P. Diévart, P., H.H. Kim, S.H. Won, Y. Ju, F.L. Dryer W., Wang, M. Oehlschlaeger. The Combustion Properties of 1,3,5-Trimethylbenzene and a Kinetic Model, *Fuel* Submitted, September, (2012).

S. Jahangirian, S. Dooley, F.M. Haas, F.L. Dryer. A Detailed Experimental and Kinetic Modeling Study of n-Decane Oxidation at Elevated Pressures, *Combust Flame* (2012) 159:30-43.

S. Jahangirian, S. Dooley, F.L. Dryer, V. Iyer, T.A. Litzinger, R.J. Santoro. Emulating the Combustion Behavior of Real Jet Aviation Fuels by Surrogate Mixtures from Solvent Blends, To be submitted to *Energy and Fuels* Oct, 2012.

X. Hui, K. Kumar, C. J. Sung, S. Dooley, F. L. Dryer. Laminar Flame Speeds and Extinction Stretch Rates of Selected Aromatic Hydrocarbons, *Fuel* (2012) 97:695–702.

H. H. Kim, S.H Won, J. Santner, Z. Chen, Y. Ju. Measurements of the Critical Initiation Radius and Unsteady Propagation of n-Decane/Air Premixed Flames, *Proc. Combust Ins*, 34 (2012). In press.

J. K. Lefkowitz, S.H Won, Y. Fenard, Y. Ju. Uncertainty Assessment of Species Measurements in Acetone Counterflow Diffusion Flames, *Proc. Combust Ins*, 34 (2012). In press.

X. Hui, K. Kumar, C. J. Sung, T. Edwards, D. Gardner, Experimental Studies on the Combustion Characteristics of Alternative Jet Fuels, *Fuel* (2012) 98:176-182.

X. Hui, K. Kumar, C. J. Sung, S. Dooley, F. L. Dryer. Laminar Flame Speeds and Extinction Stretch Rates of Selected Aromatic Hydrocarbons, *Fuel* (2012) 97:695-702.

X. Hui, C. J. Sung. Laminar Flame Speeds of Transportation-Relevant Hydrocarbons and Jet Fuels at Elevated Temperatures and Pressures, *Fuel*, (2012) submitted.

S. Dooley, S.H. Won, J. Heyne, T.I. Farouk, Y. Ju, F.L. Dryer, K. Kumar, X. Hui, C-J. Sung, H. Wang, M. A. Oehlschlaeger, V. Iyer, S. Iyer, T.A. Litzinger, R.J. Santoro, T. Malewecki, K. Brezinsky. The Experimental Evaluation of a Methodology for Surrogate Fuel Formulation to Emulate Gas Phase Combustion Kinetic Phenomena, *Combust Flame* (2012) 159: 1444-4466.

S. Gudiyella, K. Brezinsky. The High Pressure Study of n-Propylbenzene Pyrolysis, *Proc Combust Inst* (2012) 34:http://dx.doi.org/10.1016/j.proci.2012.05.007

S. Gudiyella, K. Brezinsky. High Pressure Study of n-Propylbenzene Oxidation", *Combust Flame* (2012) 159:940-958.

S. Gudiyella, K. Brezinsky. High Pressure Study of 1,3,5-Trimethylbenzene Oxidation, *Combust Flame* (2012) 159:3264-3285.

T. Malewicki, A. Comandini, K. Brezinsky. Experimental and Modeling Study on the Pyrolysis and Oxidation of Iso-Octane, *Proc Combust Inst* (2012) 34:http://dx.doi.org/10.1016/j.proci.2012.06.137

T. Malewicki, K. Brezinsky. Experimental and Modeling Study on the Pyrolysis and Oxidation of n-Decane and n-Dodecane, *Proc Combust Inst* (2012) 34:http://dx.doi.org/10.1016/j.proci.2012.06.156

T. Malewicki, S. Gudiyella, K. Brezinsky. Experimental and Modeling Study on the Oxidation of Jet A and the n-Dodecane/iso-Octane/n-Propylbenzene/1,3,5-Trimethylbenzene Surrogate Fuel, *Combust Flame* (In Press) 2012.

Theses

Zheng Chen, PhD thesis, Studies on the Initiation, Propagation, and Extinction of Premixed Flames, Mechanical and Aerospace Engineering, Princeton University, Princeton NJ. 2009

Amy Mensch. A Study On The Sooting Tendency of Jet Fuel Surrogates Using the Threshold Soot Index, M.S. Thesis, The Pennsylvania State University, May 2009.

Michael P. Burke, PhD thesis, Experiments and Kinetic Modeling of High-Pressure H_2/O_2 Flames (with CO, CO_2, and CH_4 Addition), Mechanical and Aerospace Engineering, Princeton University, Princeton NJ. 2011.

Michelle Christensen. Flow Reactor Autoignition Studies of Iso-octane at High Pressures and Low-To-Intermediate Temperatures, Ph.D. Thesis, The Pennsylvania State University, May 2012.

Soumya Gudiyella, An Experimental and Modeling Study of the Combustion of Aromatic Surrogate Jet Fuel Components, PhD Thesis, University of Illinois Chicago (2012).

Hwanho Kim, Master Thesis, Studies on the Critical Flame Initiation Radius and Unsteady Propagation of *n*-Decane / Air Premixed Flames, Mechanical and Aerospace Engineering, Princeton University, Princeton NJ.2012.

Tom Malewicki, Development of a Jet A Chemical Surrogate Model Using High Pressure Shock Tube Speciation Data. PhD Thesis, University of Illinois Chicago (2012).

Venkatesh Iyer. Effect Of Aromatic Components In Surrogate Fuels On Soot In Co-Flow Flames And A Model Gas Turbine Combustor, Ph.D. Thesis, The Pennsylvania State University, August 2012.

Xin Hui. Flame studies on Conventional, Alternative, and Surrogate Jet Fuels, and Their Reference Hydrocarbons, Ph.D. Thesis, Case Western Reserve University, December 2012 (expected)

Personnel

Investigators			
Ken Brezinsky	Co-Investigator	University of Illinois, Chicago	kenbrez@uic.edu
Fred Dryer	Principal Investigator	Princeton University	fldryer@princeton.edu
Yiguang Ju	Co-Investigator	Princeton University	yju@princeton.edu
Tom Litzinger	Co-Investigator	Pennsylvania State University	talme@engr.psu.edu
Robert Santoro	Co-Investigator	Pennsylvania State University	rjs2@psu.edu
Chih-Jen Sung	Co-Investigator	University of Connecticut	cjsung@engr.uconn.edu

Professional Staff and Visiting Researchers			
Henry Curran	Visiting Researcher	Princeton University, NUI Galway, Ireland	2008-2009
Stephen Dooley	Research Staff	Princeton University	2009-2011
Timothy Bennett	Technical Staff	Princeton University	2009-2012
Pascal Dievart	Research Staff	Princeton University	2011-2012
Tanvir Farouk	Research Staff	Princeton University	2011-2012
Xiaolong Gou	Visiting Researcher	Princeton University	2007-2009

John Grieb	Technical Staff	Princeton University	2009-2010
Saeed Jahangirian	Research Associate	Princeton University	2009-2011
Sang Hee Won	Research Associate	Princeton University	2007-2012
Kamal Kumar	Research Assist Prof	University of Connecticut	2009-2012
Gaurav Mittal	Research Associate	Case Western Reserve University	2007-2008
Wayne Metcalfe	Research Associate	Princeton University	2008-2009
Hui Xu	Research Associate	Princeton University	2007-2008
Zhiwei Yang	Research Associate	Princeton University	2007-2008

Graduate Students

Kyle Brady	Doctoral Student	University of Connecticut	2009-2012
Zheng Chen	Doctoral Student	Princeton University	2007-2008
Michelle Christensen	Doctoral Student	Pennsylvania State University	2008-2012
Apurba Das	Doctoral Student	Case Western Reserve University	2009-2012
Soumya Gudiyella	Doctoral Student	University of Illinois, Chicago	2007 - 2012
Josh Heyne	Doctoral Student	Princeton University	2009-2012

Xin Hui	Doctoral Student	Case Western Reserve University	2007-2012
Venkatesh Iyer	Doctoral Student	Pennsylvania State University	2007-2012
Tom Malewicki.	Doctoral Student	University of Illinois, Chicago	2007 - 2012
Amy Mensch	Masters Student	Pennsylvania State University	2007-2009
Pradep Singh	Masters Student	University of Connecticut	2010-2012
Undergraduate Students			
Amanda Ramcharan	Thesis Student	Princeton University	2010-2011
Jennifer Shim	Summer Student	Princeton University	2012

Table of Contents

1. Introduction

The principal advantages of hydrocarbon-based liquid transportation fuels are their high energy density and portability, properties that are especially important for strategic aircraft applications. Certainly through much of this century, liquid fuel combustion will continue to be the major mode of producing propulsive thrust for aircraft.

Real fuels are extremely complex mixtures with inherent variabilities resulting from changing petroleum/alternative fuel raw resource properties, processing, refining and finishing. Fuel physical and chemical properties must be bounded so their variations do not compromise its utility in the intended application. Fuel certification standards, e.g. **Table 1.1** [1], continue to evolve to assure that fuels are fit-for-purpose in aircraft. Fuel specification standards only loosely define the physical and chemical properties that affect multi-phase combustion.

Detail Specification for Military Turbine Fuels including JP-8, MIL-DTL-83133G, 30 Apr, 2010		
Property	**Constraint**	**ASTM Test Method**
Aromatics (vol%)	< 25	D1319
Sulfur (mass %)	< 0.3	D4294
Distillation Temperature (C)	< 105	D86
10 % recovered (mass)	< 205	D86
20, 50, 90% recovered (mass)	Report	D86
End Point	< 300	D86
Density (kg/l)	0.775-0.840	D4052
Flash Point (C)	> 38	D93
Net Heat of Combustion ((MJ/kg)	>42.8	D 4809
Freezing Point (C)	<-47	D2386
Viscosity (@-20 C) (mm^2/s)	<8	D445
Hydrogen Content (mass %)	>13.4	D3701
Smoke Point (mm) OR Smoke Point and naphthalenes less than 3% (vol)	>25 >19	D1322
Calculated Cetane Index	Report	D976

Table 1.1. An Example of Detailed Fuel Specification for Military Turbine Fuels (MIL-DTL-83133G, 30 Apr, 2010). Acceptable alternative test methods to those quoted may exist [1].

Generically, commercial and military jet fuels contain five primary types of molecular hydrocarbon classes in varying fractional amounts and molecular weight distributions, e.g., see **Fig. 1.1** [2]. Defense Agency Support Center (DESC) Petroleum Quality Information System (PQIS) statistics (e.g. [3] http://www.desc.dla.mil/DCM/Files/2009PQISreport.pdf) continue to show significant variations in fuel properties, geographically as well as from year to year. For JP-8 variations in sulfur content of (100 to 2500 ppm by weight, median at ~1000 ppm), aromatics (10 -25 (vol)%, maximum upper limit permitted, median 16 and 22%), naphthalene (centered about 1.5 (vol)%, limited to < 3%), hydrogen content (~13.6 to 14.2 (mass)%, and smoke (~19 mm to 32mm). Physical properties of JP-8 samples also varied; e.g. viscosity at -20 C ranged from ~ 3.4 to 5.9 mm^2/s, fuel density ~ 0.79 to 0.82 kg/l, initial boiling point (~100 C to 190 C), T_{10} (~161 C to 200 C) while T_{50} and T_{90} varied from ~191 C to 215 C and ~235 C to 274 C, respectively.

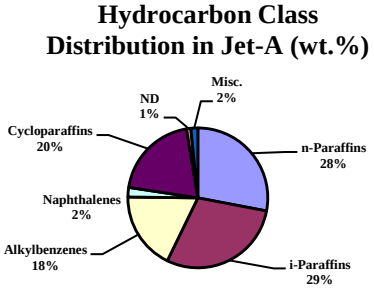

Figure 1.1. World-wide average molecular class distribution of Jet A [2]

Molecular weight distribution is the primary factor in determining fluid properties such as

surface tension, viscosity, distillation curve, and vapor equilibria. **Figure 1.2** [4] displays the molecular mass (distillation) distribution of saturated alkane, cycloalkane, and single ring aromatics, while **Figure 1.3** [5] compares the carbon number and molecular class of five different alternative gas turbine fuel blending stocks. Note that none of the present synthetic products contain aromatics. At present, however, aromatic content is required in jet fuels, due to shrinkage of elastomer seals used in aircraft fuel systems in their absence. Thus, present fuel specifications require blending of no less than 50 vol% of petroleum derived JP-8 with such synthetic materials so that sufficient aromatic content is present to prevent failure of fuel seals. Such blending modifies both the molecular class fractions as well as molecular weight distributions within each class of the fuel blend.

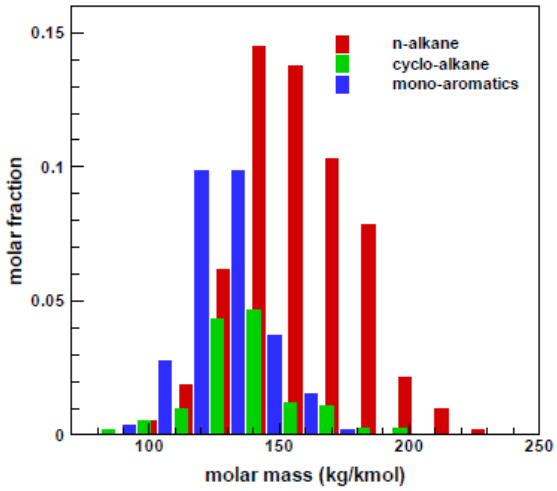

Figure 1.2. Molecular composition distribution for a specific Kersosene Jet A-1 fuel. (normal and iso-alkanes have been combined; small amounts of diaromatics and alkenes are neglected). Bars represent a fit to the real fuel composition distribution through a selection of twenty eight individual pure components. [4].

Noting the above property statistics, the relative range of physical and chemical properties over which today's gas turbine technologies achieve acceptable performance and emissions is impressive. The potential deployment of alternative fuels has also stimulated further refinements of specification standards that cover bulk thermodynamic and transport properties as well as criteria for thermal and storage stability, safety and handling, and compatibility with existing fuels, additives, and fuel-wetted aircraft materials. But the modified rules do not define more succinctly the effects of physical and chemical properties on specific combustion properties. *More quantitative description of how petroleum derived and alternative fuel physical and chemical properties affect combustion remain a critical issue in assessing existing hardware performance and in developing future propulsion systems.*

1.1. Surrogate Fuel Concepts

Even if the composition of each specific fuel sample is determined in detail (e.g. as indicated by carbon number distributions **Figure 1.4** [5], or [6]), relating their specific combustion properties to the detailed analyses requires approximations [7-11]. From fundamental insights, fuel-specific distillation curve, vapor dome, viscosity, and surface tension are all known to be properties that influence atomization, vapor deposition and mixing in multiphase systems). Additionally, fundamentals

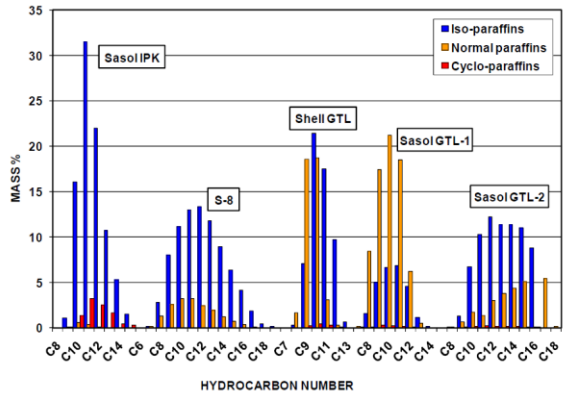

Figure 6. Molecular distributions of n-paraffins, iso-paraffins and cyclo-paraffins found in fuels produced from Fischer Tropsch processes of various primary energy resources (IPK-Coal, all others, natural gas). Presented in [11].

suggest that molecular class distribution across each distillation curve could result in local variations in vaporized chemical composition through preferential vaporization, affecting local chemical kinetic behavior.

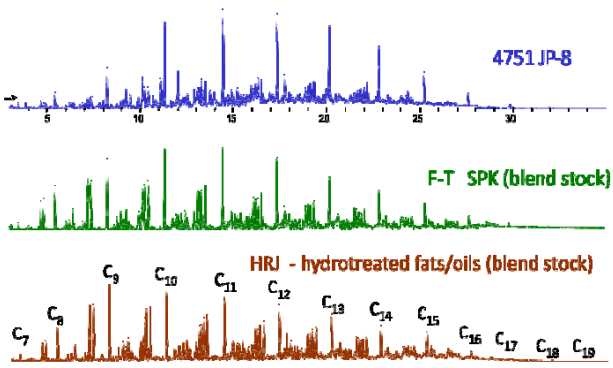

Figure 1.4. Carbon distributions of a military JP-8 fuel sample, a Fischer Tropsch synthetic paraffinic kerosene (SPK) generated from natural gas and a hydroprocessed renewable jet (HRJ) fuel derived from fats/oils [5].

Moreover, developing robust, predictive chemical kinetic models that encompass the detailed molecular chemical species composition of each fuel would be prohibitively complex, given the large numbers and types of component species present, not to mention the current availability and uncertainties of fundamental kinetic data for each component and their mixture interactions. One might argue that model reduction methodologies can be applied to yield acceptable dimensional constructs, but these will continue to reflect all of the uncertainties contained in the original model. As a result, a commonly employed concept for emulating the physical and chemical property effects of real fuels on combustion has been the use of "surrogate mixtures" (a mixture of a limited number of components, each of known molecular structure) that adequately represent the real fuel physical and/or combustion-related properties.

The generally applied procedure has been to select candidate surrogate components from the molecular classes found in the real fuel. The constructed surrogate mixture and real fuel behaviors are then compared experimentally (over a limited number of fundamental venues) or by comparing detailed computational predictions for the surrogate fuel mixture against experimental observations for the real fuel. Moreover, many studies on developing and testing surrogates have treated the target "jet" fuel as a generic material, providing little detail on its specific physical and chemical properties (sometimes not even its specification data).

Discussion continues over the relative importance of physical and chemical kinetic properties to performance of and emissions from multi-phase combustion systems, e.g. [12-16]. Few works have considered comprehensive replication of both in developing surrogate concepts and mixtures, e.g. [15, 16]. Large numbers of surrogate components are generally required, particularly for reproducing distillation curve and vapor dome properties. Replicating distribution of molecular class structure over the distillation curve generally requires even larger numbers of components from each molecular class found in the fuel [16].

On the other hand, the complexity and dimensionality of detailed kinetic models also increases substantially with the number of individual surrogate components utilized [17-19]. The number of reactions and species needed for emulating the wide range of carbon numbers and molecular structures found in jet fuels is very large, especially if molecular oxygen addition reactions associated with low and intermediate temperature regime chemistry are considered [20]. Evaluating the influence of low and intermediate temperature chemistry on gas turbine combustion properties is one of many questions raised as this project began. However, this

chemistry is also known to be of importance to compression ignition phenomena in piston engines and thus is relevant to one-fuel-forward strategic concepts.

For the near term, models for a specific real fuel that would equally weight the fidelity in reproducing the detailed physical and chemical properties of a real fuel would be intractable for computational design, and likely even for computational research. Understanding the quantitative importance of each physical and chemical property in relative terms on multi-phase combustion performance and emissions is important to guiding which aspects require most detail. Experimental and modeling studies at the applied combustion level remain important in determining these facts [5].

1.2. Overall MURI Research Goals

The overall goal of this MURI effort has been to develop concepts, metrics, advanced metrology and cross-validated critical experimental data along with new fundamental insights to produce surrogate mixtures that would accurately reflect the physical and chemical kinetic properties of each specific real fuel sample under multi-phase combustion conditions relevant to aircraft gas turbine applications. Though physical property effects need to be considered, we place initial emphasis on developing and proofing "surrogate fuel" formulation concepts for emulating fully prevaporized combustion properties.

Historically, algorithms for predicting global properties such as Cetane number, Octane number, sooting, as well as physical and chemical properties, e.g. [21-25] suggested to us that similar functional correlations might point to methodologies and rules for constructing surrogate mixtures to emulate fully prevaporized real fuel combustion properties. Earlier work on creating gasoline surrogate mixtures [26], and our analyses of the above studies along with prior involvement in [7-10] led us to *formulate overarching, kinetic/transport hypotheses for surrogate mixture formulation* [27] *as well as a select, small number of components to initially consider* [27, 28] *in order to emulate real fuel behavior. Based on our qualitative understanding of the parameters that influence kinetic and transport timescales of aliphatic and aromatic fuel mixture combustion phenomena, a prioritization of the order in which the types of molecular class structure would be considered was developed. Emphasis was placed on simple, low volume, efficient experimental methodologies for determining "fuel property targets" for real fuels, surrogate components, and their mixtures that could be used to match surrogate mixture behavior to that of a specific real fuel.*

A cross-validated and comprehensive experimental database was generated consisting of homogenous autoignition, chemical species evolution, laminar flame speed, laminar premixed and non–premixed (diffusive) strained extinction, and sooting characteristics for each component, their mixtures, and for the specific real fuel samples to be emulated. Single pulse shock tube and variable pressure flow reactor experiments produced data for highly dilute reaction conditions, while rapid compression machine, laminar premixed and non-premixed flame, and turbulent combustor experiments produced data for higher fuel/oxidizer energy densities typical of real systems.

In the efforts to evolve surrogate concepts, we emphasized comparing the surrogate mixture behaviors directly with those of specific real fuels across all of the above experimental venues.

We purposely did not depend on model predictions of surrogate mixtures in this process, since considerable uncertainties remained, even for the kinetics of well studied species such as n-alkanes, and iso-octane. Moreover, frequently the physical modeling parameters utilized in simulations can also result in uncertainties in the predictions of experimental data. Finally, experimental venues that involve kinetic/transport require kinetic model reduction that may also result in concerns as to the veracity of the predictions.

On the other hand, as the research evolved, we utilized detailed kinetic models, both those found in the literature and those developed as part of the research, to analyze the experimental comparisons and elucidate the controlling parameters in the various fundamental combustion configurations, for example, the effects of energy density, molecular transport, and chemical kinetics on laminar diffusive strained extinction.

We concluded that kinetic models for alkyl aromatics, which are central to any surrogate kinetic model, were the least developed and tested for the range of conditions of interest. As a result, kinetic model development within the MURI concentrated on alkyl aromatic submodels. Normal alkane, iso-alkane, and cycloalkane kinetic sub-models, principally those evolving at Lawrence Livermore National Laboratories, were utilized in the MURI efforts, though comparisons of our experimental observations against other models are also detailed in MURI funded publications. A separate concurrent effort supported by the Air Force [29] evolved and validated a large detailed model for alkanes, and cycloalkanes. Unlike the LLNL based work, Jet Surf [29] did not consider low and intermediate temperature kinetic regimes.

Realizing that each detailed model for a specific surrogate component and their eventual composite for describing the surrogate mixture would be very large dimensionally, model reduction and CFD code integration methods were also considered as we addressed the fundamental combustion venues we were studying that couple combustion kinetics and transport.

As the fundamental veracity of our surrogate formulation approach became more apparent, we directed kinetic modeling efforts toward developing detailed and reduced kinetic models for each of the specific surrogate components. Surrogate component and detailed surrogate mixture kinetic model development progressed significantly over the last year of the MURI, but remains incomplete in terms of model refinements and validations. However, the present modeling results summarized here show both considerable progress and promise.

The above discourse sets the background upon which the call for research under a MURI in this effort was made, briefly describes the emergence of the approach presented in our responding proposal, and the details the directions that the subsequent research took. The specific areas of effort and contributions from each of the respective laboratories involved in the MURI are outlined in the following section, followed by sections that present summaries of these research efforts. The sections are not equally weighted in terms of length due to differences in what has been and that which remains to be published in the archival literature. Some duplicative discussions of particular work may appear in several of these sections, as there were substantial collaborations amongst the various researchers, particularly in developing the surrogate component and fuel kinetic databases and in testing surrogate concepts through comparisons of real fuel and surrogate mixture combustion behaviors.

1.3. Areas of Contribution of Each Participating Group.

Four research groups collaborated in the MURI research, each contributing to specific experimental and modeling tasks. The groups included those of Dryer (Princeton1), JU (Princeton2), Sung (UCONN), Santoro and Litzinger (PSU), and Brezinsky (UIC). The responsibilities of each group generally were as follows:

1. ***Select surrogate component candidates, develop surrogate concepts and formulate prototype surrogate mixtures- Princeton1 (Dryer)***

2. ***Develop transport, thermochemical, elementary kinetic databases and validated detailed kinetic models for surrogate components. (Shared, but principally, Princeton and UIC)***

3. ***Evolve a robust, fundamental, experimental validation database to produce "fuel property target" data and to characterize autoignition, heat release rate, premixed and non-premixed laminar flame properties and sooting for each surrogate component species, representative mixtures of surrogate components and real fuels (all).***

- ***Princeton University (PU)***

Variable Pressure Flow Reactor (VPFR) Experiments
Premixed Flame Experiments
Autoignition – (Ignition Quality Testing)
Non-Premixed Flame Extinction Experiments
Molecular Weight Characterization
H/C Characterization

- ***University of Connecticut (UCONN)- C-J. Sung***

Rapid Compression Machine Experiments
Pre-mixed Flame Experiments (laminar flame speed, premixed extinction)
Non-Premixed Flame Experiments (ignition and extinction)

- ***Pennsylvania State University (PSU)- R.J. Santoro, T. Litzinger***

Threshold Sooting Index Investigations and Measurements
Fundamental Soot Laser Extinction Comparisons
High Pressure Autoignition Experiments in a turbulent reactor
Modular Gas Turbine Combustor (MGTC) Soot laser Extinction Comparisons

- ***University of Illinois, Chicago (UIC)- K. Brezinsky***

High Pressure Single Pulse Shock Tube Experiments

4. ***Derive comprehensive, validated kinetic models for component mixtures relevant to real fuel emulation over the full thermodynamic parameter space***

5. ***Identify critical performance targets for surrogate mixture behavior important to altitude relight, high speed propulsion, augmentor performance, and gas turbine environments (all)***

6. ***Develop methodologies to reproduce real fuel property targets for mixture formulation – Princeton 1, Princeton2***

7. ***Apply existing and new dimensional reduction methods to produce reduced models that can be used in numerical design tools – UCONN, Princeton2***

The integral results of these collaborative efforts are detailed in the list of archival papers and preprints papers presented in the Executive Summary.

In addition to the archival and preprinted publications listed at the end of the respective research summaries generated by each group, the research has been summarized in PowerPoint

presentations for the MURI Kick-Off Meeting in 2007 and in the annual Multi Agency Coordinating Council Review (MACCCR) Fuels Summits for 2008-2011. The MACCCR meetings served as the annual review for the MURI effort. Each of the enumerated websites below archives the PowerPoint presentations generated by each of the MURI investigator groups:

MURI Kick-off Meeting:

Sept.17-18, 2007; Princeton University **https://www.princeton.edu/~combust/MURI/**

MACCR Fuels Summit Reviews:

Sept. 8-10, 2008: Gaithersburg, MD **http://kinetics.nist.gov/RealFuels/macccr/index.html**

Sept. 15-17, 2009: Los Angeles CA **http://kinetics.nist.gov/RealFuels/macccr/macccr2009.html**

Sept. 20-22, 2010: Princeton, NJ **http://kinetics.nist.gov/RealFuels/macccr/macccr2010.html**

Sept. 20-22, 2011: Argonne, IL **http://kinetics.nist.gov/RealFuels/macccr/macccr2011.html**

Below, each of the collaborating groups presents a summary of their respective contributions to the MURI project. These individual summaries are then followed by a section delineating the overall project results and implications for future work.

1.4. References

[1] http://www.iash.net/Fuel_Specs/USIS_fuel_spec.html, "Detailed Fuel Specification for U.S. Military Turbine Fuels MIL-DTL-83133G, 30 Apr, 2010.

[2] Shafer, L.M., Striebich, R.C., Gomach, J., Edwards, T., "Chemical Class Composition of Commercial Jet Fuels and Other Specialty Kerosene Fuels". AIAA 2006-7972.

[3] Defense Energy Support Center (DESC). Petroleum Quality Information System (PQIS), http://www.desc.dla.mil/DCM/Files/2009PQISreport.pdf

[4] Le Clercq, P., Doué, N., Rachner, M., Aigner, M., "Validation of a Multicomponent-Fuel Model for Spray Computations", Proceedings of the 47th AIAA Aerospace Sciences Meeting, 5-8 June, Orlando, FL, USA. AIAA-2009-1188

[5] Edwards, T., Dryer, F.L., Moses, C., "Evaluation of Combustion Performance of Alternative Aviation Fuels", 46th AIAA/ASME/SAE/ASEE Joint Propulsion Conference & Exhibit 25 - 28 July, Nashville, TN. Paper No. AIAA-2010-7155

[6] Edwards, J.T., Bruno, T.J., "The Properties of S-8", Technical Report MIPR F4BEY6237G001, Physical and Chemical Properties Division, National Institute of Standards and Technology, Boulder, CO, November 2006.

[7] Pitz, W.J., Cernansky, N.P., Dryer, F.L., Egolfopoulos, F.N., Farrell, J.T., Friend, D.G., Pitsch, H., "Development of an Experimental Database and Chemical Kinetic Models for Surrogate Gasoline Fuels". SAE Paper 2007-01-0175.

[8] Farrell, J.T., Cernansky, N.P., Dryer, F.L., Friend, D.G., Hergart, C.A., Law, C. K., McDavid, R.M., Mueller, C.J., Patel, A.K., Pitsch, H., "Development of an Experimental Database and Kinetic Models for Surrogate Diesel Fuels". SAE Paper 2007-01-0201.

[9] Colket, M. B., et al, "Development of an Experimental Database and Kinetic Models for Surrogate Jet Fuels", Jan 2007. AIAA Paper 2007-770.
[10] Colket, M. B., et al, "Identification of Target Validation Data for Development of Surrogate Jet Fuels", January 2008. AIAA Paper 2008-972.
[11] Pitz, W.J. and Mueller, C.J., "Recent Progress in the Development of Diesel Surrogate Fuels", *Prog Energy Combust Sci* (2010) 37:330 (2011).
[12] Bruno, T. J., Smith, B. L., "Evaluation of the Physicochemical Authenticity of Aviation Kerosene Surrogate Mixtures. Part 1: Analysis of Volatility with the Advanced Distillation Curve", *Energy Fuels* (2010) 24:4266-4276.
[13] Bruno, T. J., Huber, M.L., "Evaluation of the Physicochemical Authenticity of Aviation Kerosene Surrogate Mixtures. Part 2: Analysis and Prediction of Thermophysical Properties", *Energy Fuels* (2010) 24:4277-4284
[14] Huber, M.L., Lemmon, E.W., and Bruno, T.J., "Surrogate Mixtures Models for the Thermophysical Properties of Aviation Fuel Jet A", *Energy Fuels* (2010) 24:3565 3571.
[15] Slavinskaya, N. A., Zizin, A., Aigner, M., "On Model Design of a Surrogate Fuel Formulation", *J Eng Gas Turb Power* (2010) 132(11):1501-1511.
[16] Mueller, C.J., Cannella, W.J., Bruno, T.J., Bunting, B., Dettman, H.D., Franz, J.A., Huber, M.L., Natarajan, M., Pitz, W.J., Ratcliff, M.A., Wright K., "Methodology for Formulating Diesel Surrogate Fuels with Accurate Compositional, Ignition-Quality, and Volatility Characteristics", *Energy Fuels*, May 22.. DOI: 10.1021/ef300303e
[17] Lu T. F., Law C. K., "Toward Accommodating Realistic Fuel Chemistry in Large-scale Computations. *Prog Energy Combust Sci* (2009) 35:192-215.
[18] Westbrook, C.K., Pitz, W.J., Herbinet, O., Curran, H.J., Silke, E., "A Comprehensive Detailed Chemical kinetic Reaction Mechanism for Combustion of *n*-Alkane Hydrocarbons from *n*-Octane to *n*-Hexadecane", *Combust Flame* (2009) 156:181-199.
[19] Sarathy, S.M, Westbrook, C.K., Mehl, M., Pitz, W.J., Togbe, C., Dagaut, P. Wang, H., Oehlschlaeger, M.A., Niemann, U., Seshadri, K., Veloo, P.S., Ji, C., Egolfopoulos, F., Lu, T., "Comprehensive Chemical Kinetic Modeling of the Oxidation of C2-Methyl Alkanes from C_7 to C_{20} ",*Combust Flame* (2011) 158:2338-2357.
[20] Battin-Leclerc, F., "Detailed Chemical Kinetic Models for the Low-temperature Combustion of Hydrocarbons with Application to Gasoline and Diesel Fuel Surrogates", *Prog Energy Combust Sci* (2008) 34:440-498.
[21] Gosh, P., Jaffee, B., "Detailed Composition-Based Model for Predicting the Cetane Number of Diesel Fuels", *Ind Eng Chem Res* (2006) 45:346-351.
[22] Gosh, P., Hickey, K. J., Jaffee, B., "Development of a Detailed Gasoline Composition-Based Octane Model", *Ind Eng Chem Res* (2006) 45:337-345.
[23] Yan, S., Eddings, E.G., Palotas, A.B., Pugmire, R.J., Sarofim, A.F., "Prediction of Sooting Tendency for Hydrocarbon Liquids in Diffusion Flames", *Energy Fuels* (2005) 19:2408-2415.
[24] Pepiot-Desjardins, P., Pitsch, H., Malhotra, R., S.R. Kirby, S.R., Boehman, A.L., "Structural Group Analysis for Soot Reduction Tendency of Oxygenated Fuels", *Combust Flame* (2008) 154:191–205.
[25] Katritzky, A.R., Kuanar, M., Slavov, S., Hall, C.D., "Quantitative Correlation of Physical and Chemical Properties with Chemical Structure: Utility for Prediction", *Chem Rev* (2010) 110:5714–5789.

[26] Chaos, M. Zhao, Z., Kazakov, A., Gokulakrishnan, P., Angioletti, M. and Dryer, F.L., "A PRF+Toluene Surrogate Fuel Model for Simulating Gasoline Kinetics", 5th US Combustion Meeting, University of California at San Diego, San Diego, CA, March 25-28, 2007. Paper E-26

[27] Dryer, F.L. (PI), Brezinsky, Curran, H. J., Ju, Y., Litzinger, T. A. Santoro, R. J., Sung, C-J, "Multi University Research Initiative - Generation of Comprehensive Surrogate Kinetic Models and Validation Databases for Simulating Large Molecular Weight Hydrocarbon Fuels", AFOSR Grant No. FA9550-07-1-0515.

[28] Xu, H., Yang, Z, Chaos, M., Dryer, F.L., "Surrogate Jet Fuel Mixture Formulation and Development of Experimental Databases", JANNAF 42nd Combustion Joint Sub-Committee Meeting *Modeling and Data For Combustion Simulation*, Boston Marriott Newton, Hanscom AF Base, Newton, MA, May 12-16, 2008

[29] Wang, H., Dames E., Sirjean, B., Sheen, D.A., Tangko, R., Violi, A., Lai, J.Y.W., Egolfopoulos F.N. Davidson, D.F., Hanson, R.K.,.Bowman, C.T., Law, C.K., Tsang, W., Cernansky, N.P., Miller, D.L., Lindstedt, R.P., (September 19, 2010) "A high-temperature chemical kinetic model of n-alkane (up to n-dodecane), cyclohexane, and methyl-, ethyl-, n-propyl and n-butyl-cyclohexane oxidation at high temperatures - JetSurF version 2.0", available at: http://melchioruscedu/JetSurF/JetSurF20.

Individual Group Summaries

2. Princeton University (Princeton1) F.L. Dryer

2.1. Abstract

In addition to serving as the principal coordinator of the MURI, Prof. Dryer directed the research in his own laboratory, with the principal assistance of Dr. Stephen Dooley. The efforts in his laboratory provided development of the MURI surrogate concept, as well as investigation and adaptation of Derived Cetane methodologies to characterizing gas turbine fuel reactivity. Additionally, new experimental data on real fuels, and surrogate components and their mixtures were obtained using the Princeton Variable Flow Reactor (VPFR). Finally, this laboratory in collaboration with Prof. Ju's laboratory led the development of kinetic models to be used in analyses and modeling of surrogate mixture behavior, with emphasis on comprehensive, hierarchical modeling methodologies.

2.2. Introduction

Though a substantial number of studies to develop surrogates for gas turbine fuels appeared in the literature prior to this MURI project (e.g. Refs. [1-12]), no generally proofed methodology for selecting specific surrogate components and for formulating fuel surrogate mixtures to emulate the variability of real fuel properties had emerged. Beginning in 2003[13], consideration of these issues catalyzed the formation of a Surrogate Fuels Working Group to summarize overall research status in relevant areas and attempt to provide a road map for future research directions on jet [14], gasoline[15], and diesel[16] surrogate fuels development. The selection of specific components to form mixtures that would emulate the combustion properties of a real fuel typically proceeded by selection of one or more to represent each of the chemical classes within the real fuel. At least one surrogate component of each major chemical structure class appeared to be required to characterize the chemical kinetic interactions of the components.

Even before 2003 (supported by General Motors Research and Honda Research, Japan), the PI's laboratory had already studied n-heptane, iso-octane, and toluene (ternary reference fuel, TRF) mixtures as a surrogate for fully prevaporized combustion behavior of gasoline. Component mixture variations were found to reproduce the desired combustion behaviors of energy density, flame speed, ignition delay, and chemical reactivity compared to real gasolines in fundamental experiments [17-21], if the mixture matched the H/C ratio and some measure of the chemical reactivity behavior for the real fuel. Methodologies were established to formulate ternary mixtures matching gasolines by performing reactivity experiments comparing the real gasoline and surrogate mixtures in the Princeton Variable Pressure Flow reactor (VPFR). Stoichiometry of the experiments was determined by measuring the CO_2 yield for known mass flow rates of fuel and oxygen. However, the mixture of components that produced matching H/C and reactivity did not correspond to that which reproduced the road octane number of the gasoline [21].

Noting that algorithms for predicting properties such as Cetane number [22, 23], distillation [24], and sooting tendency [25] as functions of molecular fragments, the PI hypothesized that methodologies and rules for emulating real fuel combustion behavior could be formulated to

replace mimicking the class composition of the fuel itself [26]. Modeling class composition has inherent difficulties, for example in classifying alkyl aromatics as aromatics alone and not recognizing the contributions of the alkyl portions of the molecules to the alkane classes.

Component	Molecular Formula	Structure	NTC
n-Heptane	C_7H_{18}		Yes
n-Decane	$C_{10}H_{22}$		Yes
n-Dodecane	$C_{12}H_{26}$		Yes
Iso-Octane (2,2,4 Trimethylpentane)	C_8H_{18}		Sml
Iso-Cetane (Heptamethylnonane)	$C_{16}H_{34}$		No
Methylcyclohexane	C_7H_{14}		Yes
Toluene	C_7H_8		No
n-Propyl Benzene	C_9H_{12}		?
1,3,5 Tri Methyl Benzene	C_9H_{12}		?
1-methyl naphthalene	$C_{11}H_{10}$		No

Figure 2.1. Surrogate component candidates selected for the MURI research. "NTC" denotes the presence/absence of two stage chemical kinetic behavior. Color coding: Blue- Substantial modeling and validation efforts; Orange- Model development underway; Brown- Modeling and validation data limited; Black- validation data very limited.

The background above provided overarching, qualitative, kinetic/transport insights and modeling constraints that led the MURI to select the initial surrogate component set shown in **Fig. 2.1**. Gas turbine fuels have significantly higher average molecular weights than gasolines, require consideration of sooting, had no representative criteria for "reactivity", and, at the time, lacked fundamental experimental characterization over a range of conditions encompassing propulsion applications. The limited availability of detailed kinetic models for heavier molecular weight components, particularly aromatics, also significantly influenced our overall approach. The carbon numbers of n-heptane, n-decane, iso-octane, and toluene are all less than the average value for gas turbine fuels (~12). However, n-decane, iso-octane and toluene continued to be of interest to the work, since these components had already received substantial modeling attention. Efforts were already underway at Princeton and elsewhere to develop higher carbon number n-alkane kinetics, principally for n-decane, based upon the existing n-heptane modeling [27-31]. But a carbon number of at least n-dodecane would eventually be required to form surrogate mixtures with appropriate average molecular weight. Over the conduct of this research significant advances have been made on modeling higher carbon number normal alkanes, as discussed elsewhere in this report.

The remaining components shown in **Fig. 2.1** were not selected based upon their prevalence in gas turbine fuel compositions, but because of their ability to form mixtures that could match the "(fuel) combustion property targets" (i.e. H/C, TSI, and DCN, MW_{ave} discussed below) for the ranges of parameters found for specific real jet fuels. **Figure 2.2** summarizes the relationship of prevaporized global combustion properties and combustion property targets that the MURI envisioned.

The chemical interactions of the surrogate components in a mixture permits flexible adjustment of DCN and TSI (which depends on the molecular weight of the fuel, MW_{ave}) for a fixed H/C ratio. Matching H/C ratio and average molecular weight, MW_{ave}, to that of a real fuel are important to replicating heat of reaction, flame temperature, flame speed, and local air/fuel stoichiometric location/species leakage (in mixing limited

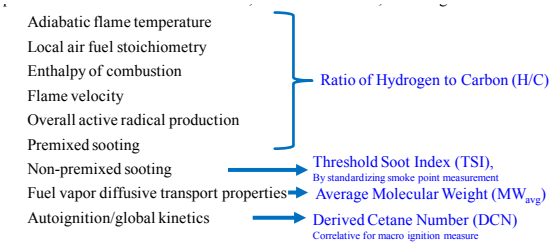

Figure 2.2. Critcal (fuel) combustion property targets that manifest in important fully prevaporized combustion behavior of each, individual real fuel, including

combustion conditions) of the real fuel. Moreover, matching H/C ratio is required to simulate total air/fuel flow rates for commensurate power with both the surrogate mixture and the real fuel. For gas turbine surrogates, the selection of several aromatic components is critical to simultaneously replicating H/C ratio, autoignition, and sooting, particularly under diffusive/mixing limited combustion conditions.

It is well known that the radical pool generated in the pyrolysis and oxidation of aromatics, with or without short chain length alkylation, is less than that generated by n-alkanes [32]. The addition of an aromatic to an n-alkane of similar molecular weight leads to destruction of the initial aromatic specie primarily as a result of hydrogen abstraction by the pool of small radicals produced in larger measure by the n-alkane. The overall radical pool in the reacting mixture is suppressed (relative to that found for the oxidation of the pure n-alkane) because the overall rate of small radical regeneration from aromatic fragments is typically slower in comparison to regeneration of small radicals from beta scission and decomposition of the intermediates formed from the alkanes.

Hydrogen atom abstraction reactions with the aromatics occur preferentially on the alkyl side chains, followed by direct oxygen attack on or beta scission of the alkyl side chain if it contains three or more carbon atoms. Abstraction of hydrogen from any methyl side chains yields much less effective radical species for regenerating H, OH, or O through their subsequent reactions than in the case of longer n-alkyl side chains. As a result, methylated single ring aromatics will inhibit the overall radical pool more effectively than alkylated single ring aromatics of similar molecular weight with long side chains. Based upon the beta-scission products yielded, we should also expect that iso-propyl or tert-butylbenzene will inhibit the radical pool growth rate of an alkane more than equal additions of n-propyl or n-butyl benzene. Similar to the xylenes, we expected that 1,2,4-trimethylbenzene (124TmB) would be reactive with molecular oxygen at low temperatures (contributing to cool flame chemistry) while 135TmB would exhibit little or no cool flame chemistry itself [33]. Though we considered both structures, the symmetry of 135TmB is more attractive in terms of modeling aspects. Thus, we chose this trimethyl benzene as a candidate component. Moreover, since nPB and 135TmB have the same molecular weight, these compounds offered an opportunity to emphasize kinetic differences upon diffusive/mixing limited combustion observations. The addition of 135TmB to an alkane will inhibit the low, intermediate, and high temperature reaction characteristics principally by competition for the small radical pool generated by the alkane.

The kinetic study of toluene and xylenes were recognized to be central to developing kinetic models for the higher carbon number alkyl aromatics. Aromatic model development for toluene was also considerably farther along than for higher alkyl aromatics. Even so, there was a clear need to advance the model development for toluene as a template and sub model for the larger aromatic species, since their kinetics also heavily involve the benzyl radical. We also utilized toluene as the aromatic fraction in early surrogate work.

The remaining combustion target, sooting, responds to both hydrogen content (in premixed environments) as well as chemical structure (in diffusion/mixing limited situations). Aromatics are considerably more active in producing soot. Small amounts of 1-methylnaphthalene were included as a potential surrogate component should a means of adjusting the overall sooting behavior to better simulate that of the real fuel be needed. However, we later found that

including this species was not required. In fact, the amount of such components in gas turbine fuels is limited by fuel certification standards.

Finally, some comment on the choices of iso-octane and methylcyclohexane as components to represent iso-alkanes and cycloalkane class structures in the fuel is in order. Neither of these choices was viewed as ideal ones. As both have carbon numbers that are considerably less than those typical of gas turbine fuels. Physical properties for iso-octane (e.g. liquid density), are also at odds with those of jet fuel. What appears to be a larger concern is that gas turbine fuels typically contain weakly branched alkane isomers rather than strongly branched structures such as iso-octane or iso-cetane.

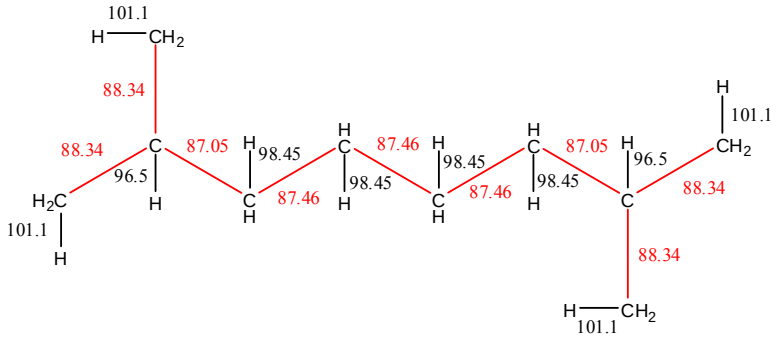

Figure 2.3. Bond dissociation energies of 2,7-dimethyloctane (kcal/mol). Values from group additivity.

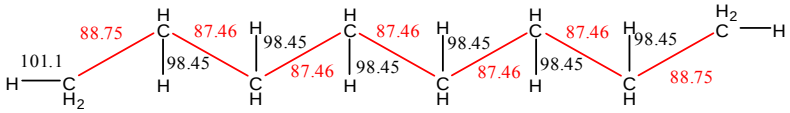

a) n-octane

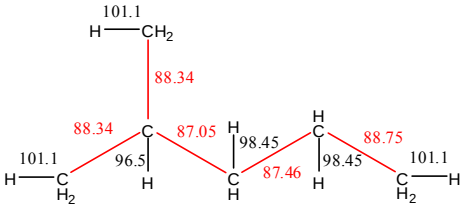

b) 2-methylpentane

Figure 2.4. Bond dissociation energies of the noted molecule. (Kcal/mol). a) n-octane ; b) 2-methylheptane. Values from group additivity

Weakly branched alkanes are not generally available from chemical suppliers and typically must be synthesized, making them exceedingly expensive as surrogate components. Similarly, higher molecular weight cycloalkanes are also exceedingly expensive. For example, n-propylcyclohexane is typically available at over $600 for 100 ml. Economic constraints alone limit the ability of researchers to produce expansive validation data over a wide range of experimental venues for either of these component structures.

While others [34] emphasized research on weakly branched and cyclo alkanes, we deferred study of these components, despite their presence in real fuels. In the case of weakly branched alkanes, we argued and shared with the community that weakly branched alkanes would not have unique consequences in the real fuel global reactivity and combustion behavior.

For example, **Fig. 2.3** depicts the bond dissociation energies of 2,7 dimethyl octane (DMOCT) as calculated using Benson's group additivity method. Based on these bond energies, there are no unusual reaction centers that emerge in comparison to other normal or weakly alkanes (**Fig. 2.4**). The presence of the branched chain creates slightly weaker C-H bonds (96.5 kcal/mol) at carbon

sites 2 and 7 of 27DMOCT, due to the stability of the tertiary radical created by hydrogen abstraction from this site. A weaker C-C bond alpha to the branched center also results for similar reasons. Similar reaction centers are also present in many other branched alkane isomers.

C – type	A	n	E_a
1^o	1.00e+13	0.0	52,290
2^o	1.00e+13	0.0	49,640
3^o	1.00e+13	0.0	48,200

Figure 2.5. Arrhenius parameters per H atom for abstraction by O_2 (cm^3/mol/s/cal).[33].

The initiation process (generation of the first radical by H abstraction by O_2) or through thermal decomposition at a C-C weaker bond location should proceed in a similar fashion to an n-alkane, especially for higher carbon number molecules. In the present example, the presence of the two weak tertiary hydrogen sites are outnumbered 4:1 by the secondary hydrogen sites on the straight chain, and also by the 12 primary hydrogen sites on the terminal carbons of the molecule. To illustrate this point, literature rate constants [33] for H atom abstraction from each of the carbon sites (primary, secondary and tertiary) by molecular oxygen were scaled by the number of each of the different carbon sites present in 27DMOCT and plotted as a function of the total rate of H abstraction by O_2, **Fig. 2.5**.

Figure 2.6 suggests that at 700-2000 K, H atom abstraction by O_2 would primarily yield secondary radicals. However, despite having only two sites, the tertiary radical plays a significant role in the total rate of abstraction, particularly below 1100 K. This is due to the significantly lower activation energy of this reaction when compared to the rate of abstraction from a primary site. Considering the most probable beta scission products (based on bond strengths) from each of the alkyl radicals we found that 27DMOCT would be less reactive than an n-alkane of equal carbon number. We therefore concluded that the reactivity could be matched with an appropriate blend of a normal alkane with isobutene (as yielded from beta scission of iso-octyl radicals, or a longer saturated branched alkane). We also could not envision how the branched centers would interact with one another in a meaningful way to significantly affect the overall combustion properties of a surrogate mixture containing n-alkanes and the more highly branched species we chose.

Cases where the chemistry might be more unique to the original molecule structure are the addition of O_2, for example in the subject iso-alkane for the secondary radical site at carbon 4. The RO_2 species formed can isomerize and abstract either of the weak tertiary hydrogen atoms through a six or seven-membered transition state. This reaction center would be impossible to recreate with the blended mixture. However, this result would only be likely to affect low temperature autoignition chemistry, and even here, our later experimental results suggests that in mixtures as complex as gas turbine fuels, this effect is at best weak.

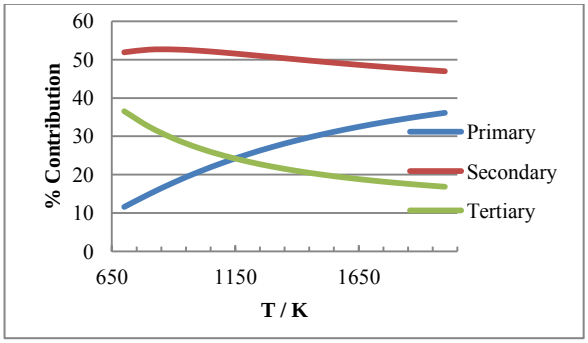

Figure 2.6. Percent contribution of 2,7-dimethyloctane + $O_2 \leftrightarrow R\bullet + HO_2$ forming a primary, secondary or tertiary radical.

The above hypotheses have been supported over the course of our work by our relative success of emulating real fuels that contain

substantial fractions of methyl- and dimethyl-isoalkanes (a synthetic gas turbine feed stock produced from natural gas, S-8) with n-dodecane/iso-octane mixtures. Later in this document, we specifically show as well that 2-methyl heptane kinetic behavior with a mixture of n-decane and iso-octane.

Similarly we argued that though cycloalkanes may be present in significant fractions of higher molecular weight propulsive fuels (see our later discussions), we would assess the need for this component as the program progressed. Methylcyclohexane (MCH) detailed mechanisms already existed [33, 36] and could be used in model projections of including MCH in surrogate mixtures. We later detail experimental and numerical work that suggests that cycloalkanes appear to add little to the control of global combustion observations of surrogate mixtures that is already achieved by n-alkane/iso-alkane/aromatic mixtures.

In summary, from kinetic and transport analyses and our collective combustion research experience, we hypothesized the above selection of surrogate fuel components, surrogate mixture requirements based upon matching the production rate of small radicals by reproducing the large molecular weight fuel fragments (?) under the constraints of mean molecular weight, H/C ratio, a measure of mixing- limited sooting tendency, the threshold sooting index (TSI), and a relative measure of global reactivity, the derived cetane number (DCN). The net rate of radical production defines the ignition and overall reaction character of the surrogate mixture. The production rate of fuel fragments (particularly H and H_2) also defines transport of reactive species from fuel rich to oxygen rich regions in non-premixed reaction zones. The combination of these two criteria determines ignition, extinction, and propagation speed for both premixed and non-premixed flames. Finally, the constraints of average molecular weight, MW_{ave}, H/C ratio, and aromatic composition are important to achieving energy density, heat of reaction, flame temperature, stoichiometric fuel/air ratio, and local air/fuel stoichiometric location, and NO_x (maximum flame temperature) in diffusion flames, and in-combustor reactivity and sooting.

In the next section, we discuss in more detail the methods that we have utilized to determine each of the (fuel) combustion property targets introduced above (**Fig. 2.2**).

Summary of Research Findings

2.3. Combustion Property Targets

The new strategy that we developed for specifying the mixture of surrogate components that would best replicate the global combustion properties of the real fuel rests on matching the *combustion property targets (H/C, DCN, TSI, and MW_{ave}) of the mixture to those of the specific real fuel of interest* [21]. Through this approach, our intent was to establish a correlation of chemical structure of the surrogate mixture that would reproduce the significant gas turbine combustion kinetic related phenomena that numerical models must reproduce (flame burning velocity and extinction, ignition delay etc.). Some but not all of the elements of our approach had been employed and discussed in previous efforts in the literature, for example the works of Violi et al. [1], Ranzi [37], and Colket et al. [38]. Our efforts also centered on defining a set of simple, direct experimental methods that would require only small amounts of the specific fuel of interest in order to determine the property target values that we wished to replicate. Moreover,

we concentrated on methods that could be equally applied to real fuel samples, surrogate components and their mixtures. It should be note as well that from the beginning we envisioned the likelihood that additional surrogate components and combustion property targets might become of interest in the future, especially in light of interests in including physical properties and in expanding the specific combustion behaviors to be considered in the future. The concepts that we have considered allow for this flexibility.

2.3.1. Hydrogen/Carbon Molar Ratio, H/C

The H/C molar ratio defines the ratio of carbon dioxide to water formed from combustion and along with the molecular weight of the fuel essentially determines the enthalpy of reaction and the adiabatic flame temperature which in turn strongly influence flame velocity as well as other flame phenomena. Though a global parameter, the hydrogen/carbon ratio of a real fuel also portrays the diversity of molecular structure and defines the local air fuel stoichiometry in mixing-limited combustion situations [39]. The overall radical population in a reacting flow is also strongly dependent on H/C. The alkane components of aviation fuel have H/C of 2.1-2.2. Aromatic components are much lower, ranging from 1-1.4 for benzene, toluene, xylene, trimethyl benzene, *n*-propyl and *n*-butyl benzene. H/C values for reported jet aviation fuels lie in the range of 1.8-2, while the non-aromatic synthetic fuels occupy the alkane range of 2.1-2.2.

Sample Description (Wright Patterson AFB)	IQT DCN	ASTM D613	ASTM D976
AFB-POSF-3602-Jet A	38.35		
AFB-POSF-3638-Jet A	44.74		
AFB-POSF-3684-JP-8	43.14		
AFB-POSF-3773-JP-8	47.79		
AFB-POSF-4177-JP-8	40.15		
AFB-POSF-4658-Jet"A"Blend	45.27		
AFB-POSF-4765 coal-based Jet A	32.95		
AFB-POSF-4795/JP-10	18.64		
AFB-POS5140-TS-1 Jet fuel	40.81		
POSF 4751 JP-8	44.43	45.2	
POSF 5018 S-8 Syntroleum GTL F-T	59.67	58.4	68
50/50 blend 4751/5018	51.60	52.9	
POSF 5172 Shell SPK GTL F-T	59.08	57.4	57
50/50 blend 4751/5172	50.75	51.1	
Sasol IPK (POSF 5642)	31.28		51

Figure 2.7. Comparison of ASTM D-6890 (Derived Cetane Number, DCN), (ASTM D-613Cetane number, CN) and ASTM D-976 Cetane Index (CI) for various real petroleum–derived, alternative and blended gas turbine fuel samples. The SASOL "IPK" sample is a fully isomerized paraffinic kerosene with no aromatic content. (Data Courtesy of T. Edwards, AFRL).

We chose to directly determine the H/C ratio of the fuel experimentally by utilizing an elemental analysis approach ASTM D-5291 [40].

2.3.2. Derived Cetane Number, DCN

The DCN of is experimentally determined from an absolute ignition delay measurement for a fuel sample produced using a particular experimental procedure. This absolute ignition delay is then converted to a DCN value through a correlation derived from similarly measured values for reference materials having known cetane numbers (CN). [41-43]. DCN is a convenient manner for

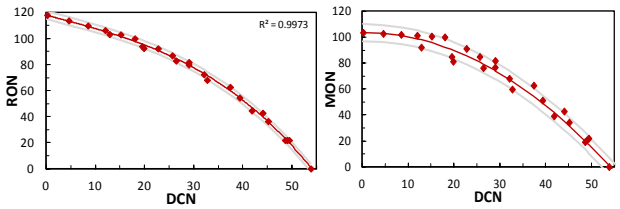

Figure 2.8. Research Octane (RON)-DCN and Motored Octane (MON)-DCN correlations based on IQT *experimental data* for ternary (n-heptane/iso-octane/toluene) reference gasoline mixtures. Gray bands are ±3.5 and ±6.5 units from best fit polynomials, respectively. From [46].

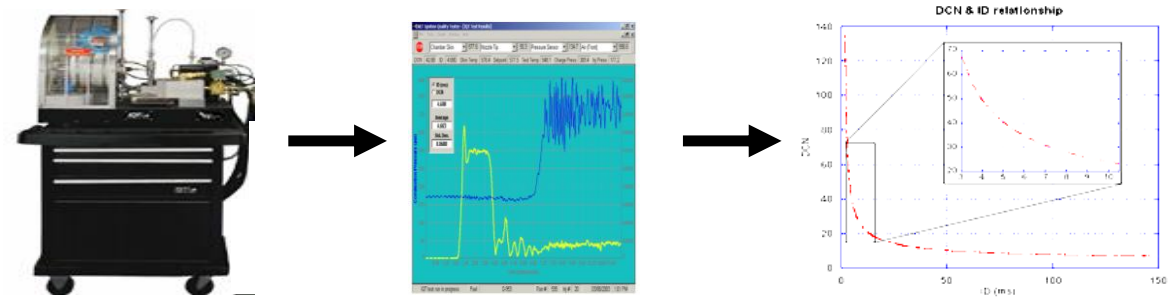

Figure 2.9. Experimental Determination of Derived Cetane Number (DCN). a) Ignition Quality Tester (AET, Inc); b) Time history of fuel injector needle opening and closing (yellow), and pressure within the combustion chamber; c) conversion of absolute ignition delay determination to a DCN.

reporting absolute ignition delay data for gas turbine fuels, as the ASTM D-6890 [43] method used in determining DCN sets forth a well developed procedure for utilizing the experimental instrumentation and includes clear uncertainty criteria.

DCN is to be differentiated from the cetane number (CN) itself as determined using a CFR engine [44] or the Cetane Index [45], which results from a correlation of Cetane Number with other parameters based upon other data typically reported as part of gas turbine fuel specifications. Cetane Index can be unreliable in terms of reflecting ignition behavior in comparison to CN or DCN as noted in **Figure 2.7**. Cetane number and DCN may also differ slightly for materials with 30<CN<65. One must take care in retrieving cetane for pure components from the literature, as all three method results may be indiscriminately reported collectively in literature results [17, 18].

The use of DCN in the MURI is strictly a means of representing the relative global reactivity amongst the fuels, components, and component mixtures tested, and in no way suggests that the determined ignition delays are directly relevant to gas turbine combustion environments. Neither is the global measurement used to differentiate among the individual contributions of the low, intermediate, and high temperature chemical kinetic regimes to the measurement. The technique is versatile in relating observables to the chemical kinetic properties of mixtures that vary in distinct functional group distributions represented by the fuel that is tested. Exemplar of this fact, we recently applied the same approach to derive correlations for Octane numbers with fuel properties as well [46]. We found that that Research Octane (RON) and Motored Octane (MON) numbers of ternary gasoline reference mixtures of n-heptane, iso-octane, and toluene, can be accurately correlated against absolute ignition delays (reported as DCN measurements) for these mixtures (**Figure 2.8**).

No a attempt was made to separate the individual contributions from fuel physical properties and fuel chemical kinetic properties to the measured ignition delays, though for the real fuels, the surrogate components, and their mixtures considered in this work all have very similar viscosity, surface tension, and vapor pressure characteristics. The DCN measurements are made under a fixed liquid fuel volume injection referenced to n-heptane, consequently any notion of fuel to air

equivalence ratio is a variable parameter implicit within the ignition delay/derived cetane number test itself.

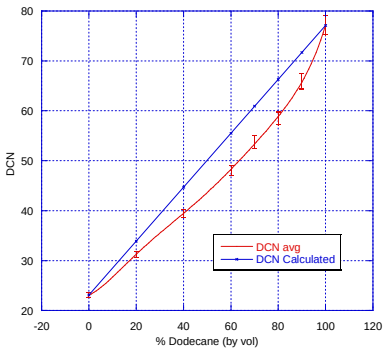

Figure 2.10. Measured and calculated DCN of methylcyclohexane/n-dodecane mixtures as a function of liquid volume fraction of n-dodecane. Calculated values are based upon the linear proportioning of the pure component DCN's.

The DCN's reported and utilized in this MURI were determined using an Ignition Quality Testing (IQT) apparatus [41, 42] and the associated ASTM D-6890 [43] procedure for determination of autoignition characteristics of diesel fuels (**Figure 2.9**). The procedure requires only about 50 ml of sample and about 20 minutes per sample test to perform. The IQT operating procedure determines an experimental ignition delay of a fuel pulse spray injection into a pressurized (22.1 atm) and heated (833K) constant volume chamber filled with dry air (reference material). Once the instrument parameters have been stabilized through a warm-up procedure, fifteen individual sample injection cycles are performed to produce the reference test state, followed by 32 individual sample injection cycles to statistically determine the specific sample absolute ignition delay. The ignition delay on each cycle is determined as the time between the injector closing time and the rise time of pressure within the chamber. The absolute ignition delay values are transformed to DCN's by calibrating the instrument performance using reference fuels, and through a pre-determined correlation of absolute ignition delay against DCN. Values reported as part of this work were determined by averaging at least three individual fuel sample tests (96 individual injections total). We found the three or more test values lay within a standard deviation of ± 0.6 DCNs of one another.

Any real fuel, surrogate component, or surrogate component mixture can be tested to yield a DCN value the same identical manner described above. It has been common in the literature to assume that the DCN of a mixture of components is linearly related to the DCN's of the individual species and the individual component liquid volume fraction. **Figure 2.10** displays the DCN's found experimentally and those predicted by linear interpolation of pure component values for methylcyclohexane/n-dodecane mixtures as a function of the liquid volume fraction of n-dodecane. To be noted is that experimentally, there is a near-linear dependence of DCN on liquid volume fractions of n-dodecane between 30 and 60%, which is inconsistent with extrapolation of the pure component DCN values. We found similar difficulties with mixtures containing iso-octane. To avoid these problems, we did not use pure component values to determine DCN's for mixtures of surrogate components.

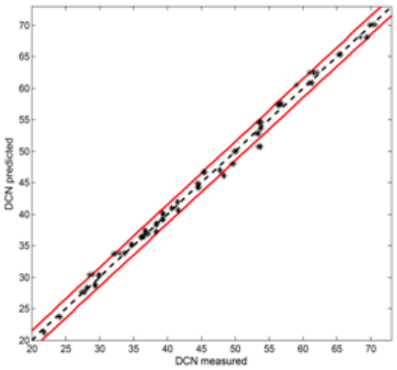

Figure 2.11. Comparison of predicted and measured DCN values for 124 individual mixtures of n-dodecane, iso-octane, n-propyl benzene, and 1,3,5 trimethyl benzene (2nd generation surrogate fuel component mixtures).

Instead, we experimentally developed an extreme vertex multidimensional map for all mixtures of the chosen surrogate components that would yield a DCN for the mixture of between 30 and 70. DCN correlations with surrogate mixture compositions

were developed for two different sets of components and their mixtures, 1st generation surrogate map for mixtures of n-decane, iso-octane, and toluene [47]; and a 2nd generation surrogate map for mixtures of n-dodecane, iso-octane, n-propyl benzene, and 1,3,5 trimethyl benzene [48]. The respective data utilized for determining surrogate mixtures in the references above appear as supplementary data in each reference. The DCN's of these two surrogate component mixtures are represented by the following two equations.

DCN(1st Gen) = 67.27*Dec + 17.12*Iso+11.32*tol + 30.89*dec*iso+7.54*dec*tol - 22.15*dec*iso*(dec - iso) + 15.15*dec*tol*(dec - tol) - 9.59*dec*tol*(dec - tol)^2.(one sigma uncertainty = +/- 0.3)

DCN(2nd Gen) = 78.09*dod + 17.28*iso + 2.89*TMB + 23.38*nPB + 38.98*dod*iso + 22.53*dod*TMB - 36.75*dod*iso*(dod - iso) + 32.86*dod*nPB*(dod - nPB) + 32.01*dod*iso*(dod - iso)^2 - 40.52*dod*nPB(dod - nPB)^2 (one sigma uncertainty = +/- 1.2)

Since the completion of the MURI, the relationship for the 2nd generation function has been further refined with additional measurements. The new functional relationship for the 2nd generation surrogate mixtures was derived by correlating 124 individual DCN determinations of various known mixtures and then tested for predictive ability against additional mixtures. The uncertainty in the new function predictions is +/- 0.93 DCN units over the entire range tested. **Figure 2.11** compares the predicted and measured values for the derived correlation. The new function produces slightly different compositions for the same DCN in comparison to the above relation, and the function will appear in future publications.

2.3.3. Threshold Sooting Index, TSI

The Threshold Sooting index is defined by Calcote and Manos [49] as;

$$TSI = a\left(\frac{Molecular\ weight}{Smoke\ point}\right) + b$$

where the smoke point is the maximum smoke free laminar diffusion flame height (*mm*) [50], molecular weight is in $g\ mol^{-1}$ and a ($mol\ mm\ g^{-1}$) and b (dimensionless) are experimental constants. The smoke point is determined from small scale experimental tests using a wick flame apparatus and ASTM D-1322 [51] procedures.

The TSI is a macro measure of the tendency of a fuel to form soot under diffusive/mixing limited conditions. The practical importance, (e.g. efficiency, pollutant formation) that a surrogate emulate the sooting tendency of a target real fuel is clear. In addition, it is logical that by constraint of this parameter, the surrogate fuel aromatic fraction ought to be similar to that of the target fuel, as TSI has been shown to be strongly dependent on aromatic component fraction [52]. As part of this MURI, Mensch et al. [53] (see section) developed a reference database for the TSI of the first and second generation surrogate components and verified the TSI linear mixture rule described by Gill and Olson [54] for their mixtures i.e.

$$TSI_{mix} = \sum_i x_i TSI_i$$

where x_i refers to the mole fraction of the i^{th} component in the mixture. Note that the determination of TSI for the real target fuel is conditional upon an accurate determination of the real fuel average molecular weight. The database presented in Mensch et al. [53] was used to compute the TSI of surrogate component mixtures studied in this MURI.

Finally, it should be noted that there has been much discussion recently of alternative correlation procedures TSI with height that eliminate consideration of molecular weight [55], or put forth alternative approaches such as Yield Soot Index (YSI) [56]. However, we support the use of TSI, both because the sooting height determination is part of the standard data collected for gas turbine fuel certification, and independent of the correlation issue, the molecular weight of the fuel remains as a separate important combustion property target of importance (see discussions below).

2.3.4. Average Fuel Molecular Weight, MW_{ave}

Gas phase fuel diffusive properties correlate strongly with molecular weight [57]. Thus, in order to emulate the diffusive properties of real aviation fuels in gas phase flame environments, a surrogate fuel must be of similar average molecular weight. The H/C ratio along with the molecular weight is strongly correlated with the average heat of combustion per mole, since for large hydrocarbons the numbers of moles of fuel species is small relative to the numbers of moles of oxidation product species. We will see later that the heat of combustion per mole is an important parameter in understanding diffusive extinction. Finally, the average molecular weight is also a parameter implicit in the determination of the TSI of molecular mixtures, and a determining factor in terms of volumetric air flow required for a specific combustion stoichiometry.

The methods presently found in the literature for determining the average molecular weight of hydrocarbon mixtures deduce this quantity using empirical correlations of more easily measurable parameters such as mixture boiling point and fluid viscosity [58-60]. These methods have typical uncertainties of as much as 20 units for the average molecular weight of jet fuels.

Early in our research, we determined average molecular weight of using the elemental H/C data and combustion observations of the amount of CO_2 formed in lean oxidation in the variable pressure flow reactor. We estimated the uncertainty in the reported values to be +/- 15 units, as reported elsewhere.

Very late in the MURI project, we developed an improved method for providing average molecular weight of fuel samples in the future [61]. The method that we have submitted in a provisional disclosure requires only small amounts of sample and yields accurate average molecular weights for a molecular weight range that spans those typical of gasoline, jet fuel, and diesel materials (**Fig. 2.12**). The uncertainty associated with this experimental method is less than +/-1.5 units.

2.4. Procedures for Testing the Combustion Property Matching Concept

In order to compare surrogate mixture and real fuel combustion behaviors, we performed the following procedures. First, the real fuel sample was characterized by:

1. Determining its MW_{avg}
2. Determining the empirical formula for C_nH_m using CHN analysis data (ASTM D5291) & the determined MW_{avg}. This procedure also yielded the H/C molar ratio.
3. Determining DCN using Ignition Quality Testing (ASTM D6890).
4. Determining the TSI from smoke point measurement (ASTM D1322) and the determined MW_{avg}.

As described earlier, an extreme vertex map of DCN as a function of the mixture composition was developed experimentally for predicting 30<DCN<70 for each chosen set of surrogate components (see below). For each composition, a mixture TSI can be produced using the database of Mensch et al [53], and analytical expressions are also available to produce values of H/C and MW_{ave}. A particular composition of surrogate components that reproduces a specific DCN value therefore also leads to values for H/C, MW_{ave}, and TSI that can be computed through these analytical expressions. While each surrogate composition has a defined H/C, MW_{ave}, and TSI, a specific DCN can be obtained with a number of *different* surrogate compositions.

To obtain the optimum global mixture composition, we produced a mapped surface for DCN as a function of surrogate composition as described above. We then determined that composition which best reproduced all of the (equally weighted) real fuel combustion property target values. The optimal solution was obtained by generating a probability function that depends on each property target functional relationship The first derivatives of the probability function with respect to each surrogate component were derived and a normalized function composed of the sum of the squares of the first derivatives was minimized to obtain the global optimal composition. Two approaches were investigated to perform this optimization. An automated minitab approach documented in [47], and more recently an in-house developed Matlab approach were both found to yield the same global solutions.

In each case, however, additional local optima on the probability surface were found that yield different compositions (in comparison to the global optimal solution) that still reproduced essentially the same four property targets. Independent of the choice of the error function values used in performing the optimization in matching the property targets of the real fuel, the fact that there are multiple solutions is indicative of the under-constrained nature of the optimization process.

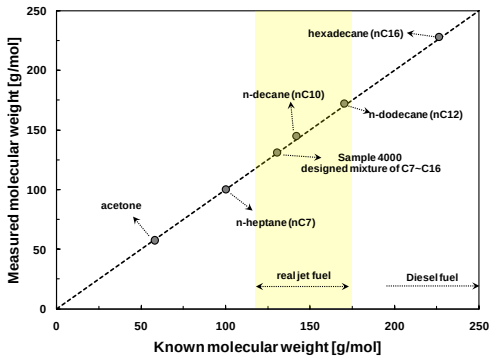

Figure 2.12. Comparison of measured and known molecular weights of pure hydrocarbons and their mMixtures [61].

Two base sets of surrogate components were utilized in our research. "First generation" surrogate mixtures [47] were composed of n-decane, iso-octane, and toluene. Mixtures of these components are constrained to a considerably

lower molecular weight range that does not encompass the average of real jet fuels. Moreover, we also found that mixtures that met the H/C and DCN targets typically would not also meet the TSI target. Emulating the average molecular weight and TSI were sacrificed in the initial concept demonstrations using 1st generation surrogate mixtures in order to have more robust kinetic modeling tools to interpret results. "Second generation" surrogate mixtures [48] were composed of n-dodecane, iso-octane, 135TmB, and nPB. It was found that mixtures of these components produced property targets that encompassed most of those found for real gas turbine fuels. The extreme vertex maps for the 1st and 2nd generation surrogates are found in the supplementary materials associated with [47] and [48], respectively.

The fully prevaporized behaviors of real fuel samples and the matching surrogate mixture were then compared experimentally in a wide range of fundamental fully prevaporized configurations, inclusive of reflected shock ignition, rapid compression machine ignition, variable pressure flow reactor reactivity, single pulse shock tube speciation, laminar premixed flames (flame speed, strained ignition, strained extinction) and opposed flow, laminar diffusion flame extinction. Reflected shock ignition data were obtained through collaborations with Prof. M.A. Oehlschlaeger of Rensselaer Polytechnic Institute. Tests were also conducted at PSU in a wick burner experiment to compare the sooting behavior of 2nd generation surrogate mixtures and real fuels under fuel/air conditions. The range of energy densities studies in this work span very dilute mixture studies in the single pulse shock tube and flow reactor studies to fuel/air conditions in other experiments. Comparisons are only summarized below with detailed discussions appearing in [47, 48].

2.5. Comparison of Pure Component Surrogate Mixtures with Fully Prevaporized Real Fuels Combustion Behaviors of Real Fuels

2.5.1. Real Fuels Used in Experimental Comparisons with Surrogate Component Mixtures

Two real gas turbine fuels were utilized in fundamentally testing of the surrogate mixture formulation concepts by comparing fundamental combustion behaviors: 1) a Jet A fuel reference mixture, (Jet A POSF 4658) prepared by Wright Patterson Air Force Research Laboratory, and 2) "S-8", a synthetic paraffinic jet fuel. POSF 4658 was produced by blending five different Jet A-1 fuels from flight lines regions distributed over the United States to produce a fuel composition that closely replicated the World Wide average found at that time. Syntroleum Inc produced S-8 materials from natural gas in several lots for the Air Force, POSF 4734 being the lot investigated in our work. Both of these particular fuels have been the subject of many laboratory studies. The molecular class distributions of these fuels have been determined using two ASTM methods, as well as by gas chromatographic/mass spectrometric analyses. Bruno and co-workers [64] report data for the molecular class distributions for the two fuels shown in **Fig. 2.13** using the mass spectrometric classification method ASTM D2789. Schafer and Edwards [67] also recently reported

Fluid	Paraffins	Monocyclo-paraffins	Dicyclo-paraffins	Alkyl-aromatics	Indanes and tetralins	Naphth-alenes
	Vol %	Vol %	Vol %	Vol %	Vol %	Vol %
Jet-A-4658	46.5	22.5	5.4	18.4	4.5	2.4
S-8-4734	80.0	17.3	0.9	0.1	0	1.9

Figure 2.13. Class composition distributions for Jet A POSF 4658 and S-8 POSF 4734, as determined using ASTM D2789 [64]

a slightly modified class distribution for POSF 4658 (**Fig. 2.14**) than those originally published [68], due to recent modifications in the method used by them (ASTM D 2425 [69])

	World Survey Average	Composite Jet A Blend (POSF-4658)
D2425 (volume %)		
Paraffins (normal + iso)	54	52
Cycloparaffins	26	28
Alkylbenzenes	14	12
Indans and Tetralins	4.8	4.9
Naphthalene	<0.3	<0.3
Naphthalenes	1.6	1.3

Figure 2.14. Class Distribution of POSF 4658 determined using ASTM D-2425 compared with the World Survey average values [68]

In addition, Bruno et al [64] also performed separate gas chromatograph/mass spectrometric analyses of both fuels to determine the most prevalent organic species found in each. The reported data are presented in terms of percent of total (uncalibrated) detector area responses for each species identified, with perhaps as much as 40% or more of the species contained in the sample being unidentified. While the class distributions of the two ASTM methods determined for POSF 4658 are quite similar, the distribution determined from these separate analyses (**Fig. 2.15**) differs substantially.

Figure 2.15. The molecular class distribution of the Jet A POSF 4658 fuel from gas chromatographic/mass spectrographic detailed analyses reported in [64]. The summary figure

As noted earlier, the molecular class distributions of real fuels have frequently been utilized to define the mixture of surrogate component classes that are to be used in emulating a real fuel. Uncertainties in these values exist not only as based upon the ASTM method used for defining the classifications, but these estimates are equally difficult to improve upon by speciated analyses, due to the inherent analytical difficulties associated in determining all of the multi-species composing the real fuel. *The MURI approach to determining surrogate composition described above does not depend on accurately quantifying the molecular class distribution, only in knowing the types of classed present in the sample.*

2.5.2. Comparison of 1st and 2nd Generation Surrogates with Jet A POSF 4658

Two papers can be found in the literature that detail comparisons of 1st and 2nd generation surrogate formulations for POSF 4658 against Jet A POSF 4658 combustion behavior over a wide range of conditions and experimental venues.

Figure 2.16 presents the Jet A POSF 4658 property targets that we determined and compares them against the global optimal target values for the global best fit 1st and 2nd generation surrogate mixtures. Though the data are report in molar units, the surrogate mixtures were prepared on a mass basis. The Jet A POSF 4658 molecular formula was determined to be $C_{10.17}H_{19.91}$. To demonstrate the accuracy of the vertex map solution for optimizing the 1st generation mixture, the measured DCN was found to be 47.4± 0.3, in good agreement with the predicted value shown in Fig. 16. Note that it is not possible for the 1st generation surrogate cannot match the molecular weight of the Jet A POSF 4658 fuel or simultaneously match the TSI and H/C parameters. Thus the 1st generation surrogate was tested against the real fuel in

	Mole Fraction				DCN	H/C	MW / g mol^{-1}	TSI
Target Real Fuel	Jet Aviation Fuel, POSF 4658				(47.1 ± 0.3)	(1.96)	(142.1 ± 20)	(21.4)
1st Generation Surrogate Fuel	*n*-decane	*iso*-octane	toluene		47.1 (47.4 ± 0.4)	2.01	120.7	14.1
	0.427	0.330	0.243					
2nd Generation Surrogate Fuel	*n*-dodecane	*iso*-octane	135TmB	nPB	47.1 (48.5 ± 0.4)	1.95	138.7	20.4 (21.4 ± 0.6)
	0.404	0.295	0.073	0.228				

Figure 2.16. Combustion Property Targets for Jet A POSF 4658 and Global Optimal Compositions and Targets for 1st and 2nd generation Surrogate Mixtures [47, 48] Values in parentheses are experimental determinations. Other values are predictions.

experiments that did not compare sooting behavior. In formulation, the matching the H/C ratio was given preference over TSI. The deficiency in diffusion limited strained extinction caused by the miss-match of molecular weight is discussed in more detail below. Also note that only later in the research did we achieve methods to determine the average molecular weight of real fuel samples with substantially improved uncertainty.

In comparison, the 2nd generation global optimized surrogate mixture more appropriately reflect *all* of the combustion property targets of the real Jet A POSF 4658 fuel. Note that all of the prediction property targets for the 2nd generation composition shown in **Fig 16** are in good agreement with experimental determinations.

Figures 2.17-2.19 compare the behavior of 1st and 2nd generation POSF 4658 surrogate mixture combustion behaviors with that of Jet A POSF 4658 over a wide range of experimental venues, involving a significant span in pressures, temperatures, equivalence ratios, and energy densities. Note that all of these comparisons result from a substantial collaboration amongst not only all of the MURI participating laboratories, but also collaborations involving Prof. M.A. Oehlschlaeger's group at RPI. All of these comparisons are discussed in detail in references [48] and [49], and only a few summary points are offered here.

In **Figure 2.17**, we note that the agreement of the 1st and 2nd POSF 4658 surrogate mixture data are essentially co-incidental with one another. Both sets also agree with that for Jet A POSF

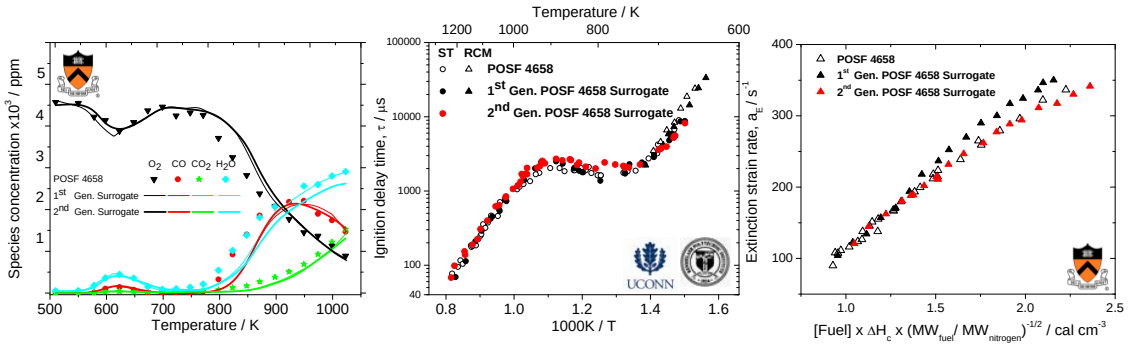

Flow reactor oxidation data for conditions of 12.5 atm, 0.3% carbon, φ= 1.0 and *t* =1.8s, for POSF 4658, 1st generation POSF 4658 and 2nd generation POSF 4658 surrogate.

Ignition delay times, φ= 1.0 in air at ~20 atm for POSF 4658, 1st generation POSF 4658 surrogate and 2nd generation POSF 4658.

Strain rates of extinction for counter flow diffusion flames at 1 atm, for 1st and 2nd generation POSF 4658 surrogate fuels v. 4658 surrogate fuels v. Transport Weighted Enthalpy (*TWE) for each fuel.

a) b) c)

Figure 2.17. Comparison of the Reaction Behaviors of 1st and 2nd Generation POSF 4658 Surrogate Mixtures with Those of Jet A POSF 4658 for the Noted Experimental Configurations and Conditions [48].

4658 within the uncertainties of the experiments themselves, except for the following issues. In the VPFR comparison in **Fig 2.17a**, while the low temperature, turnover temperature (675 K), negative temperature, and hot ignition characteristics are all essentially the same, the surrogate reactivity data appear to autothermally accelerate with reaction temperature after hot ignition (~775 K) more slowly than the real fuel. There is a similar discrepancy in results in **Fig. 2.17b** at conditions where the transition across the hot ignition condition to higher temperature behavior occurs.

However the consistency of the overall ignition delays determined in reflected shock and rapid compression machine studies is noteworthy. In **Fig. 2.17c**, the extinction behavior of the 1st generation surrogate is not consistent with that for the real fuel or the 2nd generation surrogate mixture. This inconsistency is a result of the fact that the 1st generation surrogate has a much lower average molecular weight than the 2nd generation surrogate and the real fuel. Note that the extinction strain rate is plotted in **Fig. 2.17c** as a function of the "Transport Weighted Enthalpy", a quantitative scaling analysis developed to explain the roles of molecular diffusive, molecular energy density, and chemical kinetic properties on the extinction strain rate [70]. The efforts described in [70] showed that the extinction strain rate, a_E, under diffusive counter-flow conditions can be written as $a_E = 230\ x\ R_i\ x\ [Fuel]\ x\ \Delta H_c\ x\ \left(\frac{MW_{fuel}}{MW_{Ar}}\right)^{-1/2} - 54$, where R_i is

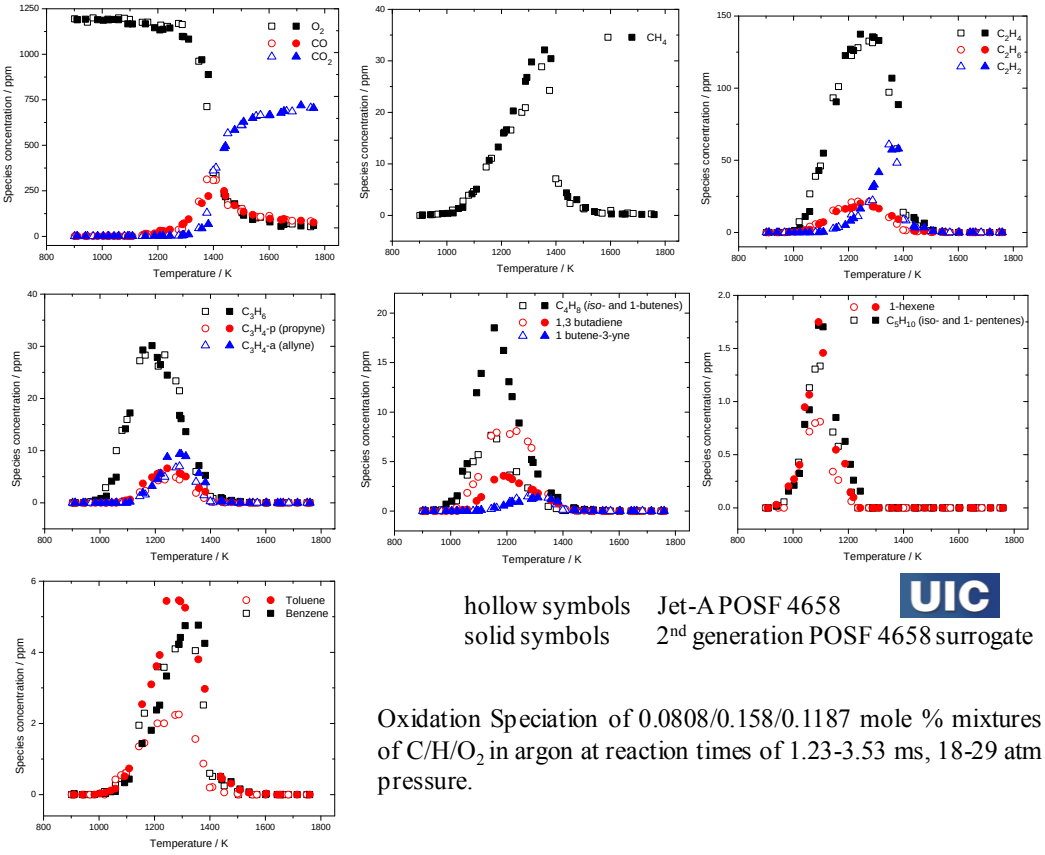

Figure 2.18. Comparison of the Reaction Behavior of 2nd Generation POSF 4658 Surrogate Mixtures with that of Jet A POSF 4658 Single Pulse Shock Tube Species Distributions at the Prescribed Reaction Temperatures. [48].

defined as the "radical index". R_i is a measure of the chemical potential of the fuel in question under diffusion flame conditions. The radical index of different fuels is expressed by comparison to normal alkane fueled flames at the same Damkohler number and TWE. All normal alkanes are defined to have a radical index value of unity.

The TWE includes the average molecular weight of the fuel and the heat of combustion per mole as important parameters. In the case of the 1st generation surrogate results shown in **Fig 2.17 c**, the average molecular weight of the fuel and the surrogate are not closely matched and so the data do not fall on the same correlated function. The radical index is an indication of high temperature reactive character in diffusion flames and is further discussed in [70] and in the Princeton2 discussions section below.

Figure 2.18 compares the single pulse species evolution for the 2nd generation POSF 4658 surrogate and Jet A POSF 4658 real fuel at comparable reaction residence time for different initial reaction temperatures [48].

To be noted here is the close agreement of surrogate and real fuel for those species that are the least reactive in the system, included alkenes, and alkyl aromatic ring species, with the exception of the butenes. The disparity in the butenes is to be expected as these species are directly resultant of oxidation of iso-octane in the surrogate, a species not present in the real fuel.

Figure 2.19 compares the laminar premixed flame behaviors of 1st and 2nd generation POSF 4658 surrogates against those of the Jet A POSF 4658 real fuel [48]. The comparisons show very

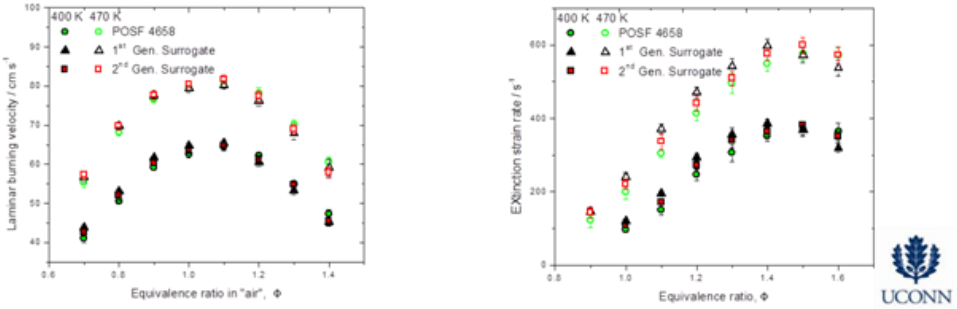

Laminar burning velocities at 1 atm: Jet-A POSF 4658 (circles), 1st gen (triangles) and 2nd gen (squares) POSF 4658 surrogates.

Extinction strain rates for premixed Fuel/O_2/N_2 at 1 atm: Jet-A POSF 4658 (circles), 1st gen (triangles) and 2nd gen (squares) POSF 4658 surrogates. $N_2/(N_2+O_2)$ =0.86.

Figure 2.19. Premixed laminar flame properties of Jet-A POSF 4658, 1st and 2nd gen POSF 4658 surrogate s at T_u = 400 K. (solid symbols) and 470 K (hollow symbols) in "Air": $N_2/(N_2+O_2)$ =0.86. [48]

good agreement on premixed flame phenomena amongst all three sets of data.

Finally, The sooting characteristics of Jet A POSF 4658 and the 2nd generation surrogate have been compared in a modified wick flame burner [48], **Figure 2.20**. No comparisons were made for sooting behavior for the 1st generation surrogate mixtures as its TSI is disparate with the Jet A POSF 4658 fuel value.

The smoke points of Jet-A POSF 4658 and the 2nd generation surrogate measured on the ASTM smoke point lamp (22.1 mm and 22.5 mm respectively) match within the experimental uncertainty of ±0.5 mm [53]. These values were slightly different on the modified wick burner (21 mm and 23 mm, respectively), and so when comparing the radial soot profiles, a non-dimensional axial co-ordinate, defined as the ratio of the measurement location to smoke point height of the fuel on the wick burner, was applied. The radial soot profiles presented in Fig. 20 are near the location of maximum soot volume fraction in these flames. Radial soot profiles for the 2nd generation surrogate fuel are shown at two non-dimensional heights that bracket the axial value of z for the real fuel data. The peak volume fractions all agree very well in terms of location and magnitude, and agreement along the centerline are within the uncertainty of the soot volume fraction measurements.

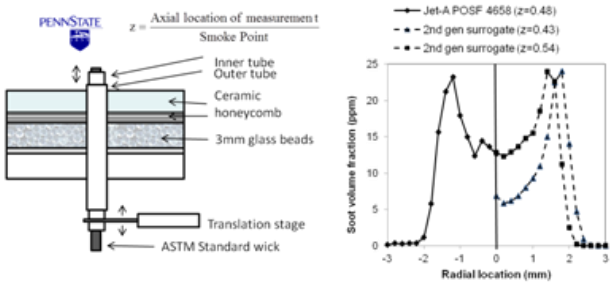

Figure 2.20. Soot volume fraction comparisons of Jet A POSF 4658 and Jet A POSF 4658 2nd Generation Surrogate Mixture in a Modified Wick Flame Burner [48].

In summary, the global combustion behaviors of the real Jet A POSF 4658 fuel and the 1st and second generation surrogate mixtures develop to match the real fuel combustion property targets agree very well across a wide range of experimental venues and parameters. This is a first demonstration to our knowledge of *a priori* comparisons of different surrogate component mixture comparisons with the same real fuel, both produced by optimizing the mixtures that best matched combustion property targets determined for the real fuel sample. As noted earlier, other surrogate mixtures of these two sets of components exist that also reproduce the property targets of the real fuel nearly as well as those demonstrated here.

Further insights as to why all of these surrogate mixtures behave similarly can be gained by comparing the "distinct thermochemical groups" that are present in each surrogate. Motivated by the success of analyses [71-77] that show correlative relationships of observables such as cetane number, octane number, and sooting with chemical group distributions, we hypothesized that a chemical group additivity analyses [78] of these 1st and 2nd generation surrogate fuels might elucidate their similar behavior. We deconstructed the surrogate mixtures into mass distributions of methyl (CH_3), methylene (CH_2), and benzyl-type ($C_6H_3X_2CH_2$) molecular groups. The presence of these moieties fundamentally define the rate constants of many of the important elementary reactions that control the global rate of fuel oxidation. As an example, **Fig. 2.21** demonstrates this group deconstruction for n-propyl benzene (nPB). Similarly, the deconstruction of n-dodecane yields two methyl groups and ten methylene groups, while 135 trimethyl benzene (135TmB) is yields two methyl groups and one benzyl-type group. Other molecular group arrangements could have been chosen, but from pure component studies [79-81], these functionalities most clearly represent the relationship between molecular structure and chemical kinetics with

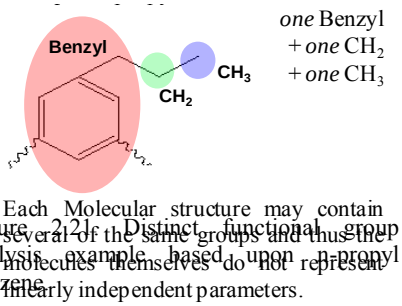

Figure 2.21. Distinct functional group analysis example based upon n-propyl benzene.

minimal ambiguity. Radical species with the radical site located at the *alpha* position to an aromatic ring are uniquely stable reaction intermediates as they essentially rely on bimolecular reactions for their consumption [80]. All alkyl aromatics have a propensity to form benzyl-type radicals as intermediate oxidation species, the actual identity of the radical species being of secondary relevance to the presence of the ring structure. The methyl and methylene groups are the primary constituents of normal and isomerized alkanes. The number of methylene groups present in a molecule defines the n-alkyl chain length. In so doing, the propensity for a radical to undergo the lowest activation energy alkyl peroxy radical isomerization, leading to low temperature chain branching is represented. Similarly at high temperatures, the yield of the key high temperature alkyl radical beta-scission intermediate, ethylene, is reasonably represented by this fundamental metric. The number of methyl groups present in a molecule is directly related to the degree of branchedness of the alkyl chain. The ratio of methyl to methylene will strongly influence the ratio to which methyl or ethyl radicals (the latter leading to the production of radical chain branching hydrogen atoms) are produced. Therefore the ratio in which these molecular groups are present in a fuel is fundamentally related to the composition of the radical pool produced. Finally, one might speculate that methylated alkanes (aka strongly branched alkanes) would even more CH and/or C groups than iso-octane. For the iso-octane component, the number of these groups relative to CH_2 or CH_3 groups is small and this is likely to remain the case for complicated real fuels, where the molecular diversity typically large.

Figure 2.22 shows the results of this molecular group analysis for the 1st generation surrogate, and several suggested 2nd generation surrogate candidates, including the one discussed in more detail above. A mass-basis comparison is chosen for to compensate for differences in average molecular weight amongst the various surrogate mixtures. Since, CH groups and quaternary C groups iso-octane as well as the H atoms associated with the benzyl type radicals are not considered, the analyses account for only ~93-94% of the mass contained within the various surrogate mixtures. The striking result is that despite the different component selections as well as the different mixture fractions for the 2nd generation candidates, all are composed of very similar building block molecular functional distributions, suggesting the existence of a universal molecular functional distribution. **Figure 2.22** also summarizes that the radical indices Ri, which is an entirely different metric calculated for the respective surrogate compositions, all fall within a very narrow range of 0.72-0.80.

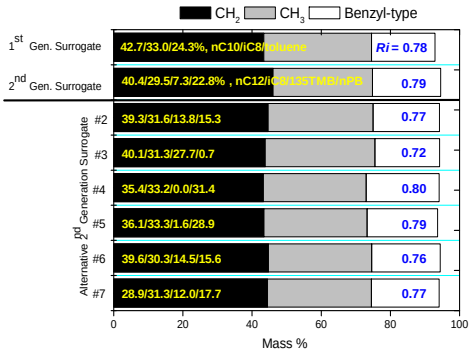

Figure 2.22. Molecular group mass contributions of 1st generation global, 2nd generation global, and 2nd generation alternative POSF 4658 surrogate fuels. Figures in yellow are the molar fractions of the respective surrogate components within each mixture.

Thus, it is apparent that the combustion property targets viewed in the context of a distinct chemical functionality concept actually serve as descriptors for a quantitative chemical structure-chemical property relationship [72] for complex combustion kinetic phenomena. Structurally oriented lumping processes [82, 83] have been used in the chemical refining industry for some time, and these approaches combined with nuclear magnetic resonance analyses of hydrocarbon structures can develop similar analyses from the atomic scale such as recently attempted by Zhang et al. [84] for modeling sooting processes and applied by Mueller and co-workers [85] for formulating diesel fuel surrogates. These techniques

relate to the present work, which in deference has through its analyses begun to order the relative importance of distinct functional groups in controlling global combustion kinetic phenomena. While other groupings may be important to these relationships, for the process of constructing relevant surrogate mixtures for gas turbine fuels, the present groupings appear to be significant to first order.

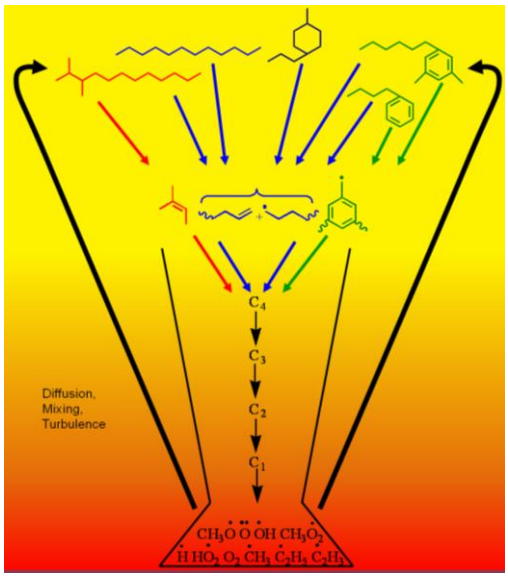

Figure 2.23. Schematic diagram of real fuel oxidation and its relationship to distinct chemical functionality.

Figure 2.23 summarizes the present findings schematically and emphasizes that emulating the detailed molecular composition of a real fuel relates to the present interpretation through the mass distribution of distinct functional groups that are represented by the particular composition. These groups are relevant because their kinetic interactions determine the small active radical pool characteristics of the overall reaction processes that control its global combustion behavior. Molecular structure correlations can yield the distinct chemical functional information for a real fuel if chemical composition is known (or perhaps from NMR spectral analysis) *But, it appears that defining the selected experimental (fuel) combustion property targets used here provide sufficient constraints with much less analytical or interpretive efforts. In fact, there is considerable flexibility offered by relaxing the criteria of having to select a particular molecular structure to represent each of those found in the real fuel.*

At present, it appears that emulating the global combustion behavior of Jet A POSF 4658 rather well does not require consideration of cyclo-alkanes. Though information on the cyclo-alkane content of this fuel is not well determined, we have addressed this question through modeling as well as experimental exercises. We modified the 1st generation surrogate composition to include

Cyclohexane or methylcyclohexane (MCH) along with n-decane, iso-octane, and toluene as components. We performed sufficient experimental studies to determine the surrogate mixtures that continue to replicate H/C and DCN combustion property targets with TSI and MW_{ave} determined as a result of the matching condition. **Figure 2.24** reports the modified 1st generation mixture compositions and projected combustion property targets. The 1st generation kinetic model discussed in [47] was then further modified by including appropriate modeling sub-components from [36, 86] to include MCH as a surrogate modeling component. **Figure 2.25** displays flow reactor reactivity and reflected shock tube ignition delay numerical modeling

Mole Fraction					DCN	H/C	MW / g mol^{-1}	TSI
Jet-A POSF 4658					47.1	1.957	142.01	21.4
1st generation surrogate	*n*-decane	*iso*-octane	Toluene		47.1	2.01	120.7	14.1
	0.427	0.33	0.243					
1st generation surrogate + cylclohexane	*n*-decane	*iso*-octane	Toluene	Cylclohexane	46.8	1.99	117.9	11.1
	0.482	0.175	0.178	0.165				
1st generation surrogate + methyl cyclohexane	*n*-decane	*iso*-octane	Toluene	Methyl cyclohexane	47.8	1.98	118.2	11.2
	0.422	0.174	0.179	0.225				

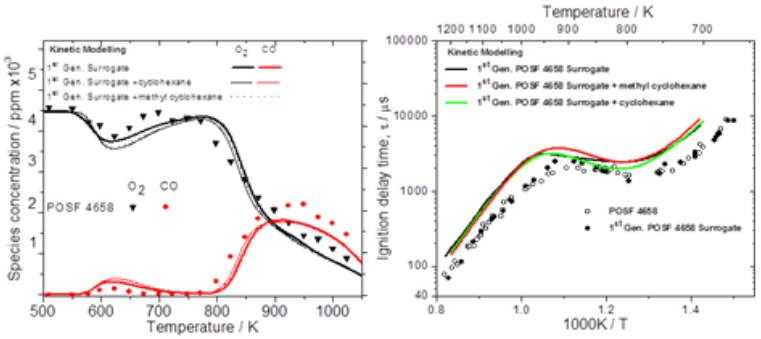

Figure 2.25. Flow reactor reactivity and reflected shock tube ignition delay of 1st generation surrogate *versus* modified 1st generation surrogate containing MCH. Model [36, 47, 86] computations (lines), experiments (symbols).

predictions for the first generation and modified 1st generation (methylcyclohexane mixtures shown in **Fig. 2.24** with the Jet A POSF 4658 experimental data with and each other. The modeling approaches are those discussed in [47]. While the modeling predictions differ from the experimental results, the results for the 1st generation and modified 1st generation mixtures are essentially the same.

We also performed a VPFR reactivity experiment with the 1st generation modified (MCH) mixture shown in **Fig. 2.24**. **Figure 2.26** compares the experimental data for the original 1st generation surrogate, the modified 1st generation surrogate and Jet A POSF4658 real fuel. Note that the inset in this figure compares the change in temperature at the sampling location relative to the initial reaction temperature, the difference being reflective of the energy release produced by the chemical reaction.

With the exception of the reactivity above the hot ignition temperature (~775K) the profiles are essentially unchanged by modifying the surrogate components used to match the real fuel property targets. The improved emulation in this region with the inclusion of MCH appears to be related to differences in heat release associated with the oxidation of the cyclo alkane decomposition products and an associated increase in auto-thermal acceleration of the reaction. Though inclusion of the cyclo alkyl functional group results in some changes in reactivity, these are relatively minor. However, should one conclude that cyclo alkyl groups should be included in the surrogate formulation, the concepts applied thus far can be extended to accommodate this (and any other) components as we have demonstrated by this test case.

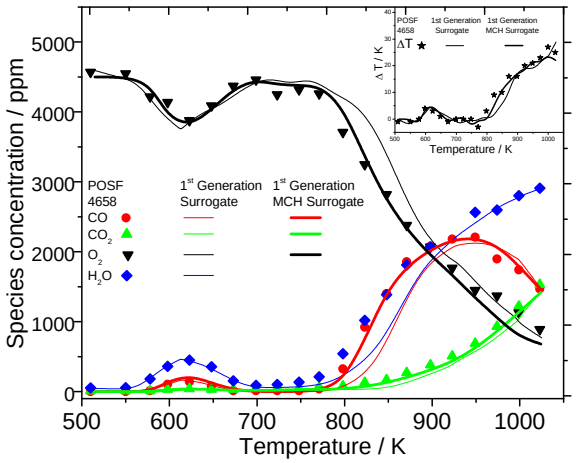

Figure 2.26. Variable Pressure Flow Reactor (VPFR) oxidation data as a function of initial reaction temperature for conditions of 12.5 atm, 0.3% carbon, φ= 1.0 and t =1.8s, for POSF-4658 (symbols), 1st generation surrogate (light lines), *and* 1st generation surrogate + methyl cyclohexane (solid lines). Inset: ΔT from heat release of the reaction.

2.5.3. Comparisons of 1st and 2nd Generation Surrogates with S-8 (POSF 4734)

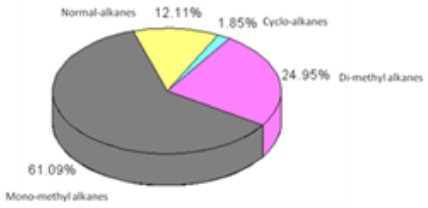

Figure 2.27. Molecular class composition of S-8 Synthetic paraffinic kerosene [87].

S-8 Synthetic produced by Syntroleum Inc was the initial synthetic fuel to be investigated by the Air Force. This synthetic liquid was produced from natural gas and is composed entirely of alkanes (no aromatics), mostly composed of mono- and di-methylated iso alkanes (**Fig. 2.27**). All materials were supplied from the same plant in Tulsa OK, in three different process runs, each of about 60-80 barrels. S-8 POSF 4734 was derived from the first process run in 2004. S-8 POSF 4820 was sampled from the second process run of 70-80 drums, while S-8 POSF 5018 was from the last purchase. This last purchase was actually flown supplying one engine on a B-52 as a 50/50 blend with (JP-8 POSF 4751). The DCN S-8 POSF 4734 was experimentally determined at Princeton to be 58.7 ± 0.7, and is to be compared with the DCN value for S-8 POSF 5018 of 59.67 determined by South West Research Institute and reported in Fig. 7 (well within the uncertainties of the two batch measurements). A more detailed description of what follows in this report has recently been published in the archival literature [87]. The achieved objectives of reported in the manuscript were:

- Reported detailed kinetic phenomena for a real non-aromatic synthetic fuel S-8 POSF 4734.
- Further tested the fundamental methodology for surrogate fuel formulation against any issues specific to synthetic aviation fuels over their petroleum derived counterparts.
- Provided an accurate and comprehensive data set for the testing and development of kinetic models for the oxidation of simple hydrocaron mixtures that have been experimentally validated as surrogate fuels for synthetic aviation fuels.
- Evaluated the state of the art in detailed model predictions using literature models against the new data and each other.

The purpose of the following brief discussion is principally to demonstrate the ability of the same surrogate concepts to yield *a priori* surrogate mixtures that replicate well the real fuel fully prevaporized combustion properties and to emphasize that fuels that are composed of mostly weakly branched alkanes can be very well emulated with surrogate mixtures that do not contain *any* weakly branched components. **Figure 2.28** reports the property targets for S-8 POSF 4734 along with those of a surrogate mixture of n-dodecane and iso-octane that closely match the H/C and DCN property targets of the real fuel, where the average molecular weight (MW) is estimated from the gas chromatographic-mass spectrometry analysis found in [66]. Note that the H/C value of 2.14-2.17 is consistent (within measurement uncertainties) with the values appearing in Naik et al. [88] and Gokulakrishnan et al. [89] as is the average molecular weight

Mole Fraction		DCN	H/C	MW / g mol^{-1}
S-8 POSF 4734		58.7±0.3	2.14-2.19	163.4±15
n-dodecane	*iso*-octane			
0.519	0.481	58.7	2.19	143.4

Figure 2.28. Property targets of S-8 POSF 4734 and a global two component surrogate composed of n-dodecane and iso-octane. [87]

determination [88]. The S-8 POSF 4734 surrogate was prepared on a mass basis and the measured DCN of 58.7 ±0.6, closely compares with the value computed from the 2nd generation surrogate extreme vertex optimization. The optimization was performed based on H/C and DCN, since the TSI is weakly dependent on alkane compositions. The molecular weight of the surrogate is approximately 20 g/mol lower than that of the target fuel. This issue was expected during the formulation and its impact considered. A principle importance of the molecular weight combustion property target is in the constraint of fuel mass diffusive properties. Hydrocarbon/air diffusion coefficients exhibit a weak power dependence to hydrocarbon molecular weight. Thus it was deduced that the ~20 g/mol mismatch in molecular weight of surrogate and target fuel for such high molecular weights would be of minor importance. This deduction was tested for by measurement of strained diffusive extinction limits, which as we discuss in depth in [Won Radical index] are heavily dependent on fuel diffusion. The close agreement of surrogate fuel and target fuel extinction limits, **Figure 2.29c** indicates the veracity of this argument.

Figure 2.29 compares the fully prevaporized combustion behaviors of, S-8 POSF 4734, the S-8 POSF 4734 surrogate and where possible to provide a frame of reference, also those of Jet A

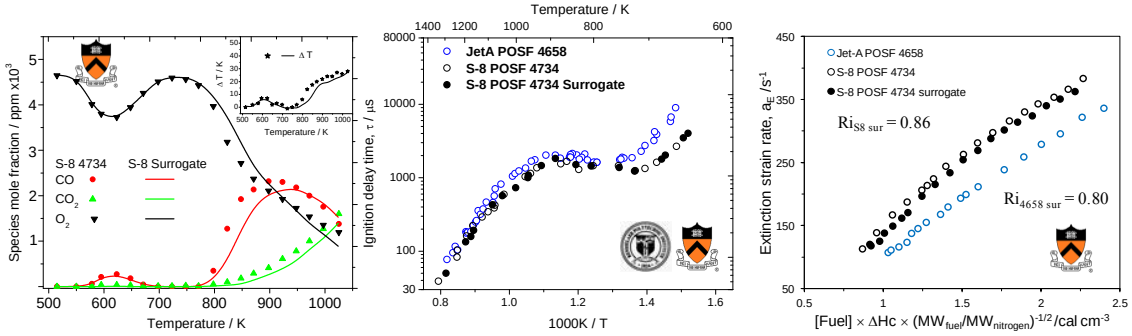

Flow reactor oxidation data for conditions of 12.5 atm, 0.3% carbon, φ= 1.0 and *t* =1.8s for S-8 POSF 4734 (symbols) and S-8 POSF 4734 Surrogate (lines), Inset; *ΔT*.

Reflected Shock ignition delay times, φ= 1.0 in air at ~20 atm for S-8 POSF 4734, S-8 POSF 4734 Surrogate.

Strain rates of extinction v TWE for counter flow diffusion flames at 1 atm, Jet-A POSF 4658, S-8 POSF-4734 and S-8 POSF 4734 Surrogate.

a) b) c)

Figure 2.29. Comparison of fully prevaporized combustion behaviors of S-8 POSF 4734, Jet A POSF 4658, and S-8 POSF 4734 Surrogate [87].

POSF 4658. Note that as expected based upon the DCNs, the Jet A sample has longer reflected shock ignition delays than the S-8 sample (**Fig. 2.29b**) and is less robust to diffusive strain than the synthetic fuel. Note also in **Fig. 2.29c** that the S-8 real fuel has a high radical index (0.86) than the Jet A sample (0.80).

One notes very good agreement between the S-8 real fuel and surrogate behavior across the entire spectrum of experimental comparisons. Based upon these comparisons it is clear that considering weakly branched alkanes as a special case for adding a molecular class to the second generation palette appears unnecessary in terms of achieving good agreement of surrogate mixture macro observable with fuels that are primarily composed of such classes. This point is even more strongly made by comparing a combustion property target matched mixture of n-decane and iso-octane formulated to the reactivity of 2-methylheptane [87]. The molecular structure of 2-methyl heptane is shown in **Figure 2.30.** It has been proposed and received extensive study as a model to develop the kinetics knowledge on weakly branched hydrocarbon

oxidation kinetics. Using the ignition quality tester at Princeton, the DCN of 2-MH is measured as 49.9 and the remaining combustion property targets of 2-MH are determined from its molecular formula. For these inputs, the 1st generation combustion property regression returns a 46.8/53.2 mole % mixture of n-decane/iso-octane as nearly an identical combustion property match for 2-methyl heptane DCN, H/C, and MWave [87], where all four combustion property targets are matched very closely. **Figure 2.30** displays the experimental reactivity data from the VPFR for 2-methyl heptane and its n-decane/iso-octane surrogate, indicating that the reactivity even on a pure component basis may be closely approximated with existing surrogate fuel components.

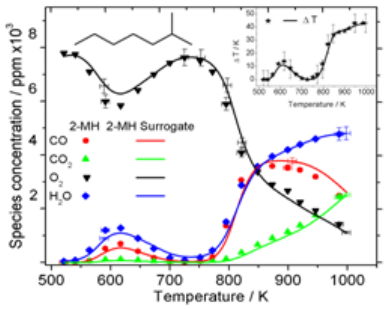

Figure 2.30. Flow reactor oxidation data for conditions of 12.5 atm, 0.5% carbon, φ= 1.0 and *t* =1.8s for 2-methyl heptane [91]: (2-MH, symbols) and the 2-methyl heptane surrogate fuel (n-decane/iso-octane 46.8/53.2 mole%, lines), Inset; ΔT.

Finally, it is important to again emphasize why comparing experiments to experiments is significantly more reliable than comparing experimental results with surrogate mixture kinetic model predictions. **Figure 2.31** compares predictions using several different models in the literature with each other and with experimental data obtained for the S-8 POSF 4734, and the S-8 POSF 4734 Surrogate. Data for Jet A POSF 4658 are also shown for comparison with the S-8 data. It is to be noted than independent of the model source, the predictions do not carry the same quality of performance in evaluating the veracity of the surrogate construction concept as do the comparisons of experiment with experiment. Moreover, it is also noted that models without low and intermediate temperature kinetic submodels (at the fuel chemistry level) do not predict the important trend of ignition delay data in terms of the transition from high to intermediate temperature behavior. The importance of these kinetic trends to gas turbine

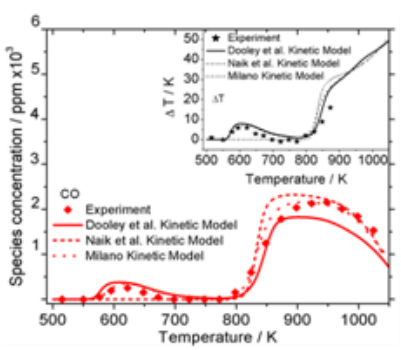

Flow reactor oxidation data for conditions of 12.5 atm, 0.3% carbon, φ= 1.0 and *t* =1.8s for the S-8 POSF 4734 Surrogate. Inset; ΔT. Symbols are experimental data; Lines are model computations.

a)

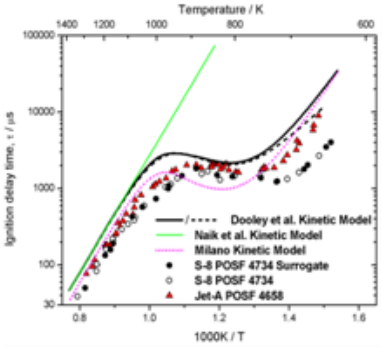

Reflected shock ignition delay times, ϕ = 1.0 in air at ~20 atm for S-8 POSF 4734, S-8 POSF 4734 Surrogate, and Jet-A POSF 4658. Symbols are experimental data; Lines are model computations. Dashed lines are computations imposing a pressure gradient of 2%/ms. All other computations are performed with assumptions of constant volume/constant internal energy.

b)

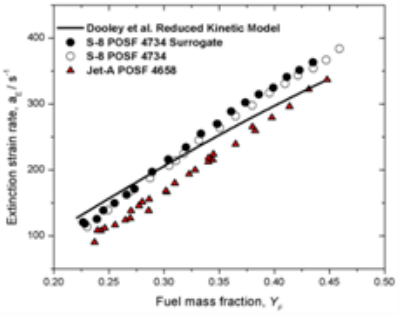

Strain rates of extinction for counter flow diffusion flames at 1 atm, S-8 POSF 4734, S-8 POSF 4734 Surrogate, and Jet-A POSF 4658. Lines are model computations. Kinetic model is a reduced version [92] derived from Dooley et al. [47].

c)

Figure 2.31. Comparisons of model predictions for the S-8 POSF 4734 Surrogate using several models in the literature [87].

combustion continues to be evaluated.

2.5.3.1. Applying Surrogate Concepts to Mixtures of Hydrocarbon Fluids

Above, we have demonstrated a simple, efficient concept for producing a surrogate mixture of several *pure* chemical species to emulate the fully prevaporized global combustion properties of a real fuel exists across a wide range of experimental venues and environmental conditions. These tests are mostly composed of studies involving fundamental laboratory experiments. In these works, the cost of the surrogate fuel mixtures to be studied has been of less concern; since most laboratory scale research involves only small quantities of test materials (< 2 Liters) Though it is noted that some types of fuel components, e.g., weakly branched alkanes or heavier alkyl aromatics, can be prohibitively expensive even in such small quantities. A particular concern motivating the present work is the much larger volumes of surrogates needed for studies in applied venues such as gas turbine rig combustors.

Infrequently, mixtures of commercially available hydrocarbon fluids ("solvents" and/or "distillation cuts") each having essentially a single molecular class structure, have been utilized in large scale testing to vary selected physical and chemical properties or to test material compatibilities with fuels. However, methodologies for formulating mixtures of several such materials that would replicate the fully pre-vaporized global kinetic behavior of a real fuel have received little attention in general and, to our knowledge, no attention in laboratory scale studies.

The MURI investigated applying the same concepts utilized to formulate the 1st and 2nd generation surrogates described above to produce mixtures of hydrocarbon fluids that replicate fully prevaporized real gas turbine fuel global kinetic properties [46, 47]. The motivating factor in this work was to consider how to test the surrogate concept in experimental configurations that require substantial amounts of fuel resources such as the turbulent dump combustor at PSU. In a later section of this final report, the approach developed was applied to compare the sooting behavior of a real fuel and surrogate mixtures formulated from hydrocarbon fluids and pure components in a model gas turbine combustor.

Surrogate mixtures composed of mixtures of hydrocarbon fluids were prepared for two different real jet fuels, Jet A (POSF 4658) and a military JP-8 (POSF 5699). Three commercial, narrow distillation cut hydrocarbon fluids were used to produce the POSF 4658 surrogate mixture. Each distillation cut fluid was composed of a well defined carbon number range and molecular class structure that matched relatively well the average molecular weight range of real jet fuels. The commercial reference names for these fluids are 1) Nor-Par 12 (NP12): a mixture of > 98% linear (mainly C_{11} - C_{12}) *n*-alkanes [95]; 2) Iso-Par L (IPL): a mixture of > 99% (mainly C_{11} - C_{14}) iso-paraffinic alkanes [96]; and 3) Solvesso Aromatic 150 (A150): a mixture of (primarily C_{10} - C_{11}) alkyl-benzenes with small amounts of naphthalene present [97]. Only about two gallons of each hydrocarbon fluids were available for this work. Some of the materials, namely Nor-Par fluids, are no longer available commercially. Thus other options for producing surrogate mixtures to emulate JP-8 POSF 5699, a real fuel to be experimentally studied in model combustor facilities at Penn State (later section in this report) were required.

Three different hydrocarbon fluids were used to formulate the surrogate mixture for JP-8 POSF 5699: 1) Exxsol D95 (D95) non aromatic fluid: a mixture of normal alkanes (primarily C_{12}

through C_{15}); 2) Solvesso Aromatic 100 (A100): a mixture of C_9 and C_{10} alkyl-benzenes; and 3) IPK UN1223 (IPK): an iso-paraffinic kerosene synthetic jet fuel obtained from the Wright Patterson Air Force Research Laboratory, Dayton Ohio. IPK (iso-paraffinic Kerosene). IPK is a wide distillation cut fluid composed entirely of iso-paraffinic components produced by Sasol.

Nor-Par, Iso-Par, Exxsol, and Solvesso alkyl aromatic (A) fluids used in this study are trademarked hydrocarbon distillation cuts produced by Exxon-Mobil Chemical Co. Generic chemical and distillation information on Exxsol, Iso-Par, and Solvesso aromatic fluids (A100 and A150) can be found at http://www.exxonmobilchemical.com/Chem-English/productsservices/hydrocarbon-oxygenated-fluids-hydrocarbon-fluids.aspx. Specific Product specifications can vary slightly from those published data, but since all of the Exxon-Mobil fluids are all narrow carbon number distillation cuts with essentially the same molecular class, their physical and chemical properties have only small variations with production lot. On the other hand, IPK is a much wider range distillation material of unknown isomerization level.

The combustion property targets of the two jet fuels, each of the hydrocarbon fluids, and the respective mixtures of these fluids were determined experimentally as described previously in this report. Each DCN measurement was performed in an identical fashion using ASTM 6890 procedures and the Ignition Quality Testing instrument. For determining mixture DCN's for the hydrocarbon fluids, binary and tertiary mixtures of the fluids used in formulating each surrogate were prepared by mass measurement to delineate the influence of each individual hydrocarbon fluid on the mixture DCN. The hydrocarbon fluid component TSI values utilized were obtained by the smoke point technique using ASTM D-1322 methodology and the average molecular weights for each of the surrogate components. The average molecular weight of each of the hydrocarbon fluid components was determined from detailed hydrocarbon speciation data. The mixture-averaged molecular weight of each of the JP-8 POSF 5699 surrogate components was estimated through a vapor pressure suppression technique with relatively high uncertainties. The uncertainties in TSI determination for the hydrocarbon fluids were conditional upon the uncertainties in determination of average molecular weights, which could be further improved upon using the methodology to determine molecular weight that was developed after the present efforts, were already completed. Finally, H/C molar ratio of each of the jet fuel samples and each of the hydrocarbon fluid surrogate components was determined experimentally using ASTM D5291 methodology.

Figure 2.32 summarizes the combustion property targets obtained for the surrogate mixture components used in formulating the Jet-A POSF 4658 and JP-8 POSF 5699 surrogate mixtures. The use of a paraffinic surrogate component with high H/C ratio, high DCN, and low TSI (e.g., D95 and NP12) and an aromatic surrogate component with low H/C ratio, low DCN and high TSI (e.g., A100 and A150) allows for independent control and matching of H/C ratio and TSI of the real fuel, but fails to reproduce the DCN of the real fuel. In order to adjust the DCN independently of the H/C ratio and TSI, a surrogate component with lower DCN, but relatively similar H/C ratio and TSI to the paraffinic component is required. In our pure

Hydrocarbon Fluid	DCN	H/C	MW / g mol^{-1}	TSI
Nor-Par 12 (NP12)	73.83	2.14	162	4.5
Iso-Par L (IPL)	31.72	2.19	173	13.1
Aromatic 150 (A150)	8.43	1.33	135	85.3
EXXSOL D95 (D95)	58.3	2.02	177	13.9
IPK UN1223 (IPK)	31.7	2.15	154-160	12.3
Aromatic 100 (A100)	7.9	1.34	121	65.6

Figure 2.32. Combustion Property Target Data for the Jet-A POSF 4658 Surrogate Components. Molecular weights are from Material Safety Datasheets. The molecular weight of IPK is estimated to be 154-160

surrogate component studies [46, 47], this role was fulfilled by *iso*-octane. However, this surrogate component is prohibitively expensive in large volumes. As an alternative, we utilized an *iso-paraffinic hydrocarbon fluid* (e.g., IPK or Iso-Par L) to formulate the surrogate mixtures that replicate all four combustion property targets of specific real jet fuel.

The combustion property target data as determined using the methods described above were delineated by an extreme vertices matrix to parameterize, in a comprehensive and consistent fashion, the DCN, H/C, MW and TSI as a function of Nor-Par 12, Iso-Par L and Aromatic 150 mole fraction. Several mixtures of Nor-Par 12, Iso-Par L, and Aromatic 150 that would be suitable as a surrogate fuel mixture for Jet-A POSF 4658 were computed statistically as

Fuel				DCN Predicted	DCN Measured	H/C	MW / g mol^{-1}	TSI
Jet-A POSF 4658				-	47.1	1.95	142 ±20	21.4
2nd Generation POSF 4658 Surrogate (mole %)				47.1	48.6	1.96	138.7	20..4
n-dodecane	iso-octane	1,3,5 trimethyl benzene	n-propyl benzene					
40.4	29.5	7.3	22.8					
Jet-A POSF 4658 Solvent Cut Surrogate Mixture (mole %)				47.4	47.3	2.03	162.1	21.4
Nor-Par 12	Iso-Par L	Aromatic150						
42.78	40.62	16.6						
JP-8 POSF 5699					49.3	1.94	153 (est.)	22.3
JP-8 POSF 5699 Solvent Cut Surrogate Mixture (mole%)					49.4	1.93	165.6 (est.)	20.8
EXXSOL D95	IPK UN1223	Aromatic100						
70.51	13.13	16.36						

Figure 2.33. Combustion property targets for the three component surrogate mixtures, typical kerosene fuels, the target fuels (Jet-A POSF 4658 and JP-8 POSF 5699) and their hydrocarbon fluid surrogate mixtures and surrogate property targets.

described earlier. A three component mixture that closely shared the DCN, TSI and H/C of the target fuel was then selected. **Figure 2.33** summarizes the combustion property targets and compositions of the Jet-A POSF 4658 1st and 2nd generation surrogates composed of pure components. The POSF surrogate mixtures have average molecular weights that reasonably approximate the real fuel targets.

Figure 2.34 compares the VPFR reactivity data for each of the real fuels and their respective hydrocarbon fluid surrogate mixtures. As the property targets for Jet A POSF 4658 and JP-8 5699 are very similar, we should expect that the reactivity data for the two real fuels should be essentially the same (**Fig. 2.33a**). **Figure 2.33b** compares the Jet A POSF 4658 and Jet A POSF 4658 hydrocarbon fluid surrogate reactivities, while **Fig. 2.33c**) compares the JP-8 POSF 5699 and JP-8 POSF 5699 hydrocarbon fluid surrogate reactivities.

The principal conclusions from these comparisons are:

- Two real fuels sharing nearly the same combustion property targets essentially have the same fully prevaporized reactivity profiles, further demonstrating the validity of the combustion property matching methodology for analyzing fuels. It is expected, but yet to be established directly by experiment, that other fundamental global combustion parameters will also be very similar. However, the likelihood of this result is already strongly supported by the fact that having the same targets would lead to the production of nearly identical 2nd

generation surrogate mixtures for both fuels, and the matched 2nd generation surrogate mixtures has show good comparisons with target fuel global combustion behavior over the entire wide range of fundamental venues and environmental parameters.

- Surrogate mixtures of hydrocarbon fluids having narrow distillation cuts of molecular class structure (i.e., Nor-Par 12 (linear alkanes), Iso-Par L (iso-paraffinic alkanes), and Aromatic 150 (alkylbenzenes)) can be used to formulate mixtures with combustion property targets (DCN, TSI, H/C molar ratio, and average molecular weight) that emulate closely those of a *specific* target jet aviation fuel. Moreover, since the same 2nd generation surrogate mixture would result from matching the property targets for both the real fuel and the hydrocarbon fluid surrogate, we should expect that the same kinetic and vapor phase transport models should reasonably predict the fully prevaporized global combustion behavior of both the real fuel and the hydrocarbon fluid surrogate.
- Surrogate mixtures formed from hydrocarbon fluids having broader ranges of molecular compositions appear to lead to improved emulation of real fuel reactivity at the onset of hot ignition regime, 800-900 K, when compared against the 2nd generation surrogate mixtures produced from mixtures of three to four pure surrogate components. It appears that this results from the richer palette of distinct functional groups and molecular chain length present in the hydrocarbon fluids.

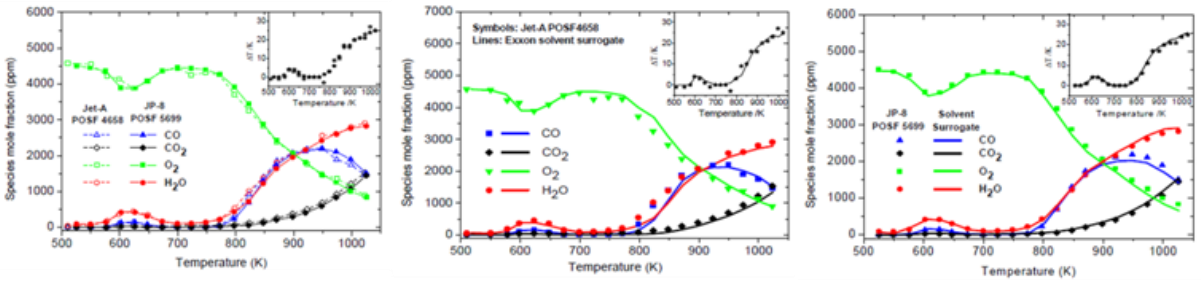

Flow reactor chemical reactivity data Jet A POSF 4658 (open symbols) and the JP-8 POSF 5699 fluid surrogate mixture (filled symbols); Inset: heat release, ΔT.

a)

Flow reactor chemical reactivity data Jet A POSF 4658 (symbols) and the Jet A POSF 4658 fluid surrogate mixture (solid lines); Inset: heat release, ΔT.

b)

Flow reactor chemical reactivity data JP-8 POSF 5699 (symbols) and the JP-8 POSF 5699 fluid surrogate mixture (solid lines); Inset: heat release, ΔT.

c)

Figure 2.34. Flow reactor chemical reactivity data for Jet A POSF 4658, JP-8 POSF 5699, and their hydrocarbon fluid surrogate mixtures. All data at 0.3% molar carbon, $\varphi = 1.0$, 12.5 atm pressure, and 1.8 s residence time.

More generally, the choice of surrogate components and class composition can differ significantly from those of the real fuel without degrading the quality of predictions. The guiding principle to maintain a reasonable emulation of the distribution of the key distinct functional groups represented by the real fuel component selection and mixture composition remains even for these more complex surrogate mixtures that do not approximate the original fuel molecular structure or structural class distribution.

Finally, this work shows that mixtures formed with hydrocarbon fluid surrogates, which are much less expensive than single molecular structural pure components, can yield close replication of fully pre-vaporized global combustion properties of a real fuel, provided the surrogate formulation emulates well the real fuel combustion property target values. The ability to formulate hydrocarbon fluid surrogate blends to emulate real fuel behavior appears to be a possible route to bridge the present experimental knowledge base developed on surrogate fuel

science to applied combustion research aimed at simplifying the integration of emerging alternative fuel feed stocks into the aircraft transportation sector. What clearly remains to be established is whether a surrogate mixture that emulates a real fuel well across the wide set of venues and parameter space tested by the MURI actually represents the envelope of parameter space important to combustion behavior in turbulent reacting conditions characteristic of propulsion systems.

The most direct manner of testing this hypothesis is to study 2nd generation surrogate mixtures in a fully prevaporized applied experimental configuration known to be relevant to applied combustion problems. This prospect is entirely feasible….provided one can accept that the fuel costs for such an experiment will be the order of $50,000 per barrel; the actual cost determined by how small such an experiment can be scaled without losing its relevance to practical devices. Estimates appear to be requiring a minimum of about a barrel of fuel. Clearly at a price equivalency for hydrocarbon fluid surrogates the order of ten times less, it is prudent to at least first explore the matter using this approach before using pure component surrogates. Moreover, if this approach appears to be viable, then hydrocarbon fluid surrogate mixtures can be utilized to evaluate the relative importance of fully prevaporized combustion kinetics and physical properties such as distillation curve and class distribution over the curve on multi-phase turbulent combustion behaviors.

2.5.4. Physical Property Emulation

The surrogate formulation strategy tested in this study is designed to produce surrogate fuels to emulate a specific range of fully prevaporized, real fuel global combustion properties that relate principally to chemical kinetic and gas phase transport phenomena. Though air-breathing energy conversion processes utilizing liquid fuels depend on these properties for ignition, chemical heat release, local reaction temperatures, rate of burning, extinction, and sooting, real systems are also multi-phase combustion phenomena, which can be affected by physical properties such as distillation curve, atomization (viscosity, surface tension), vaporization (phase relationships), mixing phenomena and chemical kinetic/turbulent parameter coupling. Ultimately, a successful computational engineering combustion model must include all of these multiphase aspects. An end goal for understanding real fuel effects on performance and emissions therefore requires encompassing as targets both the relevant chemical kinetic as well as physical property characteristics.

As noted earlier, accurate emulation of physical properties typically require a larger number of surrogate components than needed for emulation fully prevaporized global combustion properties. Moreover, local gas phase combustion properties may also be coupled to physical properties, not only through mass deposition as a result of the distillation characteristics of the fuel, but by preferential vaporization. Preferential vaporization occurs when the mass diffusive resistances inside droplets are low relative to the rate of vaporization at the droplet surface. This may result from significant internal liquid phase circulation within each droplet, or because the droplet diameter (length scale) is small relative to the diffusive length scale. As a result lower molecular weight components have more likelihood to preferentially vaporize early, and if these are alkyl aromatic rather than n-alkane in character, one is substantially more prone to rapid ignition than the other, potentially a problem for relight.

Another more subtle coupling of fuel physical properties with combustion in multi-phase combustion systems is the potential heat feedback from combustion to local liquid fuel temperatures at the atomizer. **Figure 2.35** compares the range of viscosity variations for fuel statistics gathered from 2006 - 2008, with the possible changes in viscosity with liquid temperature. Heat feed back to the atomizer potentially offers a significant coupling of combustion and variation in this important atomization parameter. Additionally, using liquid fuel as a heat transfer fluid may also affect atomizer liquid temperature. Similar coupling can also as a result of the temperature dependence of fuel surface tension.

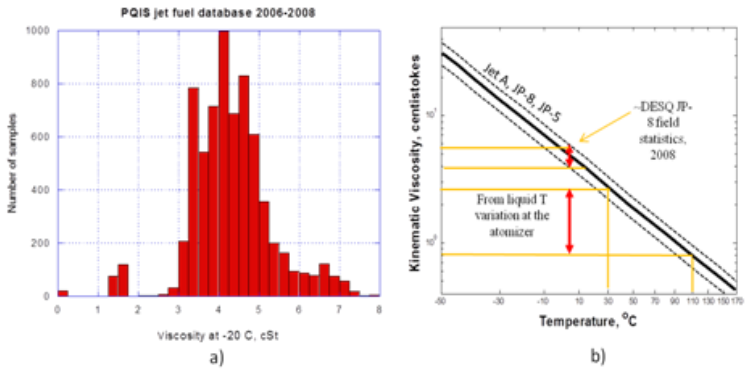

Figure 2.35. Kinematic reference viscosity statistics for the real jet fuel database for 2006-2008 [98] and the typical variation of jet fuel viscosity with liquid temperature [99].

A factor that must be emphasized, even as approaches for emulating real fuel properties are in the formative stage, is that the utility of computational design tools will be a strongly related to the complexity of the submodels for physical and chemical kinetic properties. At present, little is known as to the relative trade-offs around how accurately physical and chemical kinetic properties of a real fuel need to be replicated. For detailed kinetics, the complexity is overwhelming, even for one molecular fuel structure, not to mention mixtures of structures of different molecular weights and classes (to also address preferential vaporization impacts). The detailed kinetic model constructed for the simple three component 1st generation surrogate fuel [47] is composed of 1597 species. Thus, one cannot escape the realization that the complexity, particularly the number of surrogate components needed, is a principal factor in defining the tractability of the numerical combustion model. Consequently, it has been the explicit aim of the MURI surrogate formulation strategy to prioritize the emulation of real fuel combustion kinetic phenomena over physical properties, with as few surrogate components, and even families of components as practical. This direction is warranted even with advancements in detailed kinetic model reduction techniques (e.g. [100, 101]) and/or reaction pathway lumping approaches (e.g. [102]) to reduce the number of species required for predicting real fuel kinetic behavior. Even so, the reductions continue to embody all of the uncertainties in the numerous parameters that were estimated in constructing the detailed model. Moreover, it is to date, not well established how turbulence/chemistry coupling may be affected by model reduction methods that do not consider turbulence-related timescales in performing the reduction process. Over the past five years, other

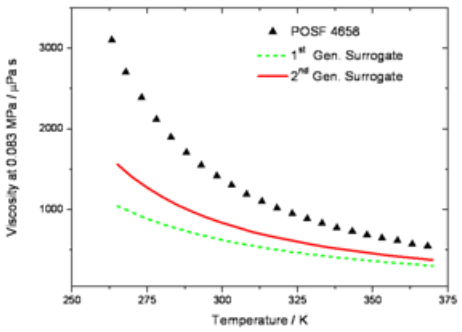

Figure 2.36. Measured viscosity for Jet-A POSF 4658 at 0.083MPa (symbols [36]) and calculated viscosities [100] at 0.083MPa for 1st generation (n-decane/iso-octane/toluene 42.7/33.0/24.3 mole %, dashed line) and 2nd generation (n-dodecane/iso-octane/1,3,5 trimethylbenzene/n-propylbenzene 40.41/29.48/7.28/22.83 mole %, solid line) POSF 4658 surrogate fuels.

researchers have placed primary emphasis on physical property emulation in developing surrogate fuel concepts [83, 103-109]. For example, Huber et al. [108] have emphasized replication of the measured liquid density and viscosity of Jet-A POSF 4658, both important properties in the liquid fuel vaporization process of gas turbines. We calculated the liquid density and viscosity behaviours of the 1st and 2nd generation surrogate fuels from the equation of state methods implemented in the REFROP code [110], and the results are compared to the measured values of Jet-A POSF 4658 in **Figures 2.36** and **2.37** respectively. Although the mixture-averaged molecular weight is considered as a *combustion* property target to constrain vapor phase mass diffusive issues, it is also appropriate to some degree as a measure of other physical properties. Thus the 2nd generation surrogate is of higher density and viscosity than the lighter 1st generation surrogate. The density of the 2nd generation surrogate is estimated to be ~5-6 % lower than the measurements of Huber et al. for Jet-A POSF 4658. However, the deviation from the measured Jet-A POSF 4658 viscosity is larger, ranging from ~50-30 % from 273-373 K. but is likely to deviate only minimally at the operating temperatures of gas turbine atomizers. These properties were not considered in formulating either the 1st or 2nd generation surrogates.

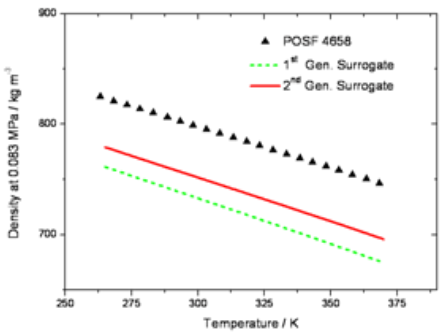

Figure 2.37. Measured density for Jet-A POSF 4658 at 0.083MPa (symbols [36]) and calculated densities [100] at 0.083MPa for 1st generation (n-decane/iso-octane/toluene 42.7/33.0/24.3 mole %, dashed line) and 2nd generation (n-dodecane/iso-octane/1,3,5 trimethylbenzene/n-propylbenzene 40.41/29.48/7.28/22.83 mole %, solid line) POSF 4658 surrogate fuels.

Notwithstanding this, it is worth highlighting that although iso-octane is an acceptable surrogate fuel component for combustion kinetic purposes (also in terms of cost), its physical properties (low density and low viscosity) and required fraction (~30 mole %) account for most of the noted deviation of 2nd generation surrogate physical properties from those of Jet-A POSF 4658. A higher carbon number, heavily isomerized species replacing iso-octane could be utilized to better approximate both chemical and physical properties.

Bruno and co-workers [106, 107] followed the above work by expounding upon the "physicochemical authenticity" of surrogate mixtures that had been previously proposed in the literature for emulating aviation kerosene. More complex Jet-A surrogates were proposed, composed of less studied molecules from a combustion kinetic view point, were shown to perform somewhat better in emulating physical properties. Bruno and Huber [107] proposed a simple ternary surrogate **(Fig. 2.38)** that had reasonable thermophysical property emulation of Jet

Mole Fraction					DCN	H/C	MW/ g mol^{-1}	TSI
Jet-A POSF 4658					47.1	1.96	142.0	21.4
1st Generation Surrogate	*n*-decane	*iso*-octane	toluene		47.1	2.01	120.7	14.1
	0.427	0.33	0.243					
2nd Generation Surrogate	*n*-dodecane	*iso*-octane	1,3,5 TmB	n-PB	48.5	1.95	138.7	20.4
	0.404	0.295	0.073	0.228				
***H-B Surrogate**	*n*-dodecane	Tetradecane	1,2,4 TmB		60.4	1.89	158.3	28.7
	0.288	0.304	0.408					

A 4658. However, the lack of any isomerized alkane is problematic in terms of the chemical properties of their recommendation. We estimated the property targets for the Huber-Bruno surrogate and found that the aromatic content is far too low to counter the high DCN values of the alkane components, and far too high to replicate the TSI of Jet A POSF 4658. In fact, the combustion property targets of many of the surrogates found in the literature are known to vary greatly both in comparison to each other and (for example) to the real fuel target ranges encompassed here e.g., see Xu et al. [26].

The *a priori* surrogate formulation methodology tested here can certainly be modified to additionally incorporate more precise physical property emulation as a specified target by, for example, incorporating higher molecular weight alkanes and strongly branched iso-alkanes, without compromise of what has been demonstrated in surrogate formulation concepts by the prior work reported here.

For example, liquid density generally increases in the following order of molecular class, iso-alkanes ≅ n-alkanes < monocycloalkanes < alkyl-aromatics < polycycloalkanes < polyaromatics [111]. It is apparent from review of the literature (e.g. [81]) that this ordering for the availability and the fidelity of kinetic models is generally the inverse. With the additional considerations of the correlation of kinetic model size to component molecular weight, and the close sharing of combustion kinetic phenomena of real fuel and simple surrogate fuels demonstrated here, the key question presently unanswered is "*to what precision must real fuel physical and combustion kinetic properties be emulated in the surrogate formulation?"* Instruction on this issue is required to realize, in an efficient manner, surrogate fuels that emulate physical and combustion kinetic properties, as originally called for by Edwards and Maurice [112]. The analysis provided here of the chemical-group-additive nature of real fuel combustion behavior should be a principle consideration of future work as this concept allows for the production of surrogate formulations of the minimal complexity.

In closing this section, a recent microgravity isolated droplet combustion study recently appeared and is the first fundamental experimental work to consider coupled liquid phase and vapour phase kinetic/transport conditions [113]. The isolated droplet combustion behavior of individual, large diameter droplets (~550 micron) of Jet A 4658 real fuel, and the POSF 4658 1st and 2nd generation surrogates burning in air at atmospheric pressure were compared. Droplet burning rates, flame diameter, and surrounding "soot" shell were compared. The 2nd generation data simulated the real jet fuel in terms of burning rate, flame and soot diameter better than the 1st generation results. The 1st generation burning rate was consistently higher, with lower sooting than the real fuel or 1st generation results. An important point to be made is that simulation of the real fuel behavior was captured well by the 2nd generation surrogate even though the distillation curve of the surrogate and real fuel are drastically different. In modeling of other isolated droplet burning experiments conducted in this same experimental facility, Farouk and Dryer [114] have shown that internal motions induced by droplet deployment and surface tension effects exist that result in rapid transport of material within the droplet. As a result one might expect "batch distillation" to be observed, but there is no indication that this process leads to the preferential vaporization conditions typically noted in the literature for binary liquid droplets composed of materials of vastly different volatility. All of these results further emphasize that the relative importance of physical and chemical properties on multiphase combustion phenomena need to be more precisely considered.

2.6. Modeling

Modeling efforts under this MURI were primarily by the Princeton groups as well as by UIC. These two studies were coordinated, with slightly different missions. The UIC effort pursued detailed kinetic model development more specifically aimed at interpreting the pulsed shock tube experimental studies performed within the group, and contributing to the understanding of those aspects that would eventually be needed to model sooting behavior. The experiments themselves produced high pressure, high temperature species descriptions for short reaction residence times as functions of initial reaction temperature and, in addition to providing general validation data, those pathways that contribute to the formation of poly aromatic hydrocarbons and soot precursors were elucidated. Additionally, experiments were performed to compare 2nd generation Jet A POSF 4658 surrogate kinetic behavior against that of Jet A POSF 4658 real fuel.

The work of Dooley et al. [47] provided a base model of n-decane, iso-octane, and toluene that were then extended and revised considerably to produce models for n-decane, n-dodecane [115] and iso-octane [116]. The UIC modeling development for aromatics stemmed from the work of Klotz [117] and Dooley et al [47]. The work of Klotz et al and Sivaramakrishnan et al. [118] were foundation for modeling experiments on m-xylene utilized in studies of sooting supported by SERDC [119]. This work supported the further model development for nPB [120] and 135 TmB [121]. All of these efforts are available in the published literature. The UIC modeling work is summarized in reporting from this group, and includes a comparison of a composite 2nd generation model against their high pressure pulsed shock tube data for the 2nd generation Jet A POSF 4658 surrogate mixture [122]. Model reduction and comparisons against a majority of other data collected by the MURI team remain to be performed.

The modeling efforts carried out at Princeton have emphasized a hierarchical approach to comprehensive kinetic modeling and initially applied modeling principally to analyze the surrogate concept. There was to the use of modeling to analyze the data obtained across the spectrum of fundamental experiments, including low, intermediate, and high temperature aspects. In addition, reduced models have been produced to consider flame phenomena, and these are now being assembled to produce a 2nd generation kinetic model that will reproduce all of the fundamental kinetic behaviors of both the pure and mixture experiments.

Early on, the Princeton groups utilized n-decane/iso-octane/toluene modeling to analyze the 1st generation surrogate concepts [47]. We redeveloped a small-species C_0-C_4 submodel based upon the recently available literature results that could be combined with the work of Lawrence Livermore National Laboratories for higher molecular weight kinetics, inclusive of those for iso-octane and normal alkanes. We chose to coordinate our efforts in this manner with those of LLNL, as we were also cognizant of a lack of information as to the importance of low and intermediate temperature regime kinetics for gas turbine applications [16]. In fact the lack of consideration of these kinetic regimes on the part of Jet Surf construction [34] led us precluded further consideration of using this resource in our modeling efforts.

In recognition that alkyl aromatics were essential components to any future surrogate model development, we also noted that aromatic kinetics for even toluene were not reproducing well much of the data present in the literature as the MURI began. Thus in our model development

efforts, we combined the chores of C_0-C_4 and aromatic modeling needs to develop a comprehensively validated model for toluene [123] oxidation. The toluene model development was also realized to be the "backbone" for larger molecular weight alkyl aromatic models of nPB and 135TmB oxidation. Normal propyl benzene model predictions have been compared against premixed laminar flame speed and strained extinction data, reflected shock tube ignition and variable pressure flow reactor data. [124]. Predictions have also been compared with laminar premixed flame speed and strained extinction [125] data generated by the MURI team.

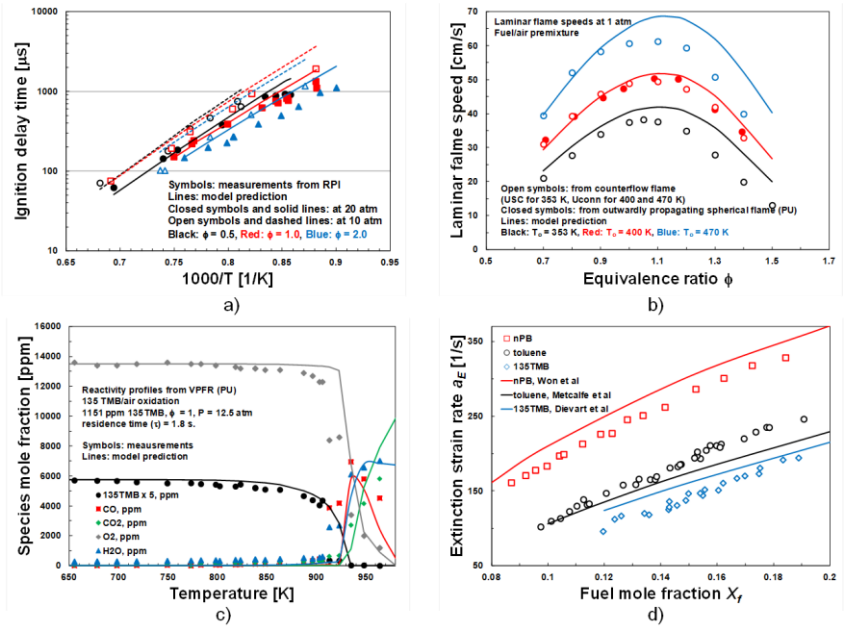

Figure 2.39. Comparisons of modeling in progress on 135 TmB [127]. a) Comparison against reflected shock tube ignition delay; b) laminar flame speed; c) Variable Pressure Flow Reactor reactivity; d) counter flow diffusive strained extinction.

Early developments of models for both were of significance in advancing our understanding of the factors controlling counterflow diffusive strained extinction [126]. A publication on a refined detailed model for nPB oxidation remains in preparation, and a full manuscript on modeling of 135TmB oxidation behavior over a wide range of experimental conditions have been submitted for review [127]. A sample of comparisons utilizing this model is shown in **Figure 2.39**.

Finally, a composite reduced model for n-dodecane/iso-octane/nPB/135TmB has been assembled and predictions are compared against several data for the 2nd generation Jet A POSF 4568 experimental studies are compared in **Fig. 2.40**.

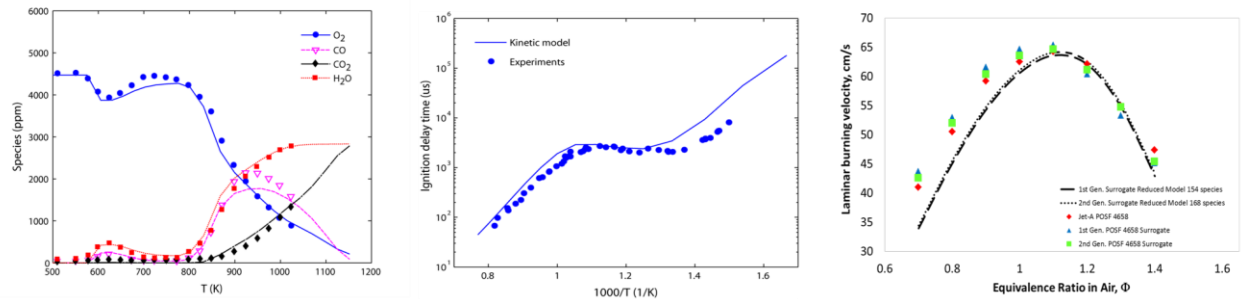

Figure 2.40. Jet A POSF 4658 2nd generation (n–C_{12}/iso-C_8/n-PB/135TmB (40.41/29.48/7.28/22.83 mole %) surrogate mixture. Lines represent kinetic model and symbols represent experimental data.

One notes significant disparities in predicting lean laminar flame speed data, and further refinements of the models are underway to address these deficiencies. More results on the modeling efforts for the 2nd generation surrogate components and their composite will be presented in early 2013 [128].

2.7. References

[1] Violi, A., Yan, S., Eddings, E.G., Sarofim, A.F., Granata, S., Faravelli, T., Ranzi, E., "Experimental Formulation and Kinetic Model for JP-8 Surrogate Mixtures", *Combust. Sci. Tech.*, (2002)174:399-417.

[2] Metghalchi, M., "Autoignition and Burning Speeds of JP-8 Fuel at High Temperature and Pressures", Contractors Meeting in Chemical Propulsion, ARO and AFOSR, 155 (2003).

[3] Lenhert, D.B., "The Oxidation of JP-8 and Its Surrogates in Low and Intermediate Temperature Regime", Ph.D. Thesis, Drexel University, Philadelphia, PA. December, 2004.

[4] Hohmann, S., Uslu, S., "Computational Fluid Dynamics for Combustion (CFD4C)", Final Report, Project GRD1-1999-10325 (2004).

[5] Eddings, E.G., Yan, S., Ciro, W., Sarofim, A.F., "Formulation of a Surrogate for the Simulation of Jet Fuel Pool Fires", *Combust. Sci. Tech.* (2005) 117:715-739.

[6] Mawid, M.A., Park, T.W., Sekar, B., Arana, C., "Detailed Chemical Kinetic Modeling of JP-8/Jet-A Ignition and Combustion", ASME Paper GT2005-68829.

[7] Agosta, A., Lenhert, D.B., Miller, D.L., Cernansky, N.P., "Development and Evaluation of a JP-8 Surrogate that Models Preignition Behavior in a Pressurized Flow Reactor", Paper E07, *Third Joint Meeting of the US Sections of the Combustion Institute*, Chicago, IL (2005).

[8] Dagaut, P, El Bakali, A., "The Combustion of Kerosene: Experimental Results and Kinetic Modeling Using 1- to 3-Component Surrogate Model Fuels", *Fuel* (2006) 85:944-956.

[9] Holley, A.T., Dong, Y., Andac, M.G., Egolfopoulos, F.N., "Extinction of Premixed Flames of Practical Liquid Fuels: Experiments and Simulations", *Combust Flame* (2006) 144:448-460.

[10] Holley, A.T., Dong, Y., Andac, M.G., Egolfopoulos, F.N. , "Ignition and Extinction of Non-premixed Flames of Single-Component Liquid Hydrocarbons, Jet Fuels, and Their Surrogates", *Proc Combust Ins* 31, doi:10.1016/j.proci.2006.07.208.

[11] Humer, S., Frassoldati, A., Granata, S., Faravelli, T., Ranzi, E., Seiser, R., Seshadri, K., "Experimental and Kinetic Modeling Study of Combustion of JP-8, Its Surrogates and Reference Components in Laminar Nonpremixed Flows", *Proc Combust Ins* 31, doi:10.1016/j.proci.2006.08.008.

[12] Gokulakrishnan, P., Gaines, G., Currano, J., Klassen, M.S., Roby, R.J., "Experimental and Kinetic Modeling of Kerosene-type Fuels at Gas Turbine Operating Conditions", *J. Eng. Gas Turb Power*, ASME Transactions: (2007) 129.

[13] Allison, T.C., Burgess, D.R., Hudgens, J.W., Manion, J.A., Matheu, D.M., Tsang, W., "Workshop on Combustion Simulation Databases for Real Transportation Fuels", Report NISTIR 7155: National Institute of Standards and Testing, Gaithersburg, MD. [online] http://kinetics.nist.gov/realfuels/content/RealFuelsReport_NISTIR7155.pdf (2003).

[14] Pitz, W.J., Cernansky, N.P., Dryer, F.L., Egolfopoulos, F.N., Farrell, J.T., Friend, D.G., Pitsch, H., "Development of an Experimental Database and Chemical Kinetic Models for Surrogate Gasoline Fuels", SAE Paper 2007-01-0175.

[15] Farrell, J.T., Cernansky, N.P., Dryer, F.L., Friend, D.G., Hergart, C.A., Law, C. K., McDavid, R.M., Mueller, C.J., Patel, A.K., Pitsch, H., "Development of an Experimental Database and Kinetic Models for Surrogate Diesel Fuels", SAE Paper 2007-01-0201.

[16] Colket, M. B., et al, "Development of an Experimental Database and Kinetic Models for Surrogate Jet Fuels", Jan 2007. AIAA Paper 2007-770.

[17] Zhao, Z., Conley, J.P., Kazakov, A., Dryer, F.L., "Burning Velocities of Real Gasoline Fuel at 353 K and 500 K", SAE Paper 2003-01-3265.
[18] Davidson, D.F., Gauthier, B.M., Hanson, R.K., "Shock Tube Ignition Measurements of *Iso*-octane/air and Toluene/air at High Pressures", *Proc. Combust. Inst.*, (2005) 30:1175-1182.
[19] Zhao, Z., Chaos, M., Kazakov, A., Gokulakrishnan, P., Angioletti, M., Dryer, F. L., "Fuel Chemistry Models for Simulating Gasoline Kinetics in Internal Combustion Engine Applications", Work-in-Progress 2C-27, 31st International Symposium on Combustion, Heidelberg, Germany (2007).
[20] Hohmann, S., Uslu, S., "Computational Fluid Dynamics for Combustion (CFD4C)", Final report, project GRD1-1999-10325 (2004).
[21] Chaos, M., Zhao, Z., Kazakov, A., Gokulakrishnan, P., Dryer, F.L., "A PRF+Toluene Surrogate Fuel Model for Simulating Gasoline Kinetics," Proceedings of the 5th Joint Meeting of the US Sections of the Combustion Institute (2007) paper E26.
[22] Murphy, M.J., Taylor, J.D., McCormick, R.L., "Compendium of Experimental Cetane Number Data", Subcontractor Report NREL/SR-540-36805: National Renewable Energy Laboratory, Golden CO. [online] http://www.nrel.gov/vehiclesandfuels/pdfs/sr368051.pdf (2004).
[23] Taylor, J.D., McCormick, R.L., Clark, W., "Report on the Relationship Between Molecular Structure and Compression Ignition Fuels, Both Conventional and HCCI", Milestone Report NREL/MP-540-36726: National Renewable Energy Laboratory, Golden, CO. [online] http://www.nrel.gov/vehiclesandfuels/pdfs/mp36726.pdf (2004).
[24] Androulakis, I.P., Weisel, M.D., Hsu, C.S., Qian, K., Green, L.A., Farrell, J.T., "An Integrated Approach for Creating Model Diesel Fuels", *Energy Fuels* (2005) 19:111-119.
[25] Yan, S., Eddings,E.G., Palotas, A.B., Pugmire, R.J., Sarofim, A.F., "Prediction of Sooting Tendency for Hydrocarbon Liquids in Diffusion Flames", *Energy Fuels* (2005) 19:2408-2415.
[26] Xu, H., Yang, Z, Chaos, M., Dryer, F.L., "Surrogate Jet Fuel Mixture Formulation and Development of Experimental Databases", JANNAF 42nd Combustion Joint Sub-Committee Meeting *Modeling and Data For Combustion Simulation*, Boston Marriott Newton, Hanscom AF Base, Newton, MA, May 12-16, 2008
[27] Battin-Leclerc, F., Fournet, R., Glaude, P.A., Judenherc, B., Warth, V., Come, G.M., Scacchi G., "Modeling of the Gas-phase Oxidation of *n*–decane from 550 to 1600 K", *Proc Combust Inst* (2000) 28:1597-1605.
[28] Bikas, G., Peters, N., "Kinetic Modeling of *n*-decane Combustion and Autoignition", *Combust Flame* (2001) 126:1456-1475.
[29] Zhao, Z., Li, J., Kazakov, A., Dryer, F.L., Zeppieri, S.P., "Burning Velocities and a High-temperature Skeletal Kinetic Model for *n*-decane", *Combust Sci Tech* (2005) 177:89-106.
[30] Chaos, M., Kazakov, A., Zhao, Z., Dryer, F.L., "Model Development and Reduction Methods for High-temperature Large Alkane Molecule Kinetics", Work-in-Progress 2E-15, *Thirty-first International Symposium on Combustion*, Heidelberg, Germany (2006).
[31] Chaos, M., Kazakov, A., Zhao, Z., Dryer, F.L., "A High-temperature Chemical Kinetic Model for Primary Reference Fuels", *Int J Chem Kinet* (2007) 39:399-414.
[32] Brezinsky, K., Litzinger, T.A., Glassman, I., "The High Temperature Oxidation of the Methyl Side Chain of Toluene", *Int J Chem Kinet* (1984) 16:1053-1074.

[33] Roubaud, A., Minetti, R., Sochet, L.R., "Oxidation and Combustion of Low Alkylbenzenes at High Pressure: Comparative Reactivity and Auto-ignition", *Combust Flame*, (2000) 121:535-541.
[34] Egolfopoulos, F. N. (PI), Bowman, C. T., Cernansky, N.P., Hanson, R. K., Law, C. K., Lu, T., Miller, D. L., Pitsch, H., Wang, H., " Development of Detailed and Reduced Kinetic Mechanisms for Surrogates of Petroleum-Derived and Synthetic Jet Fuels", AFOSR Grant No. FA9550-08-1-0040 (2007-2010).
[35] Orme, J., Simmie, J.M., Curran, H.J., "Experimental and Modeling Study of Methylcyclohexane Pyrolysis and Oxidation", *J Phys Chem A* (2006) 110:114-313.
[36] Pitz, W.J., Naik, C.V., Ní Mhaoldúin, T., Westbrook, C.K., Curran, H.J., Orme, J.P., Simmie, J.M. (2007) "Modeling and Experimental Investigation of Methylcyclohexane Ignition in a Rapid Compression Machine", *Proc Combust Inst* (2007) 31:267-275.
[37] Ranzi, E., "A Wide-Range Kinetic Modeling Study of Oxidation and Combustion of Transportation Fuels and Surrogate Mixtures", *Energy & Fuels* (2006) 20:1024-1032
[38] Colket, M.B., Edwards, T., Williams, S., Cernansky, N.P., Miller, D.I., Egolfopoulos, F.N., Dryer, F.L., Bellan, J., Lindstedt, p., Seshadri, k., Pitsch, h., Sarofim, A., Smooke, M., Tsang, W. AIAA 2008-972.
[39] Mueller, C.J. "The Quantification of Mixture Stoichiometry when Fuel Molecules Contain Oxidizer Elements or Oxidizer Molecules Contain Fuel Elements", SAE Tech. Pap. 2005-01-3705.
[40] ASTM D5291-10 Standard Test Methods for Instrumental Determination of Carbon, Hydrogen, and Nitrogen in Petroleum Products and Lubricants, ASTM International, 100 Barr Harbor Drive, PO Box C700, West Conshohocken, PA 19428-2959. United States
[41] Allard, L.N., Hole, N.J, Webster, G.D., Ryan, T.W.I., Ott, D., Beregszazy, A., Fairbridge, C.W., Cooley, J., Mitchell, K., Richardson, E.K., Elliot, N.G., Rickeard, D.J. SAE Tech. Pap. (1997) 971636.
[42] Allard, L.N., Webster, G.D., Ryan, T.W.I., Matheaus, A., Baker, G., Beregszazy, A., Read, H., Mortimer, K., Jones, G.J., SAE Tech. Pap. 2001-01-3527
[43] ASTM D6890-09 "Standard Test Method for Determination of Ignition Delay and Derived Cetane Number (DCN) of Diesel Fuel Oils by Combustion in a Constant Volume Chamber", ASTM International, 100 Barr Harbor Drive, PO Box C700, West Conshohocken, PA 19428-2959. United States
[44] ASTM D613-10a "Standard Test Method for Cetane Number of Diesel Fuel Oil", ASTM International, 100 Barr Harbor Drive, PO Box C700, West Conshohocken, PA 19428-2959. United States
[45] ASTM D976 "Standard Test Method for Calculated Cetane Index of Distillate Fuels", ASTM International, 100 Barr Harbor Drive, PO Box C700, West Conshohocken, PA 19428-2959. United States
[46] Haas, F.M. Shim, J., Ramcharan, A.M., Dryer, F.L, "Ignition Quality Evaluation of Valerate Alkyl Esters", Work in Progress Poster, 34th International Symposium on Combustion, Warsaw Poland, July 30-Aug 3.
[47] Dooley, S. Won, S.H., Chaos, M., Heyne, J., Ju, Y., Dryer, F.L., Kumar, K., Sung, C-J., Wang, H., Oehlschlaeger, M.A., Santoro, R.J., Litzinger T.A., 'Jet Fuel Surrogate Formulated by Real Fuel Properties', *Combust Flame* (2010) 157:2333-2339.
[48] Dooley, S., Won, S.H., Heyne, J., Farouk, T.I., Ju, Y., Dryer, F.L., Kumar, K., Hui, X., Sung, C-J., Wang, H., Oehlschlaeger, M.A., Litzinger, T.A., Santoro, R.J., Malewecki, T.,

Brezinsky, K., "The Experimental Evaluation of a Methodology for Surrogate Fuel Formulation to Emulate Gas Phase Combustion Kinetic Phenomena", *Combust Flame* (2012) 159: 1444-4466.

[49] Calcote, H. F., Manos, D. M., "Effect of Molecular Structure on Incipient Soot Formation," *Combust Flame* (1983) 49:289–304.

[50] Olson, D. B., Pickens, J. C., Gill, R. J., "The Effects of Molecular Structure on Soot Formation II. Diffusion Flames," *Combust Flame* (1985) 62:43–60

[51] ASTM D1322 "Standard Test Method for Smoke Point of Kerosine and Aviation Turbine Fuel", ASTM International, 100 Barr Harbor Drive, PO Box C700, West Conshohocken, PA 19428-2959. United States

[52] Hunt, R. A. J., "Relation of Smoke Point to Molecular Structure," *Ind Eng Chem* (1953) 45(3):602–606.

[53] Mensch, A., Santoro, R. J., Litzinger, T. A., Lee, S.-Y., "Sooting Characteristics of Surrogates for Jet Fuels," *Combust Flame* (2010) 157(6):1097-1105.

[54] Gill, R. J., Olson, D. B., "Estimation of Soot Thresholds for Fuel Mixtures," *Combust Sci Tech* (1984) 40:307–315.

[55] Li, L., Sunderland, P.B. "An Improved Method of Smoke Point Normalization", *Combust Sci Technol* (2012) 184: 829-841.

[56] McEnally, C. S., Pfefferle, L. D., "Improved Sooting Tendency Measurements for Aromatic Hydrocarbons and Their Implications for Naphthalene Formation Pathways," *Combust Flame* (2007) 148:210-222.

[57] Holley, A.T., You, X.Q., Dames, E. Wang, H., Egolfopoulos, F.N., *Proc Combust Inst* (2009) 32:1157-1163

[58] ASTM D2502 "Standard Test Method for Estimation of Mean Relative Molecular Mass of Petroleum Oils from Viscosity Measurements", International, 100 Barr Harbor Drive, PO Box C700, West Conshohocken, PA 19428-2959. United States

[59] ASTM D2503, "Standard Test Method for Relative Molecular Mass (Molecular Weight) of Hydrocarbons by Thermoelectric Measurement of Vapor", ASTM International, 100 Barr Harbor Drive, PO Box C700, West Conshohocken, PA 19428-2959. United States

[60] Schneider, D.F. "Select the Right Hydrocarbon Molecular Weight Correlation", Strauss Engineering, Inc, PMB 339, 2951 Marina Bay Drive, #130, League City, Tx 77573 (1998).

[61] Dryer, F.L., Won, S.H., Dooley, S., "A Measurement Process for the Determination of the Mixture Averaged Molecular Weight of Complex Mixtures", Provisional Patent Disclosure, Princeton University, Princeton NJ 08544. February 17, 2012.

[62] Dooley, S. Won, S.H., Chaos, M., Heyne, J., Ju, Y., Dryer, F.L., Kumar, K., Sung, C-J., Wang, H., Oehlschlaeger, M.A., Santoro, R.J., Litzinger T.A., Jet Fuel Surrogate Formulated by Real Fuel Properties", *Combust Flame* (2010) 157:2333-2339.

[63] Dooley, S., Won, S.H., Heyne, J., Farouk, T.I., Ju, Y., Dryer, F.L., Kumar, K., Hui, X., Sung, C-J., Wang, H., Oehlschlaeger, M.A., Litzinger, T.A., Santoro, R.J., Malewecki, T., Brezinsky, K., "The Experimental Evaluation of a Methodology for Surrogate Fuel Formulation to Emulate Gas Phase Combustion Kinetic Phenomena", *Combust Flame* (2012) 159: 1444-4466.

[64] Bruno, T.J., Laesecke, A., Outcalt, S.L., Seelig, H-D., Smith, B.L., "Properties of a 50/50 Mixture of Jet-A + S-8", NISTIR 6647, National Institute of Standards and Technology Thermophysical Properties Division 325 Broadway, Boulder, CO 80305, March 2007.

[65] ASTM D2789, "Standard Test Method for Hydrocarbon Types in Low Olefinic Gasoline by Mass Spectrometry", ASTM International, 100 Barr Harbor Drive, PO Box C700, West Conshohocken, PA 19428-2959. United States.
[66] Widegren, J.A., Bruno, T.J., "Thermal Decomposition Kinetics of the Aviation Turbine Fuel Jet A", *Ind Eng Chem Res* (2008) 47:4342-4348.
[67] Shafer, L.M., Edwards, T. "Speciated Naphthalene Analysis in Liquid Transportation Fuels", 12th International Conference on Stability, Handling, and Use of Liquid Fuels, Sarasota, Florida USA 16-20 October 2011.
[68] Shafer, L, Striebich, R., Gomach, J., Edwards, T., "Chemical Class Composition of Commercial Jet Fuels and Other Specialty Kerosene Fuels", AIAA Paper 2006-7972.
[69] ASTM D2425, "Standard Test Method for Relative Molecular Mass (Molecular Weight) of Hydrocarbons by Thermoelectric Measurement of Vapor Pressure", ASTM International, 100 Barr Harbor Drive, PO Box C700, West Conshohocken, PA 19428-2959. United States.
[70] Won, S.H., Dooley, S., Dryer, F.L., Ju, Y., "A Radical Index for the Determination of the Chemical Kinetic Contribution to Diffusion Flame Extinction of Large Hydrocarbon Fuels", *Combust Flame* (2011) 159:541-551.
[71] Yang, Y., Boehman, Al., Santoro, R.J., "A Study of Jet Fuel Sooting Tendency using the Threshold Sooting Index (TSI) Model", *Combust. Flame* (2007) 149:191-205
[72] Katritzky, A.R., Kuanar, M., Slavov, S., Hall, C.D., "Quantitative Correlation of Physical and Chemical Properties with Chemical Structure: Utility for Prediction", *Chem Rev* (2010) 110:5714–5789.
[73] Gosh, P., Jaffee, B., "Detailed Composition-Based Model for Predicting the Cetane Number of Diesel Fuels", *Ind Eng Chem Res* (2006) 45:346-351.
[74] Gosh, P., Hickey, K. J., Jaffee, B., "Development of a Detailed Gasoline Composition-Based Octane Model", *Ind Eng Chem Res* (2006) 45:337-345.
[75] Albahri, T.A., "Structural Group Contribution Methods for Predicting the Octane Number of Pure Hydrocarbon Liquids", *Ind Eng Chem Res* (2003) 42:657-662.
[76] Pepiot-Desjardins, P., Pitsch, H., Malhotra, R., S.R. Kirby, S.R., Boehman, A.L., "Structural Group Analysis for Soot Reduction Tendency of Oxygenated Fuels", *Combust Flame* (2008) 154:191–205.
[77] Yan, S., Eddings, E.G., Palotas, A.B., Pugmire, R.J., Sarofim, A.F., "Prediction of Sooting Tendency for Hydrocarbon Liquids in Diffusion Flames", *Energy Fuels* (2005) 19:2408-2415.
[78] Benson, S.W., *Thermochemical Kinetics,* 1976, John Wiley and Sons, Inc., New York
[79] Simmie, J.M., "Detailed Chemical Kinetic Models for the Combustion of Hydrocarbon Fuels", *Prog Energy Combust Sci* (2003) 29:599-634.
[80] Battin-Leclerc, F., "Detailed Chemical Kinetic Models for the Low-temperature Combustion of Hydrocarbons with Application to Gasoline and Diesel Fuel Surrogates", *Prog Energy Combust Sci* (2008) 34: 440-498.
[81] Battin-Leclerc, F., Blurock, E., Bounaceur, R., Fournet, R., Glaude, P.A., Herbinet, O., Sirjean, B., Warth, V., "Towards Cleaner Combustion Engines through Ground Breaking Detailed Chemical Kinetic Models", *Chem. Soc. Rev.*, (2011) 40:4762-4782.
[82] Zhang, H.R., Eddings, E.G., Sarofim, A.F., Mayne, C.L., Yang, Z., Pugmire, R.J., "Selection of Surrogates for Jet Fuels," in *Combustion Generated Fine Carbonaceous Particles*, eds. H. Bockhorn, A. D'Anna, A.F. Sarofim, H. Wang, KIT Scientific Publishing (ISBN 978-3-86644-441-6), 2009.

[83] Mueller, C.J., Cannella, W.J., Bruno, T.J., Bunting, B., Dettman, H.D., Franz, J.A., Huber, M.L., Natarajan, M., Pitz, W.J., Ratcliff M.A., Wright, K., "Methodology for Formulating Diesel Surrogate Fuels with Accurate Compositional, Ignition-Quality, and Volatility Characteristics", *Energy Fuels* (2012) 26:3284-3303.
[84] Quann, R.J., Jafee, S.B., "Structure-Oriented Lumping: Describing the Chemistry of Complex Hydrocarbon Mixtures", *Ind Eng Chem Res* (1992) 31:2483-2497.
[85] Quann, R.J., Jafee, S.B., "Building Useful Models of Complex Reaction Systems in Petroleum Refining", *Chem Eng Sci* (1996) 51:1615-1635.
[86] Silke, E.J., Pitz, W.J., Westbrook, C.K., "Detailed Chemical Kinetic Modeling of Cyclohexane Oxidation", *J Phys Chem A* (2007) 111:3761-3775.
[87] Dooley, S. Won, S.H., Ju, Y., Dryer, F.L., Wang, H., Oehlschlaeger, M.A., "The Combustion Kinetics of a Synthetic Paraffinic Jet Aviation Fuel and a Fundamentally Formulated, Experimentally Validated Surrogate Fuel", *Combust Flame* (2012) 159: 3014-3020.
[88] Naik C.V., Puduppakkam K. V., Meeks E., Wang Y.L., Feng Q., Tsotsis T.T., " Detailed Chemical Kinetic Mechanism for Surrogates of Alternative Jet Fuels", *Combust Flame* (2011) 158:434-445.
[89] Gokulakrishnan P., Klassen M. S., Roby R.J., "Ignition Characteristics of a Fischer Tropsch Synthetic Jet Fuel", Proceeding of the International Gas Turbine Institute, ASME Turbo-Expo, Berlin, Germany, Paper # GT2008-51211.
[90] Ranzi E., Frassoldati A., Granata S., Faravelli T., "Wide-Range Kinetic Modeling Study of the Pyrolysis, Partial Oxidation, and Combustion of Heavy n-Alkanes" *Ind Eng Chem Res* (2005) 44:5170-5183. http://www.chem.polimi.it/CRECKModeling/kinetic.html (Version POLIMI_TOT1112)
[91] Jahangirian S., Healy D., Sarathy M., Dooley S., Mehl M., Pitz W.J., Dryer F.L., Curran H.J., Westbrook C.K. "Experimental and Modeling Study of 2-methylheptane Oxidation in a Flow Reactor, Shock Tube, and Rapid Compression Machine" *Fall Meeting of The Eastern United States Section of The Combustion Institute*, University of Connecticut, October 2011.
[92] Sun W., Chen Z., Gou X., Ju Y., "A Path Flux Analysis Method for the Reduction of Detailed Chemical Kinetic Mechanisms" *Combust Flame* (2010) 157:1298-1307.
[93] Sarathy S.M., Yeung C., Westbrook C.K., Pitz W.J., Mehl M., Thomson M.J., "An Experimental and Kinetic Modeling Study of n-octane and 2-methylheptane in an Opposed-Flow Diffusion Flame" *Combust Flame* (2011) 158:1277-1287.
[94] Jahangirian S., Dooley S., Haas F. M., Dryer F.L., "A Detailed Experimental and Kinetic Modeling Study of n-Decane Oxidation at Elevated Pressures" *Combust. Flame* (2012) 159:30-43.
[95] NORPAR 12 Hydrocarbon Fluid, Materials Safety Data Sheet, Product Code 133598, Exxon Company, Houston TX 72252-2180, Issue Date 01/21/00.
[96] ISOPAR-L Hydrocarbon Fluid, Materials Safety Data Sheet, Product Code 133465, Exxon Company, Houston TX 72252-2180, Issue Date 01/21/00
[97] AROMATIC 150 Product Safety Summary, ExxonMobil Chemical Company, Houston, TX 77079-1398, updated June 2009.
[98] Petroleum Quality Information System, DESQ Report, 2009. http://www.desc.dla.mil/DCM/Files/2009PQISreport.pdf.

[99] Handbook of Aviation Fuel Properties—2004 Third Edition, CRC Report No. 635, CRC, Inc., Alpharetta, GA 30022.
[100] Lu, T., Law, C.K., "Toward Accommodating Realistic Fuel Chemistry in Large-Scale Computation", *Prog Energy Combust Sci* (2009) 35:192-215.
[101] Liang, L., Stevens, J.G., Raman, S., Farrell, J.T., "The Use of Dynamic Adaptive Chemistry in Combustion Simulation of Gasoline Surrogate Fuels *", Combust Flame* (2009) 156:1493-1502.
[102] Ranzi, E., Dente, M., Bozzano, G., Goldaniga, A., Faravelli, T., "Lumping Procedures in Detailed Kinetic Modeling of Gasification, Pyrolysis, Partial Oxidation and Combustion of Hydrocarbon Mixtures", *Prog Energy Combust Sci* (2001) 27:99-139.
[103] Slavinskaya, N., Zizin, A., Aigner, M., "On Model Design of a Surrogate Fuel Formulation", *J Eng Gas Turb Power* (2010) 132:111501-1-11.
[104] Bruno, T.J., Ott, L.S., Lovestead, T.M., Huber, M.L., "Relating Complex Fluid Composition and Thermophysical Properties with the Advanced Distillation Curve Approach", *Chem Eng Technol* (2010) 33:363-376.
[105] Bruno, T.J., "Improvements in the Measurement of Distillation Curves. 1. A Composition-Explicit Approach", *Ind Eng Chem Res* (2006) 45:4371-4380.
[106] Bruno, T.J., Smith, B.L., "Evaluation of the Physicochemical Authenticity of Aviation Kerosene Surrogate Mixtures. Part 1: Analysis of Volatility with the Advanced Distillation Curve", *Energy Fuels* (2010) 24:4266-4276.
[107] Bruno, T.J., Huber, M.L., "Evaluation of the Physicochemical Authenticity of Aviation Kerosene Surrogate Mixtures. Part 2: Analysis and Prediction of Thermophysical Properties", *Energy Fuels* (2010) 24 :4277-4284.
[108] Huber, M.L., Lemmon, E.W., Bruno, T.J., "Surrogate Mixture Models for the Thermophysical Properties of Aviation Fuel Jet-A", *Energy Fuels* (2010) 24:3565-3571.
[109] Alnajjar, M., Cannella, B., Dettman, H., Fairbridge, C., Franz, J., Gallant, T., Gieleciak, R., Hager, D., Lay, C., Lewis, S., Ratcliff, M., Sluder, S., Storey, J., Yin, H., Zigler, B., CRC Report No. FACE-1 (2010), Coordinating Research Council, Inc., Alpharetta, GA.
[110] Lemmon, E.W. Huber, L.H., McLinden, M.O., NIST Standard Reference Database 23: Reference Fluid Thermodynamic and Transport Properties-REFPROP, Version 9.0, National Institute of Standards and Technology, Standard Reference Data Program, Gaithersburg, 2010.
[111] NIST Chemistry WebBook, NIST Standard Reference Database Number 69, Eds. P.J. Linstrom and W.G. Mallard.
[112] Edwards, T., Maurice, L.Q., "Surrogate Mixtures to Represent Complex Aviation and Rocket Fuels", *J Prop Power* 17 (2001) 461-466.
[113] Liu, Y.C., Savas, A.J., Avedisian, C.T., "Surrogate Fuel Development Based on Droplet Combustion: Comparison of Multi-component Mixtures with an Aviation Fuel", 50th AIAA Aerospace Sciences Meeting including the New Horizons Forum and Aerospace Exposition 09 - 12 January 2012, Nashville, Tennessee. Paper No. AIAA 2012-1253
[114] Farouk, T.I., Liu, Y.C., Savas, A.J., Avedisian, C.T., Dryer, F.L., "Sub-millimeter Sized Methyl Butanoate Droplet Combustion: Microgravity Experiments and Detailed Numerical Modeling", *Proc Combust Ins* (2012) 34. http://dx.doi.org/10.1016/j.proci.2012.07.074
[115] Malewicki, T., Brezinsky, K., "Experimental and Modeling Study on the Pyrolysis and Oxidation of n-Decane and n-Dodecane", *Proc Combust Ins* (2012) 34. http://dx.doi.org/10.1016/j.proci.2012.06.156.

[116] Malewicki, T., Comandini, A., Brezinsky, K., "Experimental and Modeling Study on the Pyrolysis and Oxidation of iso-Octane", *Proc Combust Ins* (2012) 34. http://dx.doi.org/10.1016/j.proci.2012.06.137
[117] Klotz, S., Brezinsky, K., Glassman, I., "Modeling, the Combustion of Toluene-Butane Blends", *Proc Combust Ins* (1998) 27:337-344. *Base Model for Toluene. AFOSR No. 91-0431.*
[118] Sivaramakrishnan, R., Tranter, R.S., Brezinsky, K., "High-pressure, High-temperature Oxidation of Toluene", *Combust Flame* (2004) 139:340-350. *Base model for higher alkyl aromatics. DOE/BES DE-FG0298ER14897.*
[119] Gudiyella, S., Malewicki, T., Comandini, A., Brezinsky, K., "High Pressure Study of m-Xylene Oxidation", *Combust Flame* (2011) 158:687–704. *Base model for higher alkyl aromatics. SERDP, PN WP1575.*
[120] Gudiyella, S., Brezinsky, K., "High Pressure Study of n-Propylbenzene Oxidation", *Combust Flame* (2012) 159:940–958.
[121] Gudiyella, S., Brezinsky, K., "High Pressure Study of 1,3,5-Trimethylbenzene Oxidation", *Combust Flame* (2012). http://dx.doi.org/10.1016/j.combustflame.2012.06.014
[122] Malewicki, T., Gudiyella, S., Brezinsky K., "Experimental and Modeling Study on the Oxidation of Jet A and the 2nd Generation Surrogate Fuel", *Combust Flame* (2012) Accepted.
[123] Metcalfe, W. K., Dooley, S., Dryer, F. L., "Comprehensive Detailed Chemical Kinetic Modeling Study of Toluene Oxidation", *Energy Fuels* (2011) 25:4915-4936.
[124] Won SH, Dooley S, Dryer FL, Ju Y. Kinetic effects of aromatic molecular structures on diffusion flame extinction. *Proc Combust Inst* (2011) 33(1):1163–70.
[125] Wang H, Oehlschlaeger MA, Dooley S, Dryer FL. "A Shock Tube and Kinetic Modeling Study of the Autoignition of n-propylbenzene", In: 7th US national technical meeting of the combustion institute, Atlanta, GA; 2011
[126] Dooley, S., Diévart, P., Kim, H.H., Won, S.H., Ju, Y., Dryer F.L., Wang, W., Oehlschlaeger, M. "The Combustion Properties of 1,3,5-Trimethylbenzene and a Kinetic Model", *Fuel* Submitted, September, (2012).
[127] Hui, X., Kumar, K., Sung, C-J., Dooley, S., Dryer, "Laminar Flame Speeds and Extinction Stretch Rates of Selected Aromatic Hydrocarbons", *Fuel* (2012) 97:695–702.
[128] Dooley, S., Dryer, F.L., Farouk, T.I., Won, S.H., "Reduced Kinetic Model for the Combustion of Jet Propulsion Fuels", 51st AIAA Aerospace Sciences Meeting, Grapevine, Texas. 7-10 January 2013.

2.8. Archival Publications

S. Dooley, S.H. Won, M. Chaos, J. Heyne, Y. Ju, F. L. Dryer, K. Kumar, C-J. Sung, H. Wang, M. A. Oehlschlaeger, R.J., Santoro, T. A. Litzinger. A Jet Fuel Surrogate Formulated by Real Fuel Properties, *Combust Flame* (2010) 157:2333-2339.

S. Jahangirian, S. Dooley, F.M. Haas, F.L. Dryer. A Detailed Experimental and Kinetic Modeling Study of n-Decane Oxidation at Elevated Pressures, *Combust Flame* (2012) 159:30-43.

S.H. Won, S. S. Dooley, F.L. Dryer, Y. Ju. Kinetic Effect of Molecular Structure on Extinction Limit of Aromatic Diffusion Flames, *Proc Combust Ins* (2011) 33:1163-1170.

S.H. Won, S. Dooley, F. L. Dryer, and Y. Ju. A Radical Index for the Determination of the Chemical Kinetic Contribution to Diffusion Flame Extinction of Large Hydrocarbon Fuels, *Combust Flame* (2011) 159:541-551.

S. Dooley, S.H. Won, J. Heyne, T.I. Farouk, Y. Ju, F.L. Dryer, K. Kumar, X. Hui, C-J. Sung, H. Wang, M. A. Oehlschlaeger, T.A. Litzinger, R.J. Santoro, T. Malewecki, K. Brezinsky, The Experimental Evaluation of a Methodology for Surrogate Fuel Formulation to Emulate Gas Phase Combustion Kinetic Phenomena, *Combust Flame* (2012) 159: 1444-4466.

S. Dooley, S.H. Won, Y. Ju, F.L. Dryer, H. Wang, M. A. Oehlschlaeger. The Combustion Kinetics of a Synthetic Paraffinic Jet Aviation Fuel and a Fundamentally Formulated, Experimentally Validated Surrogate Fuel, *Combust Flame* (2012) 159: 3014-3020.

X. Hui, K. Kumar, C. J. Sung, S. Dooley, F. L. Dryer. "Laminar Flame Speeds and Extinction Stretch Rates of Selected Aromatic Hydrocarbons, *Fuel* (2012) 97:695–702.

S. Dooley, P. Diévart, P., H.H. Kim, S.H. Won, Y. Ju, F.L. Dryer W., Wang, M. Oehlschlaeger. The Combustion Properties of 1,3,5-Trimethylbenzene and a Kinetic Model. *Fuel* Submitted, September, (2012).

S. Jahangirian, S. Dooley, F.L. Dryer, V. Iyer, T.A. Litzinger, R.J. Santoro. Emulating the Combustion Behavior of Real Jet Aviation Fuels by Surrogate Mixtures from Solvent Blends, To be submitted to *Energy and Fuels* Oct, 2012.

2.9. Abstracts and Preprints

S. Dooley, S.H. Won, M. Chaos, J. Heyne, Y. Ju, F. L. Dryer, K. Kamal, C. J. Sung, H. Wang, M. A. Oehlschlaeger, R. J. Santoro, T. A. Litzinger, A Jet Fuel Surrogate Formulated By Real Fuel Properties, *Technical Meeting of the Western States Section of the Combustion Institute*, Boulder, Colorado, March 23, 2010.

V. Iyer, S. Iyer, S. Dooley, M. Linevsky, T. Litzinger, C. Mordaunt, R. Santoro, F. L. Dryer. Comparison of Sooting Propensity of JP-8 with its Surrogates in a Wick Burner and a Model Gas Turbine Combustor, Fall Technical Meeting of the Eastern States Section of the Combustion Institute Hosted by the University of Connecticut, Storrs, CT Oct. 9-12, 2011.

S. Jahangirian, S. Dooley, F.L. Dryer, V. Iyer, T.A. Litzinger, R.J. Santoro. Emulating the Combustion Behavior of Real Jet Aviation Fuels by Surrogate Mixtures from Solvent Blends, Fall Technical Meeting of the Eastern States Section of the Combustion Institute Hosted by the University of Connecticut, Storrs, CT Oct. 9-12, 2011.

V. Iyer, S. Dooley, S. Iyer, F.L. Dryer, T. A. Litzinger, C. J. Mordaunt and R. J. Santoro. Emulating the Sooting Propensity of JP-8 with Surrogate Fuels from Solvent Mixtures, 50th AIAA Aerospace Sciences Meeting, 9-12 January 2012, Nashville TN.

S. Dooley, F.L. Dryer, T.I. Farouk, S.H. Won, "A Reduced Kinetic Model for the Combustion of Jet Propulsion Fuels", 51st AIAA Aerospace Sciences Meeting, Grapevine, Texas. 7-10 January 2013. Abstract Accepted.

2.10. Presentations

Invited Speaker, "Combustion Chemistry for Petroleum-Derived and Alternative Fuels: Surrogate Fuel Mixtures and Models", University of Illinois, Urbana-Champaign, December 4, 2007.

F.L. Dryer, Invited Speaker, "Petroleum Derived and Low Carbon Intensity Alternative Aircraft Fuels: Long term Production and Real Fuel Modeling Concepts", Institute for Combustion Engines (VKA), RWTH Aachen University, Aachen Germany, June 26, 2008.

F.L. Dryer, Invited Speaker, "Petroleum Derived and Low Carbon Intensity Alternative Aircraft Fuels: Long term Production and Real Fuel Modeling Concepts", United Technology Research Center, East Hartford, CT, September 22, 2008.

F.L. Dryer, Invited Speaker, "Alternative Fuels: Long term Production and Real Fuel Modeling Concepts", Argonne National Laboratory, Argonne, IL, May 4, 2009.

F.L. Dryer, Invited Panel Speaker, "Evaluation of Combustion Performance of Alternative Aviation Fuels", 46th AIAA/ASME/SAE/ASEE Joint Propulsion Conference & Exhibit, Nashville, TN, July 25-28, 2010.

Invited Speaker, College of Engineering & CS MMAE Distinguished Speaker Series, University of Central Florida, Orlando, FL, Nov. 18,19, 2010.

F.L. Dryer, Invited Speaker, "Progress on the Formulation and Kinetic Modeling of Jet Fuel Surrogates: Synthetic Paraffinic Kerosenes", 49th Aerospace Sciences Meeting, Marriott Conference Center, Orlando, Fl, Jan. 4-8, 2011

F.L. Dryer, Invited Speaker, "Recent Studies on High-Hydrogen-Content Power Generation and Liquid Jet Aircraft Fuels," *GE Energy Combustion Symposium, GE Energy*, Greenville, SC, January 25−26, 2011.

F.L. Dryer, Invited Topical Speaker, "Surrogate Mixtures for Describing Real Fuel Combustion: Challenges and Recent Progress," 7th *US National Combustion Meeting (Combustion Institute)*, Georgia Institute of Technology, Atlanta, GA, March 20−23, 2011.

F.L. Dryer, Invited Speaker, "Surrogate Mixtures for Describing Real Fuel Combustion: Challenges and Recent Progress," *Technology Watch Day on Future Biofuels*, Tailor-Made Fuels from BioMass (TMFB), RWTH Aachen University, Aachen City, Germany, May 24, 2011.

F.L. Dryer, Invited Speaker, "Emulating the Combustion Behavior of Real Petroleum-Derived and Alternative Fuels", Bilger Lecture, 2011 Australian Combustion Symposium, University of Newcastle, Whitesands Conference Centre, Shoal Bay Resort and Spa, NSW Australia, November 28 – 30, 2011.

F.L. Dryer, Invited Speaker, "Aircraft Transportation Fuels for the 21st Century" , Siemens Energy Center, UCF College of Engineering & Computer Science , Orlando, FL, April 6, 2012

F.L. Dryer, Invited Speaker, "Formulating Surrogate Fuel Compositions and Models for Emulating Petroleum Derived and Alternative Jet Aviation Fuels", National Institute of Standards and Technology, Boulder , CO, May 3, 2012.

F.L. Dryer, Invited Speaker, "Formulating Surrogate Fuel Compositions and Models for Emulating Petroleum Derived and Alternative Jet Aviation Fuels", Colorado State University, Fort Collins, CO, May 4, 2012.

2.11. Graduate Theses

None

2.12. Personnel

Graduate Students: Francis M. Haas, Joshua Heyne

Undergraduate Students: Amanda Ramcharan, Jennifer Shim

Professional Research Staff: Stephen Dooley, Tanvir Farouk, Saeed Jahangirian, Wayne Metcalfe, Peter Veloo

Professional Technical Staff: Timothy Bennett, Joseph Sivo, John Grieb

3. Princeton University (Princeton2) – Y. Ju

3.1. Abstract

The research led by Prof. Yiguang Ju at Princeton University for the MURI program has covered a broad range of fundamental studies in both experiments and numerical modeling. In the experiments, three experimental platforms, a counterflow burner system, and a heated spherical combustion chamber have been developed and successfully utilized to provide the fundamental insights in the evaluation of surrogate formulation methodology. New experimental data for model validation and new concept of transport weighted enthalpy and radical index were developed to understand flame chemistry and surrogate model construction as well as fuel screening. In numerical modeling, a detailed chemical kinetic model for 1,3,5-trimethylbezene oxidation has been developed. In model reduction, a multi-generation path flux analysis algorithm and a multi-time scale integration scheme are developed and they have served as a major numerical tool for the MURI research team and others in combustion community.

3.2. Introduction

One of the research thrusts at Princeton University led by Prof. Yiguang Ju was to develop the experimental platforms which can provide fundamental database of flames particularly for large hydrocarbon liquid fuels. Thus, the surrogate formulation methodology can be evaluated through experiment-to experiment comparisons between the targeted jet fuel and the surrogate mixtures, so that the ambiguity from modeling results can be eliminated. Two experimental platforms have been developed; a counterflow burner system to investigate the extinction behaviors of premixed and non-premixed flames and a heated spherical combustion chamber to determine the laminar flame speed and critical flame initiation radius in various pressure conditions. The counterflow burner system has been utilized to mainly provide the database of diffusion flame extinction for various molecular classes from n-alkanes, iso-alkanes, aromatics, real jet fuels, and their surrogate mixtures. A theoretical scaling analysis has been carried out to provide a new concept and tool, the transport-weighted enthalpy and radical index, to advance the understanding of flame chemistry and to screen surrogate mixtures and alternative fuels. The heated spherical combustion chamber has provided the measurements of laminar flame burning velocities and insights of flame initiation processes, the critical flame initiation radius for both n-alkanes and aromatic fuels. Since most of the results have been already published in the literature, these studies will be briefly summarized later.

The second research thrust was the development of chemical kinetic model for 1,3,5-trimethylbenzene oxidation, based on the toluene model, developed by Prof. Dryer's group at Princeton University. Although 1,3,5-trimethylbenzene has been identified as one of component fuels in the MURI 2nd generation surrogate mixtures, the absence of chemical kinetic model for this molecule has limited the modeling capability of the MURI team. The newly developed model has been comprehensively validated against wide range of measurements, ignition delays from shock tube, laminar flame speeds, extinction limits of premixed and non-premixed flames, and reactivity profiles from flow reactor. The model has been embedded in the MURI 2nd generation surrogate model and currently under the test against the experimental database accumulated in MURI teams.

The third research thrust is to develop numerical schemes which can allow us to handle extremely large chemical kinetic models developed for jet fuel surrogate under the MURI works. Two new numerical approaches, a multi-timescale (MTS) method and a multi-generation path flux analysis (PFA) method to reduce the detailed chemical kinetic model and integrate the reaction system computationally efficiently without loss of model fidelity have been developed. The MTS method can increase computation efficiency in combustion modeling by almost one-order with the same combustion kinetics. The PFA method considers the indirect couplings among the species in multi-generation of fuel oxidation. It can capture most of important fuel oxidation pathways and provides the better and precise predictability of the reduced model against global combustion properties, such as ignition delay, laminar flame burning velocity, and flame extinction. Moreover, the MTS and PFA methods have been embedded into an in-house DNS code, adaptive simulation of unsteady reactive flow (ASURF), to compute the unsteady flame propagation processes both efficiently and precisely. The PFA method has been extensively utilized in the broad avenue of MURI research program to validate the developed chemical kinetic models. The ASURF with PFA embedded has been also utilized to identify the roles of chemical kinetics and transport in unsteady n-decane/air premixed flame propagation, which has never been studied before.

Summary of Research Findings

3.3. Determination of fuel-specific chemical kinetics in diffusion flame extinction

The extinction limits of diffusion flame have been extensively measured in a counterflow configuration, since it provides a simple experimental platform to validate both chemical kinetics and transport models simultaneously [1-19]. As such, previous studies have mainly focused on simply evaluating the performance of chemical kinetic model of single pure component against the experimental measurements and analyzing the model performance using sensitivity or path flux analysis. It has been reported that the extinction limits of diffusion flames are mainly controlled by the complicated interactions among the energy density, transport, and chemical kinetics of fuel. However, there have been lacks of understandings on how these three aspects affect diffusion flame extinction quantitatively. Thus, it becomes a challenging problem if one wants to do fuel-to-fuel comparison based on diffusion flame extinctions. It becomes more problematic for the complicated large hydrocarbon mixtures to evaluate the performance of suggested surrogate mixture against real jet fuel.

Consequently, in this research task one of the main objectives in this MURI study is to develop a new method, which can isolate the contributions from energy density and transport from that of chemical kinetics of fuels in diffusion flame extinction for surrogate mixture validation. In order to achieve this goal, we have

1) *developed a counterflow burner system* which allows us to handle large hydrocarbon liquid fuels,

2) i*nvestigated the role of aromatic blending on n-alkane diffusion flames in extinction limits* to specify how the chemical kinetics controls the extinction limits,

3) *extended our knowledge to C_9 aromatic isomers to identify how the molecular structure of aromatic fuels affects the extinction limits* of diffusion flames by separating it from the effects of energy density and diffusion transport,

4) *developed a new flame extinction concept and correlation, the radical index and transport-weighted enthalpy* to isolate the contributions from energy density and transport impacts and to clearly demonstrate the chemical kinetic contribution. This universal correlation has been derived in a function of radical index and transport-weighted enthalpy for extinction limits of large hydrocarbon fuels, which encompass all the molecular classes (n-alkanes, iso-alkanes, and aromatics) and are tested in the entire MURI work. The result provided a predictable tool on the extinction limits of diffusion flames for the complicated surrogate mixture.

3.3.1. Development of counterflow burner system for the study of large hydrocarbon liquid fuels

The experimental configuration consisted of a counterflow burner, a vaporization system, flow controllers, an online Fourier transform infrared (FTIR) spectrometer, and a laser induced fluorescence imaging system as schematically shown in **Fig. 3.1**. The liquid fuel vaporization system includes a double concentric nozzle and a stainless steel chamber. The liquid fuels were supplied through the inner channel and the preheated nitrogen carrier gas flows co-axially along the outer channel to raise the temperature of the liquid fuel and to provide fuel atomization in the stainless steel chamber (300 cc volume). The liquid fuels were injected through the central nozzle with 0.2 mm inner diameter. The temperature of nitrogen co-flow into the nozzle was elevated by using an in-line electric heater (Omega) and monitored by a K-type thermocouple at the outlet of heater. To reduce the heat loss from the chamber and avoid fuel condensation, the outer surface of the chamber was surrounded by two electrical knuckle heaters. The temperature at the inside of the chamber was also monitored by a K-type thermocouple and used as a feedback to the electric heaters to maintain the temperature at 500 K at all flow rates. To confirm that there was no fuel thermal decomposition or concentration fluctuation at the specified

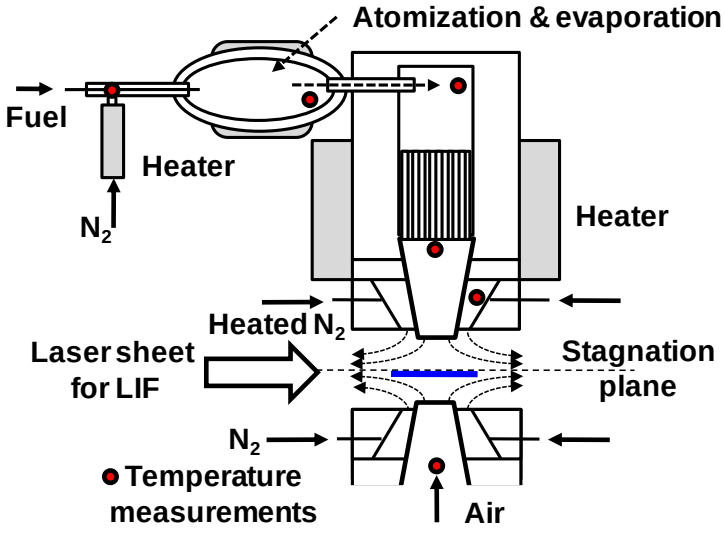

Figure 3.1. Schematic of experimental setup

vaporizing temperature, an FTIR spectrometer was used to detect production of hydrocarbon fuel molecules. No fuel fragments were observed and the fluctuation of fuel concentration was found to be less than 1 % of fuel mole fraction. The flow rate of liquid fuels was controlled by using a volumetric syringe pumps (ISCO, Model 314 or Harvard Apparatus, PHD 22/2000). The flow rates of nitrogen carrier gas and nitrogen co-flow in the counterflow flame were controlled by using calibrated sonic nozzles.

The vaporized fuel and nitrogen gaseous mixture was directly transported to the upper burner of the counterflow system. The upper burner was heated to 500 K and the temperatures at both the nozzle exit and 50 mm upstream from the nozzle exit were monitored. The electrical heater was PID controlled to maintain the fuel flow temperature at 500 K during the entire experimental process. The temperature variation during the variation of flow rate and fuel concentration was found to be within 10 K. However, at the steady state condition, the temperature change was maintained within 1 K. For the oxidizer stream, dry air was utilized and the temperature was also monitored and maintained at 298 K. All experiments were conducted at 1 atmosphere. The nozzle diameter of the fuel and oxidizer was 20 mm and the distance between two nozzles was varied from 9 to 15 mm consistently with repeatable results. The fuel and oxidizer nozzles were 50 mm long and 20 mm long honeycombs were installed 20 mm upstream from the nozzle exits. The flow uniformity at the nozzle exit was also confirmed by using a particle image velocimetry (PIV) system (TSI, Model 610034). To further verify the one-dimension approximation in the experiments, counterflow flame experiments with 13 mm i.d. nozzles were also conducted later. Consistent extinction strain rates for two different nozzle sizes were obtained, indicating that two-dimensional effects are negligible.

To measure the extinction strain rate precisely, two different methodologies were adopted and compared. First, the extinction strain rate was measured by gradually increasing the flow velocities of both the fuel and oxidizer in a small increment (~1% of strain rate) for fixed fuel fraction by matching the momentum of fuel and oxidizer streams to fix the stagnation plane halfway between the two nozzles. The second method was to decrease the fuel fraction by slowly decreasing the liquid fuel flow rate of volumetric syringe pump for fixed strain rate while maintaining a momentum balance. The results of the two methods showed good agreement within ± 5 % error. The strain rate a is defined as the gradient of axial flow velocities from the fuel and oxidizer sides, taking into account the density difference between fuel and oxidizer as below [17],

$$a = \frac{2U_o}{L}\left(1+\frac{U_f}{U_o}\sqrt{\frac{\rho_f}{\rho_o}}\right) \tag{1}$$

Here, ρ represents the density, U is flow velocity at the nozzle exit, L is the distance between fuel and oxidizer nozzles, and subscript f and o indicate fuel and oxidizer, respectively.

A planar laser induced fluorescence (PLIF) system was used to measure the distribution of OH radicals. The PLIF system consisted of an Nd:YAG laser (Spectra-Physics, Lab-170-10), a dye laser (Sirah, CSTR-G-30), and an ICCD camera (Princeton Instrument, PI-MAX2). The $Q_1(6)$ transition of OH is excited at the wavelength of 282.93 nm. To confirm the linear LIF regime, local OH LIF signals at different locations were monitored by increasing the laser power, and the

local saturation of LIF intensity was observed only at laser powers higher than 15 mJ/pulse. Accordingly, in experiments the pulse energy was maintained at 5 mJ/pulse. A laser sheet was produced using a 100 mm focal length concave cylindrical lens and a 500 mm focal length convex cylindrical lens. The focus of sheet beam was aligned to the center between the burner nozzles and the height of sheet beam was 80 mm. The fluorescence signal was captured at an angle of 90 degrees through UG-11 and WG-305 optical filters to reduce noise.

Estimation of the LIF quenching rate is important to minimize the uncertainty of measurements [20, 21]. The quenching rate of the LIF signal for n-decane/toluene diffusion flames was estimated by considering the major species numerically. However, the greater caution is required in the case of aromatic diffusion flames, since the current kinetic model does not fully describe the formation of PAHs, which has higher absorption coefficients at UV ranges as well as unknown quenching coefficients [22]. To determine the quenching effect of LIF signals, OH LIF images were sequentially taken with 2ns gate width by varying the delay time from the laser Q-switch output at the same flow condition for all aromatic fuels. The results were processed to obtain the decay curve of OH LIF signal normalized by the peak OH LIF signals. The LIF emission lifetime was around 8.26 ns from linear fitting for toluene diffusion flame. 1,2,4-trimethyl benzene (124TMB), 1,3,5-trimethylbenzene (135TMB), and n-propyl-benzene (nPB) diffusion flames reveal 1%, 21%, and 30% reduction of LIF emission lifetime compared to that of toluene, respectively. Since the measured emission lifetime was of the same order of the present laser pulse duration (~8 ns), the time resolution for OH excitation was not good enough to resolve the details of LIF signal decay characteristics. Nevertheless, the present method still showed the capability to observe the variation of decay time. Finally, the OH LIF intensities of different fuels have been normalized by their respective emission lifetimes to account for the different quenching effects of different fuels.

3.3.2. The kinetic coupling between aromatics and n-alkanes in diffusion flame

In order to investigate how the aromatic component will affect the extinction limits of n-alkane diffusion flame, which will be a typical case for jet fuel surrogate, the kinetic effects of toluene blending on the n-decane diffusion flame extinction limit by changing the radical pool concentration and heat release have been studied both experimentally and numerically. The

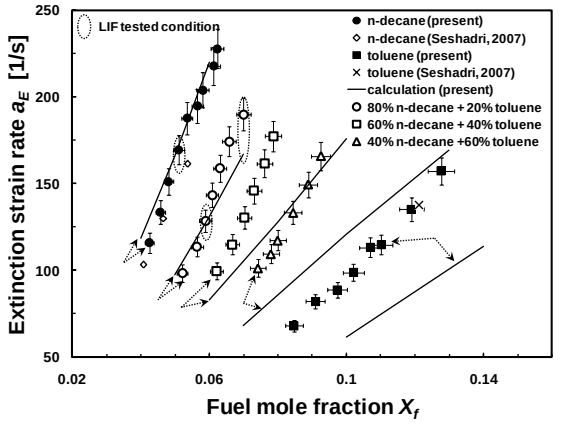

Figure 3.2. Extinction strain rates with fuel mole fraction for n-decane, toluene, and blended fuels.

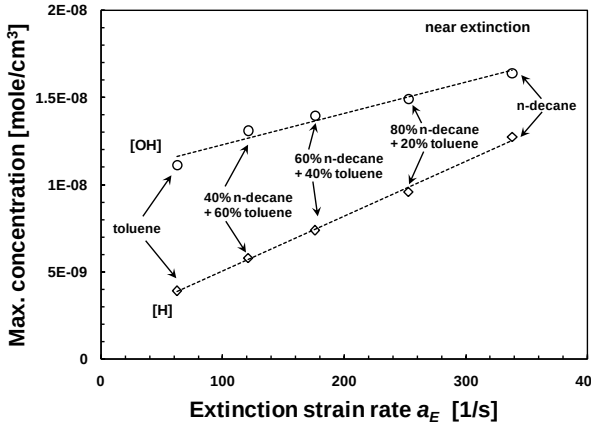

Figure 3.3. Calculated maximum radical concentrations with extinction strain rate for various blending condition at X_f = 0.1. (dashed lines: linear curve fits)

results showed that the extinction strain rate of n-decane/toluene/nitrogen flames decreased significantly with an increase of toluene addition (**Fig. 3.2**) and depended linearly on the maximum OH concentration (**Fig. 3.3**). It was found that the maximum OH concentration, which depends on the fuel H/C ratio, can be used as an index of the radical pool and chemical heat release rate via the reaction of OH with others. Experimental results further demonstrated that toluene addition in n-decane dramatically reduced the peak OH concentration via H abstraction and radical recombination reactions and accelerated flame extinction via kinetic coupling between toluene and n-decane mechanisms. Comparisons between experimentally measured OH concentrations with and without toluene addition in n-decane with numerical predictions revealed that the tested toluene mechanisms significantly over-predicted the radical destruction rate, leading to under-predicted extinction limits and OH concentrations (**Fig. 3.4**). In addition, sensitivity analysis of diffusive transport showed that in addition to n-decane and toluene, the transport of OH and H also affected considerably the extinction limit. The results suggested that an explicit prediction of the extinction limits of aromatics and alkane blended fuels can be established by using H/C ratio (or radical index) and the mean fuel molecular weight which represent the rates of radical production and the fuel transport, respectively.

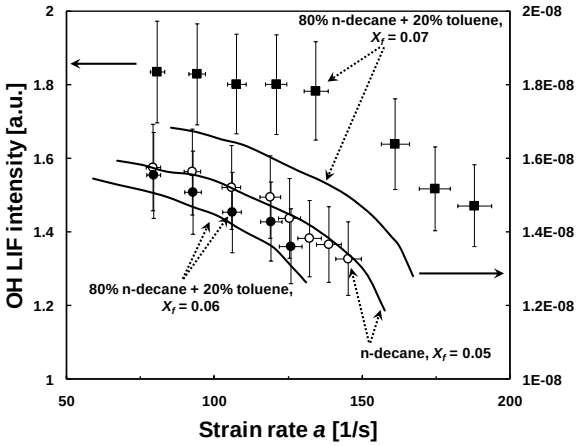

Figure 3.4. Comparison of OH radical with strain rate between LIF experiment and numerical calculation for n-decane and blended fuels. (symbol: experiment, line: calculation)

3.3.3. Effects of molecular structure on diffusion flame extinction for aromatic fuels

To understand the kinetic effects of molecular structure of aromatic fuels, the extinction limits of diffusion flames were investigated experimentally and numerically in the counterflow

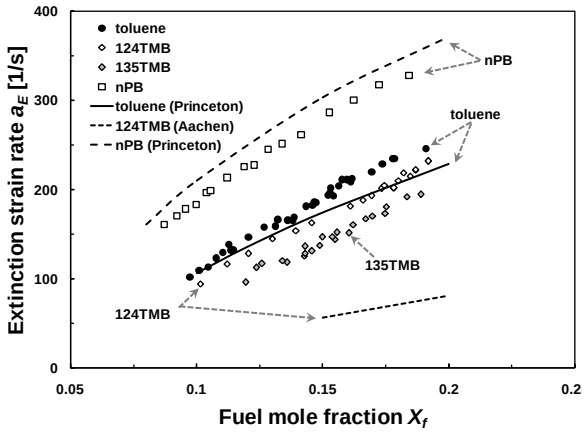

Figure 3.5. Experimental measurements on extinction strain rates of aromatic diffusion flames and comparison to numerical calculations.

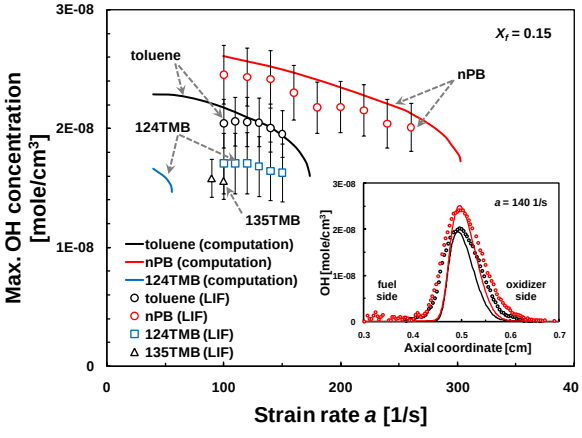

Figure 3.6. Maximum OH concentration as a function of strain rate for aromatic diffusion flames at X_f = 0.15. Inset: Comparisons of OH spatial profiles for nPB (red) and toluene (black) at a = 140 s^{-1}.

configuration for toluene, n-propylbenzene (nPB), 1,2,4-trimethylbenzene (124TMB), and 1,3,5-trimethylbenzene (135TMB). A semi-detailed nPB kinetic model is developed. The maximum OH concentrations have been quantitatively measured with planar LIF techniques.

Extinction limits of aromatic fuels are found to be dramatically changed according the molecular structure, ranked from highest to lowest as nPB, toluene, 124TMB, and 135TMB as shown in **Fig. 3.5**. The comparison between experiments and modeling reveals that the toluene and nPB models are able to properly reproduce the experimental results, whereas the 124TMB model under-estimates the formation of OH, thus leads to under-estimation of extinction limits as shown in **Fig. 3.6**. The analysis on the production and consumption pathways of OH shows production predominantly by three elementary chain-branching reactions, whereas the consumption pathways consist of chain propagation and termination reactions producing heat formation and fuel fragmentation [23]. It was also demonstrated that at the low strain rate, OH consumption through reactions with fuel fragments are negligible compared to that of heat formation, so that the maximum OH concentration is relatively insensitive to the change of strain rate. However, the maximum OH concentration starts to decrease significantly as strain rate nears the extinction limits, since the OH is being consumed considerably by the fuel fragments. Furthermore, it was found that nPB is mainly decomposed thermally at relatively low temperatures, whereas toluene and 124TMB are decomposed by H abstraction reactions by the H atom, which leads to a reduction of OH concentration. The OH index determined from LIF measurements is proposed to represent the radical pool production capability for the aromatics fuels. Finally, a linear correlation of extinction strain rates with OH index and fuel mole fraction was demonstrated in **Fig. 3.7** for all aromatic diffusion flames, allowing the kinetic effects of molecular structure on extinction of diffusion flames to be identified with OH concentration (OH index).

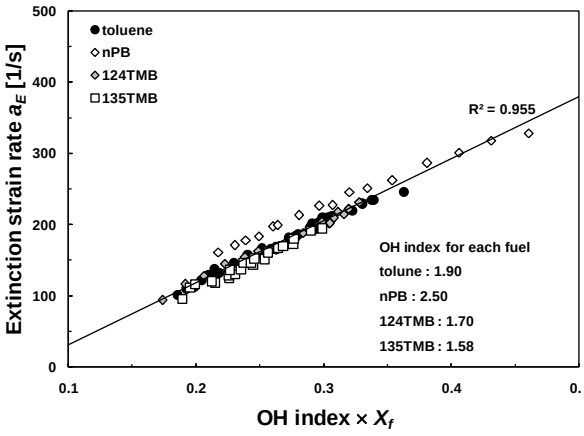

Figure 3.7. Linear correlation of extinction strain rate with fuel mole fraction and OH index for toluene, nPB, 124TMB, and 135TMB diffusion flames.

3.3.4. A new flame extinction concept: Radical Index and Transport-Weighted Enthalpy, to quantify fuel chemistry and transport in diffusion flames for large hydrocarbon fuels

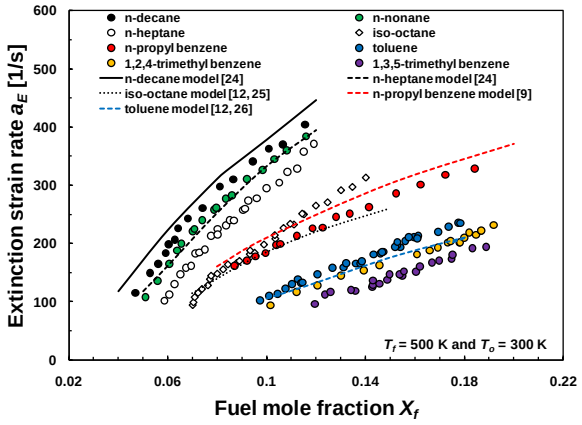

Figure 3.8. Extinction strain rates verses fuel mole fraction for n-decane, n-nonane, n-heptane, iso-octane, n-propyl benzene, toluene, 1,2,4-trimethyl benzene and 1,3,5-trimethyl benzene; symbols: experiments, line: numerical computations.

The extinction limits of diffusion flames have

been measured experimentally for a series of fuels including n-alkanes, iso-alkanes, and aromatic functionalities, specifically n-decane, n-nonane, n-heptane, iso-octane, toluene, n-propyl benzene, 1,2,4- and 1,3,5-trimethyl benzenes. Numerical computations for n-decane, n-heptane, iso-octane, n-propyl benzene and toluene, have been performed. The tested models reproduce the experimental measurements of extinction limits reasonably well as shown in **Fig. 3.8**. A scaling analysis reveals that to the first order the extinction limits of diffusion flames are proportional to the enthalpy of combustion and binary diffusion coefficient of fuels. A simple analysis on the diffusivity shows that binary diffusion coefficient of fuel is inversely proportional to the square-root of fuel molecular weight, especially for larger hydrocarbon fuels (>100 g/mole). In order to normalize the thermal and mass transport effects, the enthalpy flux via the diffusion process is evaluated by considering the enthalpy of combustion and fuel molecular weight, named as a *transport-weighted enthalpy*.

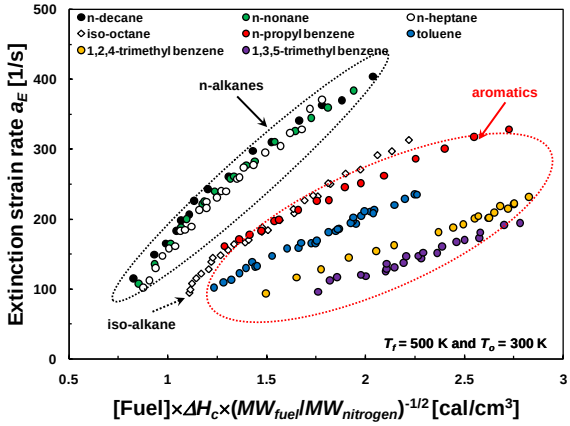

Figure 3.9. Extinction strain rates as a function of transport weighted enthalpy for all tested fuels; ΔH_c , enthalpy of combustion, *MW,* molecular weight.

$$\textit{Transport-weighted enthalpy} = [\text{Fuel}] \times \Delta H_c \times (MW_{fuel}/MW_{nitrogen})^{-1/2}$$

Here, [Fuel] is fuel concentration [mole/cm^3], ΔH_c is enthalpy of combustion [cal/mole], and *MW* is molecular weight of fuel [g/mole].

For the tested fuels, it is shown that the kinetic contribution to the extinction limit of diffusion flames owing to fuel chemistry can be elucidated by the transport-weighted enthalpy metric as shown in **Fig. 3.9**. To quantify the kinetic contribution of fuel chemistry, *a radical index* is

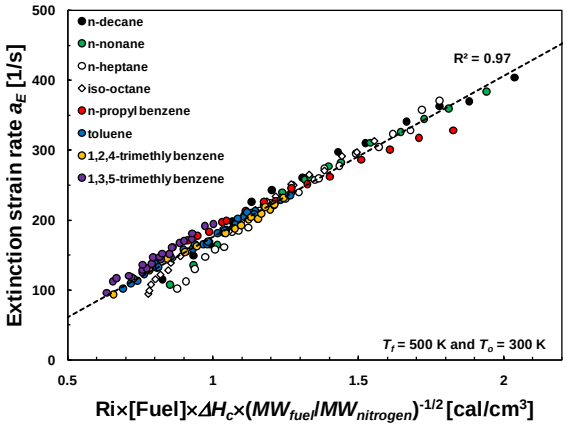

Figure 3.10. Universal correlation of extinction strain rates of all tested fuels in terms of Ri × [fuel] × ΔH_c × ($MW_{fuel}/MW_{nitrogen}$)$^{-1/2}$; line: linear fit of all experimental measurements.

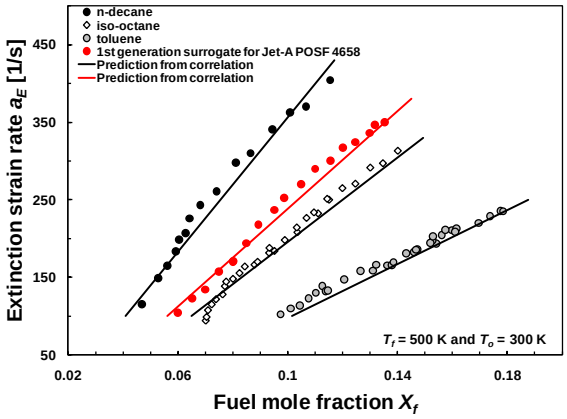

Figure 3.11. Demonstration of predictability with universal correlation for 1st generation surrogate mixture.

introduced based on the capability of a fuel to populate the OH radical concentration within the flame structure. The concept is fundamentally evaluated by analysis of both numerical computation and LIF measurements. Finally, the extinction strain rates of all studied hydrocarbon fuels are found to be the same as shown in **Fig. 3.10** when compared by the product of transport weighted enthalpy and the radical index, demonstrating a fundamental universal correlation for diffusion flame extinction. In addition, the predictability of the extinction limit by the universal correlation is successfully tested against the measured extinction limits of a multi-component surrogate fuel mixture as shown in **Fig. 3.11**. The radical index for a multi-component surrogate fuel mixture can obtained by the summation of radical index multiplied with mole fraction of each component in the mixture. The radical index and transport weighted enthalpy metrics provide important tools to understand the impact of fuel chemistry on flame extinction, thus allow for fundamental meaning to be derived from the comparison of the flame phenomena of surrogate fuels to those of target real fuels.

3.4. Critical flame initiation radius and unsteady propagation of premixed flames

Measuring flame speeds and understanding of the entire process from flame initiation to propagation is of great importance for successful relight and stability of gas turbine engines. One scientific question is whether a kinetic model which can reproduce the steady state flame speed can reproduce the unsteady flame trajectories. In order to address this issue fundamentally, the flame trajectories of outwardly propagating premixed flames have been rigorously investigated in spherical or cylindrical chambers mainly with gaseous hydrocarbon fuels. Jet fuel has an average carbon number of about twelve, thus lean jet fuel/air mixtures have a Lewis number far larger than the critical value, which may play a significant role on flame initiation and propagation processes. Furthermore, the existence of aromatic components reduces the reactivity, increasing the global activation energy. Accordingly, the development of spherical combustion chamber, which can measure laminar flame speeds and also observe entire process of flame initiation and propagation at various pressure conditions, particularly for large liquid hydrocarbon fuels, has been one of the main research thrusts in MURI.

The goals in this research task is to,

1) develop a heated spherical combustion chamber which enables combustion studies of liquid fuels with low vapor pressures,

2) examine quantitatively the unsteady flame propagation by simultaneously measuring both laminar flame speeds and critical flame initiation radius in the unsteady flame propagation,

3) identify the roles of chemical kinetics and transport impacts on this unsteady transition both experimentally and numerically. The n-decane/air mixtures have been tested at various equivalence ratios and pressures, since *n*-alkane plays a significant role in populating the active radical pool and controlling the high temperature reactivity of jet fuel and its surrogate mixture.

3.4.1. Development of a heated spherical combustion chamber for liquid fuel combustion

The experimental setup is composed of a nearly constant pressure spherical combustion bomb, fuel vaporization chamber, oven, and pressure release system as shown in **Fig. 3.12**. The spherical bomb has a 20 cm inner diameter. Two 250 μm diameter tungsten electrodes are installed at the top and bottom of the bomb and the upper electrode is mounted with a linear motion device to control the distance between the electrodes. The bomb is housed inside of an oven heated by two electrical heaters (total 2200 W) with an electric fan to achieve a uniform temperature distribution. K-type thermocouples are installed at the top and bottom of the oven to monitor temperature uniformity. The temperature inside the bomb is maintained at 400 K by PID controller and a K-type thermocouple. The inlet lines and vaporization chamber are also heated to the same temperature as the oven.

The bomb is filled with a combustible mixture using the partial pressure method. *n*-Decane (99% purity) is vaporized in a vaporization chamber (500 cm^3). Nitrogen (99.9%) and oxygen (99.5%) are added to the bomb through heated tubing. A pressure release system is installed for safety [24]. Flame propagation is visualized using a high speed Schlieren imaging [24]. Experimental data for flame radius less than 2.5 cm are used for the analysis to avoid the compression effect [24]. The pressure inside of the bomb rises less than 3 % when the flame radius reaches 2.5 cm, which is the upper limit of all experiments. Therefore, the near constant pressure assumption can be held [24, 25]. The confinement effects can be neglected because of the large inner diameter of the spherical bomb, so that the unstretched burned flame speed can be extracted from the linear relationship between burned flame speed and stretch rate $K = (2/R_f) \times (dR_f/dt)$. The laminar flame speed S_u^0 is found by using the calculated equilibrium density ratio.

The experimental uncertainties have been analyzed considering the errors due to pressure readings, temperature fluctuations, mixture concentration fluctuations, high-speed visualization, and data analysis. Errors from the Schlieren system were negligible because of the high speed (15000 fps) and high spatial resolution (86 pixel/cm). The overall uncertainty due to pressure, temperature and mixture fluctuations on laminar flame speed was estimated to be 1.1 - 7.2 % depending on the equivalence ratio using the RMS sum of each uncertainty estimated from [26]

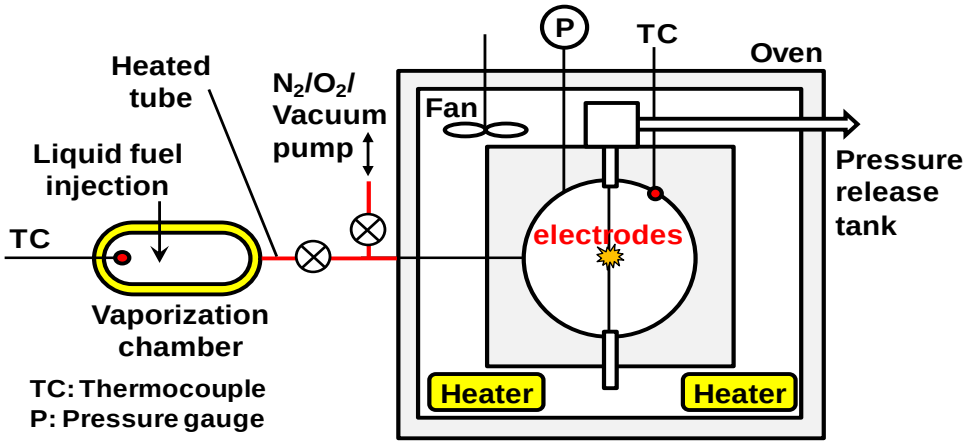

Figure 3.12. Schematic of experimental setup.

and [27]. The critical radius R_c was determined at the point that the flame trajectory started to deviate from the linear correlation, similar to [28]. The uncertainty in R_c was defined by the radius giving a 1% change in R^2 for the linear correlation between stretch rate and flame speed.

3.4.2. Numerical method for unsteady flame propagation with detailed kinetics

Chemical kinetic models from Chaos et al. [29] and Sirjean et al. [30] are used in calculations. The models are reduced with the Princeton Chem-RC software [31] for computational efficiency. The laminar flame speeds are calculated with CHEMKIN PREMIX [32]. Flame speeds have been calculated up to more than 600 grid points for all flame speed calculations to confirm no dependence on the number of grid points. The comparison between the detailed and reduced models has been made to validate the reduced model.

Unsteady flame propagation is computed using the Adaptive Simulation of Unsteady Reacting Flow (A-SURF-1D) code [25]. The details of the compressible reactive flow governing equations, numerical schemes, initial and boundary conditions, and code validation can be found elsewhere [25]. In all simulations, the spherical combustion bomb radius is set to be R_0 = 10 cm to match the experimental condition. A reflective boundary condition with constant temperature is used at the wall. An initial hot spot with a given radius R_{HOT} and temperature of 1800 K located in the center of the chamber is used to initiate the ignition. In order to match the initial flame trajectories between the experiment and simulation, the size of the ignition hot pocket R_{HOT} is varied between 1 and 3.5 mm. The laminar flame speeds computed from A-SURF with a linear extrapolation are within 4% of PREMIX, justifying the appropriateness of linear extrapolation employed in experiments.

3.4.3. Laminar flame speeds

The laminar flame speeds have been measured for *n*-decane/air mixtures for equivalence ratio ϕ from 0.7 to 1.4 at initial pressures between 0.7 and 5 atm and the initial temperature, T_u = 400 K. **Figure 3.13(a)** shows the measured and predicted flame speeds along with published data at atmospheric pressure. For lean mixtures, the measured laminar flame speeds are slightly lower than those from the nonlinear extrapolation of counterflow flames [33], but considerably lower than those from the linear extrapolation using the same configuration [10]. On the rich side, the present measurements are between the two

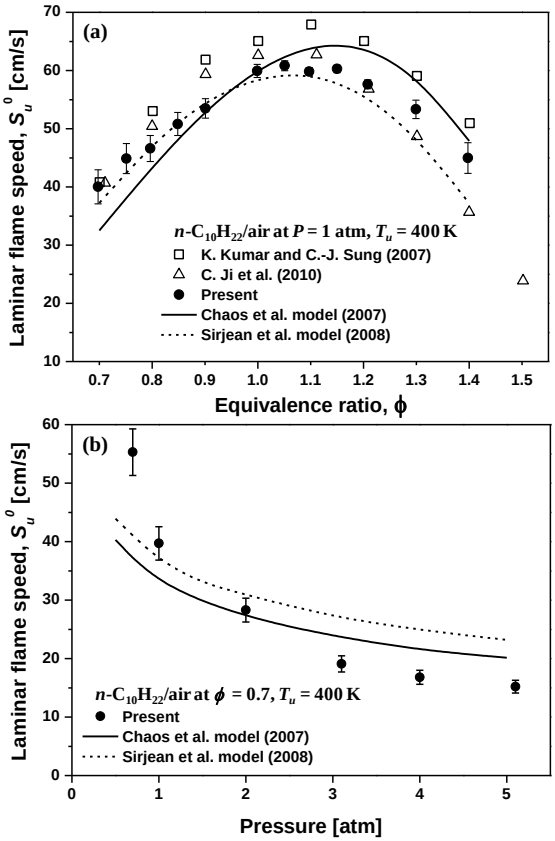

Figure 13. Experimentally and numerically determined laminar flame speed S_u^0 of n-$C_{10}H_{22}$/air mixtures at P = 1 atm, T_u = 400 K (a), and at ϕ = 0.7, T_u = 400 K (b).

sets of counterflow flame measurements, showing large uncertainty in the measurements of laminar flame speed. Both kinetic models under-predict the laminar flame speeds on the lean side, but exhibit very different predictions on the rich side. At $\phi = 0.9$, however, both models predict the same flame speed as the experiment. This condition will be used later to examine the fidelity of the kinetic models, whether they can predict both laminar and unsteady flame speeds simultaneously.

The laminar flame speeds at pressures from 0.7 to 5 atm for $\phi = 0.7$ are measured and compared with the predictions in **Fig. 3.13(b)**. The result shows that the laminar flame speed decreases as pressure increases. Note that both models predict the laminar flame speed reasonably well at 1 and 2 atm, but fail to capture the pressure dependence of laminar flame speed in the entire pressure range, indicating the importance of kinetic model validation over a wide range of pressures.

3.4.4. Observation of three flame regimes

Figures 14(a) and 14(b) show the unsteady burned gas flame speed S_b with flame radius and stretch rate, respectively, for $\phi = 0.7$. The result in **Fig. 3.14(a)** shows the existence of three distinct flame regimes; spark assisted ignition kernel propagation (Regime I), unsteady transition from spark ignition to normal flame propagation (Regime II), and normal flame propagation (Regime III). In regime I, the flame speed rapidly decreases with the increase of ignition kernel size right after ignition due to the reduced excess enthalpy from the spark ignition energy. If the ignition energy is lower than a critical value, the ignition kernel will extinguish and ignition will fail [28, 34-35]. The unsteady flame trajectory in regime I strongly depends on the ignition energy [36, 37]. If the ignition energy is larger than a critical value, a transition between ignition and flame propagation occurs in regime II. The flame speed in this regime increases rapidly within 2 milliseconds. The fast transition is attributed to a change in flame structure, which will be discussed later with numerical simulations. At the end of regime II, the flame structure becomes close to that of the normal flame. As the flame radius increases and the stretch rate decreases, the normal flame structure approaches that of the unstretched planar laminar flame.

The different flame regimes can be more clearly demonstrated in the stretch rate coordinate in **Fig. 3.14(b)**. The flame trajectory exhibits two turning points. One represents the transition from regime I to II, and the other from regime II to III. In regime I, the initial kernel development occurs at relatively higher stretch rate from about 200 to 600 sec^{-1} with small flame radii. The flame speed decreases with the decrease of stretch due to the ignition energy dissipation. This dependence reconfirms that the ignition kernel propagation is driven by the excess enthalpy from the ignition energy. It takes about 5.7 ms to reach the first

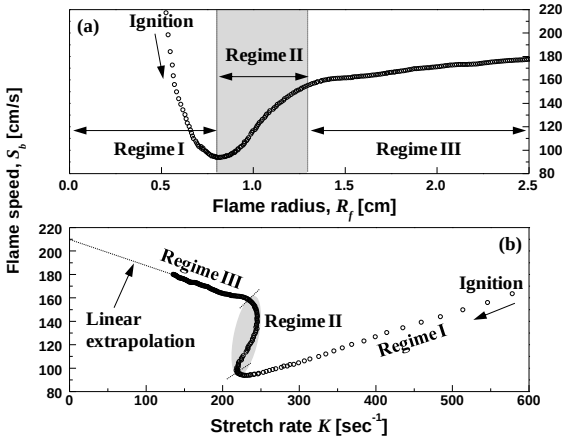

Figure 3.14. Flame speed S_b as a function of flame radius R_f (a), and stretch rate K (b) for n-$C_{10}H_{22}$/air at $\phi = 0.7$, P = 1 atm, and T_u = 400 K.

turning point. After the first turning point in regime II, the stretch rate has little change due to the simultaneous rapid increases of both the flame radius and the flame speed over 2 ms until the second turning point when the transition to the normal flame occurs.

3.4.5. The critical flame initiation radius

The dramatic change of flame trajectories has been observed previously with a mixture of large *Le* such as rich hydrogen/air [28, 35], and lean ethanol/air [6] using spherical or cylindrical chambers. Mostly, the normal flames (regime III) have been used to extrapolate the laminar flame speeds. Detailed studies on the other regimes are limited, although Bradley et al. [38] hypothesized the physical meaning of the second turning point as the extinction limit of the premixed flame. It is found that the radius at the minimum flame speed in Fig. 14(a), the first turning point in the present study, is critical for successful ignition [36], but it varies with ignition energy. However, the critical radius is independent from the ignition source when the ignition energy is low [28]. Therefore, the critical radius has been proposed as the radius above which an ignition kernel can lead to a successful ignition (i.e. transition from either regime I or II to III) [34].

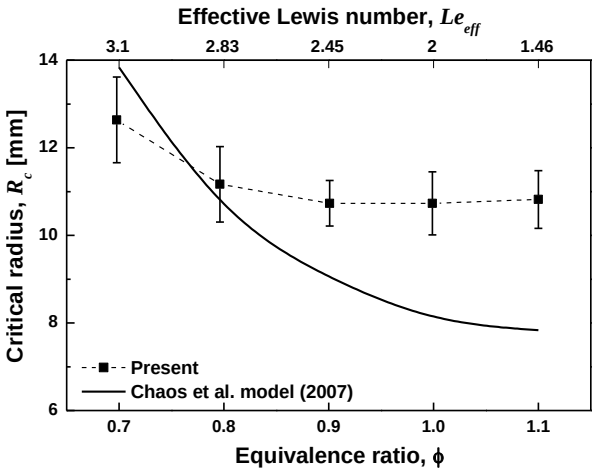

Figure 3.15. Critical radius R_c as a function of equivalence ratio and effective Lewis number Le_{eff} for n-$C_{10}H_{22}$/air at P =1 atm and T_u = 400 K.

Figure 3.15 shows the experimentally measured and numerically predicted critical radius R_c as a function of equivalence ratio and effective Lewis number, Le_{eff}. The effective Lewis number is a weighted average of the individual fuel and oxidizer Lewis numbers [39]. The critical radius increases rapidly above 10 mm as the equivalence ratio decreases and Le_{eff} increases. Numerical prediction gives a good trend of the equivalence ratio dependence, but fails to predict the quantitative values.

The dependence of the critical radius on pressure for an equivalence ratio of 0.7 is shown in **Fig. 3.16.** The critical radius increases rapidly with the decrease of pressure. In general, it has been known that the flame thickness increases as the pressure decreases. This implies that ignition at low pressure will be extremely difficult, thus requires a large ignition energy to overcome the large critical radius. The kinetic model qualitatively predicts the increase of critical radius, but again fails quantitatively.

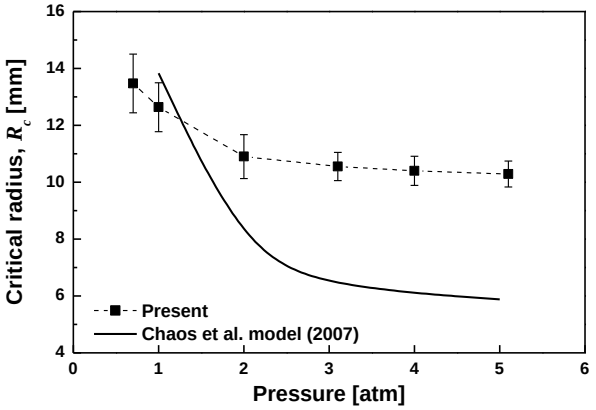

Figure 3.16. Critical radius R_c as a function of pressure for n-$C_{10}H_{22}$/air at ϕ = 0.7 and T_u = 400 K.

3.4.6. *Numerical results of unsteady flame trajectory*

In order to answer the first question of whether a kinetic model which can predict the steady state laminar flame speed well, can also predict the unsteady flame propagation, numerical simulations have been performed with A-SURF [25]. We choose an equivalence ratio of 0.9, at which both models, Chaos et al. [29] and Sirjean et al. [30], reproduce the measured laminar flame speed at P = 1 atm and T_u = 400 K (Fig. 13(a)). Although both models predict the same laminar flame speed, the flame trajectories in regime I and II as well as the critical radius differ significantly from the experimental results and also between the models. To further investigate the impact of ignition energy, the flame trajectories with the Chaos et al. [29] model have been calculated while altering the initial hot pocket size, R_{HOT}, from 2.5 mm to 3.5 mm. The results show that the model accurately predicts the behavior of flame trajectory in regime III regardless of R_{HOT}, but fails to predict the transitional behaviors in regimes I and II. Although the actual ignition process in the simulation is not identical to the experiment due to spatial non-uniformity and radical deposition in spark ignition, it is noteworthy that two tested kinetic models show different trajectories in the same computational conditions. The models also fail to predict the critical radius and regime III, where the ignition process has no effect on the trajectory for large *Le* mixture. In this regards, the critical radius and unsteady normal flame propagation can be a new validation target of a chemical kinetic model in addition to the laminar flame speed.

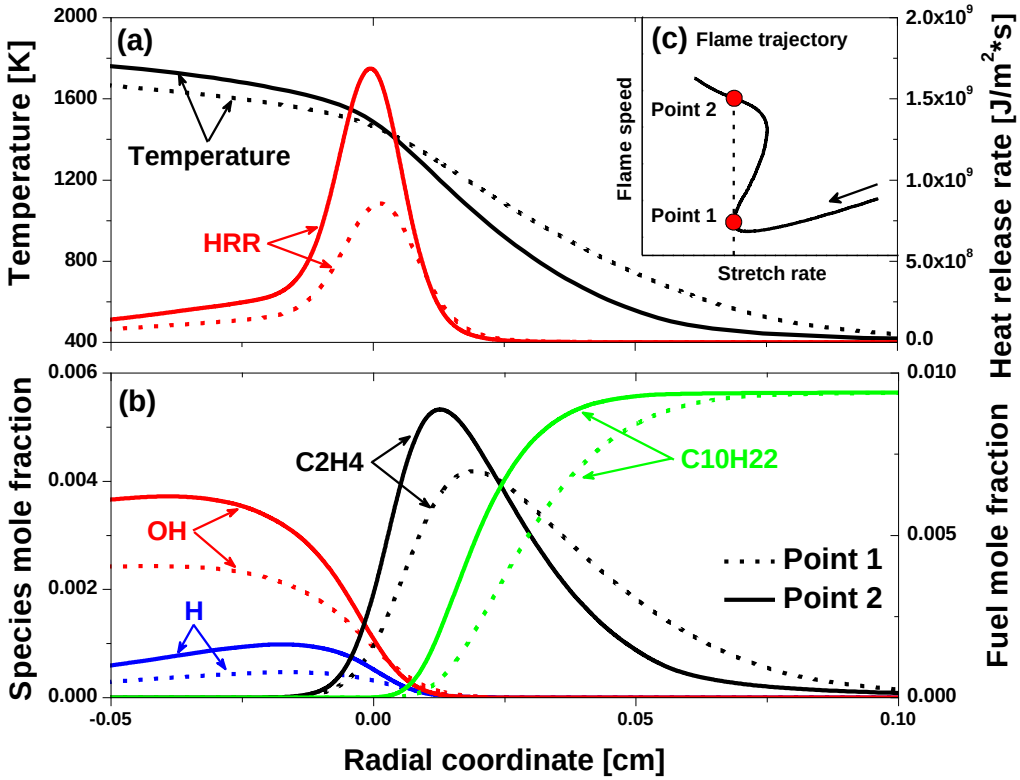

Figure 3.17. Flame structures for the first turning point (Point 1) and regime III (Point 2) at stretch rate K = 210 sec^{-1}: Temperature and heat release rate (a), Species and fuel mole fraction (b), Flame trajectory (c) for *n*-$C_{10}H_{22}$/air at ϕ = 0.7, P = 1 atm and T_u = 400 K. (the point of maximum heat release rate is shifted to the origin)

As mentioned above, the time duration for regime II is only 2 ms, during which a strong change of flame structure and flame chemistry occurs. Figure 17(c) shows the conditions plotted in **Fig. 3.17(a) and (b)** at $\phi = 0.7$. These conditions are given by the first turning point and a point in regime III at the same stretch rate. Figure 17(b) shows the mole fractions of fuel, ethylene (C_2H_4), H atom, and OH radical at these conditions. The locations of the maximum heat release rates are chosen as the origin of the coordinates. Significant changes in the distributions of heat release rate (HHR) between the two cases are shown in **Fig. 3.17(a)** compared to the change of temperature profiles. Considering that the heat release rate in a flame is strongly governed by the rate of radical pool population and its consequent impact on fuel decomposition [40], the result in Fig. 8 indicates the considerable difference in flame chemistry between these two flame regimes. After the energy deposition from the ignition source, the fuel is immediately consumed and a strong radical pool is established. In regime I, the populated radical pool starts to diffuse out, exhibiting the monotonic decay of radical concentration toward the upstream. At the first turning point, point 1 in **Fig. 3.17(c)**, finally the localized peak of radical concentration appears in the reaction zone, indicating that the flame may be *NOT self-sustained*, but able to overcome the sub-limit strong positive stretch with help from the reduced initial ignition energy. Thus, the time scale between ignition and the first turning point in regime I can be regarded as the delay time for the effect of initial ignition energy and the sub-limit strong stretch, which is a function of ignition energy, mixture Lewis number, and flame chemistry.

Unlike flames in regime I, flames in regime II are *self-sustained* without assistance from the

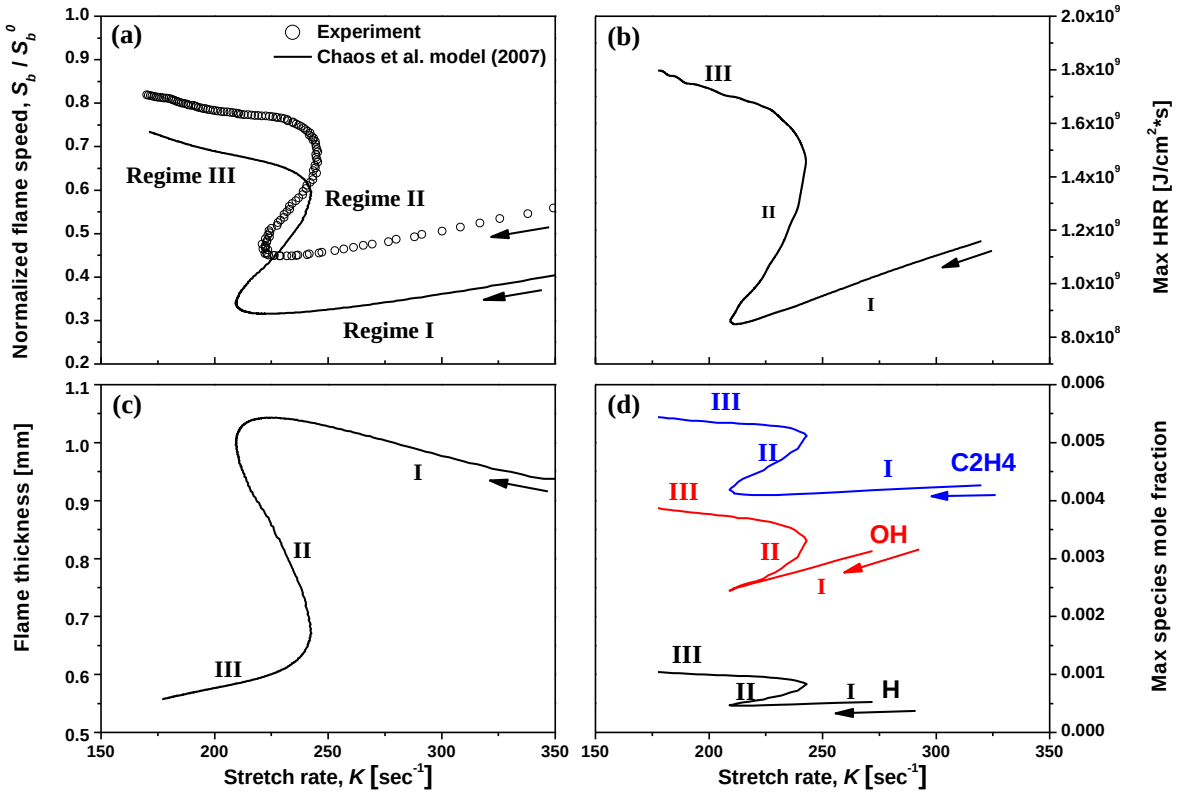

Figure 18. Normalized flame speed S_b / S_b^0 (a), maximum heat release rate (b), flame thickness (c), and maximum species mole fraction (d) as a function of stretch rate for n-$C_{10}H_{22}$/air at $\phi = 0.7$, $P = 1$ atm and $T_u = 400$ K.

ignition energy. However, the flame is still strongly stretched and has a lower flame temperature due to broadening of the reaction-diffusion zone causing decreased fuel diffusion to the reaction zone. Chemical kinetic flux analyses have been performed to identify the role of chemical kinetics for flames in regime II. The fuel, *n*-decane is mainly decomposed through H abstraction reactions via OH radical, and then converted to C_2H_4 through the sequential unimolecular decomposition reactions [41, 42]. C_2H_4 consumption plays an important role in radical pool growth, forming C_2H_3, which leads to production of HCO, CH_2O, and H atoms quickly at high temperature, populating the radical pool (**Fig. 3.17(b)**). Consequently, the fuel consumption is promoted by the acceleration of the chain branching reactions, so that the premixed flame structure is fully established by the positive feedback loop of fuel consumption and radical pool growth. The kinetic analysis reconfirmed that flames in regime II are self-sustained.

The changes of the flame trajectory, maximum heat release rate, flame thickness, and maximum mole fractions of key intermediate species are shown in **Fig. 3.18** in the stretch coordinate. These quantities differ dramatically in the different flame regimes. Normalized flame speed shown in **Fig. 3.18(a)** qualitatively agrees with experimental result, but differs quantitatively. As the flame in regime II evolves, the flame speed increases and the flame thickness (defined as $(T_{ad}-T_0)/(\max|dT/dx|)$ [43]) decreases, **Fig. 3.18(c)**. The reduced flame thickness accelerates the diffusion of fuel and further raises the flame temperature, leading to an increase in the radical pool concentration at the transition to regime III. This is why at the same stretch and equivalence ratio, the flame can have different structures. Note that since the flame temperatures and diffusion fluxes of a flame in regime I and II are lower than that of a flame at the same stretch in regime III, the chemical kinetics play different roles in regime I and II compared to that of normal flames.

Both experimental and numerical results in **Fig. 3.18** show that the flame exhibits the unsteady transition (regime II), which can be conceptually regarded as the middle branch in the *S*-Curve [13, 44]. Classically, the middle branch flame (or weak flame) is often thought unstable. Contrary to the conventional knowledge, the results in **Fig. 3.18** indicate that the weak flame regime can be observed and is an attractor of the unsteady flame propagation. Therefore, the existence of the weak flame and its short evolution time (2ms) in regime II have an important implication for near limit turbulent combustion where the normal flamelet may not be applicable. Moreover, the big difference in flame structures between regime II and III suggests that the flame trajectories in regime II cannot be used to extrapolate unstretched flame speed either linearly or nonlinearly.

3.5. Development of chemical kinetic model for 1,3,5-trimethylbenzene oxidation

Although 1,3,5-trimethylbenzene (135TMB) has been utilized as a component of 2nd generation POSF 4650 surrogate, the chemical kinetic modeling work for jet fuel surrogate has been limited due to the absence of 135TMB oxidation kinetic model. Thus, in order to provide modeling avenue in surrogate modeling work in MURI, the detailed chemical kinetic model for 135TMB oxidation has been developed.

The combustion phenomena of 135TMB have been studied at a range of thermodynamic conditions in different experimental facilities. Constant residence time flow reactor oxidative reactivity measurements show this trimethylated aromatic not to exhibit the low temperature reactivity typical of the alkylperoxy radical initiated low temperature chain branching mechanism. Reflected shock ignition delay measurements of 1,3,5-trimethylbenzene/air mixtures show the ignition delay time to decrease with increased equivalence ratio, temperature and pressure. Both behaviours are phenomenologically consistent with similar observation for toluene [45]. The laminar burning velocity of 1,3,5-trimethylbenzene/air freely propagating flames have also been measured and share close agreement to those measured by Hui et al. [46] in the counter flow flame configuration.

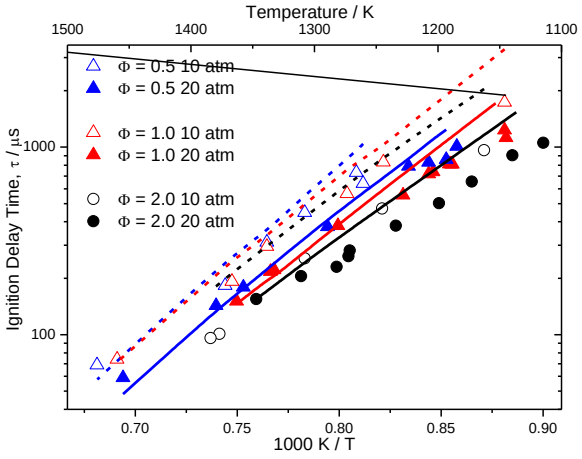

Figure 3.19. Measured (symbols) and computed (lines) reflected shock ignition delays for 1,3,5-trimethylbenzene/air mixtures. Hollow symbols and dashed lines are ~10 atm conditions, solid symbols and solid lines are ~20 atm conditions. Stoichiometric combustion is identified by an equivalence ratio of unity.

In order to facilitate the numerical modelling of high distillate real transportation fuels through the surrogate fuel concept, a chemical kinetic model has been constructed for the global combustion behaviour of 135TB. It is demonstrated that 135TMB exhibits a thermochemical environment similar to that of toluene. Given the paucity of data on the elementary oxidation reaction kinetics for 1,3,5-trimethylbenzene, this thermochemical similarity is utilized, to prescribe the oxidation mechanism and reaction rate constants by analogy to the much better understood toluene system. Without any arbitrary adjustment, the model parameters reasonably reproduce the global combustion reactivity measurements described above, including observable trends with mixture composition and initial thermodynamic condition. Ignition delays are reproduced to with a factor of 1.8 in the worst case (**Fig. 3.19**), laminar burning velocities are reproduced to within a factor of 1.19 (**Fig. 3.20**), and flow reactor reactivity to within ~15-20 K (**Fig. 3.21**). In addition the calculations of the kinetic model also reproduce the suitable data available in the literature to a precision of 60 % for laminar burning velocity, ~35 % for premixed and

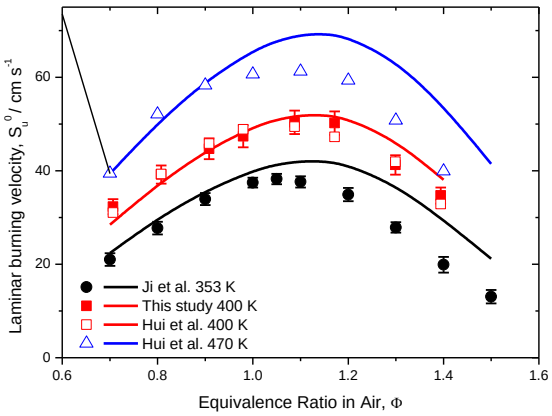

Figure 3.20. Laminar burning velocities of 1,3,5-trimethylbenzene/air mixtures at 1 atm. Symbols are experimental data [32, 34] and lines are model computations. Stoichiometric combustion is identified by an equivalence ratio of unity

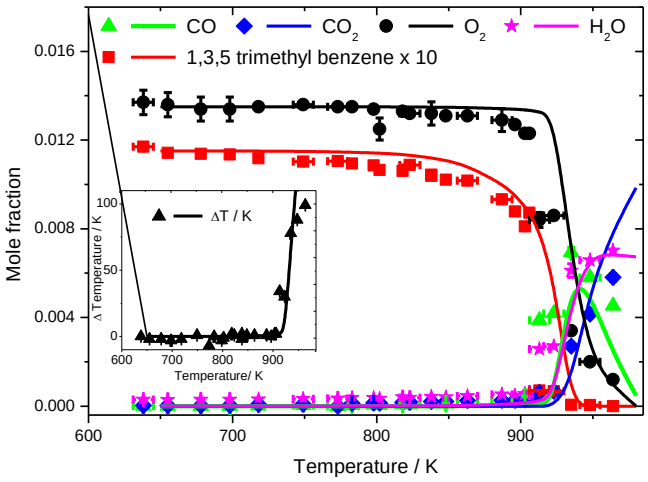

Figure 3.21. Flow reactor oxidation data for conditions of 12.5 atm, 0.1111 mole % 1,3,5-trimethylbenzene in N_2, $\phi = 1$ at 1.8 s residence time. Inset; heat release due to chemical reaction (ΔT). Symbols are experimental data and lines are model computations.

diffusive extinction limits, and (negative) ~7% for premixed extinction limits.

The 1,3,5-trimethylbenzene oxidation mechanism is analysed at conditions representative of each of the combustion phenomena measured. At all conditions, it is suggested that 1,3,5-trimethylbenzene combustion occurs principally by hydrogen abstraction from a methyl position to yield the 2,4, dimethyl benzyl radical which reacts bimolecularly, depending on condition, to form, 2,4, dimethyl benzaldehyde and 1,2-bis(3,4 dimethyl phenyl)ethane as the major stable intermediate species of mechanistic significance.

The oxidation process was observed to be driven through H/O atom reactions 1,3,5 trimethyl benzene at flame configurations, whereas OH/HO_2 radical reactions drive 1,3,5 trimethyl benzene reactivity at lower temperatures. The chemical mechanism describing the destruction of the benzene ring, releasing CO, is a key step that requires future consideration to yield improved prediction of detailed speciation of small intermediate species in the oxidation. Detailed measurements of a mechanistic nature are required to further test the suggestions of the kinetic model.

3.6. Development of numerical schemes for multi-time scale modeling and multi-generation path flux analysis for chemical kinetic model reduction

3.6.1. Development of Multi-generation Path Flux Method for Chemical Kinetic Mechanism Reduction

In this study, instead of using the absolute reaction rate such as DRG method [50], we use the production and consumption fluxes to identify the important reaction pathways. In order to consider the conservative flux information, we introduce a different definition of the interaction coefficients, which contain the flux information for both the first and second generation. Note that although in the present studies, only two generation fluxes are considered, the method can be extended to any generations.

The interaction coefficients for production and consumption of species *A* via *B* of first generation are defined as:

$$r_{AB}^{pro-1st} = \frac{P_{AB}}{\max(P_A, C_A)} \qquad (1)$$

$$r_{AB}^{con-1st} = \frac{C_{AB}}{\max(P_A, C_A)} \qquad (2)$$

Here P_{AB} and C_{AB} denote, respectively, the production and consumption rates of species *A* due to the existence of species *B*. By using the production and consumption fluxes of the first generation, The interaction coefficients which are the measures of flux ratios between *A* and *B* via a third reactant (M_i) for the second generation are defined as:

$$r_{AB}^{pro-2nd} = \sum_{M_i \neq A,B} (r_{AM_i}^{pro-1st} r_{M_iB}^{pro-1st}) \qquad (3)$$

$$r_{AB}^{con-2nd} = \sum_{M_i \neq A,B} (r_{AM_i}^{con-1st} r_{M_iB}^{con-1st}) \qquad (4)$$

The summation here includes all possible reaction paths (fluxes) relating *A* and *B*.

In theory, different threshold values can be set for different interaction coefficients. For simplicity, we can lump all the interaction coefficients together and set only one threshold value,

$$r_{AB} = r_{AB}^{pro-1st} + r_{AB}^{con-1st} + r_{AB}^{pro-2nd} + r_{AB}^{con-2nd} \qquad (5)$$

The coefficient defined above is used to evaluate the dependence/importance of species *B* to species *A* in the present study.

The methodology can identify the important multi-generation pathways. Different sized reduced mechanisms [29, 51] for n-decane and n-heptane ignition, extinction, and steady and unsteady

flame propagation are generated and examined. As shown in **Fig. 3.22**, comparison between the present PFA method and the DRG method for ignitions show that with the same or smaller sized reduced mechanisms, PFA has better accuracy than DRG to reproduce ignition of n-decane/air mixtures in a broad temperature and pressure range.

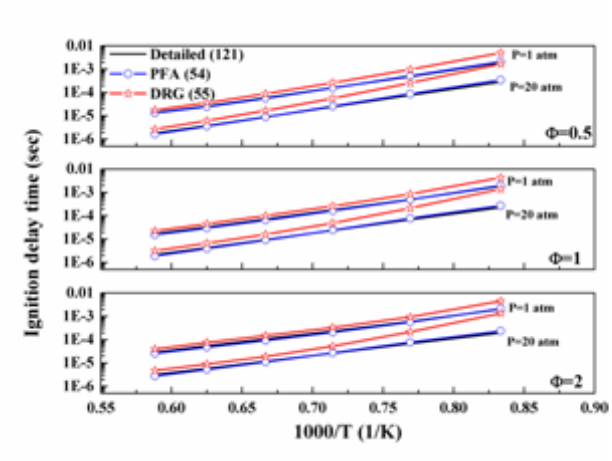

Figure 3.22. Comparison of ignition delay times of lean, stoichiometric, and rich n-decane-air mixtures for various temperatures and pressures predicted by using reduced mechanisms generated by PFA and DRG as well as detailed mechanism.

To demonstrate that the improvement of PFA over DRG is not for a particular size of reduced mechanism, **Fig. 3.23** shows the relations between the number of species in the reduced mechanisms of n-decane and the discrepancies of ignition delay time predicted by DRG and PFA methods at 1200 K, 1 and 20 atmospherics. It is seen that PFA improved the prediction accuracy significantly in a broad range of species numbers especially when the number of species in the reduced mechanism is less than 73. Therefore, the improvement of PFA in generating reduced mechanism is consistent with our flux analysis and is originated from the better prediction of species fluxes. This PFA method for model reduction has been extensively used in MURI team to reduce the developed chemical kinetic models for model validations against flame configurations.

3.6.2. Development of Multi-time scale method

Combustion is a multi-scale problem in nature. An on-grid dynamic multi-time scale (MTS) method and a hybrid multi-time scale (HMTS) method are developed to model multi-timescale combustion problems with detailed and reduced kinetic mechanisms. The basic idea of the multi- timescale (MTS) method is as follows. First of all, in each simulation a base time step, t_{base}, is specified based on the interest of the physical problem and the information needed at sub-time scale to construct models at the physical timescale of interest. Then, based on the base time step and the estimated characteristic time of each species, all the species will be divided into different groups according to their timescales. At each time step of t_{base}, from the fastest

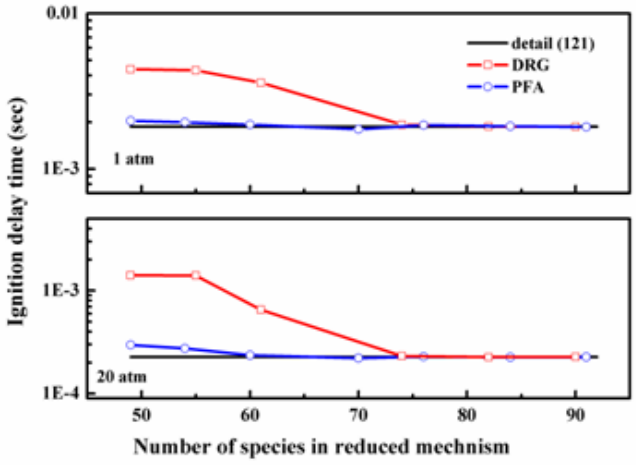

Figure 3.23. Ignition delay time comparisons of detailed and reduced mechanisms with different sizes of reduced mechanisms.

group (Δt_F) to the slowest group (Δt_S), all the groups are calculated with their own time steps by using a first-order explicit Euler scheme until a converging criterion with both absolute and relative errors is met.

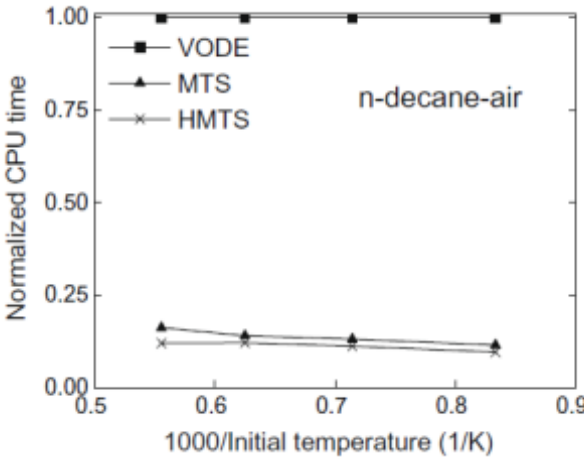

Figure 3.24. Comparison of CPU time for n-decane ignition for different initial temperatures at 1 atm.

Comparisons of homogeneous ignition delay time, temperature and species distributions of hydrogen, methane, and n-decane–air mixtures [29, 51] in a broad range of temperatures, pressures, and equivalence ratios show that both MTS and HMTS are robust and accurate enough to reproduce the results of the VODE method [52] but can reduce computation time by one-order. **Figure 3.24** is one example showing the comparisons of the normalized CPU time between MTS, HMTS, and the VODE solver for ignition of the stoichiometric n-decane/air mixture at 1 atmospheric pressure and different temperatures. It is seen that both MTS and HMTS increases the computation efficiency about one-order in the entire temperature range with the same kinetic mechanism.

It is also shown that the computation efficiency of multi-time scale method increases with the increase of the kinetic mechanism size and the decrease of base time step. Furthermore, numerical simulations demonstrate that the multi-timescale method does not require accurate estimation of the species timescale and that the present definition of species timescale is consistent with the projected timescale by the CSP method. Applications of the multi-timescale method to the unsteady flame simulations of outwardly propagating spherical n-decane–air flames reveal that the multi-timescale method is promising and computationally efficient for direct numerical simulations of transient combustion processes. The integration of the multi-timescale method with the path flux analysis based mechanism reduction approach further demonstrates that a significant increase the computation efficiency can be achieved.

3.7. References

[1] A.T. Holley, X.Q. You, E. Dames, H. Wang, F.N. Egolfopoulos, Proc. Combust. Inst. 32 (1) (2009) 1157-1163.

[2] S. S. Vasu, David F. D., R. K. Hanson, Combust. Flame 152 (1-2) (2008) 125-143.

[3] G. Mittal, C. -J. Sung, Combust. Flame 155 (3) (2008) 431-439.

[4] A. Violi, S. Yan, E.G. Eddings, A.F. Sarofim, S. Granata, T. Faravelli, E. Ranzi, Combust. Sci. Tech. 174 (2002) 399-417.

[5] A. Agosta, N.P. Cernansky, D.L. Miller, T. Favarelli, E. Ranzi, Exp. Therm. Fluid Sci. 28 (2004) 701–708.

[6] C. Guéret, M. Cathonnet, J.-C. Boettner, F. Gaillard, Proc. Combust. Inst. 23 (1990) 211-216.
[7] P. Dagaut, A. El Bakali, A. Ristori, Fuel 85 (2006) 944-956.
[8] J.A. Cooke, M. Bellucci, M.D. Smooke, A. Gomez, A. Violi, T. Faravelli, E. Ranzi, Proc. Combust. Inst. 30 (2005) 439–446.
[9] C. Ji, X. You, A. T. Holley, Y. L. Wang, F. N. Egolfopoulos, H. Wang, Propagation and Extinction of Mixtures of Air with n-Dodecane, JP-7, and JP-8 Jet Fuels, *46th AIAA Aerospace Science Meeting and Exhibit*, Reno, Nevada, 2008, AIAA 2008-974.
[10] K. Kumar, C. –J. Sung, Combust. Flame 151 (1-2) (2007) 209-224.
[11] S. Humer, A. Frassoldati, S. Granata, T. Faravelli, E. Ranzi, R. Seiser, K. Seshadri, Proc. Combus. Inst. 31 (2007) 393-400.
[12] A. T. Holley, Y. Dong, M. G. Andac, F. N. Egolfopoulos, T. Edwards, Proc. Combust. Inst. 31 (2007) 1205-1213.
[13] A. Liñán, Acta Astronautica 1 (7-8) (1974) 1007-1039.
[14] S. H. Chung, C. K. Law, Combust. Flame 52 (1983) 59-79.
[15] B. H. Chao, C. K. Law, Combust. Flame 92 (1-2) (1993) 1-24.
[16] C. -J. Sung, J. B. Liu, C. K. Law, Combust. Flame 102 (4) (1995) 481-492.
[17] K. Seshadri, F.A. Williams, Int. J. Heat Mass Transfer 21 (2) (1978) 251–253.
[18] Y. Ju, H. Guo, K. Maruta, J. Fluid Mech. 23 (1997) 315-334.
[19] G. Dixon-Lewis, Proc. Combust. Inst. 23 (1990) 305-324.
[20] Q. V. Nguyen, R. W. Dibble, C. D. Carter, G. J. Fiechtner, R. S. Barlow, Combust. Flame 105 (4) (1996) 499-510.
[21] N. L. Garland, D. R. Crosley, Proc. Combust. Inst. 21 (1986) 1693-1702.
[22] K. C. Smyth, C. R. Shaddix, D. A. Everest, Combust. Flame 111 (3) (1997) 185-194.
[23] S. H. Won, W. Sun, Y. Ju, Combust. Flame 157 (2010) 411-420.
[24] X. Qin, Y. Ju, Proc. Combust. Inst. 30 (2005) 233-240.
[25] Z. Chen, Studies on the Initiation, Propagation, and Extinction of Premixed Flames, Ph.D. thesis, Princeton University, 2008.
[26] C. Ji, E. Dames, Y. L. Wang, H. Wang, F. N. Egolfopoulos, Combust. Flame 157 (2010) 277–287.
[27] M. P. Burke, M. Chaos, F. L. Dryer, Y. Ju, Combust. Flame 157 (2010) 618-631.
[28] Z. Chen, M. P. Burke, Y. Ju, Proc. Combust. Inst. 32 (2009) 1253-1260.
[29] M. Chaos, A. Kazakov, Z. Zhao, F.L. Dryer, Int. J. Chem. Kinet. 39 (2007) 399-414.
[30] B. Sirjean, E. Dames, D. A. Sheen, X.-Q. You, C. Sung, A. T. Holley, F. N. Egolfopoulos, H. Wang, S. S. Vasu, D. F. Davidson, R. K. Hanson, H. Pitsch, C. T. Bowman, A. Kelley, C. K. Law, W. Tsang, N. P. Cernansky, D. L. Miller, A. Violi, R. P. Lindstedt, A high-temperature chemical kinetic model of n-alkane oxidation, JetSurF version 0.2, September 08, 2008 available at <http://melchior.usc.edu/JetSurF/Version0_2/Index.html>
[31] W. Sun, X. Gou, Z. Chen, Y. Ju, Combust. Flame 157 (2010) 1298-1307., available at < http://engine.princeton.edu/>
[32] R.J. Kee, F.M. Rupley, J. Miller, Report No. SAND89-8009B, Sandia National Laboratories, 1989.

[33] C. Ji, E. Dames, Y. L. Wang, H. Wang, F. N. Egolfopoulos, Combust. Flame 157 (2010) 277–287.
[34] Z. Chen, Y. Ju, Combust. Theory Modell.11 (2007) 427-453.
[35] A. P. Kelley, G. Jomaas, C. K. Law, Combust. Flame 156 (2009) 1006-1013.
[36] Z. Chen, M. P. Burke, Y. Ju, Proc. Combust. Inst. 33 (2011) 1219-1226.
[37] Z. Chen, Combust. Flame 158 (2011) 291-300.
[38] D. Bradley, M. Lawes, M. S. Mansour, Combust. Flame 156 (2009) 1462-1470.
[39] J. K. Bechtold, M. Matalon, Combust. Flame 127 (2001) 1906-1913.
[40] S. H. Won, S. Dooley, F. L. Dryer, Y. Ju, Combust. Flame 159 (2012) 541-551.
[41] S.M. Sarathy, C.K. Westbrook, M. Mehl, W.J. Pitz, C. Togbe, P. Dagaut, H. Wang, M.A. Oehlschlaeger, U. Niemann, K. Seshadri, P.S. Veloo, C. Ji, F.N. Egolfopoulos, T. Lu, Combust. Flame 158 (2011) 2338-2357.
[42] S. Jahangirian, S. Dooley, F. M. Haas, F. L. Dryer, Combust. Flame 159 (2012) 30-43.
[43] C.K. Law, C.J. Sung, Prog. Energ. Combust. 26 (2000) 459–505.
[44] F.E. Fendell, J. Fluid Mech. 21 (1965) 281-303.
[45] W. K. Metcalfe, S. Dooley, F. L. Dryer, Energy Fuels 25 (2011) 4915-4936.
[46] X. Hui, A. K. Das, K. Kumar, C.-J. Sung, S. Dooley, F. L. Dryer, Fuel 97 (2012) 695-702.
[47] Z. Zhao, M. Chaos. A. Kazakov, F.L. Dryer, Int. J. Chem. Kinet. 40 (2008) 1-18.
[48] K. Yasunaga, F.Gillespie, J.M. Simmie, H.J. Curran, Y. Kuraguchi, H. Hoshikawa, T. Yamane, Y. Hidaka, J. Phys. Chem. A 114 (2010) 9098-9109.
[49] K. Yasunaga, J.M. Simmie, H.J. Curran, T. Koike, O. Takahashi, Y. Kuraguchi, Y. Hidaka,, Combust. Flame 158 (2011) 1032-1036.
[50] T. Lu, C.K. Law, Proc. Combust. Inst. 30 (2005) 1333-1341.
[51] M. Chaos, A. Kazakov, Z. Zhao, F.L. Dryer, S.P. Zeppieri, Reduced High-Temperature Mechanisms for Large Paraffins - n-Hexadecane, in: Eastern States Fall Technical Meeting of the Combustion Institute, Orlando, FL, USA, 2005.
[52] P.N. Brown, G.D. Byrne, A.C. Hindmarsh, Siam J. Sci. Stat. Comput. 10 (5) (1989) 1038–1051.

3.8. Archival Publications

1. Y. Ju, W. Sun, M. P. Burke, X. Gou, Z. Chen. Multi-timescale Modeling of Ignition and Flame Regimes of n-Heptane-Air Mixtures near Spark Assisted Homogeneous Charge Compression Ignition Conditions, *Proc Combust Inst* (2011) 33:1245-1251.
2. Y. Ju, X. Gou, W. Sun, Z. Chen. An On-Grid Dynamic Multi-Timescale Method with Path Flux Analysis for Multi-Physics Detailed Modeling of Combustion (invited review paper), Journal of the Combustion Society of Japan, Vol.51, 2009.
3. W. Sun, Z. Chen, X. Gou, Y. Ju. A Path Flux Analysis Method for the Reduction of Detailed Chemical Kinetic Mechanisms, *Combust Flame* (2010) 157:1298-1307.
4. X. Gou, W. Sun, Z. Chen, Y. Ju. A Dynamic Multi-Timescale Method for Combustion Modeling with Detailed and Reduced Chemical Kinetic Mechanisms, *Combust Flame,* (2010) 157:1111-1121.
5. S.H. Won, W. Sun, Y. Ju. Kinetic Effects of Toluene Blending on the Extinction Limit of n-Decane Diffusion Flames, *Combust Flame* (2010) 157:411-420.

6. S. Dooley , S.H. Won , M. Chaos, J. Heyne, Y. Ju, F. L. Dryer, K. Kumar, C-J. Sung, H. Wang, M. A. Oehlschlaeger, R.J., Santoro, T. A. Litzinger. A Jet Fuel Surrogate Formulated by Real Fuel Properties, *Combust Flame* (2010) 157:2333-2339.
7. Z. Chen, X. Gou, Y. Ju. Studies on the Outwardly and Inwardly Propagating Spherical Flames with Radiation Heat Loss, *Combust Sci Technol* (2010) 182: 124–142.
8. Z. Chen, M. P. Burke, Y. Ju. On the Critical Flame Radius and Minimum Ignition Energy for Spherical Flame Initiation, *Proc Combust Inst* (2011) 33:1219–1226.
9. S.H. Won, S. Dooley, F.L. Dryer, Y. Ju. Kinetic Effect of Molecular Structure on Extinction Limit of Aromatic Diffusion Flames, *Proc Combust Ins* (2011) 33:1163–1170.
10. S.H. Won, S. Dooley, F. L. Dryer, Y. Ju, A Radical Index for the Determination of the Chemical Kinetic Contribution to Diffusion Flame Extinction of Large Hydrocarbon Fuels, *Combust Flame* (2011) 159:541-551.
11. S. Dooley, S-H. Won, J. Heyne, T.I. Farouk, Y. Ju, F.L. Dryer, K. Kumar, X. Hui, C-J. Sung, H. Wang, M. A. Oehlschlaeger, T.A. Litzinger, R.J. Santoro, T. Malewecki, K. Brezinsky. The Experimental Evaluation of a Methodology for Surrogate Fuel Formulation to Emulate Gas Phase Combustion Kinetic Phenomena, *Combust Flame* (2012) 159: 1444-4466.
12. S. Dooley, S.H. Won, Y. Ju, F.L. Dryer, H. Wang, M. A. Oehlschlaeger. The Combustion Kinetics of a Synthetic Paraffinic Jet Aviation Fuel and a Fundamentally Formulated, Experimentally Validated Surrogate Fuel, *Combust Flame* (2012) 159: 3014-3020.
13. H. H. Kim, S.H Won, J. Santner, Z. Chen, Y. Ju. Measurements of the Critical Initiation Radius and Unsteady Propagation of n-Decane/Air Premixed Flames, *Proc. Combust Inst*, 34 (2012). In press.
14. J. K. Lefkowitz, S.H Won, Y. Fenard, Y. Ju. Uncertainty Assessment of Species Measurements in Acetone Counterflow Diffusion Flames, *Proc. Combust Inst*, 34 (2012). In press.

3.9. Abstracts and Preprints at Conference presentation.

1. S.H. Won, W. Sun, Y. Ju. Kinetic Effects of Toluene Blending on the Extinction Limit of n-Decane Diffusion Flames, *6th U.S. National Combustion Meeting*, Ann Arbor, Michigan (2009).
2. W. Sun, Z. Chen, X. Gou, Y. Ju, "A Path Flux Analysis Method for the Reduction of Chemical Kinetic Mechanisms," *6th U.S. National Combustion Meeting*, Ann Arbor, Michigan (2009).
3. Y. Ju, W. Sun, X. Gou, Z. Chen. Direct Modeling of Auto-Ignition and Flame Propagation with Temperature and Concentration Gradients by Using Dynamic Multi-Timescale Method, AIAA-2010-606, 48th AIAA Aerospace Sciences Meeting, 2010.
4. S.H. Won, W. Sun, Y. Ju. Measurements of Extinction Limits and OH Radicals of Trimethylbenzene/n- Decane Diffusion Flames, AIAA-2010-197, 48th AIAA Aerospace Sciences Meeting, 2010.
5. S.H. Won, W. Sun, Y. Ju. Kinetic Effects of Toluene Blending on n-Decane Diffusion Flame Extinction Limit, AIAA-2009-993, 47th AIAA Aerospace Sciences Meeting, 2010.
6. P. Dievart, H-H. Kim, S. Dooley, S.H. Won, Y. Ju.1,3,5-trimethyl benzene: Laminar flame speeds measurements and kinetic modeling," 2011 Fall Technical Meeting of the Eastern States Section of the Combustion Institute, University of Connecticut, Storrs, CT, October 9-12, 2011.

3.10. Graduate Theses

1. Zheng Chen, PhD thesis, Studies on the Initiation, Propagation, and Extinction of Premixed Flames, 2009

2. Michael P. Burke, PhD thesis, Experiments and Kinetic Modeling of High-Pressure H_2/O_2 Flames (with CO, CO_2, and CH_4 Addition), 2011.

3. Hwanho Kim, Master Thesis, Studies on the Critical Flame Initiation Radius and Unsteady Propagation of *n*-Decane / Air Premixed Flames, 2012.

3.11. Personnel

- Graduate students: Michael P. Burke, Xiaolong Gou, Zheng Chen, Hwanho Kim, Wenting Sun
- Research staff: Sanghee Won, Xiaolong Gou, Pascal Dievart

3.12. Invited Presentations

Y. Ju, Invited Keynote Lecture, "Combustion towards Alternative Fuels for 21st Century Transportation," The Fifth International Conferences on Flow Dynamics, Sendai, Japan.

Y. Ju, Aug. 10, 2009, Department Seminar, "A Dynamic Multi-Timescale Method with Reaction Path Flux Analysis for Combustion Modeling with Detailed and Reduced Chemistry," Institute of Mechanics, Chinese Academy of Science.

Y. Ju, Invited Keynote Lecture, Dec.12-17, 2009, "The Challenges and Advance of Combustion Research for Renewable Transportation Fuels," GCOE Energy Forum, Okinawa, Japan.

Y. Ju, Department Seminar, April 9, 2010, "Kinetic and Transport Effects on Combustion Enhancement by Non-Equilibrium Plasma," University of Connecticut.

Y. Ju, Invited Lecture, July 31, 2010, "Fuels Chemistry and Surrogate Modeling," Workshop on Combustion Science in an Energy-Constrained World, Tsinghua University, China

Y. Ju, Invited Lecture, Aug.9-10, 2010,"A Dynamic Multi-Timescale Method for Kinetic Model Reduction and Direct Numerical Simulation of HCCI Combustion," Combustion and Fuels Workshop, Shanghai Jiaotong University, China,

Y. Ju, Department Seminar, Combustion Research towards Alternative Transportation Fuels, University of Kansas. May 3, 2011.

Y. Ju, Invited Lecture, Alternative Fuels for Air and Ground Transportation:Combustion Modeling and New Technology, University of Texas at El-Paso, Feb.29, 2012.

Y. Ju, Invited Lecture, Combustion Theory and Modeling towards Alternative Fuels, Purdue University, April 12, 2012.

Y. Ju, Invited Lecture, Challenges and opportunities of Combustion towards sustainable energy, Stanford University, May 23, 2012.

Y. Ju, Invited Lecture, The Role of Chemistry and Transport in Flame Dynamics, the 1st workshop on flame chemistry, Warsaw, July 28-29, 2012.

4. University of Connecticut (UCONN) – C.J. Sung

4.1. Abstract

This article presents an overview of the findings of the research group led by the Co-Investigator, Chih-Jen Sung. The research was conducted under the MURI program at Case Western Reserve University (2007−2009) and the University of Connecticut (2009−2012). The specific contributions of this Co-Investigator to the MURI effort were in the topic areas of Rapid Compression Machine Experiments, Premixed Flame Experiments, and Non-Premixed Flame Experiments. High pressure autoignition delay data were obtained for liquid fuels relevant to aero-propulsion applications. Experimental measurements of the laminar flame speed and extinction stretch rate in the premixed configuration were also conducted for neat surrogate components, fuel blends, and conventional and alternative jet fuels. The premixed flame experiments were carried out for preheated conditions and at elevated pressures. Furthermore, a novel high pressure apparatus capable of studying non-premixed ignition at pressures up to 30 atmospheres was designed, fabricated, and tested.

4.2. Introduction

Jet-A is used in civilian aircrafts and constitutes a significant fraction of the US refinery yield, while JP-8 is used as a fuel for military jet aircrafts. A better understanding of the combustion characteristics of real jet fuels is central to the process of developing more efficient and less polluting aero-combustors. Autoignition delay time is one of the fundamental combustion properties, which markedly differ for different types of commercial fuels. This property has conventionally been associated with the octane or cetane rating of a given fuel, and is generally used to assess the compatibility of the fuel with the intended end use in a reciprocating or rotary internal combustion engine. Furthermore, the understanding of autoignition chemistry for real fuels can provide insights into the development of the corresponding comprehensive reaction mechanisms. Recognizing the complex dependence of the autoignition delay times on physicochemical parameters such as temperature, pressure, and equivalence ratio, it is essential to acquire experimental data of high fidelity over a wide range of conditions for model validation.

In addition, an important validation target for combustion mechanisms has been the laminar flame speed. The laminar flame speed is a global marker for the reactivity and exothermicity of a given fuel/oxidizer mixture. Another important global validation target for the flame environment is the extinction stretch rate. The extinction stretch rate represents a kinetics-affected phenomenon and characterizes the interaction between a characteristic flame/flow time and a chemical time.

Currently, petroleum-derived kerosene type fuels are used to power civilian and military aircrafts. Flight tests have been conducted to demonstrate the feasibility of using synthetic jet fuels in military aircrafts. One such synthetic jet fuel produced by Syntroleum is S-8. This alternative jet fuel is produced by the Fischer–Tropsch process using synthesis gas derived from natural gas, and is entirely composed of n- and iso-paraffins. There are significant differences in the physical and chemical properties between jet fuels derived from naturally occurring petroleum, such as Jet-A and JP-8, and their synthetic counterparts, such as S-8. These

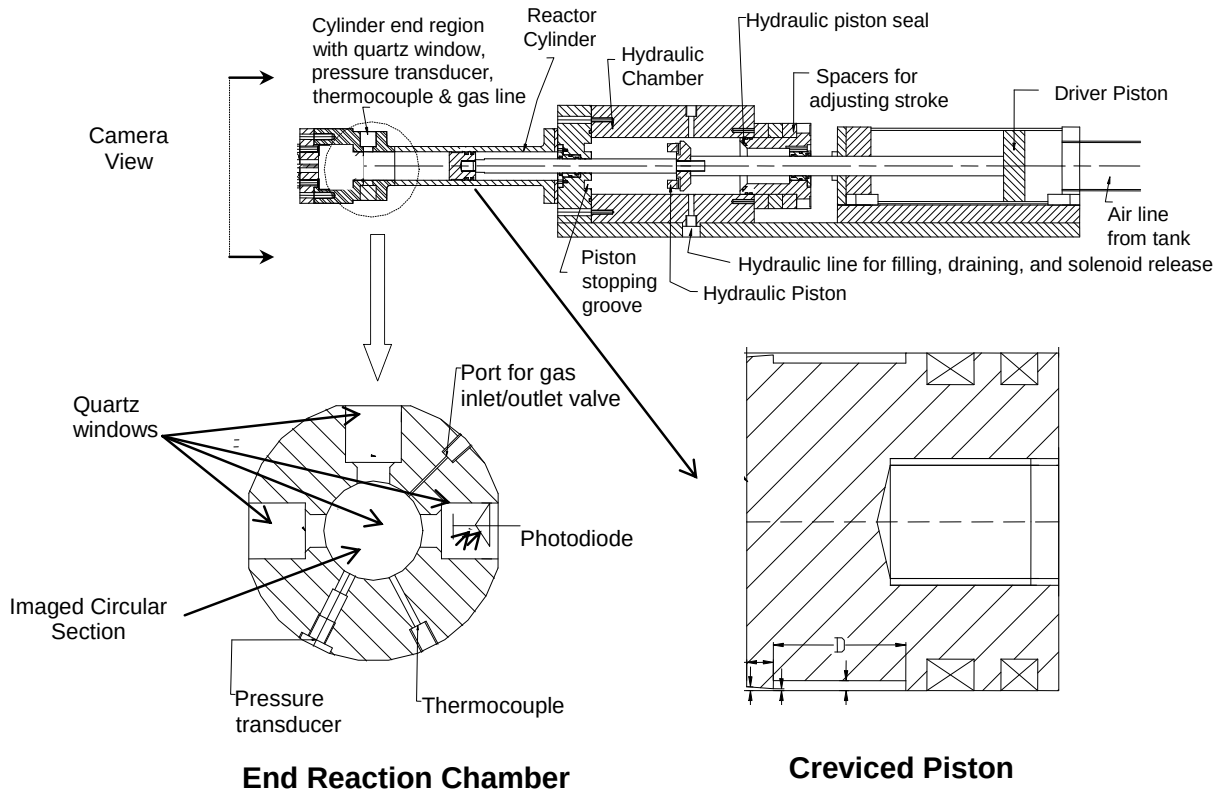

Figure 4.1. Schematic of the Rapid Compression Machine (RCM).

differences need to be well understood in order to facilitate a smooth transition from petroleum based fuels to synthetic fuels. The differences in the chemical composition between S-8 and Jet-A affect several factors, including density, heating value, carbon-to-hydrogen ratio, etc., and impact broad engine performance parameters such as fuel efficiency and emissions.

Summary of Research Findings

4.3. Autoignition Experiments

4.3.1. Jet-A and JP-8

Ignition delay times of Jet-A/oxidizer and JP-8/oxidizer mixtures were measured using a heated Rapid Compression Machine (RCM) at compressed charge pressures corresponding to 7, 15, and 30 bar, compressed temperatures ranging from 650 to 1100 K, and equivalence ratios varying from 0.42 to 2.26. The premixed fuel/oxidizer charge is fed to the reactor chamber of the RCM and then compressed. **Figure 4.1** shows the schematic of our RCM.

The pressure time record of the compression event and the subsequent ignition is obtained. A pressure time record of a typical two-stage ignition event using Jet-A is shown in **Fig. 4.2**. **Figure 4.2** is also used to illustrate the definitions of the first-stage, second-stage, and overall ignition delay times.

When using air as the oxidant, two oxidizer-to-fuel mass ratios of 13 and 19 were investigated. Jet-A was found to exhibit shorter overall ignition delay times as compared to JP-8. Special emphasis was placed on studying the low-to-intermediate temperature ignition trends. For the conditions studied, the experimental results demonstrate two-stage ignition characteristics for both Jet-A and JP-8. In addition, the overall ignition delay times exhibit a NTC-type behavior in the range of T_C=690–760 K, depending on the compressed pressure. This NTC behavior is observed to be more prominent at lower compressed pressures, as shown in **Fig. 4.3.**

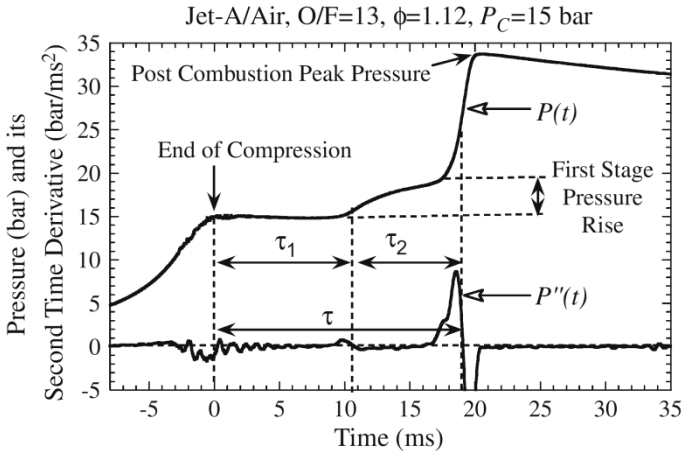

Figure 4.2. Definitions of ignition delays.

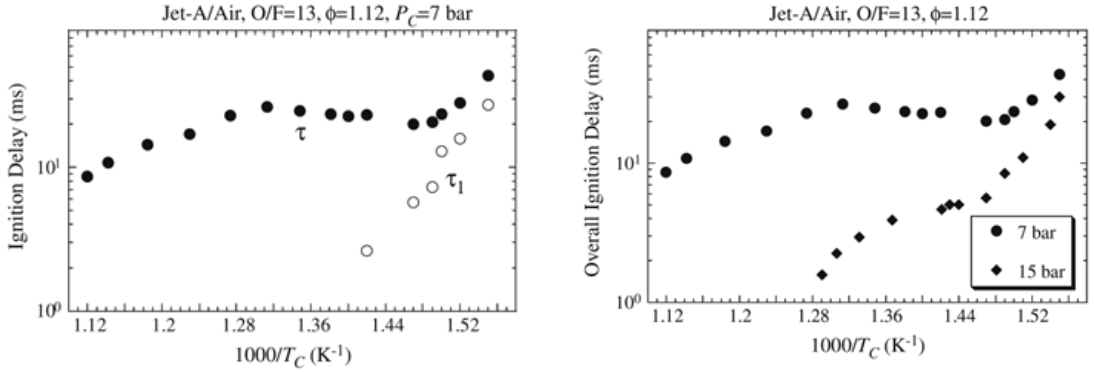

Figure 4.3. (a) NTC trend for Jet-A ignition delays, and (b) pressure effect on NTC trend.

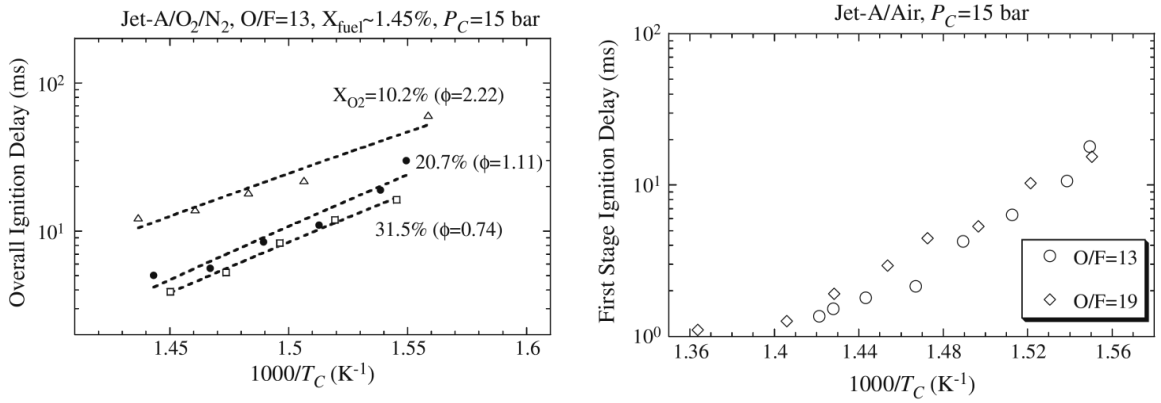

Figure 4.4. (a) Effect of ϕ on overall ignition delay, and (b) Effect of ϕ on 1st-stage ignition delay

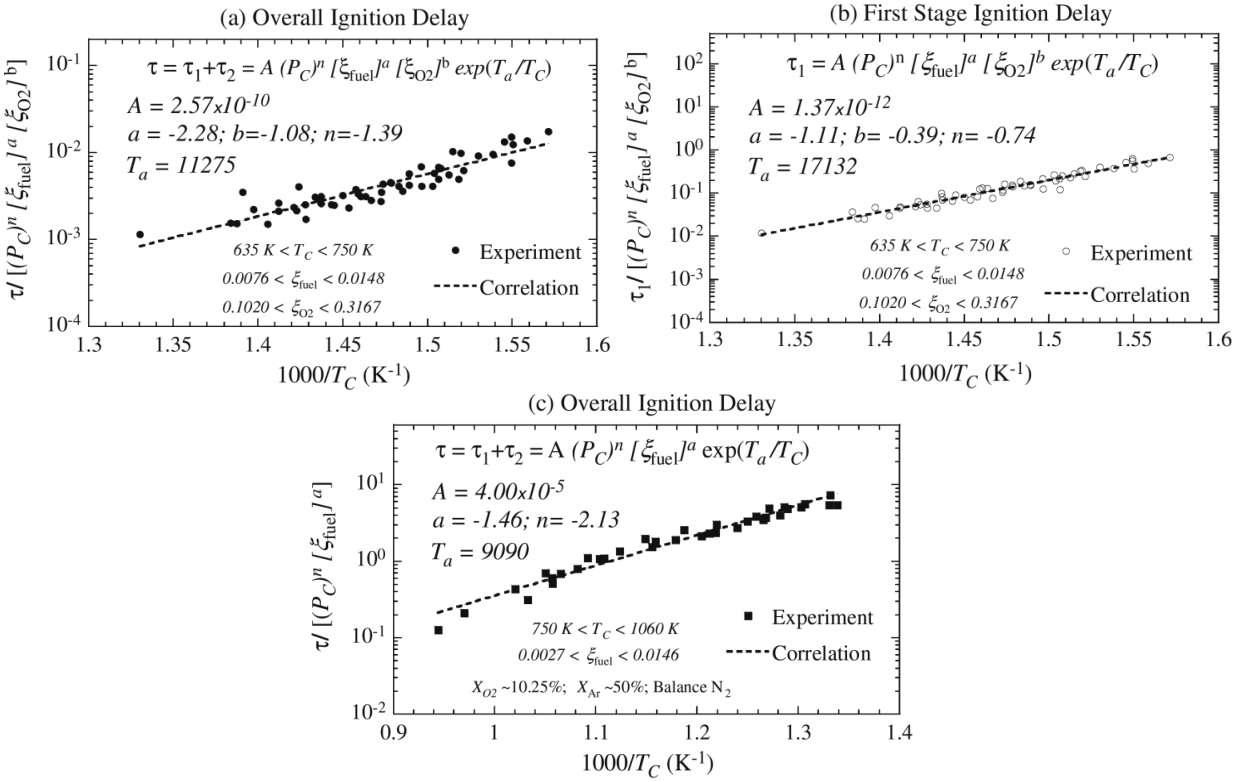

Figure 4.5. Ignition delay correlations for Jet-A: (a) overall ignition delay for Jet-A/O_2/N_2 mixtures,(b) first-stage ignition delay for Jet-A/O_2/N_2 mixtures, and (c) overall ignition delay for Jet-A/O_2/N_2/Ar mixtures.

The equivalence ratio is found to have a very strong influence on the overall ignition delay time, but not on the first-stage ignition delay, as shown in **Figs. 4.4(a) and 4.4(b).** As shown in **Figs. 4.4(a) and 4.4(b)** the first-stage ignition delays also exhibit a weaker dependence on the compressed gas pressure when compared to the overall ignition delays. Compressed charge temperature appears to be the major controlling parameter for the first-stage ignition delay.

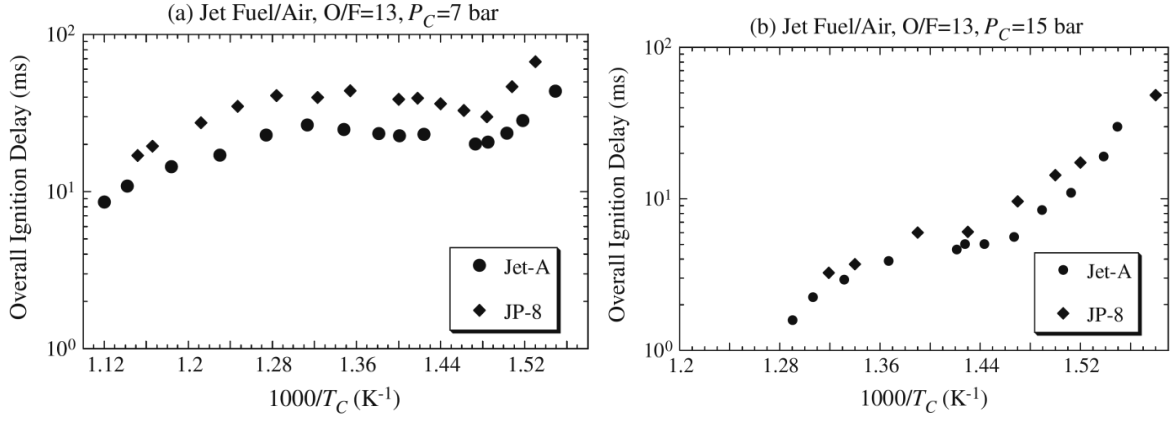

Figure 4.6. (a) Effect of P on overall ignition delay, and (b) Effect of P on first-stage ignition delay.

Furthermore, the oxygen concentration is found to have a strong influence on the overall ignition delay by primarily increasing (decreasing) the second-stage ignition delay for lower (higher) oxygen content. The influence of the key operating variables on the ignition delays has been summarized in the form of a correlation in the temperature range which does not exhibit NTC of the ignition delay times. The correlation plot and the parameters are shown in **Figs. 4.5(a)-(c)** for the first-stage and overall delays and are valid for the conditions indicated in the plots.

A comparison of the overall ignition delay times for Jet-A/air and JP-8/air mixtures under similar conditions is shown in **Fig. 4.6**. **Figures 4.6(a) and 4.6(b)** respectively compare the overall ignition delays at P_C=7 and 15 bar, with a fixed oxidizer-to-fuel mass ratio of O/F=13. The general trend of the Arrhenius plot is quite similar for Jet-A and JP-8. As noted earlier, JP-8 exhibits a longer overall ignition delay time as compared to Jet-A. On comparison of **Figs. 4.6(a) and 4.6(b),** it can be seen that the difference in overall ignition delay for two jet fuels becomes smaller as the pressure increases. Additionally, as observed for Jet-A, JP-8 exhibits a more prominent NTC trend at lower pressures.

4.3.2. S-8, Jet-A, and JP-8

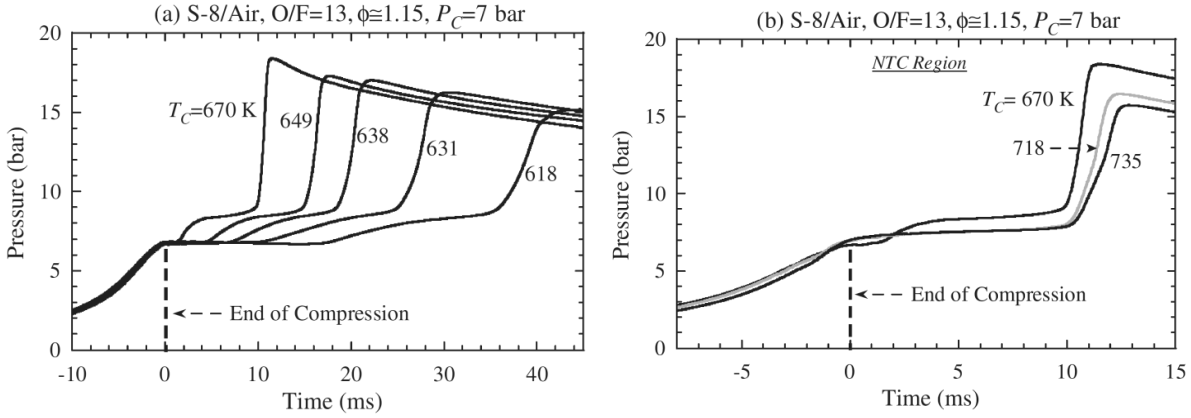

Figure 4.7. (a–b) Pressure traces for S-8/air mixtures with oxidizer-to-fuel mass ratio of 13 at P_C=7 bar.

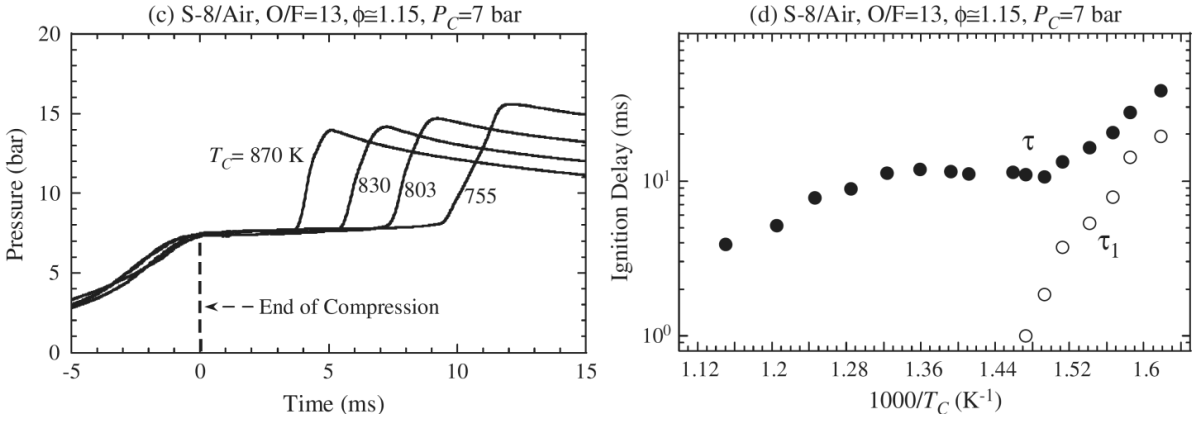

Figure 4.7. (c) Pressure traces and (d) ignition delay times for S-8/air mixtures with oxidizer-to-fuel mass ratio of 13 at P_C=7 bar.

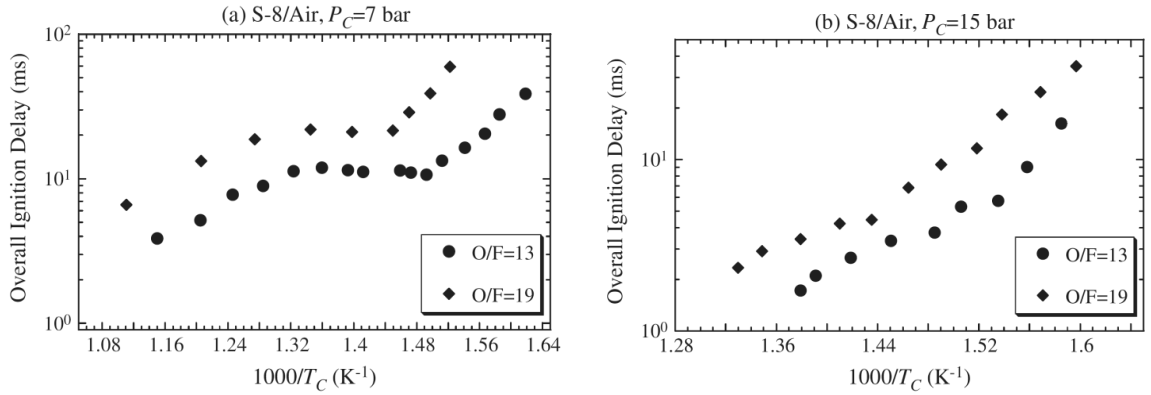

Figure 4.8. Overall ignition delays for S-8/air mixtures with varying oxidizer-to-fuel mass ratios at (a) P_C=7 bar and (b) P_C=15 bar.

Autoignition characteristics of an alternative (non-petroleum) and two conventional jet fuels were investigated and compared using a heated rapid compression machine. The alternative jet fuel studied is known as ‘‘S-8”, which is a hydrocarbon mixture rich in C_7–C_{18} linear and branched alkanes and is produced by Syntroleum via the Fischer–Tropsch process using synthesis gas derived from natural gas. Specifically, ignition delay times for S-8/oxidizer

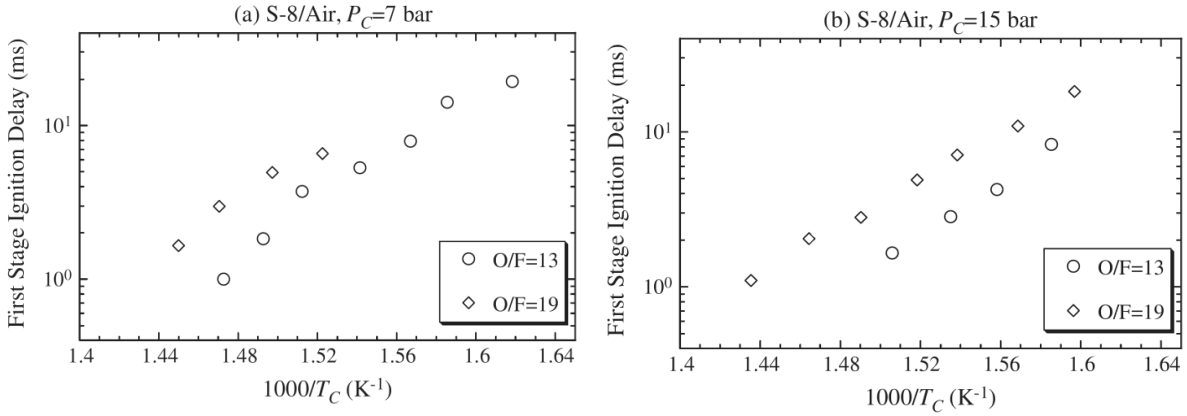

Figure 4.9. Overall ignition delays for S-8/air mixtures with varying oxidizer-to-fuel mass ratios at (a) P_C=7 bar and (b) P_C=15 bar.

mixtures are measured at compressed charge pressures corresponding to 7, 15, and 30 bar, in the low-to-intermediate temperature region ranging from 615 to 933 K, and for equivalence ratios varying from 0.43 to 2.29. The low-to-intermediate temperature ignition trends were the focus of this study. A comparison between the autoignition delay times for conventional (Jet-A and JP-8) and alternative (S-8) jet fuels was systematically carried out. For the conditions investigated, the ignition delay times for all the three jet fuels exhibit a NTC-type behavior in the range of TC=690–760 K, depending on the compressed charge pressure. This NTC behavior is amplified at lower compressed pressures. The NTC trend is shown in **Fig. 4.7**.

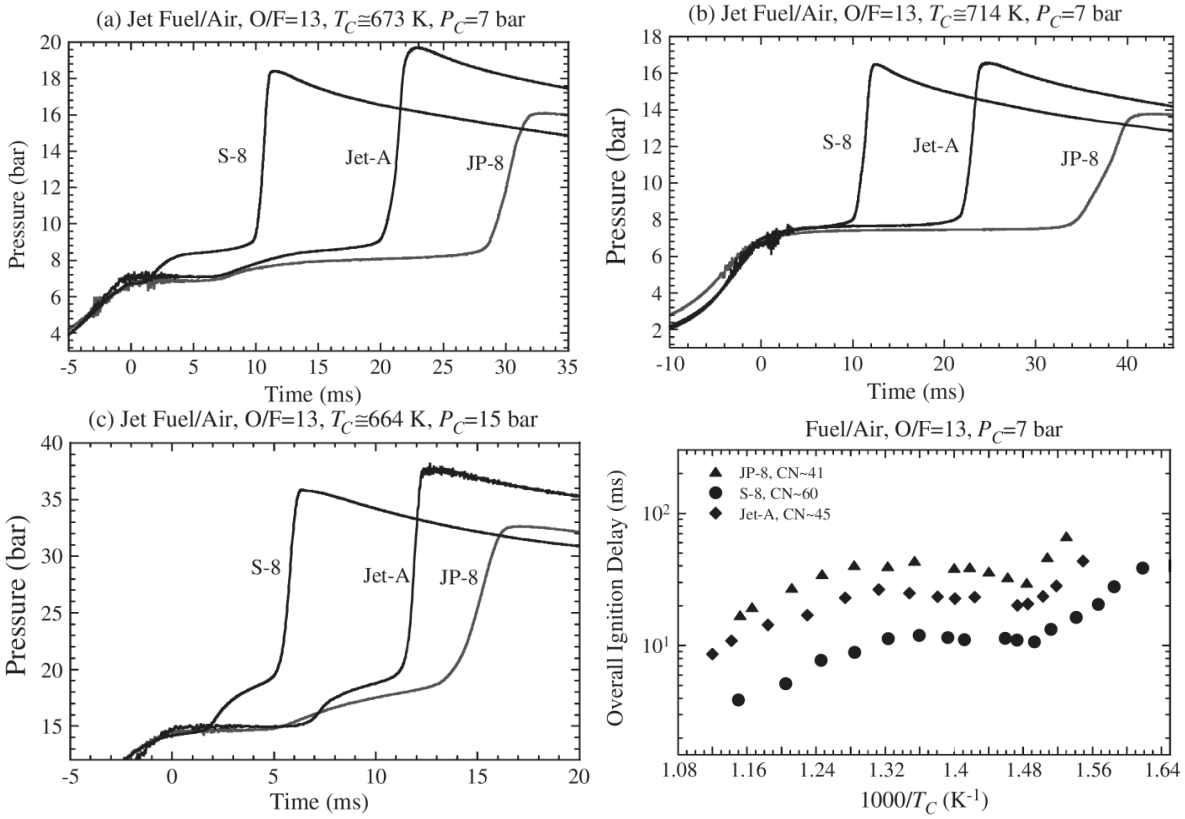

Figure 4.10. Comparative pressures traces for autoignition of S-8/air, Jet-A/air, and JP-8/air mixtures.

The effects of varying fuel loading on the ignition delay for S-8/air mixtures corresponding to an oxidizer-to-fuel mass ratio of O/F= 13 (ϕ~1.15) and O/F=19 (ϕ~0.78) were also studied. For both mixture compositions, the oxygen mole percentage is similar at X_{O2}~20.8%, while the mole percentages of S-8 are X_{fuel}=1.46% and 1.00% for O/F=13 and 19, respectively. **Figure 4.8** shows the effect of varying oxidizer-to-fuel mass ratio on the overall ignition delay for P_C=7 and 15 bar.

The corresponding plot for the first-stage ignition delay comparison is shown in **Fig. 4.9**. Although the first-stage ignition delay is also seen in **Fig. 4.9** to slightly decrease with decreasing oxidizer- to-fuel mass ratio, the extent of reduction is lesser than the overall ignition delay. The comparison of **Figs. 4.9(a) and 4.9(b)** further shows that for the same O/F value, the first-stage ignition delays are only slightly affected by the compressed charge pressure.

Under similar conditions of pressure, temperature, and oxidizer-to-fuel mass ratio, the ignition propensity of S-8 is the highest, followed by Jet-A and JP-8. While the first-stage ignition delays for Jet-A and JP-8 are similar, S-8 has a shorter first-stage ignition delay. Regarding the overall ignition delay, JP-8 is the slowest and S-8 is the fastest, with Jet-A in-between the two.

The comparative experimental pressure traces for the three jet fuels with air as an oxidizer are shown in **Fig. 4.10**. **Figure 4.10(a) and (b)** compare the pressure traces corresponding to a

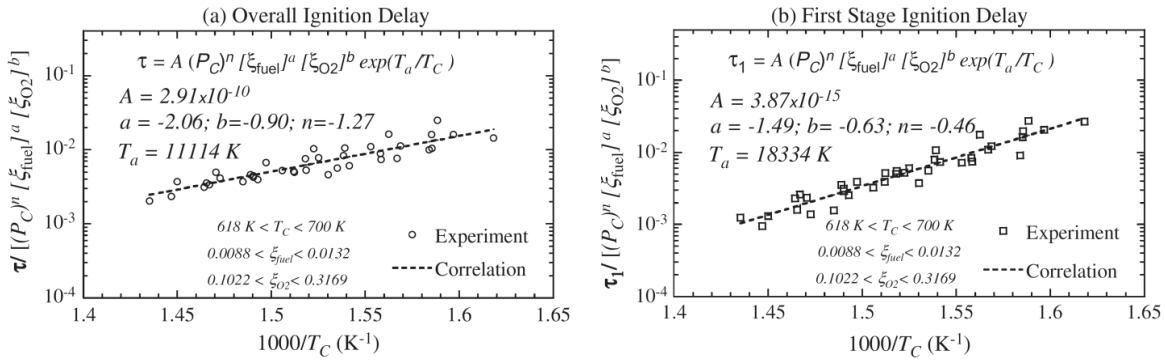

Figure 4.11. Ignition delay correlations for S-8/air mixtures with varying conditions.

compressed pressure of P_C=7 bar and an oxidizer-to-fuel mass ratio of O/F=13. **Figure 4.10(a)** demonstrates the ignition characteristics comparison in a relatively lower temperature case of approximately T_C=673 K, which is outside the NTC regime. All three jet fuels are seen to exhibit a clear two-stage ignition response. The alternative jet fuel, S-8, displays the shortest ignition delay, with both the first and second stage ignition delays being smaller as compared to the two conventional jet fuels, namely Jet-A and JP-8. An interesting point to be noticed is the relatively different overall ignition delay times for Jet-A and JP-8 despite having a nearly coincident first-

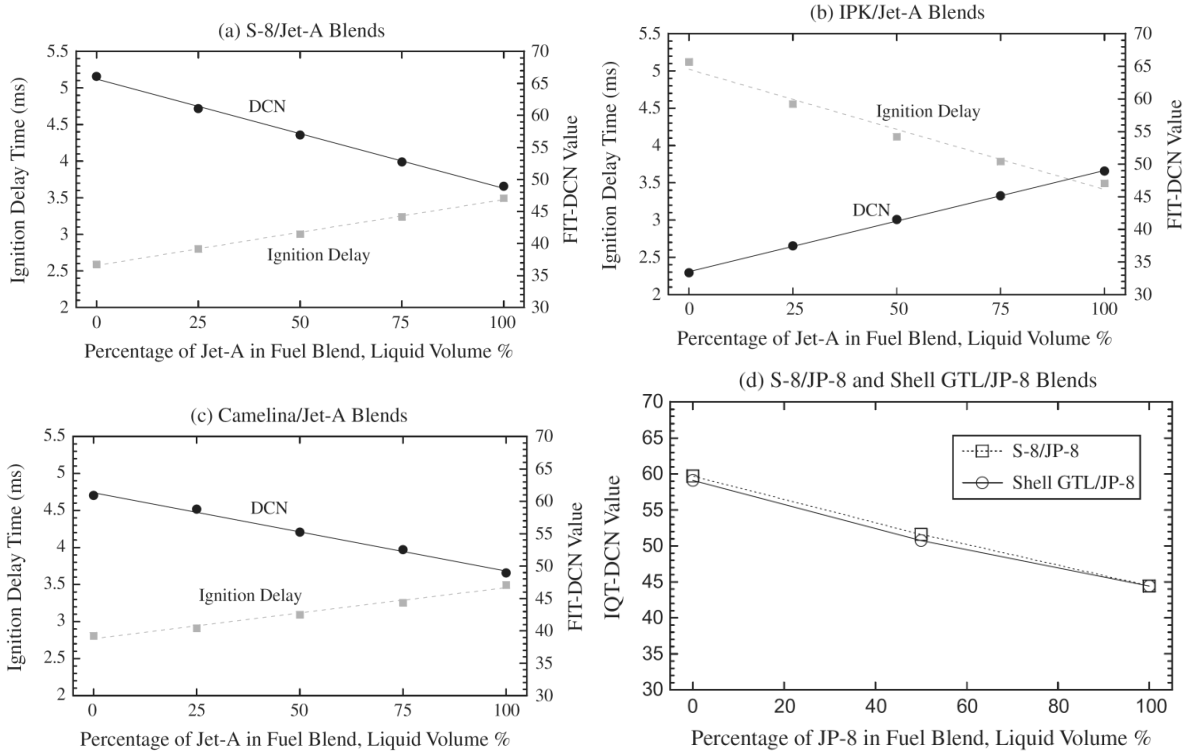

Figure 4.12. (a)-(c) Measured ignition delays and derived cetane numbers of binary fuel blends in accordance with ASTM D7170 and (d) measured derived cetane numbers of binary fuel blends based on ASTM D6890 taken from Bessee GB, Hutzler SA,Wilson GR; AFRL-RZ-WP-TR-2011-2084; April 2011.

stage activity. It is seen that the second-stage ignition delay for the JP-8 fuel is relatively longer leading to a correspondingly larger overall ignition delay as compared to Jet-A. A similar trend for the relative ignition delay times for the three jet fuels at a higher compressed gas temperature, which lies within the NTC region, is observed in **Fig. 4.10(b).** The relatively suppressed first-stage activity is also noted in **Fig. 4.10(b). Figure 4.10(c)** compares the results at a higher compressed pressure of P_C=15 bar under the similar temperature condition as **Fig. 4.10(a),** showing the same trends for both first and second stage ignition responses, as discussed earlier.

The equivalence ratio is found to have a very strong influence on the overall ignition delay time for all the three jet fuels. The first-stage ignition delays exhibit a weaker dependence on the compressed gas pressure when compared to the overall ignition delays. Compressed charge temperature appears to be the major controlling parameter for the first-stage ignition delay. The effects for S-8 were obtained in the form a correlation shown in **Fig. 4.11**.

4.3.3. SPK, HRJ, Jet-A and JP-8

Furthermore, conventional Jet-A and six alternative jet fuels, including three Fischer–Tropsch ‘‘Synthetic Paraffinic Kerosene’’ (SPK) fuels and three ‘‘Hydrotreated Renewable Jet’’ (HRJ) fuels, were experimentally investigated to obtain their fundamental combustion characteristics in

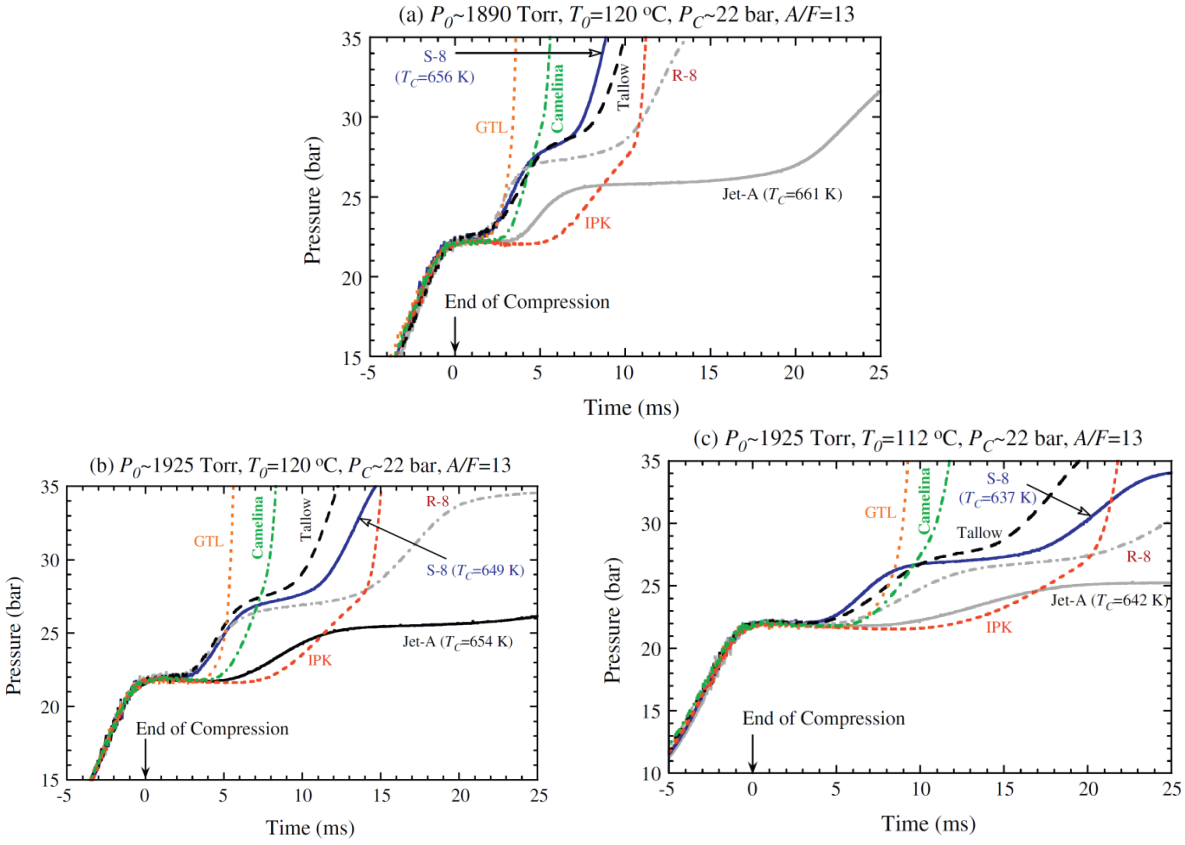

Figure 4.13. Comparative autoignition responses of Jet-A and alternative jet fuels at A/F=13, P_C=22 bar, and varying compressed charge temperatures.

terms of Derived Cetane Number (DCN) and autoignition response. The ignition delay times and DCNs for each jet fuel and selected binary blends of Jet-A and alternative jet fuel were determined by using a Fuel Ignition Tester in accordance with the ASTM D7170 method, as shown in **Fig. 4.12**.

In addition, the autoignition response for fuel/air mixtures was recorded and compared in a heated Rapid Compression Machine, conducted at an air-to-fuel mass ratio of 13 and under a compressed pressure of 22 bar, as shown in **Fig. 4.13**. By changing the compression ratio and initial temperature, the trend of autoignition behavior over a range of compressed temperatures was studied. The DCNs of alternative jet fuels are higher than that of Jet-A except for Sasol IPK. This is because Jet-A contains about 20% aromatics while IPK consists mostly of iso-paraffin and cyclo-paraffin, all of these compositions are less reactive compared to n-paraffins. The blending DCNs of binary mixtures of conventional and alternative jet fuels showed a linear relation between DCN and blending fuel composition. Such a linear dependence of DCN on blending ratio could be due to the similar volatility range and hydrocarbon distribution for alternative jet fuels. The autoignition response results demonstrated that alternative jet fuels ignite faster than Jet-A, and autoignition behavior can be very sensitive to the fuel composition and structure.

4.4. Premixed Flame Experiments

4.4.1. Jet-A and S-8

The laminar flame speed and extinction stretch rates of conventional (Jet-A) and alternative (S-8) jet fuels were obtained experimentally. Experimental results indicate that while Jet-A and S-8 exhibit similar flame propagation characteristics, the extinction response is markedly different. The alternative jet fuel, S-8, is found to produce a robust flame in terms of the capacity to resist a stretch induced blowoff, as compared to the conventional Jet-A fuel. The difference is most

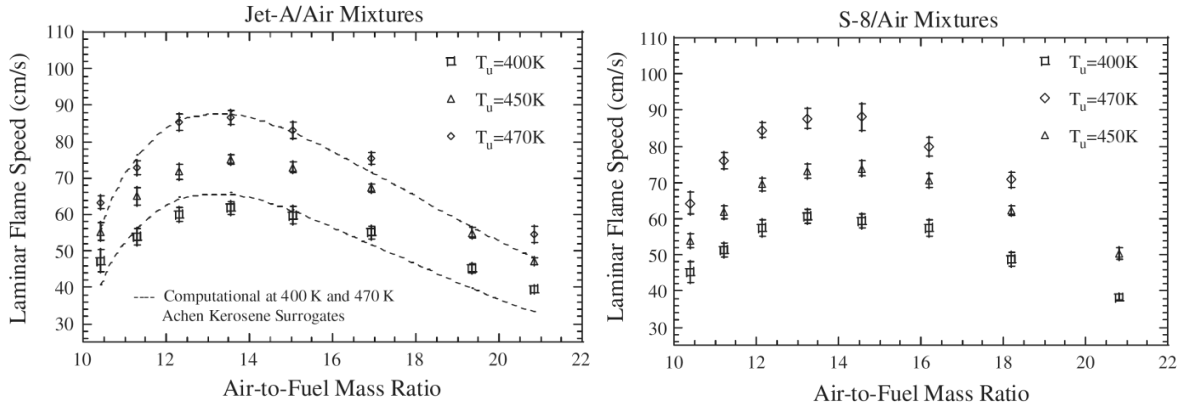

Figure 4.14. Laminar flame speeds of (a) Jet-A/air and (b) S-8/air mixtures as a function of air-to-fuel mass ratio. Simulated Mechanism: Honnet S, Seshadri K, Niemann U, Peters N;.Proc Combust Inst 2009; 32:485–92.

likely on account of the fuel structure effects and their influence on the relative sensitivity of the global combustion responses. A comparison of the current results for real jet fuels with neat alkane components is used to partially confirm the fuel structure effects. These experimental flame parameters provide a set of relevant fundamental combustion data for the validation and optimization of the existing reaction mechanisms. The measured laminar flame speeds of Jet-A/air and S-8/air mixtures as a function of air-to-fuel mass ratio for three different mixture preheat temperatures, T_u=400, 450, and 470 K, are shown in **Figs. 4.14(a) and 4.14(b)**, respectively. The 'air' used in the current experiments is synthesized by mixing oxygen and nitrogen in the molar ratio of 1:3.76. The error bars in **Fig. 4.14** indicate the 95% confidence interval estimate of the laminar flame speed obtained by using linear extrapolation technique. Moreover, the error bars are representative of the scatter and the number of data points in the raw dataset.

The measured extinction stretch rates for Jet-A/O_2/N_2 and S-8/O_2/N_2 mixtures at 400 K preheat temperature as a function of equivalence ratio are shown in **Figs. 4.15(a) and 4.15(b)**. Here, the molar ratio of $N_2/(N_2+O_2)$ is 0.84, i.e. the oxidizer consists of 84% nitrogen and 16% oxygen by mole. Experimentally, two modes of extinction, based on the separation between the twin flames, were observed. Specifically, the extinction of lean counterflow flames of Jet-A/O_2/N_2 and S-8/O_2/N_2 mixtures occurs with a finite separation distance, while that of rich flames exhibits a merging of two luminous flamelets.

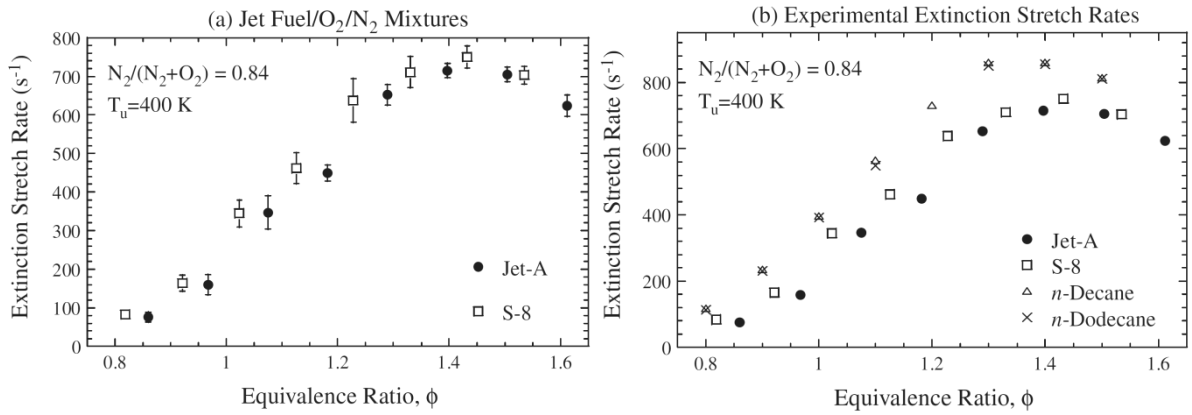

Figure 4.15. (a) Experimental extinction stretch rates for jet fuels and (b) comparative extinction stretch rates for jet fuels, n-decane, and n-dodecane.

While the kinetic mechanism for a recently reported kerosene surrogate is seen to predict the laminar flame speeds satisfactorily at some equivalence ratios, noticeable discrepancies are

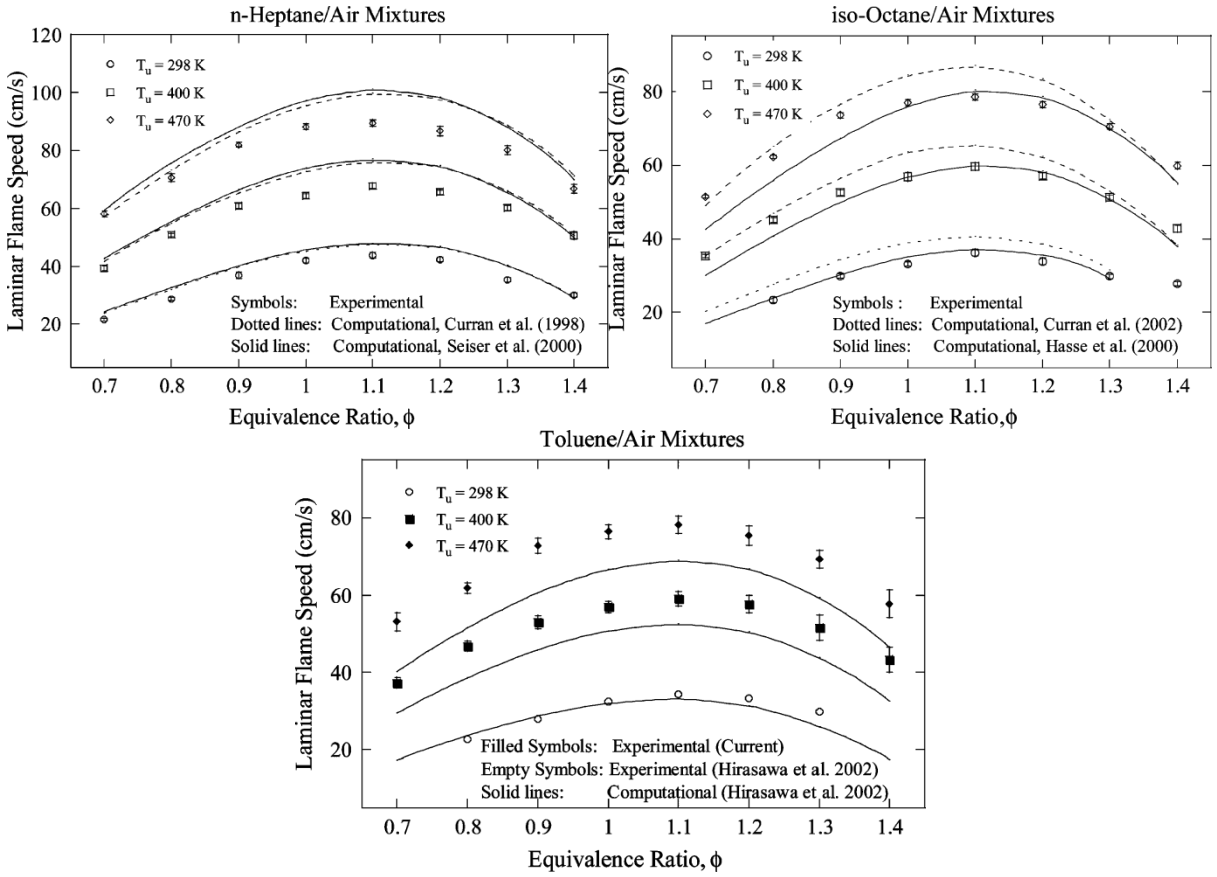

Figure 4.16. Experimental laminar flame speeds for gasoline surrogate components.

identified for the extinction stretch rate predictions, although the trend is well predicted. Therefore, further kinetic modeling and experimental studies are needed for a better understanding of the combustion chemistry for real jet fuels.

4.4.2. Surrogate Components for Gasoline and Kerosene

Laminar flame speeds and extinction stretch rates were experimentally obtained for typical surrogate components of gasoline and kerosene-type fuels at atmospheric pressure conditions, as shown in **Figs. 4.16 and 4.17**, respectively. Among the gasoline surrogate components studied, n-heptane exhibits the highest laminar flame speed, while the laminar flame speeds of iso-octane and toluene are found to be quite similar. The same trend holds true for extinction stretch rates of gasoline surrogate components. Detailed kinetic schemes for n-heptane and iso-octane are found to over-predict the experimental data. On the other hand, the iso-octane mechanisms well-predicts the present experimental results of laminar flame speeds and extinction stretch rates.

The results for key kerosene surrogate components show that n-decane has the highest laminar flame speed, followed by n-dodecane and methylcyclohexane. Despite that, the laminar flame speeds and the extinction stretch rates for n-decane and n-dodecane are considered to be quite similar. There is a fair prediction of laminar flame speeds by some of the recent kinetic schemes, although the extinction stretch rates are generally over-predicted. In addition, the recent detailed

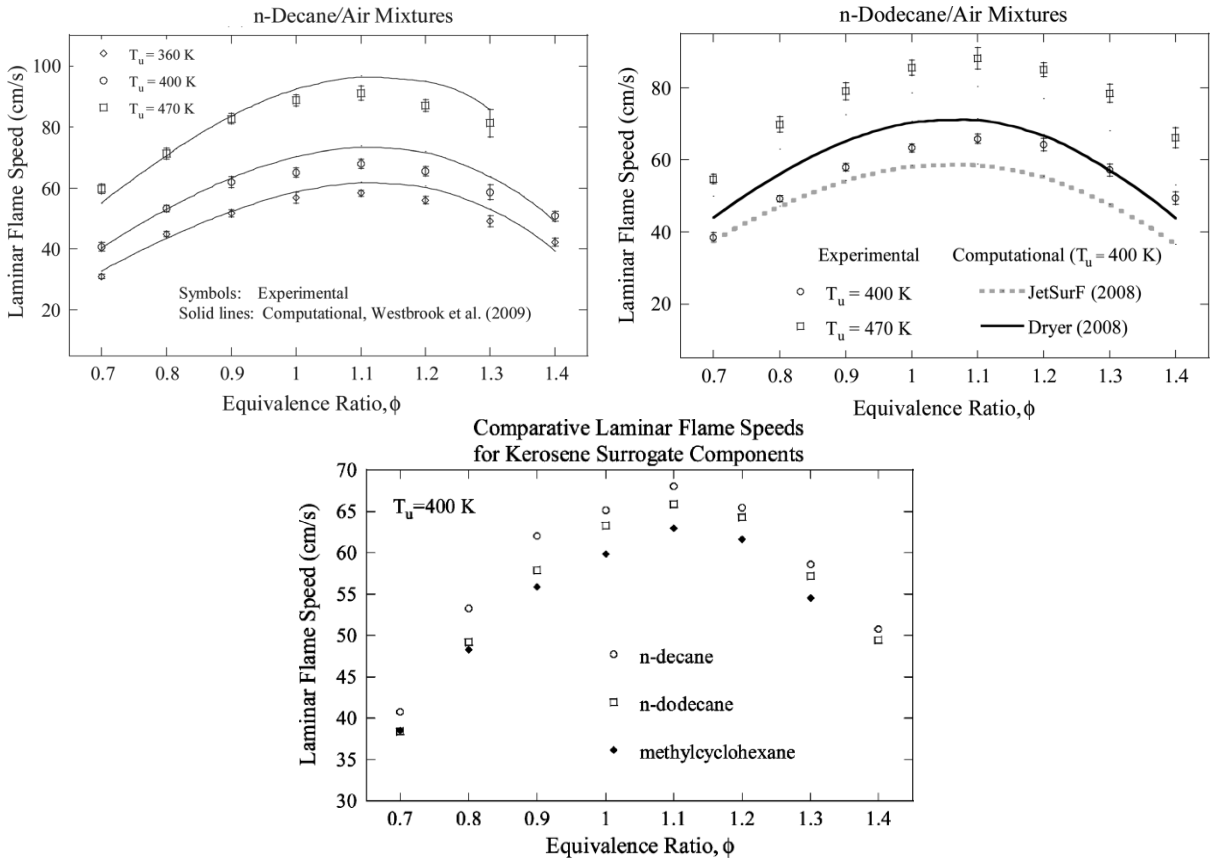

Figure 4.17. Experimental laminar flame speeds for kerosene surrogate components.

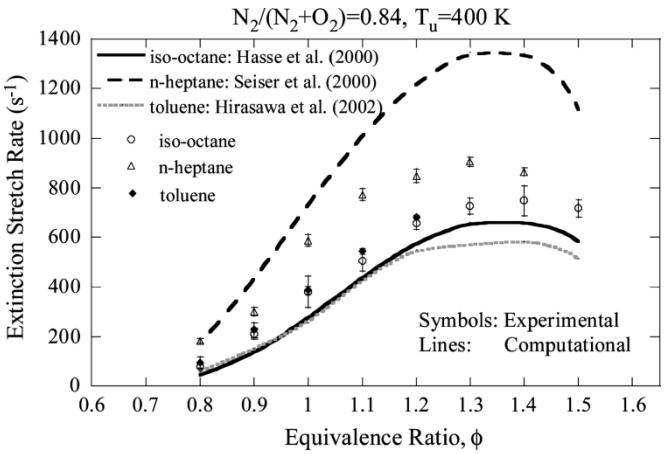

Figure 4.18. Experimental extinction stretch rates for gasoline surrogate components.

kinetic scheme adequately captures the trend for n-decane laminar flame speeds, as both a function of the equivalence ratio and the mixture preheat temperature. It is found that n-alkanes exhibit the highest flame speeds followed by cycloalkane. The branched alkane and the aromatic exhibit the lowest laminar flame speeds, although their values are quite similar.

Moreover, the n-alkane flames are more resistant to stretch-induced extinction as compared to branched alkane and aromatic flames, as demonstrated in **Fig. 4.18**. **Figure 4.19** compares the experimental and computed stretch induced extinction limits for n-alkane components relevant to kerosene type fuels.

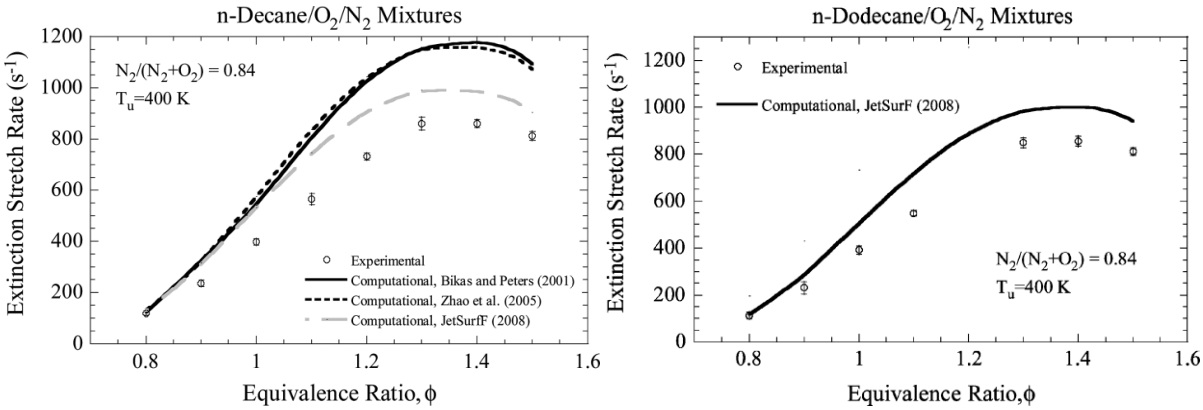

Figure 4.19. Comparison of experimental and computational extinction stretch rates for kerosene surrogate components.

Furthermore, the sensitivity analysis yields some interesting insight into the influence of kinetics as well as transport properties. It is found that both the flame propagation and extinction phenomena are very sensitive to kinetics as well as transport. The range of variation for a given level of perturbation in the kinetics and transport parameters has also been quantified.

4.4.3. Aromatic Hydrocarbons

In addition, laminar flame speeds and extinction stretch rates have been experimentally and numerically determined in toluene, n-PB, 1,2,4-TMB, and 1,3,5-TMB premixed flames under atmospheric pressure. The experimental results of laminar flame speed and extinction limit shown in **Figs. 4.20 and 4.21**, respectively, demonstrate that n-PB has the highest reactivity followed by toluene and TMBs.

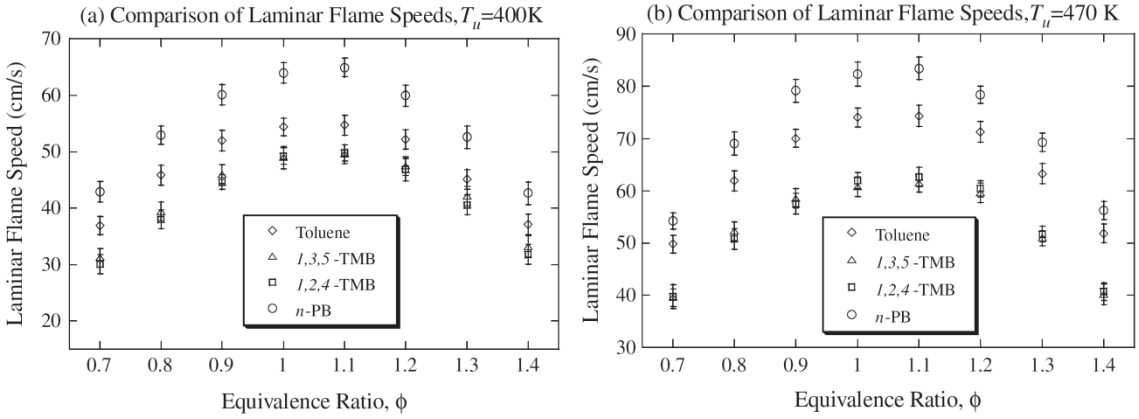

Figure 4.20. Experimental laminar flame speeds for aromatic hydrocarbons at (a) 400 K and (b) 470 K.

The simulation results were shown to be in reasonable agreement with the present experimental data, except that the 1,2,4-TMB model significantly under-predicts the extinction stretch rates. Sensitivity analysis of the present models demonstrated that both flame phenomena are mostly sensitive to chain-branching and heat release reactions.

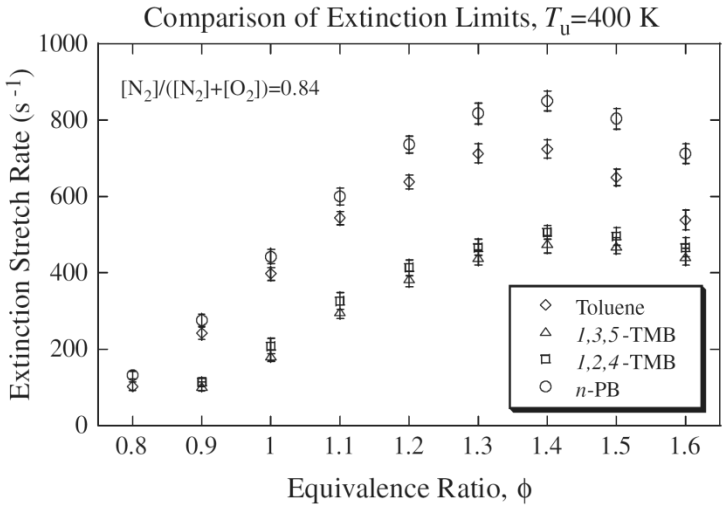

Figure 4.21. Experimental extinction stretch rates for aromatic hydrocarbons.

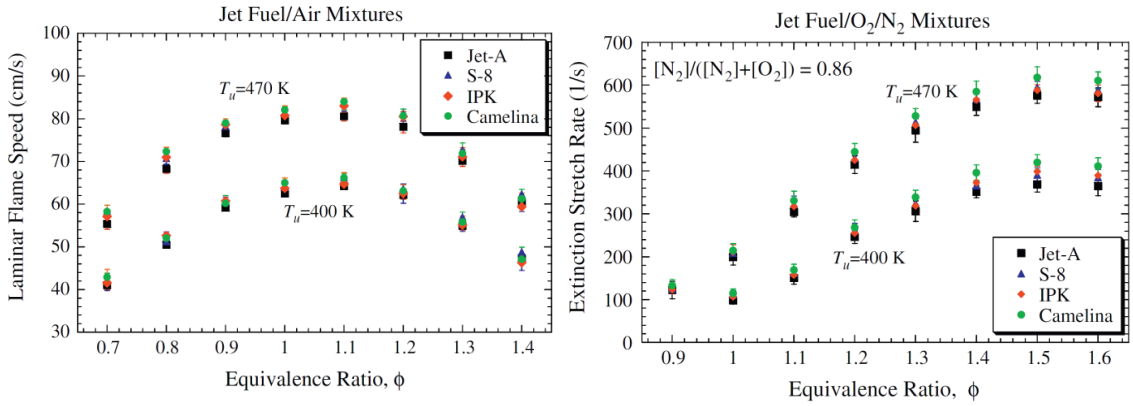

Figure 4.22. Experimental laminar flame speeds and extinction stretch rates for conventional and alternative jet fuels.

Among all the aromatics, n-PB has the highest resistance to extinction, followed by toluene and TMBs in descending order. Comparing the extinction limits of n-PB and toluene, n-PB is consistently higher than toluene and the difference becomes larger when the fuel/oxidizer mixtures become rich.

Further flux analysis revealed that the present models produce high reactivity of n-PB as a result of C_2 species and the accompany radicals produced during the disintegration of propyl side chain, while the high concentration of resonantly-stable benzylic radicals is responsible for the low reactivity of TMB. Continuing efforts are underway to refine the n-PB model employed herein and develop 1,3,5-TMB model so as to encompass a larger range of experimental venues. We also note that mechanistically revealing experiments will be particularly useful in developing higher fidelity models for these alkyl aromatics.

4.4.4. SPK, HRJ, and Jet-A

Further, conventional Jet-A and six alternative jet fuels, including three Fischer–Tropsch ‘‘Synthetic Paraffinic Kerosene’’ (SPK) fuels and three ‘‘Hydrotreated Renewable Jet’’ (HRJ) fuels, were experimentally investigated to obtain their laminar flame speeds and extinction stretch rates, as shown in **Fig. 4.22**. The laminar flame speeds and extinction stretch rates were measured in the premixed twin-flame configuration by using a counterflow burner. The flame data at two unburned mixture temperatures of 400 K and 470 K were respectively reported over an equivalence ratio range of ϕ=0.7–1.4 for the laminar flame speeds and of ϕ=0.9–1.6 for the extinction stretch rate measurements. The comparison of fundamental combustion properties for Jet-A and various alternative jet fuels provides insights into understanding the impact of fuel properties on combustion performance and developing a cost-effective combustion testing program that includes fundamental characterization.

Laminar flame speed data showed no discernible difference between alternative jet fuels and Jet-A, while extinction stretch rate data illustrated that alternative jet fuels are more resistant to extinction than Jet-A. The lower extinction limit of Jet-A could also be caused by its aromatic

content. Recognizing the importance of characterizing both physical and chemical properties of alternative jet fuels, the present investigation showed that the fundamental combustion experiments can be helpful in understanding the influence of fuel properties on combustion performance.

4.5. Archival Publications

G. Mittal, C. J. Sung. Homogeneous Charge Compression Ignition of Binary Fuel Blends. *Combust Flame* (2008) 155:431-439.

G. Mittal, M. Chaos, C. J. Sung, F. L. Dryer. Dimethyl Ether Autoignition in a Rapid Compression Machine: Experiments and Chemical Kinetic Modeling. *Fuel Processing Technology* (2008) 89(12):1244-1254.

K. Kumar, G. Mittal, C. J. Sung. Autoignition of n-Decane under Elevated Pressure and Low-to-Intermediate Temperature Conditions. *Combust Flame* (2009) 156:1278-1288.

G. Mittal, C. J. Sung. Autoignition of Methylcyclohexane at Elevated Pressures, *Combust Flame* (2009) 156:1852-1855.

K. Kumar, C. J. Sung. An Experimental Study of the Autoignition Characteristics of Conventional Jet Fuel/Oxidizer Mixtures: Jet-A and JP-8, *Combust Flame* (2010) 157:676-685.

K. Kumar, C. J. Sung. Flame Propagation and Extinction Characteristics of Neat Surrogate Fuel Components, *Energy and Fuels* (2010) 24: 3840-3849.

K. Kumar, C. J. Sung. A Comparative Experimental Study of the Autoignition Characteristics of Alternative and Conventional Jet Fuel/Oxidizer Mixtures, *Fuel* (2010) 89:2853-2863.

S. Dooley, S. H. Won, M. Chaos, J. Heyne, Y. Ju, F. L. Dryer, K. Kumar, C. J. Sung, H. Wang, M. A. Oehlschlaeger, R.J., Santoro, T. A. Litzinger. A Jet Fuel Surrogate Formulated by Real Fuel Properties, *Combust Flame* (2010) 157:2333-2339.

K. Kumar, C. J. Sung, X. Hui. Laminar Flame Speeds and Extinction Limits of Conventional and Alternative Jet Fuels, *Fuel* (2011) 90: 1004-1011.

G. Mittal, M. P. Raju, C.J. Sung. Vortex Formation in a Rapid Compression Machine: Influence of Physical and Operating Parameters, *Fuel* (2011) 94: 409-417.

S. Dooley, S.H. Won, J. Heyne, T.I. Farouk, Y. Ju, F.L. Dryer, K. Kumar, X. Hui, C-J. Sung, H. Wang, M. A. Oehlschlaeger, T.A. Litzinger, R.J. Santoro, T. Malewecki, K. Brezinsky. The Experimental Evaluation of a Methodology for Surrogate Fuel Formulation to Emulate Gas Phase Combustion Kinetic Phenomena, *Combust Flame* (2012) 159:1444-4466.

X. Hui, K. Kumar, C. J. Sung, S. Dooley, F. L. Dryer. Laminar Flame Speeds and Extinction Stretch Rates of Selected Aromatic Hydrocarbons, *Fuel* (2012) 97:695-702.

X. Hui, K. Kumar, C. J. Sung, T. Edwards, D. Gardner, Experimental Studies on the Combustion Characteristics of Alternative Jet Fuels, *Fuel* (2012) 98:176-182.

X. Hui, C. J. Sung. Laminar Flame Speeds of Transportation-Relevant Hydrocarbons and Jet Fuels at Elevated Temperatures and Pressures, *Fuel*, submitted.

4.6. Abstracts and Preprints

G. Mittal, M. Chaos, C. J. Sung, F. L. Dryer. A Rapid Compression Machine Study of Dimethyl Ether Autoignition, Fall Technical Meeting of the Eastern States Section of the Combustion Institute, University of Virginia, VA, 2007.

K. Kumar, C. J. Sung. An Experimental Study of the Autoignition Characteristics of Jet-A/Oxidizer Mixtures in a Rapid Compression Machine, Spring Technical Meeting of the Western States Section of the Combustion Institute, University of Southern California, CA, 2008.

G. Mittal, C. J. Sung. An Experimental Study of Autoignition of Methylcyclohexane, Technical Meeting of the Central States Section of the Combustion Institute, Tuscaloosa, AL, 2008.

K. Kumar, C. J. Sung. Autoignition of Conventional and Alternative Jet Fuels, Second International Symposium on Jet Propulsion and Power Engineering, Guilin, China, 2008.

K. Kumar, C. J. Sung, X. Hui. Laminar Flame Speeds and Extinction Limits of Conventional and Alternative Jet Fuels, Forty-Seventh Aerospace Sciences Meeting, AIAA Paper No. 2009-991, 2009.

K. Kumar, C. J. Sung. Autoignition of Jet Fuels under High Pressure and Low-to-intermediate Temperatures, Forty-Seventh Aerospace Sciences Meeting, AIAA Paper No. 2009-1527, 2009.

K. Kumar, C. J. Sung. Autoignition of Fully Blended Jet Fuels and Neat Hydrocarbons: Effect of Cetane Number, Sixth Joint Meeting of the U.S. Sections of the Combustion Institute, Ann Arbor, MI, 2009.

K. Kumar, X. Hui, C. J. Sung. Fundamental Combustion Properties of Jet Fuels, Sixth Joint Meeting of the U.S. Sections of the Combustion Institute, Ann Arbor, MI, 2009.

K. Kumar, C. J. Sung. Flame Propagation and Extinction Characteristics of Neat Hydrocarbon Surrogate Fuel Components, Sixth Joint Meeting of the U.S. Sections of the Combustion Institute, Ann Arbor, MI, 2009.

S. Dooley, S.H. Won, M. Chaos, J. Heyne, Y. Ju, F. L. Dryer, K. Kamal, C. J. Sung, H. Wang, M. A. Oehlschlaeger, R. J. Santoro, T. A. Litzinger. A Jet Fuel Surrogate Formulated By Real Fuel Properties, Technical Meeting of the Western States Section of the Combustion Institute, Boulder, Colorado, March 23, 2010.

X. Hui, A., K. Das, K. Kumar, C.J. Sung. Laminar Flame Speeds and Extinction Stretch Rates of Selected Aromatic Hydrocarbons, Forty-Ninth Aerospace Sciences Meeting, Paper No. AIAA-2011-241, 2011.

K. Kumar, X. Hui, A. K. Das, C. J. Sung. Autoignition, Flame Propagation, and Extinction of Binary Fuel Blends of n-Decane/Ethylene and n-Decane/Methane, Forty-Ninth Aerospace Sciences Meeting, Paper No. AIAA-2011-315, 2011.

S. Dooley, S. H. Won, J. Heyne, Y. Ju, F. L. Dryer, K. Kumar, C. J. Sung, H. Wang, M. A. Oehlschlaeger, T. A. Litzinger, and R. J. Santoro. The Formulation of Surrogate Fuels to Emulate the Combustion Behavior of Real Jet Aviation Fuels, Seventh Joint Meeting of the U.S. Sections of the Combustion Institute, Atlanta, GA, 2011.

K. Kumar, C. J. Sung. Autoignition of Selected Alkyl-Benzenes in a Rapid Compression Machine, Fall Technical Meeting of the Eastern States Section of the Combustion Institute, University of Connecticut, Storrs, CT, 2011.

4.7. Presentations

C.J. Sung. Energy Sustainability: Burning Issues and Green Aviation, Department of Aerospace Engineering, University of Michigan, Ann Arbor, MI, April 10, 2009.

C.J. Sung. Burning Issues in Energy Sustainability and Green Aviation, Department of Mechanical Engineering, University of Connecticut, Storrs, CT, April 15, 2009.

C.J. Sung. The Role of Chemical Kinetics in Green Combustion, Department of Chemical, Biological and Pharmaceutical Engineering, New Jersey Institute of Technology, Newark, NJ, February 15, 2010.

C.J. Sung. Rapid Compression Machine Studies on Autoignition of Next Generation Fuels, Argonne National Laboratory, Washington, DC, August 24, 2010.

C.J. Sung. Autoignition, Flame Propagation, and Extinction of Alternative and Conventional Jet Fuels, Invited Session on Assessment of Alternative Fuel Fundamental Combustion Properties from Test and Analysis, Forty-Ninth Aerospace Sciences Meeting, Orlando, FL, January 4, 2011.

C.J. Sung. Combustion of Next Generation Fuels, Indo-US Workshop on Biofuel Combustion and Sprays, Indian Institute of Science, Bangalore, India, June 22, 2011.

C.J. Sung. Combustion Evaluation of Alternative Jet Fuels, Keynote Speech at the Second International Symposium on Aircraft Airworthiness, Beijing, China, October 27, 2011.

4.8. Graduate Theses

Both Mr. Xin Hui and Mr. Kyle Brady are still working on their Ph.D. dissertations.

4.9. Personnel

Dr. Gaurav Mittal, Dr. Kamal Kumar, Mr. Xin Hui, Mr. Kyle Brady, Mr. Pradeep Singh

5. The Pennsylvania State University (PSU) – R.J. Santoro, T.A. Litzinger

5.1. Abstract

The MURI tasks conducted at Penn State focused on two general topics: (1) the use of Threshold Sooting Index (TSI) to characterize soot formation for Jet A and surrogate mixtures simulating Jet A; (2) measurements of the autoignition iso-octane at low to intermediate temperatures and high pressures. With respect to TSI, significant progress was made in characterizing the soot formation of pure compounds, mixture of these compounds and in conjunction with work at Princeton University in the formulation of surrogate mixtures for Jet A. Among the major accomplishments were: (1) The mixture rule to characterize multicomponent surrogates was shown be a linear relation proportional to the mole fraction of the individual components in the fuel in agreement with previous work; (2) Multi-component surrogates for Jet A were formulated and shown to replicate the TSI value for Jet A while also meeting the three other parameters selected to formulate a surrogate; (3) Spatially resolved radial profiles of soot volume fraction using a wick burner for the formulated surrogate and Jet A agreed very well in terms of peak soot volume fraction and profile shape. These measurements established that surrogates not only have a similar TSI but also the same distribution of soot through the two flames. (4) Studies done in the a high pressure model gas turbine combustor comparing a surrogate composed of alkane and aromatics solvents with JP-8 of equal TSI values established that they have the same mean soot volume fractions as a function of equivalence ratio that varied for stoichiometric to a fuel rich equivalence ratio of 1.8.

Studies of autoignition of iso-octane were conducted in a high-pressure flow reactor. A novel methodology was employed in which the minimum equivalence ratio required for ignition, or threshold equivalence ratio, at specific conditions of pressure, temperature, and residence time was measured. Autoignition delay times were obtained at pressures of 15, 17.5, 20, and 22.5 atm, for a temperature range of approximately 640-850 K. Residence times of approximately 70, 100, 125, 155, and 175 ms were investigated over equivalence ratios ranging from 0.25 to 0.8. Results showed an onset of autoignition for all pressures at approximately 640K and as temperature increased, the threshold equivalence ratio decreased. A distinct negative temperature coefficient (NTC) region, where the inverse of this dependence occurs, was observed starting between 700 K and 725 K and ending at approximately 775 K. Above this temperature, the threshold equivalence ratio again, decreased with increasing temperature. Pressure also had a strong effect on ignition delay with an overall decrease in threshold equivalence ratio with increasing pressure. Results were compared with two chemical kinetics models. Good agreement was shown with a model from Lawrence Livermore National Laboratory (LLNL) for the conditions studied in this work. The main discrepancy between the experimental and model results was the over prediction by the model of the threshold equivalence ratio in the NTC region. The second model from Chemical Reaction Engineering and Chemical Kinetics (CRECK) gave similar results as the experiment for the temperature at the onset of autoignition, but showed no presence of the NTC region that was observed experimentally and predicted by the LLNL model. Finally, the LLNL model was also used to provide a better understanding of the oxidation process of iso-octane through reaction pathway and temperature sensitivity analyses. The results showed the importance of the location of H-atom abstraction from the iso-octane molecule in determining

how reactions proceed. H-atom abstraction from the tertiary site on iso-octane served to slow overall reactivity, while abstraction from the primary and secondary locations increased overall reactivity. The fate of the hydrogen peroxide molecule was shown to be especially important in the NTC region.

5.2. Introduction

5.2.1. Motivation Background, and Objectives

Combustion modeling is necessary for the development of efficient and accurate numerical design methodologies for engines. By modeling proposed changes to engine designs ahead of time, the number of costly and time consuming engine tests can be reduced. As the desire grows to employ alternative liquid fuels, energy sources such as coal and bio-feedstocks will be used. Often the alternative fuels from these sources have significantly different chemical or physical properties than the original petroleum based fuel. Modeling the combustion of the alternative fuels will become important to predict any effects on engine performance and emissions.

The concept of surrogate fuels developed from a need to model the combustion of practical liquid fuels used in existing and future engine designs. A surrogate fuel is a mixture of a small number of pure compounds that can mimic the combustion of a real fuel, whether it is derived from petroleum or an alternative source. Practical fuels are often composed of thousands of components, which can vary with location and time of year [1]. The variation is acceptable because specifications generally require fuels to meet certain values on empirical tests, but do not specify composition. This resulting multi-component and variable nature of practical fuels introduces overwhelming complexity to the chemical kinetic modeling task. A surrogate fuel requires a much simpler chemical kinetic model than would be needed for the practical fuel. Therefore, with surrogate fuels to represent the real fuel, designing engines and developing new fuels using modeling becomes possible.

In automobile engines, the technique of substituting surrogates for practical fuels has been used successfully to model the combustion of gasoline. However, developing functioning surrogates for aviation jet fuels is more difficult for several reasons. Jet fuel has a higher average molecular weight than gasoline, which means chemical kinetic models of the individual mixture components of a jet fuel surrogate are harder to develop. Also, the specifications for jet fuels are relatively broad and include fuels with a rather wide range of properties, implying composition can vary significantly [2].

To be useful, the surrogate fuel must match key combustion processes with reasonable fidelity, and models must be carefully constructed, which presents some challenges. Rules for selecting surrogate components and matching mixtures against real jet fuels have not been previously defined. One of the goals of this Multi-disciplinary University Research Initiative (MURI) was to develop a methodology for designing surrogates that can be applied to any fuel. The successful methodology developed to formulate a surrogate relies on matching only a few important combustion- and fuel-related parameters. These crucial parameters include: hydrogen to carbon (H/C) ratio, molecular weight, autoignition characteristics, and sooting tendency. The work described in this section of the Final Report focuses on the development and use of a

parameter for sooting tendency as well as autoignition measurements of iso-octane, which is one of the selected components of the surrogate fuels studied.

The surrogate fuel should be able to accurately simulate in-combustor soot formation as well as soot emissions of Jet A. The sooting characteristics of Jet A are important because radiation from soot formed in the combustor heats and stresses the combustor liner. Soot particles that escape from the combustor may also deposit in the turbine section or exit the engine leaving a plume containing easily detected particles.

Studies of sooting tendency of hydrocarbon fuels have been done in a number of combustors and burners. A simple diffusion flame has been especially useful, as it is a key element of the United States Air Force (USAF) specifications for jet fuel with respect to soot. In diffusion flames, the threshold of soot breakthrough is identified as the condition at which soot particles are observed to exit the flame, and is commonly referred to as the smoke point (*SP*). Measurements show that the smoke point occurs at different flame heights for different fuels. Thus, the smoke point has been used as an important predictor of soot formation for years. The Threshold Soot Index (TSI), which is a linear function of the molecular weight of the fuel divided by the smoke point, can be used as a measure of sooting tendency for fuels for which these quantities are known [3]. TSI has been chosen to be the sooting tendency parameter for the present effort because of its consistency and relationship to the smoke point measurement.

The selection of surrogate components for the aviation jet fuel, Jet A, reflects the type of molecular structures in the real fuel, as well as the availability of chemical kinetic models for which validation data already exist, or are under investigation as part of the MURI collaborative projects or elsewhere. As an initial approach, the surrogate for Jet A is formulated using hydrocarbons from the three main classes of compounds present in the fuel: n-alkanes, iso-alkanes, and aromatics. Higher carbon number n-alkanes and iso-alkanes are selected in order to achieve the typical H/C ratio and autoignition properties of Jet A. Aromatic compounds, which are the most influential to TSI, are chosen with consideration of the length, location and number of alkyl branches on the benzene and naphthalene rings. Thus, the critical parameters for the MURI methodology, such as TSI, are selected to match those of the practical fuel by varying the composition of the surrogate once the base components have been selected.

Five objectives were identified for this section of the study and are described next.

- The first objective was to generate a consistent set of TSI data for all the compounds that are being considered for formulating surrogate mixtures. Determining a consistent set of TSI values required measuring the TSI values for a number of hydrocarbons. In addition to the candidate surrogate compounds, more compounds were tested to allow a better comparison to previous studies. Previous sooting tendency measurements include the flame height, the fuel consumption rate at the smoke point, as well as the volume fraction of soot, known as soot yield. TSI data derived from all three types of measurements were incorporated into the final set of TSI values.
- A second objective was to verify that for binary mixtures TSI values followed a linear mixing rule based on the mole fraction of the candidate surrogate compounds.
- A third objective was to verify that different hydrocarbon molecules from the same class could be used to formulate equivalent mixtures, in terms of the TSI values, using the

linear mixing rule. Confirming mixture equivalence required testing the mixtures to verify that their measured TSI values conformed to the mixture rule.

- The fourth objective was to test the TSI of a surrogate mixture that was formulated to match the measured TSI of Jet A. Comparisons were made using measurements made in a standard smoke point lamp, a wick burner and model gas turbine operating at elevated pressure. Overall, this research attempted to show that TSI is an effective method for sooting tendency prediction for real jet fuels.
- The final objective was to determine the autoignition time for iso-octane, which was one of the pure components of the surrogate fuel composition.

Summary of Research Findings

5.3. Threshold Sooting Index Investigations and Measurements

5.3.1. Experimental apparatus and methodology

A description of the experimental apparatus can be found in Ref. [20]. With respect to the methodology, we follow that of Calcote and Manos [3] who recognized that previous smoke point studies all demonstrated that a similar qualitative ordering of hydrocarbon classes (e.g. alkanes < iso-alkanes < cycloalkanes < alkenes < alkynes < benzenes < naphthalenes) could be reproduced in different studies, but actual values of smoke points and trends with carbon number were not consistent. The trends for some hydrocarbon classes were increasing with carbon number and others decreasing, and even these trends were not the same in all cases. Previous studies had also concluded that sooting tendency exhibited trends with C/H ratio and carbon-carbon bond strengths, but the relationships did not apply to all compounds. In addition, the accepted definition of tendency to soot, *K/SP*, did not take into account the effect of fuel molecule size on flame height. As the molecular weight increases, the flame height increases because more oxygen must diffuse into the flame to consume a unit volume of fuel [3]. Calcote and Manos [3] noted that the molecular weight of a fuel was approximately linearly proportional to the number moles of air needed to consume a mole of fuel and was a convenient proxy for moles of air per mole of fuel.

Calcote and Manos [3] attempted to resolve these issues by defining the Threshold Soot Index (TSI), which considered all the literature data on smoke point and accounted for the differences in each smoke point apparatus used. To quantitatively compare sooting tendencies between hydrocarbons, they proposed that TSI have a scale from 0 to 100. The molecular weight, *MW*, of the fuel tested was incorporated into the definition for TSI,

$$TSI = a\left(MW/SP\right)+b\,, \tag{1}$$

For the case of mixtures, the smoke point approach of Gill and Olson [4] was adopted. In this work a TSI mixture rule for diffusion flames was investigated. The smoke point data from ten pure compounds, measured on an ASTM [5] smoke point wick lamp, were compared to the suggested TSI values reported in Ref. [3], using a linear regression to obtain the apparatus-specific constants for TSI. Gill and Olson assessed the validity of the mixture rule of a linear sum of the component TSI values weighted by their mole fractions, x_i,

$$TSI_{mix} = \sum_i x_i TSI_i \,, \qquad (2)$$

using six binary fuel blends and two tertiary fuel blends. The binary mixtures were decalin/1-methylnaphthalene, iso-octane/tetralin, iso-octane/decalin, ethyl-benzene/cumene, iso-octane/cumene, and iso-octane/cyclooctadiene. There was good agreement between the TSI values measured on the smoke point lamp and those predicted with Eq. (2). This work provided another benefit for using TSI over smoke point, a method to predict the sooting tendency of mixtures.

5.3.2. TSI for Pure Compounds

The smoke points and TSI values measured in the present study for pure compounds are given in **Table 5.1**. The experiment specific constants were calculated to be a = 4.07 (±0.4) mm (g/mol)$^{-1}$ and b = - 4.8 (±2.3). The relative uncertainty in TSI is also reported.

Table 5.1 Smoke point height, TSI, and relative uncertainty in TSI for pure compounds.

Pure Compound	Formula	*MW* (g/mol)	*SP* (mm)	TSI = 4.07 * (*MW/SP*) - 4.8	Uncertainty δTSI/TSI
cyclohexylbenzene	$C_{12}H_{16}$	160.26	8.9	69	7%
1-methylnaphthalene	$C_{11}H_{10}$	142.20	5.5	100	10%
decalin	$C_{10}H_{18}$	138.26	22.7	20	5%
tetralin	$C_{10}H_{12}$	132.21	7.1	71	8%
1,2-dihydronaphthalene	$C_{10}H_{10}$	130.19	5.8	87	10%
1,2,4-trimethylbenzene	C_9H_{12}	120.20	7.2	63	8%
1,3,5-trimethylbenzene	C_9H_{12}	120.20	7.3	62	8%
n-propylbenzene	C_9H_{12}	120.20	8.5	53	7%
iso-octane	C_8H_{18}	114.23	40.0	6.8	10%
m-xylene	C_8H_{10}	106.17	7.8	51	8%
methylcyclohexane	C_7H_{14}	98.19	40.8	5.0	13%
toluene	C_7H_8	92.14	8.4	40	8%
benzene	C_6H_6	78.12	9.1	30	7%

To supplement the set of TSI values for potential surrogate components, previous TSI and Yield Sooting Indices (YSI) [7,8] data sets were also considered. However, TSI values from the present study were not directly comparable because the previously reported TSI and YSI values were scaled differently. The first TSI scale, defined by Calcote and Manos [3], was based on two compounds tested by Hunt [6], and subsequent data sets were scaled from the initial TSI values corresponding to the Hunt data. Following the work by Calcote and Manos [3], researchers scaled new TSI data based on the average of previously reported values. To ensure consistent comparison of previous TSI results to those of this study, the scaling procedure was redone based on the TSI data set shown in **Table 5.1**. To compare separate data sets, it was required that at least two compounds be common to both studies. The studies that fit this criterion are shown in Table 2. These sources measured different parameters, including flame height at the smoke point, fuel mass flow rate at the smoke point, and maximum soot volume fraction in the doped methane flame studied by McEnally and Pfefferle [7,8]. **Table 5.2** also lists the units in which the data were measured. The measured quantities were rearranged into parameters proportional to sooting tendency (TSI or YSI), which are listed in the "TSI or YSI Parameter" column in Table 2. The TSI values were determined using the method, described by Olson *et al.* [9], of performing a linear regression between the TSI values in Table 1 and the corresponding TSI or YSI parameters from each prior study. The resulting regression equation defined the apparatus specific constants, a and b, and the R^2 correlation coefficient for each data set.

Table 5.2 Sources of sooting threshold data for pure hydrocarbons, which measured two or more compounds in common with this work.

Sources	Measured Quantity	Units	TSI or YSI Parameter
Minchin, 1931 [10]	*SP*	mm	*MW/SP*
Clarke *et al.*, 1946 [11]	*SP*	mm	*MW/SP*
Hunt, 1953 [6]	*SP*	mm	*MW/SP*
Schalla & McDonald, 1953 [12]	$\dot{m}$	mg/s	$MW/\dot{m}$
Olson *et al.*, 1985 [9]	$\dot{m}$	mg/s	$MW/\dot{m}$
Gill and Olson, 1984 [4]	*SP*	mm	*MW/SP*
McEnally & Pfefferle, [7]	$f_{v,max}$	--	$f_{v,max}$
McEnally & Pfefferle, 2008 [8]	$f_{v,max}$	--	$f_{v,max}$

An example of such a regression is presented in **Figure 5.1**, with the measured TSI values in Table 1 plotted against the equivalent TSI parameter, *MW/SP*, from Minchin [10] and Clarke *et*

al. [11]. The regression line, with the equation TSI = 2.76*(*MW/SP*) - 9.7, defines the TSI scale for data from Minchin [10], and the points represent the corresponding TSI values from **Table 5.1** for the same compounds. The TSI scale for data from Clarke *et al.* [11] lies along the line defined by equation TSI = 5.07*(*MW/SP*) - 2.7. The closer the R^2 value is to one, the smaller the differences between TSI values in **Table 5.1** and those from the previous study. The agreement between TSI values in **Figure 5.2** is reasonable; however, there are some considerable differences between the data points and the line for a given *MW/SP*.

The plots, which scale the remaining sources of soot threshold data, are shown in **Figures 5.3 and 5.4.** As can be seen in these plots, the TSI constants differ for each study, even for studies which measure the same quantity, confirming that the constants are experiment dependent. Also, the agreement between the TSI values varies and is reflected in the R^2 value.

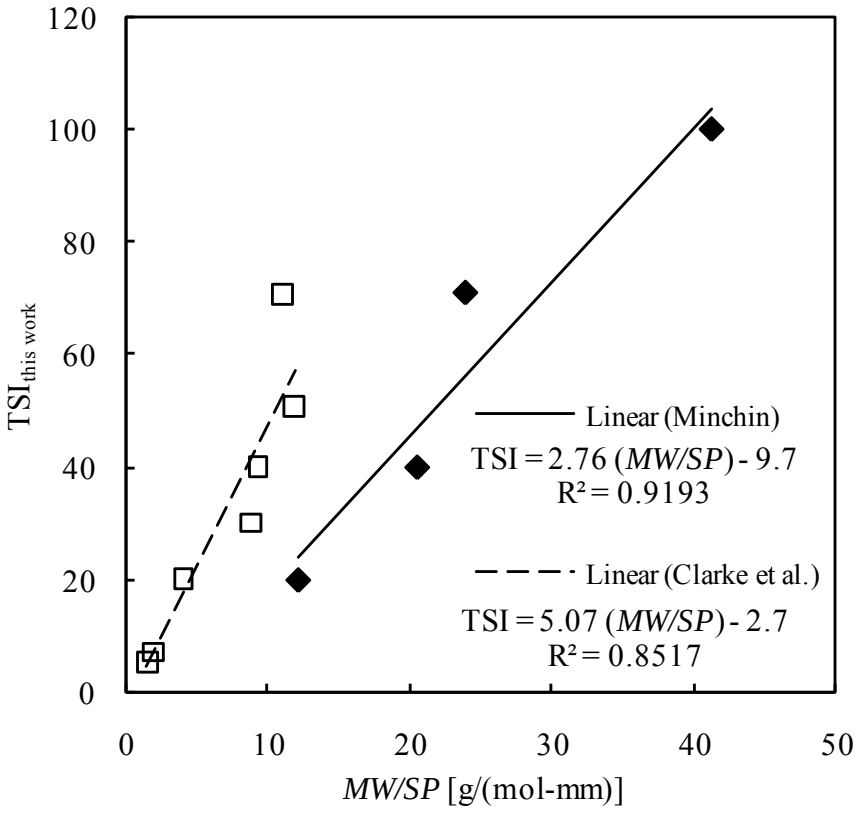

Figure 5.1 Scaling of TSI data. TSI values obtained in this work plotted against *MW/SP* data from Minchin, [10] and Clarke *et al.*, [11]. Linear fit defines TSI for a given *MW/SP* from those studies.

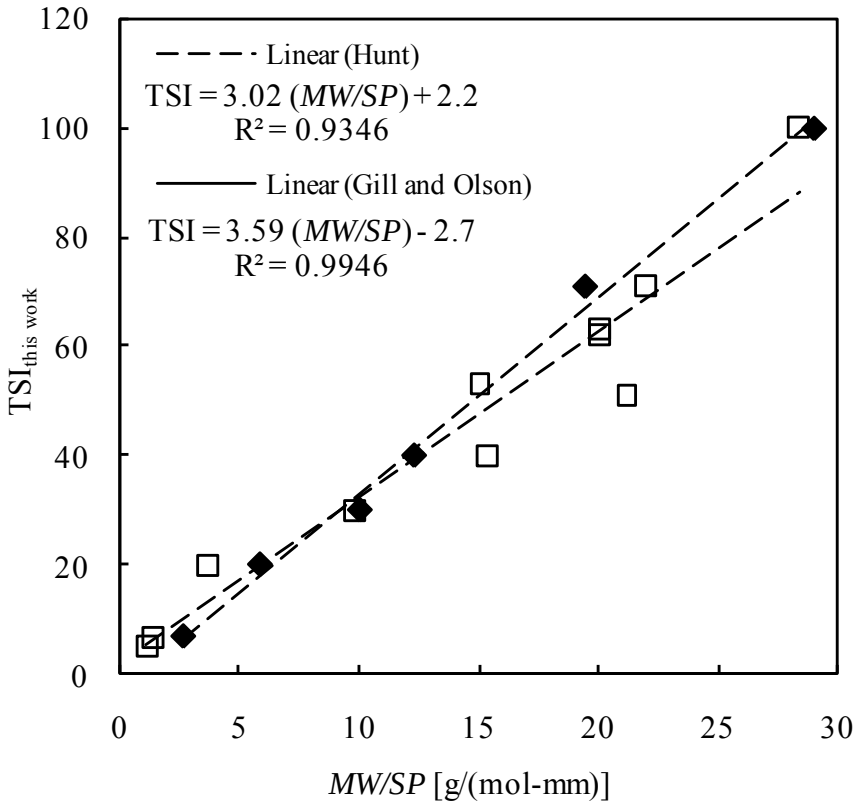

Figure 5.2 Scaling of TSI data. TSI values obtained in this work plotted against *MW/SP* data from Hunt [6] and Gill and Olson [4]. Linear fit defines TSI for a given *MW/SP* from those studies.

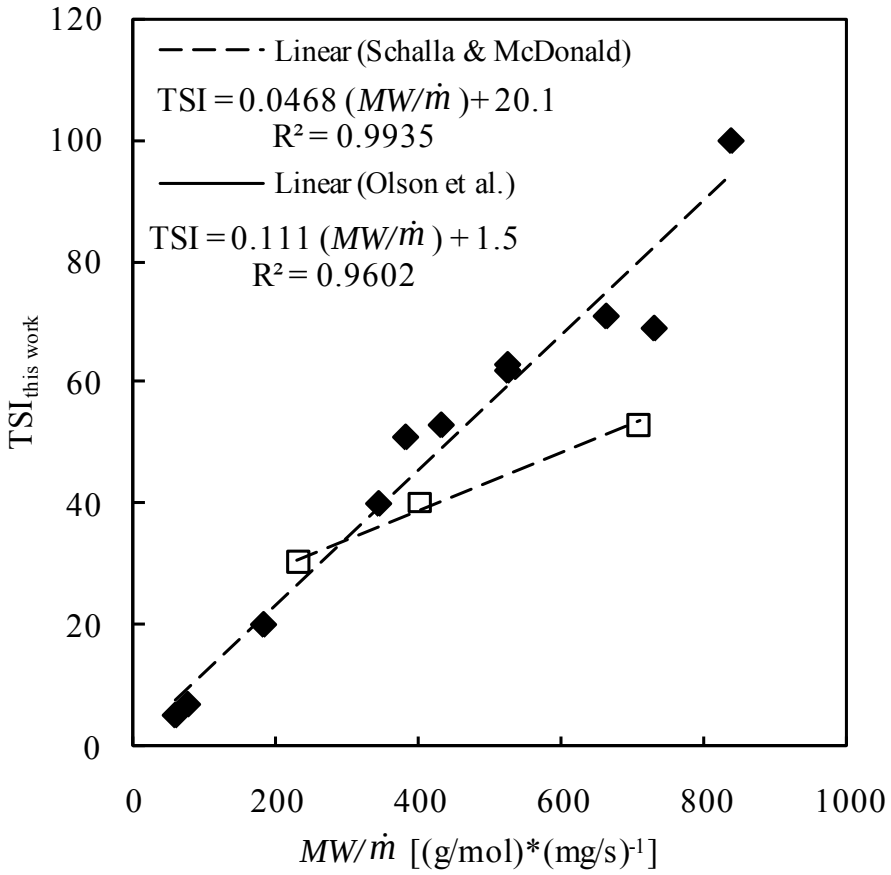

Figure 5.3 Scaling of TSI data. TSI values obtained in this work plotted against $MW/\dot{m}$ data from Schalla and McDonald [12] and Olson *et al.* [9]. Linear fit defines TSI for a given $MW/\dot{m}$ from those studies.

Since McEnally and Pfefferle [7,8] only reported YSI values, the raw $f_{v;max}$ data were not available to be scaled using the same procedure as the soot threshold data. Instead the YSI values were directly rescaled to minimize the differences from the measured TSI values in **Table 5.1. Figure 5.4** shows the measured TSI values in **Table 5.1** plotted against the reported YSI values from Refs. [7,8]. The equations from the linear regressions convert YSI to the same scale as the TSI values in **Table 5.1**. The two YSI studies are treated separately because the experimental conditions were slightly different. In the first study, the pure fuel vapor was introduced directly into the methane fuel stream. By contrast, in the second study less volatile compounds were able to be tested because the pure fuel was dissolved into a solvent, 2-heptanone, and then vaporized and introduced into the fuel stream. As **Figure 5.4** shows, the conversions to TSI are slightly different for each YSI study.

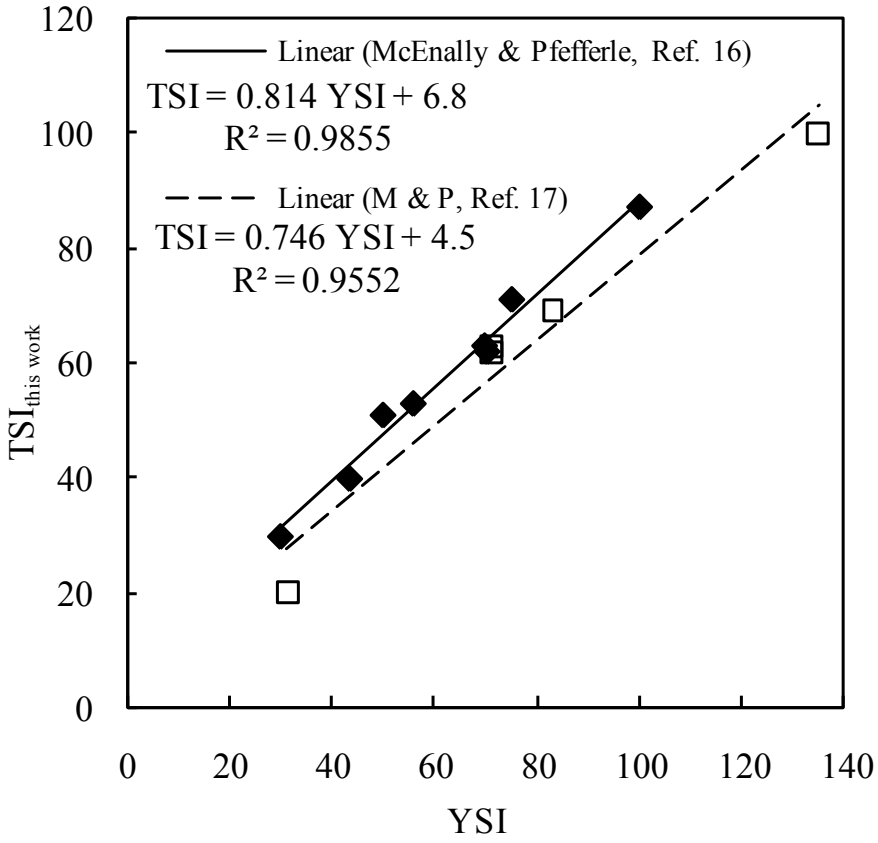

Figure 5.4 Scaling of TSI data. TSI values obtained in this work plotted against YSI from McEnally and Pfefferle [7,8]. Linear fit defines TSI for a given YSI from those studies.

The R^2 value was used as the criterion to determine which data sets to include in the final compilation of TSI values. Only the data sets that had $R^2 > 0.95$, namely Refs. [4,8,9,12,13] along with data from Table 1 were included in the average values. An encouraging fact is that all of the sooting tendency data taken since the 1980's correlated well with the data measured here. With the exception of the work of Schalla & McDonald [12], the older studies did not correlate as well.

The rescaled TSI values, the experimental constants, and the average TSI values, are shown in **Table 5.3**. The TSI values for the compounds for which smoke points could not be measured with the ASTM standard apparatus were obtained other ways. The TSI values of n-decane and n-dodecane were found from the study by Olson *et al.* [9], in which they measured the smoke point mass flow rate in an apparatus that could measure higher smoke points than the ASTM apparatus. As for iso-cetane, no smoke point measurements were found in the literature. However, Yan *et al.* [13] did provide an estimated TSI value of iso-cetane based on a polynomial regression model that correlated known TSI values with structural groups present in the fuel molecule. From the correlation, they estimated iso-cetane had a TSI of 14.6. In the present study,

a method was developed using binary mixtures to check the estimated TSI from Yan *et al.*, as discussed in section 1.2.

Table 3 TSI values for compounds considered in this work. Data include TSI values TSI values measured in this study, rescaled[a] TSI values from studies with $R^2 > 0.95$, Schalla and McDonald [12], Olson *et al.* [9], Gill and Olson [4], and McEnally and Pfefferle [7,8], and an average of these TSI values.

Pure Compound	Formula	*MW* (g/mol)	TSI - Penn State	Rescaled TSI - S&M [11,12]	Rescaled TSI - Olson *et al.* [14,19]	Rescaled TSI - G&O [4]	Rescaled YSI - M&P [16,17]	Rescaled YSI - M&P [17,18]	Average Value
			a = 4.07, b = -4.8	a=0.0468, b=21.1	a=0.111, b=1.5	a=3.59, b=-2.7			
iso-cetane	$C_{16}H_{34}$	226.45	22[b]						22 (14.6)[d]
n-dodecane	$C_{12}H_{26}$	170.34			7.0 (5.4)[c]				7.0 (5.1)
cyclohexylbenzene	$C_{12}H_{16}$	160.26	69		82.4 (82.9)			66 (83)	72 (78)
n-decane	$C_{10}H_{22}$	142.29			5.4 (3.9)				5.4 (4.2)
1-methylnaphthalene	$C_{11}H_{10}$	142.20	100		94.4 (95.6)	101 (95)		105 (135)	100 (91)
decalin	$C_{10}H_{18}$	138.26	20		21.4 (20.1)	18 (18)		28 (31)	22 (15)
tetralin	$C_{10}H_{12}$	132.21	71		74.9 (74.2)	67 (63)	67.9 (75.1)		70 (61)
1,2-dihydronaphthalene	$C_{10}H_{10}$	130.19	87				88.2 (100.0)		88 (100)
1,2,4-trimethylbenzene	C_9H_{12}	120.20	63		59.5 (57.9)		63.6 (69.8)	57 (71)	61 (52)
1,3,5-trimethylbenzene	C_9H_{12}	120.20	62		59.5 (57.9)		64.0 (70.3)	57 (71)	61 (52)
n-propylbenzene	C_9H_{12}	120.20	53	53 (76)	49.1 (47.6)		52.3 (55.9)		52 (47)
iso-octane	C_8H_{18}	114.23	6.8		9.6 (8.0)	6.7 (7.3)			7.7 (6.4)
m-xylene	C_8H_{10}	106.17	51		43.6 (42.0)		47.5 (50.0)		47 (49)
methylcyclohexane	C_7H_{14}	98.19	5.0		7.7 (6.0)				6.4 (4.9)
toluene	C_7H_8	92.14	40	39 (43)	39.4 (37.9)	41 (39)	42.2 (43.5)		40 (44)
benzene	C_6H_6	78.12	30	31 (26)		33 (32)	31.2 (30.0)		31 (29)

[a,c]"Rescaled" is defined as the TSI values that would be determined on the Penn State smoke point apparatus.

[b]Calculated from a mixture of 81% iso-cetane and 19% 1,2,4-trimethylbenzene by mole.

[c]Individual TSI values in parentheses are those originally reported by the authors or in Ref. [9] in the case of the Schalla and McDonald TSI values.

[d]Average TSI values in parentheses are those most often cited in the literature. They are the average TSI values as suggested in Ref. [9], with the exception of iso-cetane (from Ref. [13]) and 1,2-dihydronaphthalene (Ref. [7]).

In **Table 5.3**, the previous TSI values as they were reported in Refs. [4,7–9] are shown in parentheses for comparison. Although the data sets from Refs. [9] and [4] have not changed, much from their original values, the other three data sets did change significantly with the rescaling. Because TSI and YSI are relative parameters, the absolute quantities depend on the compounds and original values used to define the scale.

For Schalla and McDonald [12], the TSI was originally scaled using more compounds than the ones listed, and TSI is sensitive to the quality of *each* data point included. Because of the inherent subjectivity of the smoke point measurement, this could be an issue. The quality of any of these data is unknown, and the best way to assess whether two studies obtained similar results is to find the correlation between the compounds in common, as was done here. The rescaling of the three compounds in common with this work, acted to shift the TSI values of the aromatics tested by Schalla and McDonald almost exactly to the TSI values measured here, and therefore meeting the criterion that had been set.

The differences observed for the YSI data sets can be explained by the original values used to define the scale. For the first YSI data set, the original scale was defined assuming a TSI of 100 for 1,2-dihydronaphthalene. By contrast, here the TSI of 1-methylnaphthalene was set to 100. In the second YSI data set, 1-methylnaphthalene turned out to have a higher TSI than 1,2-dihydronaphthalene. Therefore, in the rescaling both YSI data sets are lower than the original reported values.

In parentheses next to the average TSI values in **Table 5.3** are the TSI values suggested by Olson *et al.* [9], except for iso-cetane and 1,2-dihydronaphthalene, which were not included in Ref. [9]. For iso-cetane, it is the TSI estimated in Ref. [13], and for 1,2-dihydronaphthalene, it is the YSI measured in Ref. [7]. The set of TSI values in parentheses is the set of TSI values most often cited in the literature. To show that the rescaling procedure has reduced deviations in TSI values, the total root mean square deviation from the average TSI values was calculated. For the rescaled TSI values, the root mean square deviation was 3.0 TSI units, as compared to 7.5 TSI units for the values in parentheses.

Some of the major changes in average TSI values were for the three C_9H_{12} aromatic compounds, propylbenzene, and 1,2,4-trimethylbenzene and 1,2,5-trimethylbenzene. The TSI values for propylbenzene and both trimethylbenzenes increased by more than 10%. The deviation between studies in Table 3 was ±4 TSI units for four studies, rather than ±6 TSI units for two studies cited in Olson *et al.* [9].

The average TSI for 1-methylnaphthalene, 100, as opposed to 91 from Ref. [9], reflects the original TSI assigned to it. In Calcote and Manos [3], a linear adjustment that reduced the TSI of 1-methylnaphthalene, was made to keep the scale within 0 and 100. Although not included in the previous TSI average suggested by Olson *et al.* [9], the YSI of 1-methylnaphthalene was 135 when McEnally and Pfefferle chose to assign 1,2-dihydronaphthalene a YSI of 100. With the YSI studies rescaled using more than two compounds, the YSI of 1-methylnaphthalene reduced to within ±10% of 100. Since the previously reported average TSI (91) and YSI (135) for 1-methylnaphthalene were so different, it could have been argued that the two sooting tendency parameters were not comparable. However, the rescaling of these studies shows that TSI and YSI

are complementary measures of sooting tendency, when considering the compounds in **Table 5.3**.

Another consequence of the rescaling of the YSI data was that the TSI of 1,2-dihydronaphthalene reduced from 100 to 88. However, according to Hunt's results, the TSI of naphthalene was *higher* than 1-methylnaphthalene, and McEnally and Pfefferle showed that 1,2-dihydronaphthalene and naphthalene were equivalent in YSI. Therefore, either the smoke points found by Hunt are not correct, or the *TSI* values of 1,2-dihydronaphthalene and naphthalene are not equivalent. Further studies on the TSI of naphthalene, which is a solid at room temperature, are needed to resolve this discrepancy.

5.3.3. TSI for Binary Mixtures

The TSI values of binary mixtures were studied to verify the mixture rule proposed by Gill and Olson [4], Eq. (2), as well as to verify the TSI values of certain compounds, such as iso-cetane and 1-methylnaphthalene. A total of six binary mixtures, which are listed in **Table 5.4**, were studied. The component composition in terms of mole fraction ranged from zero to one in all cases where the smoke points could be measured. The binary mixture data are plotted versus mole fraction in **Figures 5.5 and 5.6**. The points represent the measured TSI values, which were calculated from the *MW/SP* of each mixture. Appendix A lists the measured smoke points and TSI values.

Table 5.4 List of binary mixture components and surrogate mixture composition.

Binary Mixture Components	Surrogate Mixture	Liquid Volume Fraction
1,2,4-trimethylbenzene / iso-cetane	3-component A	63.2% iso-cetane 22.0% n-dodecane 14.8% 1,3,5-trimethylbenzene
toluene / iso-octane	3-component B	62.4% iso-cetane 20.4% n-dodecane 7.2% 1-methylnaphthalene
n-dodecane / m-xylene		
1-methylnaphthalene / 1,2,4-trimethylbenzene	4-component A	67.8% iso-octane 21.1% n-dodecane 8.3% 1,3,5-trimethylbenzene 2.8% 1-methylnaphthalene
1-methylnaphthalene / decalin		
1-methylnaphthalene / methylcyclohexane	JP-8 surrogate (22)	53.0% iso-octane 24.0% n-dodecane 23.0% 1,3,5-trimethylbenzene

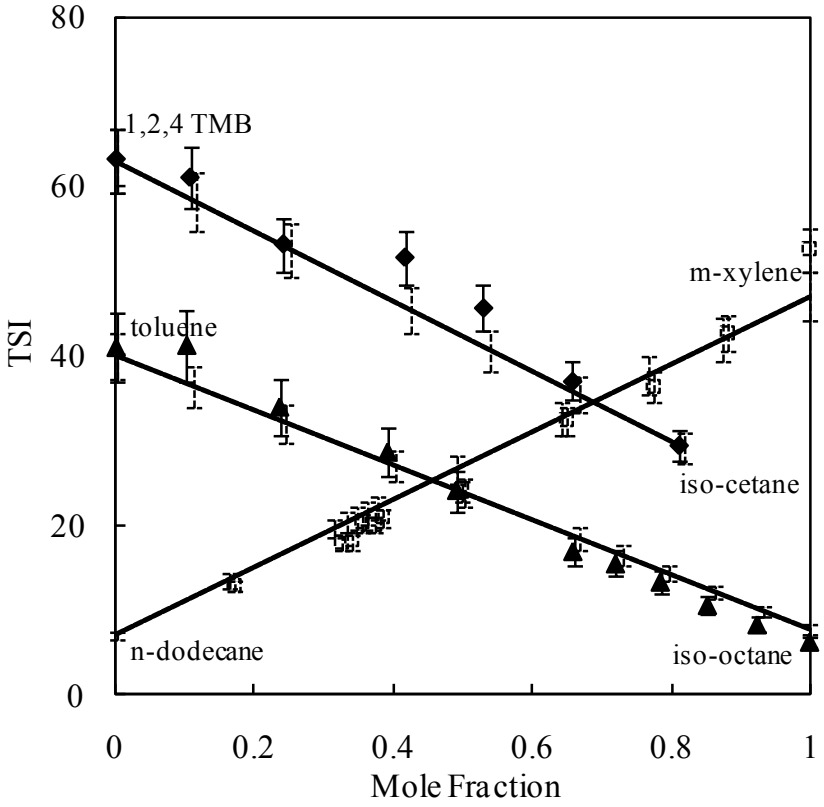

Figure 5.5 Variation of TSI with mole fraction for three binary mixtures. Points are measured TSI values, and lines are TSI values calculated from pure component values. To differentiate between the error bars, those for calculated TSI values are represented as dashed lines and are offset by 0.01 in mole fraction.

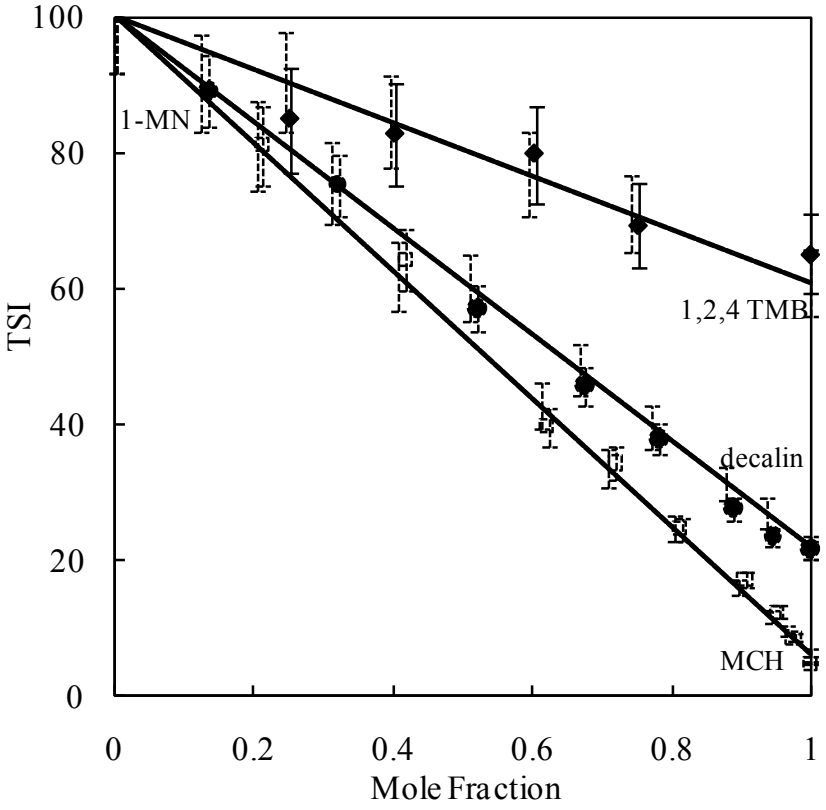

Figure 5.6 Variation of TSI with mole fraction for three binary mixtures containing 1-methylnaphthalene (1-MN). Points are measured TSI values, and lines are TSI values calculated from pure component values. To differentiate between the error bars, those for calculated TSI values are represented as dashed lines and are offset by 0.01 in mole fraction.

As described in the uncertainty analysis, the error bars for the measured TSI values, which range from ±5-8%, largely represent the uncertainty due to the smoke point measurement. Because the uncertainty in composition was so small, error bars for mole fraction are not shown. Using the pure component average TSI values from **Table 5.1** in the mixture rule, Eq. (2), the lines, representing the calculated TSI values, were constructed. The uncertainties associated with the calculated TSI values are shown as dashed error bars, and are due to the uncertainty in the individual component TSI values and mole fraction. Since the uncertainty in mole fraction is small, the error bars are dominated by the uncertainty in individual component TSI values. Although the individual component TSI values used were the average values listed in **Table 5.1**, the uncertainty was taken to be the same as the uncertainty estimated for the data found in this study. The total uncertainty in the predicted mixture TSI values (±6-9%) was generally about the same as the measured TSI mixture uncertainty. For all the mixtures tested, the error bars of the measured TSI points lie within the error bars of the calculated TSI line. It can then be concluded that the linear mixture rule, Eq. (2), applied to these mixtures in addition to the mixtures already reported in Ref. [4].

One binary mixture, 1-methylnaphthalene/decalin was also studied in Gill and Olson [4]. Examination of the three mixture data points taken in Ref. [4] to the TSI values found for comparable mixtures shows that they are very similar to those found here. The experimental constants that were used, a = 3.32 mm*(g/mol)$^{-1}$, b = -1.47, are similar to the rescaled constants found in this study for Ref. [4], a = 3.59 mm*(g/mol)$^{-1}$, b = -2.7. Therefore the TSI values using the new scale are similar to the TSI values reported using the original Gill and Olson scale.

To derive a TSI value for pure iso-cetane, a binary mixture containing as much iso-cetane as possible without losing the ability to measure the smoke point was tested. The mixture contained 81% iso-cetane and 19% 1,2,4-trimethylbenzene, molar mixture. Based on the linear mixture rule, Eq. (2), the TSI of the mixture was equal to the linear sum of the component's individual TSI values weighted by their mole fractions, called TSI_{calc}, defined for this mixture in Eq. (3). The TSI of the mixture was also found from the *MW* and *SP* of the mixture, called TSI_{meas}, defined in Eq. (4). As a component of the mixture, iso-cetane's TSI was found by equating the TSI_{meas} to the TSI_{calc}, and solving for $TSI_{i\text{-}cet}$ in Eq. (3).

$$TSI_{calc} = TSI_{1,2,4TMB} x_{1,2,4TMB} + TSI_{i-cet} x_{i-cet} \tag{3}$$

$$TSI_{meas} = a\left(MW_{mix} / SP_{mix}\right) + b \tag{4}$$

This calculation yielded a TSI for iso-cetane of 22. This is about seven TSI units (51%) higher than the value estimated by Yan *et al.* [13]. When the measured TSI values were compared with the calculated TSI values using 22 for iso-cetane, the error bars overlapped as seen in **Figure 5.5**.

Three binary mixtures containing 1-methylnaphthalene were tested to obtain additional data on its pure compound TSI value. Since 1-methylnaphthalene had the highest *MW/SP*, it was one of the two compounds that were assigned a TSI value. Therefore, the *MW/SP* for 1-methylnaphthalene partly defined the scale for the rest of the compounds. Unlike the other end point of the scale, methylcyclohexane, 1-methylnaphthalene had a very small smoke point height, around 5 mm. Because of the low flowrate associated with a smoke point of this height, this short flame was very stable, and the smoke point was easy to identify. However, the uncertainty was large because the resolution of the scale was only 1 mm. By mixing 1-methylnaphthalene with compounds that have a higher smoke point, the relative error in the smoke point measurement could be reduced. Because the mixture points with the highest 1-methylnaphthalene content still had very low smoke points, all the mixtures containing any 1-methylnaphthalene were used to derive its TSI.

A TSI value was obtained for 1-methylnapthalene by taking linear fits to all the measured points for the three binary mixtures, as shown in **Figure 5.6**. If the fit line is extrapolated back to the point where the mixture is entirely 1-methylnaphthalene, a TSI for 1-methylnaphthalene can be obtained. This is equivalent to inserting zero for the mole fraction of the other component in the equations of the fit lines in **Figure 5.7**. For the mixtures with 1,2,4-trimethylbenzene, decalin, and methylcyclohexane, the calculated TSI values for 1-methylnaphthalene were 94, 100, and 102, respectively. These values were well within the estimated uncertainty of ±10% of 100, the TSI found for the pure compound. Therefore, the calculated TSI values were consistent with its assigned TSI of 100.

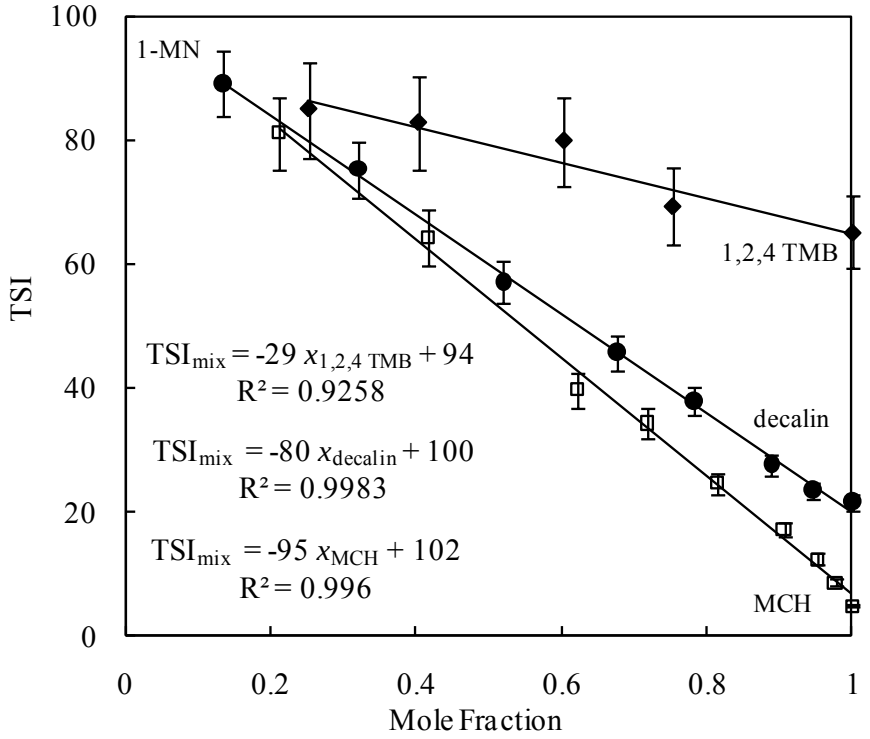

Figure 5.7 Binary mixtures containing 1-methylnaphthalene, used to calculate the TSI for pure 1-methylnaphthalene from the fit lines.

5.3.4. Achieving Matching TSI Values with Different Compounds

Three mixtures were investigated to evaluate the effect of different aromatic compounds on the match between predicted and measured TSI values. N-dodecane, a normal alkane with 12 carbon atoms, and iso-cetane, an iso-alkane with nine carbon atoms on the base chain and seven branches of methyl groups, were used as the base components in these mixtures. The aromatic compounds chosen were 1-methylnaphthalene and 1,3,5-trimethylbenzene. Although 1-methylnaphthalene could be used to achieve sooting characteristics in a surrogate, the chemical kinetic models for the trimethylbenzenes are further along in development than those for naphthalene compounds. Therefore, it was of interest to demonstrate that either or both of these compounds could be used to formulate surrogate mixtures.

The composition of the mixtures, as listed in **Table 5.5**, was formulated by the MURI team to match the four parameters of H/C ratio, MW, TSI, and cetane number (used to characterize auto-ignition) of JP-8. The first two surrogates, referred to as "3-component A" and "3-component B," contain a different aromatic compound in proportions required to maintain three parameters. In the same manner, the surrogate called "4-component A" was made containing both aromatic compounds. The mixture compositions were selected by the MURI team before any of the TSI values in this study were measured, so the TSI values for individual components at that time were taken from Refs. [9] and [13] to calculate predicted TSI values of the mixtures, using Eq.

(5). The MURI team's target TSI for the surrogates was 22, the TSI for JP-8. The TSI of JP-8 was estimated from the average JP-8 smoke point from Ref. [14], the average JP-8 composition [2] leading to a *MW* of 153.3 g/mol, and the experiment specific constants reported in Gill and Olson [4]. In Table 6, the predicted TSI values listed are instead calculated using the average TSI values reported in Table 3, so the predicted TSI values are higher than the originally intended TSI of 22. The increase in TSI is mainly due to an increase in the TSI used for iso-cetane from 14.6 to 22, and an increase in the TSI used for 1,3,5-trimethylbenzene from 52 to 61. Still, the predicted TSI values of the three mixtures differ from each other only by one TSI unit. Thus the predicted TSI values of the mixtures are still equivalent within the accuracy of the TSI method, ±10%.

The MW, H/C ratio, measured smoke point, as well as calculated and measured TSI values for the surrogates are listed in **Table 5.5**. The measured TSI values were calculated from the smoke point of the mixture, using the constants obtained for this study, a = 4.07 mm $(g/mol)^{-1}$ and b = 4.8. The data for both three-component mixtures and the four-component mixture showed good agreement between the predicted and measured TSI values. Again, a difference of one TSI unit is within the uncertainty for TSI measurement. The surrogate mixture results in **Table 5.5** successfully demonstrated that either or both aromatic compounds can be used to match a specified TSI value.

Table 5.5 Composition, smoke point height, measured TSI, and predicted TSI of three MURI surrogate mixtures for JP-8.

Surrogate	Molar Composition	*MW* (g/mol)	H/C ratio	*SP* (mm)	Measured TSI	Predicted TSI
3-component A	52% iso-cetane 23% n-dodecane 25% 1,3,5-trimethylbenzene	186.8	2.00	22.5	29.0	28
3-component B	64% iso-cetane 23% n-dodecane 13% 1-methylnaphthalene	202.5	2.00	24.2	29.3	29
4-component A	57.6% iso-octane 22.8% n-dodecane 14.7% 1,3,5-trimethylbenzene 5% 1-methylnaphthalene	193.9	2.01	24.0	28.1	28

5.3.5. Matching the TSI of JP-8 with a Surrogate

A drum of JP-8 was obtained for use in the MURI program, and its smoke point height was measured on three different occasions. The results, as shown in **Table 5.6**, are within the range of JP-8 smoke points (19-31 mm) as reported in Ref. [14]. Assuming an average composition of $C_{11}H_{21}$ as reported in Ref. [2], an average TSI value of 22 was obtained for this batch of JP-8. The measured TSI of 22 was the same as the original JP-8 TSI estimated by the MURI team.

Table 5.6 Smoke point height and TSI results for JP-8 samples taken from the same batch of fuel.

	MW (g/mol) estimated	*SP* (mm)	Measured TSI
JP-8	153.3	22.8	22.6
JP-8	153.3	22.2	23.3
JP-8	153.3	23.8	21.4
Average	**153.3**	**23.0**	**22**

A fourth surrogate mixture was devised with a target TSI of 22, and a target H/C ratio between 1.844 and 2.067 [14]. This mixture, called "JP-8 surrogate (22)," is defined in Table 7. This mixture was comprised of n-dodecane, iso-octane, and 1,3,5-trimethylbenzene. Although these three components were chosen, it would have been possible to design the surrogate with other components, e.g. n-dodecane, iso-cetane, and 1-methylnaphthalene. Iso-octane was used because it has a lower TSI value than iso-cetane. In addition to iso-cetane, iso-octane was also being considered as a potential base iso-alkane, and it was desired to show that measured and predicted TSI would still match with an iso-octane surrogate. As shown in **Table 5.7**, the measured and predicted TSI values differ by two TSI units. Although this difference is larger than the mixtures presented in **Table 5.6**, it is within ±10%. These results indicated that a surrogate fuel composed of only a few components can be formulated to match the sooting tendency of JP-8.

Table 5.7 Composition, smoke point height, measured TSI, and predicted TSI for a surrogate matching JP-8 in TSI and H/C ratio.

Surrogate	Molar Composition	*MW* (g/mol)	H/C ratio	*SP* (mm)	Measured TSI	Predicted TSI
JP-8 surrogate (22)	54% iso-octane 18% n-dodecane 28% 1,3,5-trimethylbenzene	125.9	1.98	17.8	24.0	22

One drawback of including iso-octane in "JP-8 Surrogate (22)" is the effect of lowering the mixture *MW*. Although TSI and H/C ratio can be maintained, further research is needed to show that differences in *MW* are not important to the combustion characteristics.

5.3.6. Conclusions

From the work described above, first it can be concurred that the TSI if mixtures obey a linear relations proportional to the molar fraction of each mixture component. Second, the four parameter methodology using H/C. MW, TSI and cetane number can be used to match the TSI of JP-8 with the flexibility of substituting different components with appropriate mole fractions to select components for the chemical kinetic is known or is currently under investigation.

5.4. Fundamental Soot Laser Extinction Comparisons

5.4.1. Experimental apparatus and methodology

A laminar co-flow diffusion flame burner has been widely used to study detailed soot formation processes under controlled laboratory conditions [15]. The design of the burner used for the current study combines features of the laminar co-flow diffusion flame burner used for gaseous fuels [15] and the ASTM smoke point lamp [5]. A schematic of the burner assembly is shown in

Figure 5.8. The burner consists of two concentric, closely fitting brass tubes (inner tube 4.7 mm inner diameter, outer tube 6 mm inner diameter) in which an ASTM standard wick is installed. The wick provides a simple way of delivering liquid fuels without requiring the complexity of a vaporizer. The outer tube is surrounded by an annular honeycomb structure to condition a laminar co-flow of air. The outer diameter of the burner assembly is 100 mm. The annular space surrounding the brass tube is packed with 3 mm glass beads and a series of fine wire mesh screens. The inner tube and wick are mounted on a translation stage to enable movement relative to the outer tube; this movement allows control of the flame height. A brass chimney with a height of 400 mm (not shown in the figure) is used to minimize the effects of room air currents on the flame. Slots are machined in the chimney to provide optical access. The co-flow air is metered using a flow control valve and monitored using a laminar flow element (Teledyne Hasting LAFM-5) and mass flow meter, which has a working range of 0 – 5 SCFM. A more detailed description of this system can be found in Iyer et al. [16,17] and Iyer [18].

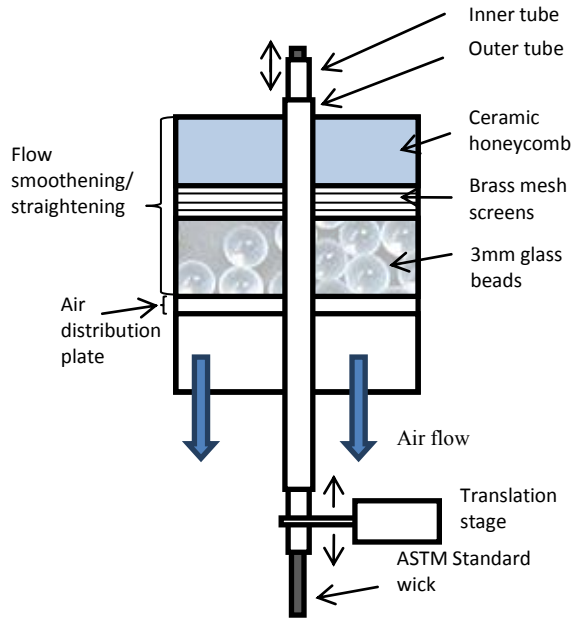

Figure 5.8 Schematic of the wick burner

The soot volume fractions are determined using a laser extinction technique. In this technique, the ratio of the measured transmitted to incident light intensity is used to determine the soot

volume fraction assuming the particle sizes are in Rayleigh limit [15]. The measurements were carried out using the CVI Melles Griot (05-LHP-121) 2 mW, 632.8 nm wavelength helium-neon laser. The optical configuration for the system is shown in **Figure 5.9**. The laser power was monitored continuously using a beam splitter and a PIN-10D silicon photodiode. The incident beam was chopped at a frequency of 1015 Hz using a Stanford Research Systems SR530 chopper. The laser beam was focused using a 400 mm focal length lens and the intensity of the transmitted light was measured using another photo diode. The output signals from the photodiodes were processed through trans-impedance and lock-in amplifiers to minimize interference from extraneous radiation, and data were acquired using a National Instruments® data acquisition system and a custom-written LabVIEW® program. The beam attenuation, I_t/I_0, was calculated from the photodiode signals: I_t being the intensity of the beam transmitted through the flame; and I_0 the intensity of the incident beam. The line-of-sight measurements obtained at different radial locations spaced 0.2 mm apart were deconvoluted using an Abel inversion technique described by Dasch [19]. For the inversion process, the flame was divided into two halves and each half was deconvoluted separately.

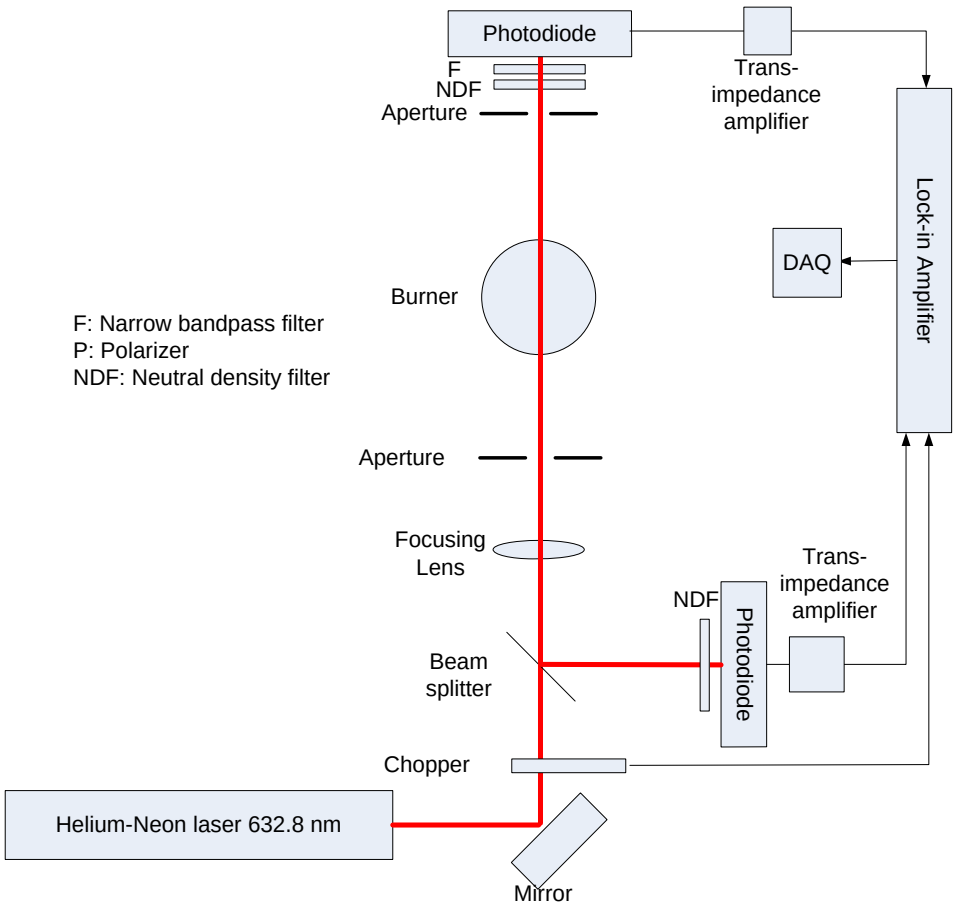

Figure 5.9 Optical set-up for laser extinction on the wick burner.

5.4.2. Results

In order to correlate the sooting tendencies of all the fuels studied on the wick burner, and to compare them with measurements on the ASTM apparatus, the threshold soot index (TSI) was used. It was necessary to calibrate the wick burner in order to obtain the experiment specific constants - a and b. This was achieved by plotting the smoke point measurements obtained on the wick burner against previously reported TSI values [20], similar to the method used by Olson et al. [9]

The smoke point flame heights were measured on the wick burner following the ASTM procedure [5] for the pure hydrocarbon fuels listed in Table 5.8. The values shown in Table 5.8 are the average of three readings. The MW/SP values with units of g-mol^{-1}-mm^{-1} were calculated for the compounds which were common to this work and that of Mensch et al. [20]. These values were plotted against TSI values reported by Mensch et al. as shown in **Figure 5.10**. An uncertainty-weighted linear regression was fit to the data points. The slope and the intercept of the fit yielded the values a = 3.62 mm-mol-g^{-1} and b = -4.3. Thus the TSI value for any compound on the wick burner will be given as –

$$\boldsymbol{TSI = 3.62\left(\frac{MW}{SP}\right) - 4.3} \tag{5}$$

where MW is the molecular weight of the compound in g mol^{-1} mm^{-1}, and SP is the smoke point flame height of the compound on the wick burner in mm. The TSI values for the pure compounds studied on the wick burner are shown in **Table 5.8**. An uncertainty of ±10% was calculated for the TSI values.

Table 5.8 Smoke point and TSI for pure hydrocarbon compounds on the wick burner.

Compound	Formula	Molecular Weight (g/mol)	Smoke Point (mm)	TSI = 3.62*(MW/SP) – 4.3	TSI Mensch [20]
Decalin	$C_{10}H_{18}$	138.3	21.5	19.0	22
Toluene	C_7H_8	92.1	7	43.3	40
m-Xylene	C_8H_{10}	106.2	7	50.6	47
1,3,5-Trimethylbenzene	C_9H_{12}	120.2	6	68.2	61
Tetralin	$C_{10}H_{12}$	132.2	6	75.5	70
1-Methylnaphthalene	$C_{11}H_{10}$	142.2	5	98.7	100
n-Propylbenzene	C_9H_{12}	120.2	7	57.9	52
Iso-propylbenzene	C_9H_{12}	120.2	6	68.2	-
n-Dodecane	$C_{12}H_{26}$	170.3	-	7.0*	7.0
Iso-octane	C_8H_{18}	114.2	-	8.0*	7.7

* TSI determined from binary mixtures with aromatic compounds.

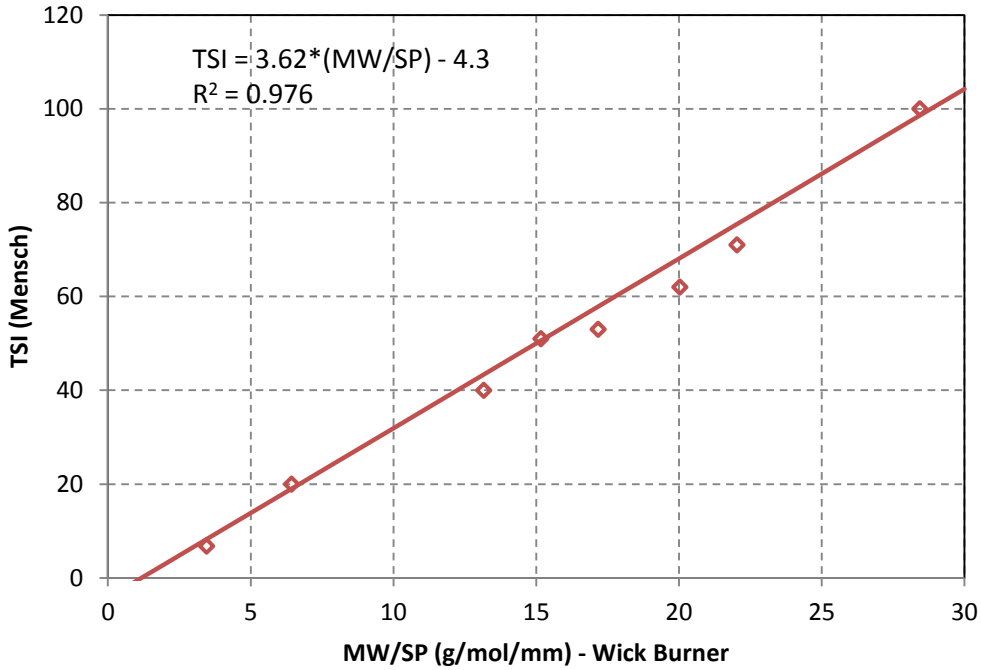

Figure 5.10 TSI calibration curve for the wick burner. TSI values are taken from Mensch [20]. Line represents uncertainty-weighted least square fit to wick burner smoke point data yielding TSI = 3.62*(MW/SP) – 4.3.

The Jet A POSF 4658 fuel was the primary fuel used for the MURI research. The combustion property targets used to formulate the surrogate fuels were the derived cetane number (DCN) = 47.1, average molecular weight = 142.1 g/mol, hydrogen-to-carbon (H/C) ratio = 1.95, and Threshold Soot Index (TSI) = 21.4. DCN was measured in an Ignition Quality Testing (IQT) apparatus [21], the average molecular weight was determined by a vapor pressure suppression technique, and the H/C ratio was obtained by the mass measurement of the ratio CO_2/H_2O from a complete combustion analysis. All these measurements were made at Princeton University, and the details can be found in Dooley et al. [21,22]. The TSI was calculated from a smoke point measurement of 22.1 mm on the ASTM apparatus as part of this work, using the constants a = 4.07 g^{-1}-mol-mm, b = -4.8 from the work of Mensch et al. [20].

A three-component surrogate mixture (1st generation surrogate) [21] was devised by the MURI team to match DCN, MW, and H/C ratio of Jet A POSF 4658. The surrogate was n-decane/iso-octane/toluene mixture of 42.67/33.02/24.31 mole %. A measured TSI of 13.7 was in agreement with the predicted TSI of 14 (calculated using the TSI of surrogate constituents). No soot volume fraction measurements were performed on the wick burner for the 1st generation surrogate because it did not match the TSI of Jet A POSF 4658.

Next, a four-component surrogate (2nd generation surrogate) composed of (molar composition) 40.41% n-dodecane, 29.48% iso-octane, 7.28 % 1,3,5-trimethylbenzene, and 22.83% n-propylbenzene was formulated [22]. This mixture had predicted values of H/C of 1.96, molecular weight of 138.7 g/mol, a TSI of 21.4, and DCN 47.1. A TSI of 20.3 was determined from smoke point measurements on the ASTM apparatus for this surrogate mixture; this value matched the

calculated TSI and also the TSI of Jet A POSF 4658 within the experimental uncertainty of ±10%. Experiments were performed in the wick burner to determine if the 2nd generation surrogate produced similar soot fields to those of Jet A POSF 4658. Radial extinction scans were conducted at different heights in the wick burner flames at their smoke point. The Jet A POSF 4658 and the 2nd generation surrogate had smoke points of 22.1 mm and 22.5 mm, respectively, on the ASTM smoke point lamp.

One would expect that introducing a co-flow would suppress the soot emission from the flame since mixing is enhanced by the co-flow, hence the fuel flow would need to be increased to recover the smoke point. This would result in a higher smoke height in the presence of co-flow air [23]. However, as observed by Rakowsky and Hunt [24], other factors of the burner design such as chimney height and chimney diameter also affect the smoke point. The nature and extent of the effect was different for different classes of fuels. The differences in the experimental configurations of the ASTM smoke point lamp and wick burner resulted in small differences in the experimentally observed smoke point between the two apparatuses. On the wick burner, a smoke point of 21 mm was obtained for Jet A POSF 4658 and 23 mm for the 2nd generation surrogate.

In order to compare the soot profiles of these flames, a non-dimensional axial co-ordinate was defined as the ratio of the measurement location to the smoke point flame height of each respective flame on the wick burner. This definition is analogous to that of Santoro et al. [15] because the diffusion flame height is proportional to Q/D [25], where Q is the volumetric flow rate and D is the diffusion co-efficient.

An exemplar plot showing I/I_0 profiles for four different non-dimensional heights in the Jet A POSF 4658 flame is presented in **Figure 5.11**. The non-dimensional heights of z = 0.36, 0.48, 0.60, and 0.71 corresponded to heights of 7.5 mm, 10 mm, 12.5 mm, and 15 mm in the flame, respectively. The line-of-sight extinction coefficients were calculated from these profiles, the two halves of the profiles were deconvolved separately, and then the local soot volume fractions were calculated. The radial soot volume fraction profiles for Jet A POSF 4658 at the same four non-dimensional heights are shown in Figure 5.12. The results in **Figure 5.12** show that the two halves of the flame look quite similar. Profiles from only the right half of the flames will be shown for the remainder of the fuels for easy comparison.

The soot profiles are consistent with the typical shapes obtained for laminar diffusion flames of Santoro et al. [15] and follow similar trends. The soot concentrations are higher in the annular region of the flame at lower heights. As the height increases, the soot concentration increases to a maximum and then decreases. There is little soot in the central region of the flame at lower heights but the concentration increases with height. The maximum value of soot volume fraction occurs in the annular region at a height approximately midway along the flame.

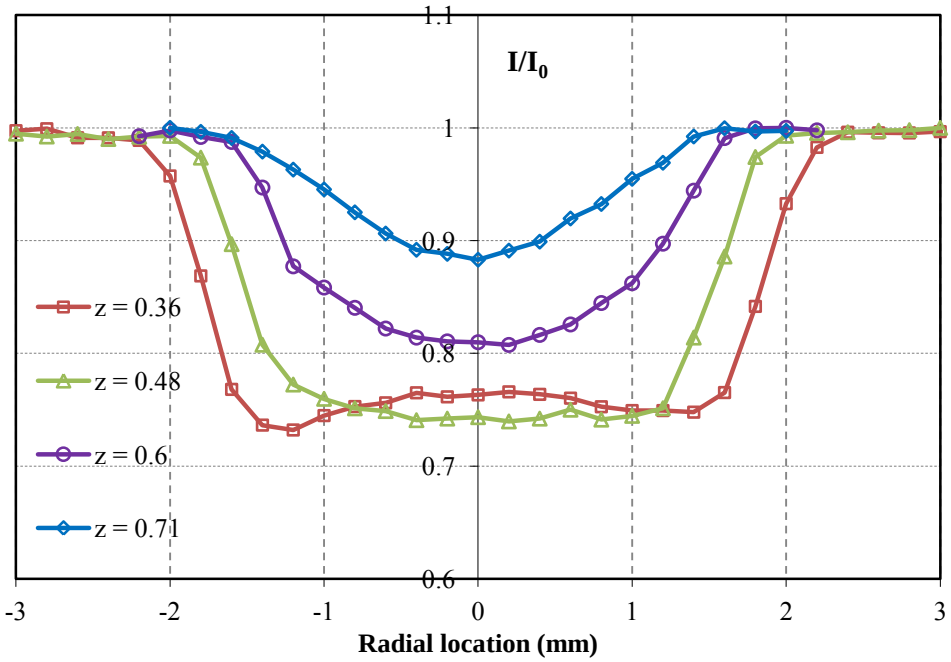

Figure 5.11 I/I_0 profiles for Jet A POSF 4658 at four heights.

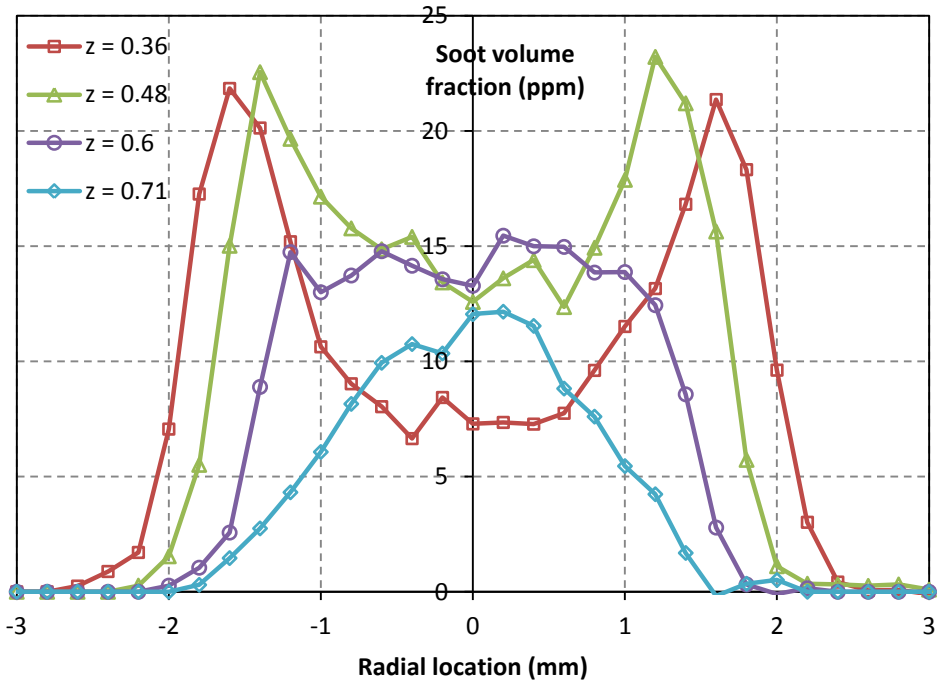

Figure 5.12 Radial soot volume fraction profiles for Jet A POSF 4658 at four heights.

In **Figure 5.13** radial profiles of soot volume fractions for the 2nd generation surrogate are presented on the right hand side and Jet A POSF 4658 on the left hand side. The profile for

POSF 4658 at each non-dimensional location was compared to two non-dimensional locations of the surrogate that fell on either side of each non-dimensional location of POSF 4658. In previous similar work [26], the uncertainty in the local soot volume fraction was estimated to be ±15%, such is represented by the error bars.

The z = 0.36 location for POSF 4658 is compared with z = 0.33 and z = 0.43 for the surrogate in **Figure 5.13a**. The soot volume fractions observed for both fuels along the flame centerline and in the annular region are comparable within the uncertainty of the technique. z = 0.48 corresponds to the location of the maximum soot volume fraction in the POSF 4658 flame. As seen from **Figure 5.13b**, the radial profiles of POSF 4658 at z = 0.48 and the 2nd generation surrogate at z = 0.54 also behave similarly, peaking at radial locations of 1.2 mm and 1.4 mm respectively. The peak soot volume fractions observed for POSF 4658 and surrogate fuels are very closely matched at a volume fraction of approximately 24 ppm. At z ~ 0.6 and 0.7, the centerline soot volume fractions are in agreement while there are small differences in the annular region. Overall the soot profiles for POSF 4658 and its TSI-matched surrogate are in good agreement.

The mis-match of z locations in the above data may correspond to different times in the soot formation and oxidation processes. In order to allow better comparisons between POSF 4658 and the surrogate, measurements need to be made at matching z locations for the two fuels.

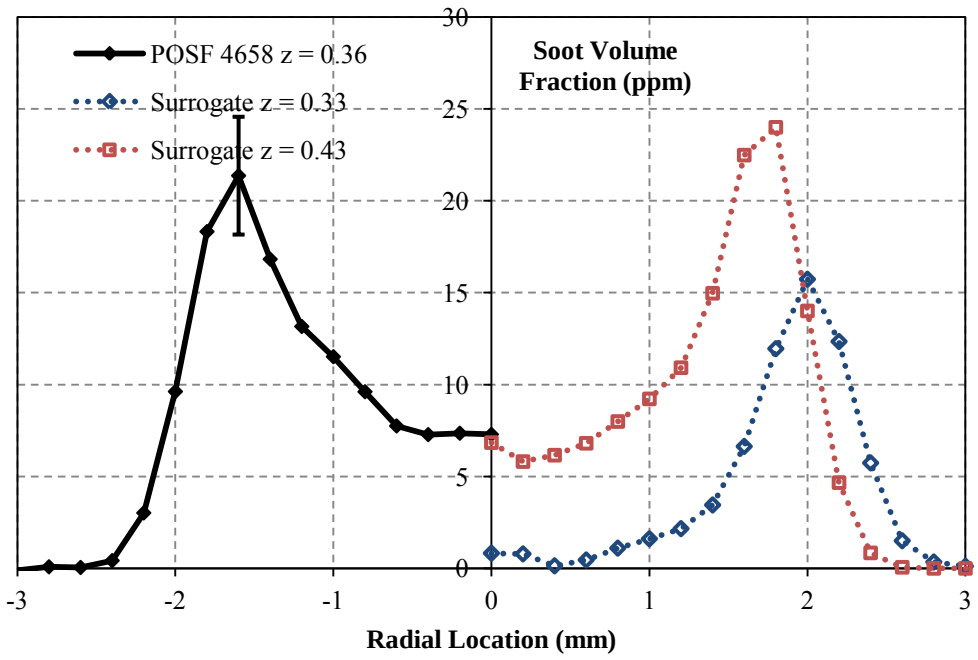

Figure 5.13 (a)

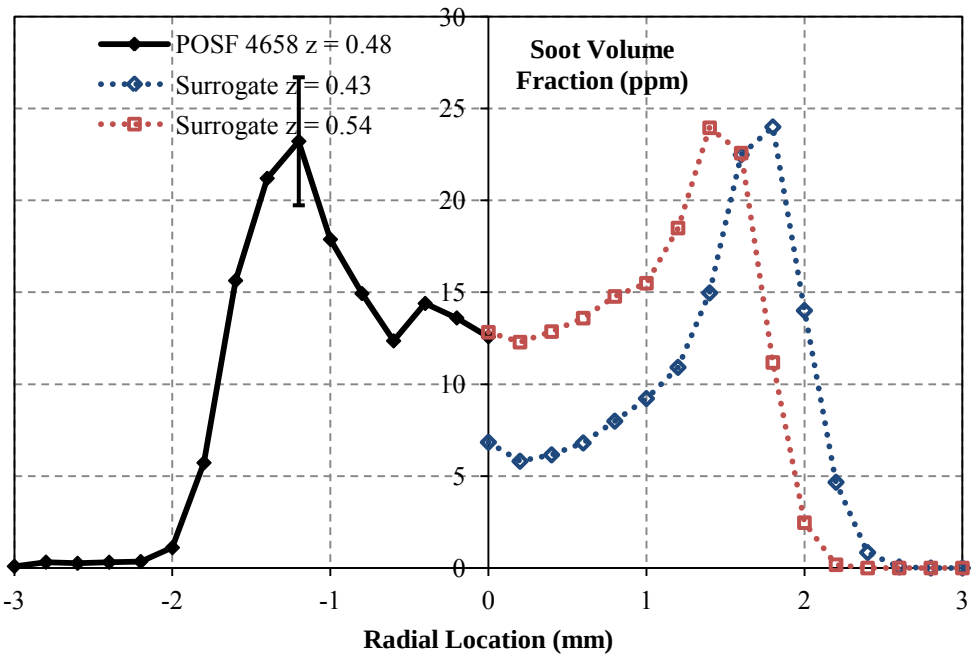

Figure 5.13 (b)

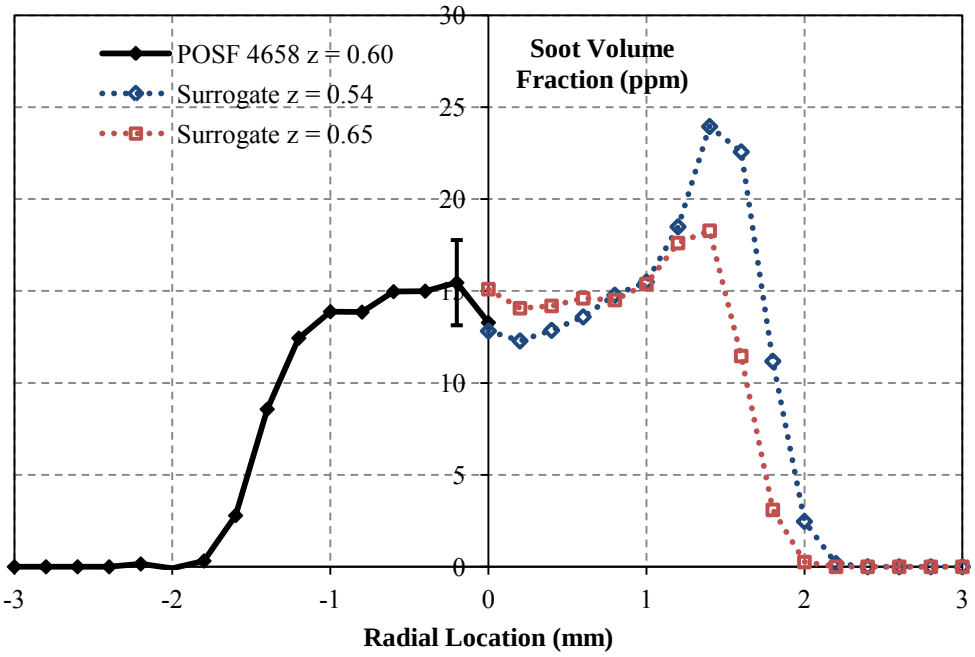

Figure 5.13 (c)

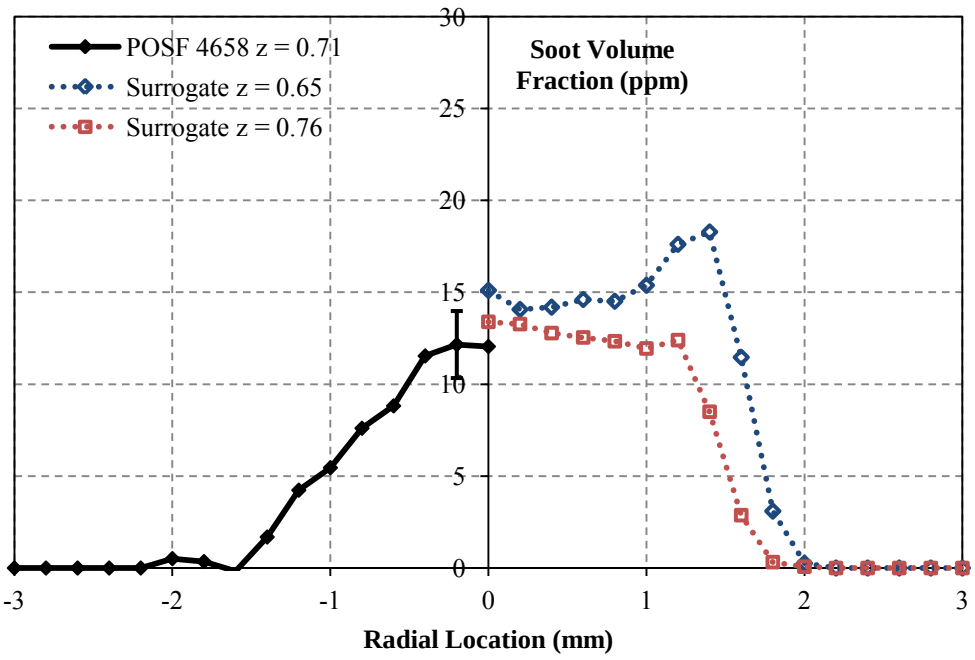

Figure 5.13 (d)

Figure 5.13 Radial soot profiles for Jet A POSF 4658 (left) and 2nd generation surrogate (right).

5.4.3. Surrogates for JP-8 POSF 5699

Only a small quantity of the Jet A POSF 4658 fuel was available, permitting tests only on the ASTM apparatus and on the wick burner. Testing on the model gas turbine combustor was not possible since large quantities of fuel (~ 6 gallons) are needed for every test on the combustor. JP-8 POSF 5699 was available in large enough quantities for testing on the ASTM apparatus, the wick burner, and the gas turbine combustor.

Jet A POSF 4658 and the two surrogates with pure hydrocarbon components (1st and 2nd generation) were tested in a wide range of laboratory experiments [21,22] – shock tube studies, rapid compression machine, flow reactor, fundamental laminar flame configurations, and spatial variation of soot volume fraction in a wick burner (2nd generation only). In addition to the fundamental experiments, it was important to compare the combustion behavior of the target fuel and its surrogates in more realistic combustion environments. Large volumes of fuel were required to run such experiments and it was prohibitively expensive to run surrogates formulated from pure hydrocarbon constituents in such experiments. To enable the study of surrogates in combustion devices, workers at Princeton University extended the MURI surrogate fuel methodology to formulate surrogate fuels from commercially available hydrocarbon solvent blends. These solvent blends were more economical and available in large quantities. The methodology using solvent fuels was tested through experiments on the ASTM apparatus, the wick burner, and the model gas turbine combustor.

Three fuels were selected as potential surrogate constituents for JP-8 POSF 5699 – two narrow cut solvent blends, Exxsol D95 and Aromatic-100, manufactured by Exxon-Mobil, and an iso-

paraffinic kerosene synthetic jet fuel obtained from the Wright-Patterson Air Force Base. The D95 was primarily composed of C_{12} through C_{15} straight- and branched-chain alkanes, the A100 consisted of C_3 and C_4 alkyl-benzenes, and the IPK consisted of C_8 through C_{12} iso-paraffinic alkanes.

TSI values for JP-8 POSF 5699 and the three solvent fuels were obtained based on smoke point data from the ASTM apparatus. JP-8 POSF 5699 had a smoke point of 22 mm on the ASTM apparatus, and a TSI of 22.3. DCN and H/C ratio were measured at Princeton University. The molecular weight of JP-8 POSF 5699 was estimated by assuming an approximate composition of $C_{11}H_{21}$ [2]. Molecular weights reported in the material safety data sheet (MSDS) were used for D95 and A100 while that of IPK was measured at Princeton. The combustion property targets of JP-8 POSF 5699 and solvent surrogate components are summarized in **Table 5.9**.

Table 5.9 Combustion property targets for JP-8 POSF 5699 and the solvent fuels.

Fuel	DCN	H/C	TSI	MW, g mol^{-1}
JP-8 POSF 5699	49.3	1.935	22.3	153
Exxsol D95 (D95)	58.3	2.02	13.9	177
Aromatics 100 (A100)	7.9	1.34	65.6	121
Iso-paraffinic Kerosene UN1223 (IPK)	31.7	2.15	12.3	160

The procedure for surrogate fuel formulation was similar to that followed in previous work [21,22]. For preliminary tests, a 67.9/32.1 mole % mixture of Exxsol D95/Toluene was formulated as JP-8 POSF 5699 surrogate #1 with TSI as the only combustion property target. A TSI of 21.7 was measured for JP-8 POSF 5699 surrogate #1 that matched the TSI of POSF 5699 within experimental uncertainty. The use of only two solvents, one of low H/C and low DCN (A100) and the other of high H/C and high DCN (D95) did not allow for independent control of all four combustion property targets to match the measured values of the real fuel. Since the objective of this study was to determine the usefulness of the TSI parameter in predicting overall soot volume fractions in a practical combustor, the TSI was initially given priority over the DCN. An 83.8/16.2 mole % mixture of Exxsol D95/Aromatics 100 was formulated as JP-8 POSF 5699 surrogate #2 (see **Table 5.10**). This mixture closely shared the TSI and H/C of the target fuel and the DCN was reasonably approximated to within 3 DCNs (see **Table 5.10**).

In order to adjust the DCN independently of the H/C, a high H/C, low DCN surrogate component was required. The IPK with H/C 2.15 and DCN 31.7 was used along with D95 and A100 to produce a surrogate fuel – JP-8 POSF 5699 surrogate #3, which shared all four combustion property targets of JP-8 POSF 5699.

Table 5.10 Mixture mole fractions and combustion property targets for surrogate formulation.

Mole %							
D95	**A100**	**IPK**	**Toluene**	**DCN**	**H/C**	**MW g mol^{-1}**	**TSI**
JP-8 POSF 5699 Surrogate #1							
67.9	0.0	0.0	32.1	--	1.75*	149.8*	21.7
JP-8 POSF 5699 Surrogate #2							
83.8	16.2	0.0	0.0	52.0	1.91	167.9	21.5
JP-8 POSF 5699 Surrogate #3							
70.5	16.4	13.1	0.0	49.4	1.93	165.6	20.8

*H/C and MW for JP-8 POSF 5699 surrogate #1 are estimated from constituent values, all other values are experimental determinations.

All the flames were set to their smoke points for soot volume fraction measurements on the wick burner. A smoke point of 22.0 mm was obtained for JP-8 POSF 5699. For JP-8 POSF 5699 surrogates #1, #2, and #3, the smoke points were 22.0 mm, 26.3 mm, and 25.0 mm, respectively, on the wick burner.

The radial soot volume fraction profiles for JP-8 POSF 5699 at three heights are shown in **Figure 5.14**. The two halves of the flame look quite similar indicating that the flames are symmetric. Therefore, only one half of the profiles will be compared in the results. Also a comparison to Jet A POSF 4658 in **Figure 5.15** shows that Jet A POSF 4658 and JP-8 POSF 5699 are very similar in terms of the centerline soot volume fractions, peak soot volume fraction, and the radial locations of the peak.

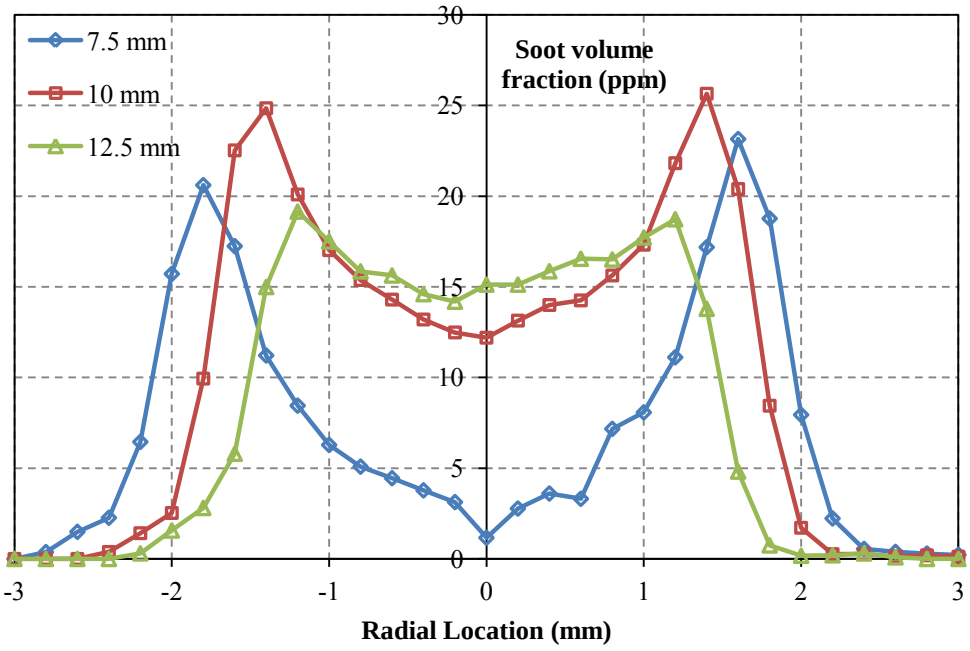

Figure 5.14 Radial soot volume fraction profiles for JP-8 POSF 5699 at three heights.

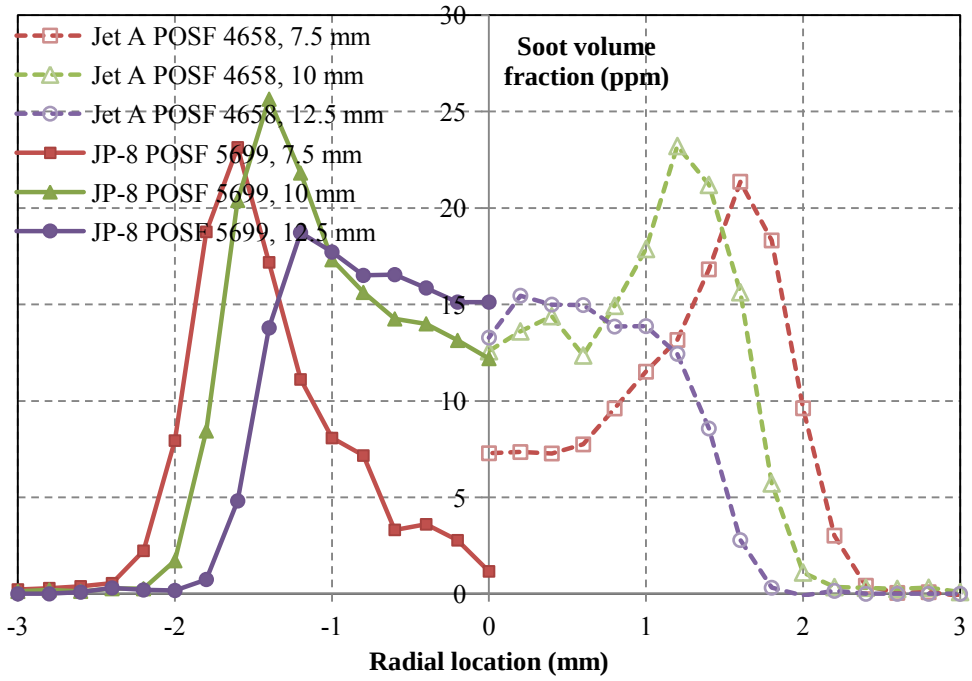

Figure 5.15 Comparison of radial soot volume fractions for JP-8 POSF 5699 (left) and Jet A POSF 4658 (right)

Soot volume fraction measurements for JP-8 POSF 5699 and the three surrogates were made at four fixed locations above the burner: 7.5 mm, 10 mm, 12.5 mm, and 15 mm. The error bars

represent ±15% uncertainty in the soot volume fractions. A non-dimensional axial co-ordinate z, defined in the same way as the Jet A POSF 4658 studies, was utilized in order to adjust for the different smoke points of the fuels. The profiles grouped according to similar z values are presented in

Figure 5.16. At heights of $z \sim 0.34$ to 0.4, JP-8 POSF 5699 surrogate #3 has the best match with JP-8 POSF 5699 in terms of the maximum soot volume fraction and the radial location of the maximum, as seen from

Figure 5.16**a**. The centerline value of surrogate #3 is higher than that of JP-8 POSF 5699. Surrogates #2 and #3 have lower peak soot volume fraction than JP-8 POSF 5699 at these heights.
The comparison of soot volume fractions approximately midway along the flames, corresponding to $z \sim 0.45$ to 0.5, is shown in

Figure 5.16**b**. The soot volume fraction reaches its peak value for all the flames in this region. The profiles for surrogates #1 and #3 agree well with that of JP-8 POSF 5699. The peak soot volume fraction for JP-8 POSF 5699 surrogate #2 is about 20% lower than JP-8 POSF 5699. The agreement between the centerline soot volume fraction and the radial location of the peak volume fraction is good for all the surrogates and JP-8 POSF 5699.

Figure 5.16**c** presents a comparison of JP-8 POSF 5699 and the three surrogates at $z \sim 0.57$ to 0.6. Compared to the lower heights, the soot volume fraction in the annular region is lower and that along the centerline is higher at these heights. Surrogates #1 and #3 compare very well with JP-8 POSF 5699 whereas surrogate #2 has lower soot volume fractions. There is very good agreement in the centerline volume fractions for all the fuels.

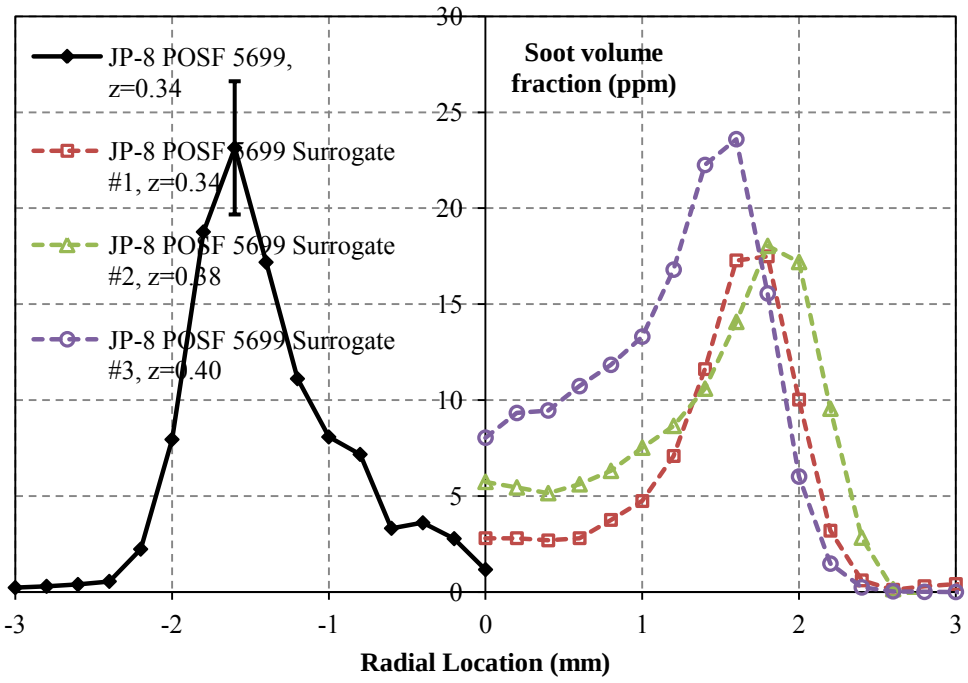

Figure 5.16(a) z ~ 0.34 to 0.4

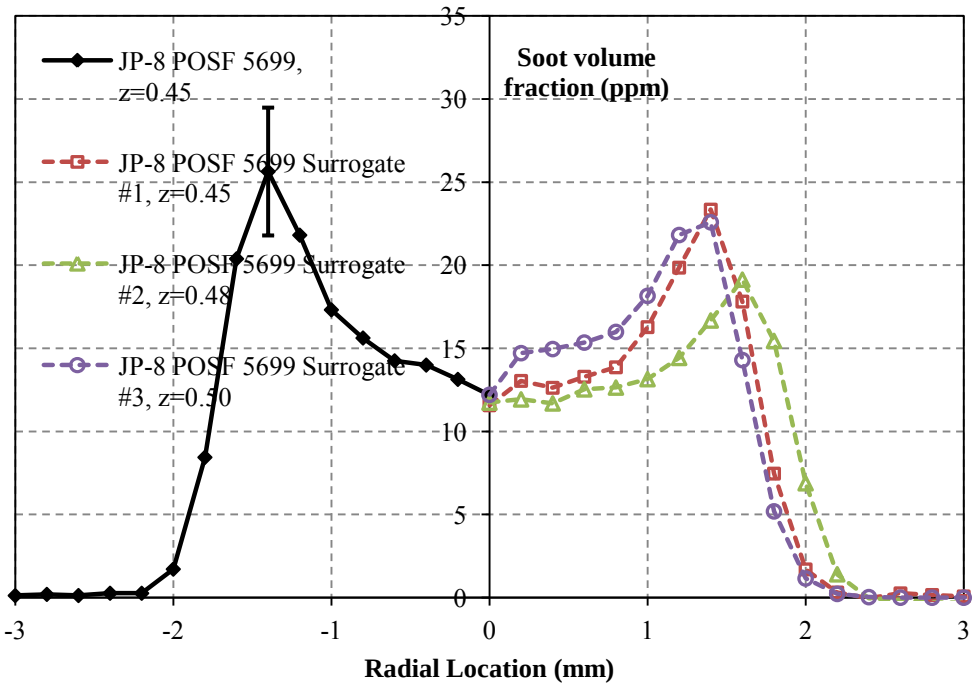

Figure 5.16(b) z ~ 0.45 to 0.5

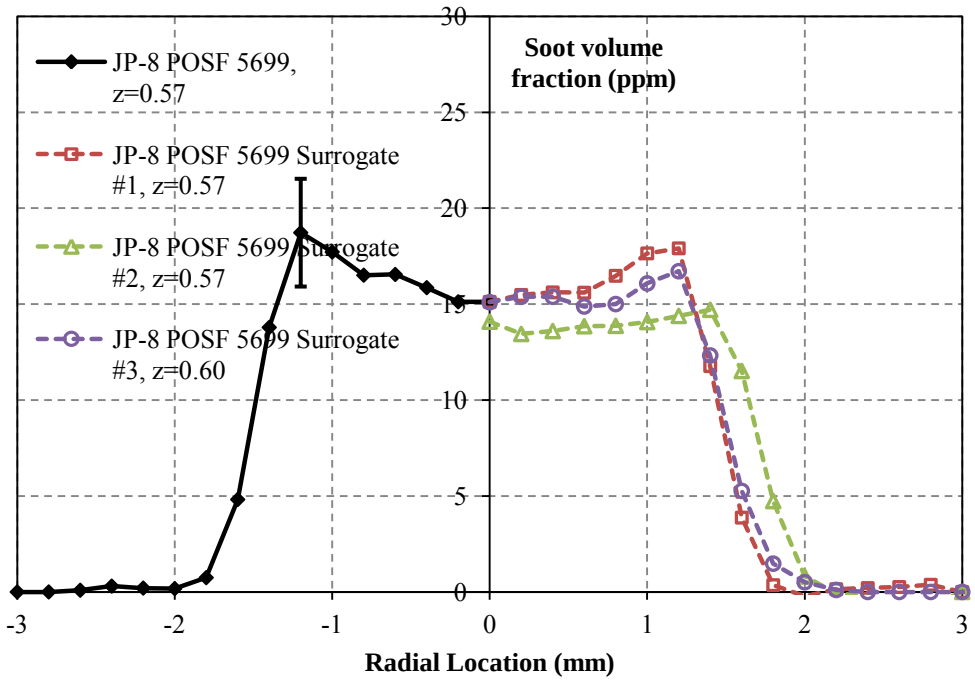

Figure 5.16(c) z ~ 0.57 to 0.6

Figure 5.16 Radial soot profiles for JP-8 POSF 5699 (left) and the solvent-based surrogates (right) at non-matching z locations.

In the above data, it is likely that some of the differences between JP-8 POSF 5699 and the surrogates are caused by the mis-match of z locations which may correspond to different times in the soot formation and oxidation processes. In order to allow comparisons between JP-8 POSF 5699 and the surrogates at matching z values, it was necessary that the measurements were made at matching z locations for all the fuels. Five locations were picked for the JP-8 POSF 5699 flame: 7.5 mm, 10 mm, 12.5 mm, 15 mm, and 17.5 mm heights above the burner. The z values at these heights as calculated for the JP-8 POSF 5699 flame were z = 0.34, 0.45, 0.57, 0.68 and 0.8. Data for the three surrogates were then obtained at these five z locations. The plots are shown in **Figure 5.17**. The JP-8 POSF 5699 profiles appear on the left while the surrogate data are shown on the right. At z = 0.34, JP-8 POSF 5699 Surrogates # 1 and 2 have the best match with JP-8 POSF 5699 in terms of the maximum soot volume fraction. Surrogate #3 has about 20% lower maximum soot volume fraction. All the fuels agree well in terms of the centerline soot and the location of the maximum soot.

The soot volume fraction reaches its peak value for all the flames midway along the flame. At z = 0.45, all the surrogates show good agreement with JP-8 POSF 5699 in terms of the peak soot volume fraction, location of the peak, and the centerline soot volume fraction. The peak soot

volume fraction values are 22.7 ppm for JP-8 POSF 5699, 23.4 ppm for surrogate #1, 21.5 ppm for surrogate #2, and 21.8 ppm for surrogate #3.

At higher locations, the annular region of soot reduces and the concentrations are higher along the centerline. At z = 0.57, 0.68, and 0.8, the centerline soot volume fractions for all the fuels match within experimental uncertainty. Overall, the surrogates, which have the same TSI value as JP-8 POSF 5699, also have very similar soot volume fraction profiles.

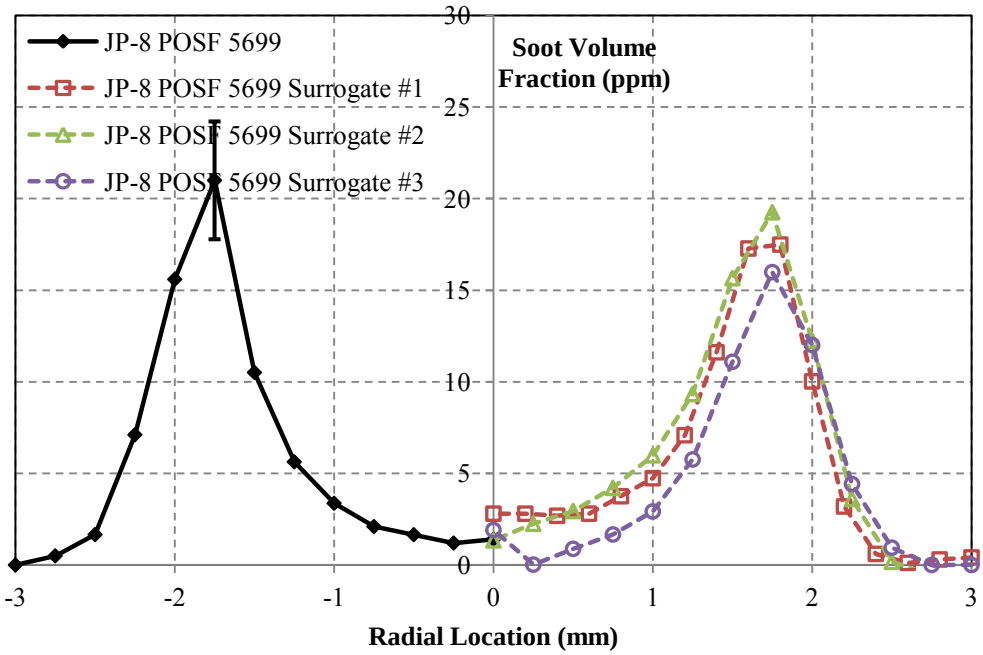

Figure 5.17(a) z = 0.34

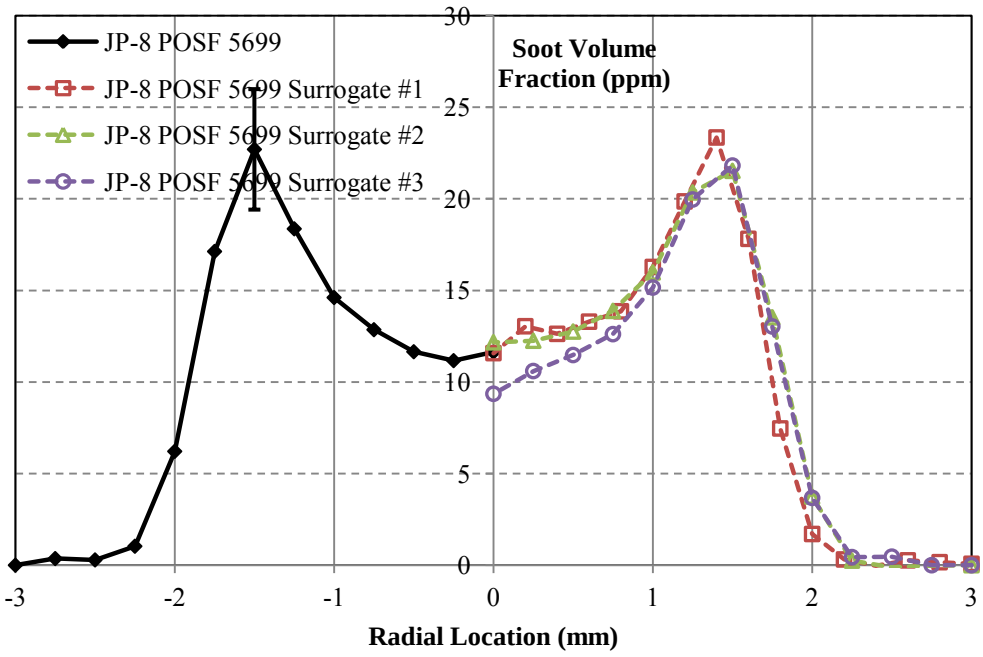

Figure 5.17(b) z = 0.45

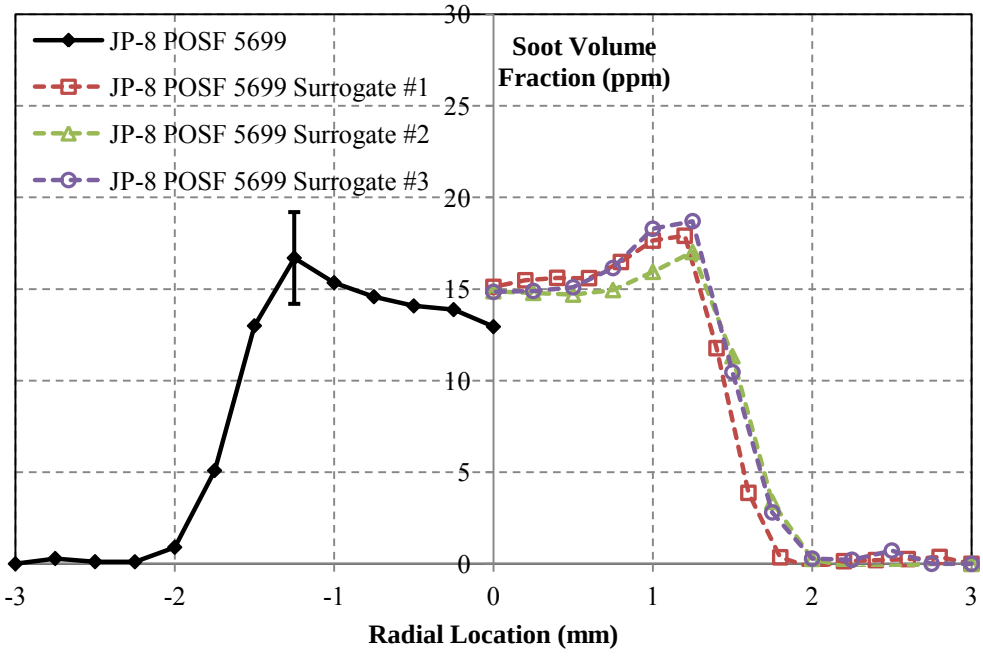

Figure 5.17(c) z = 0.57

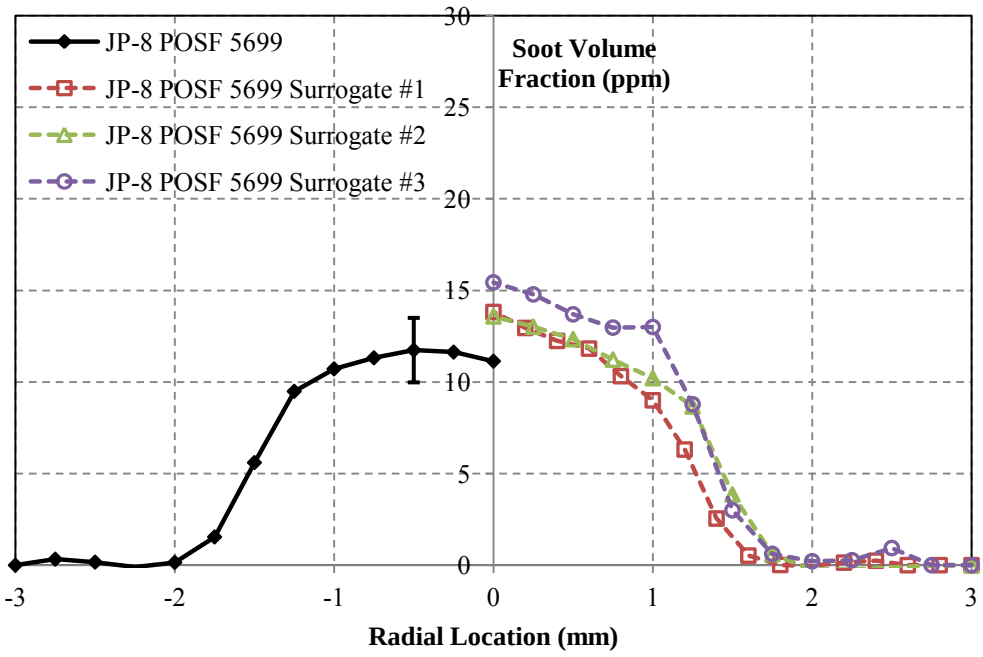

Figure 5.17(d) z = 0.68

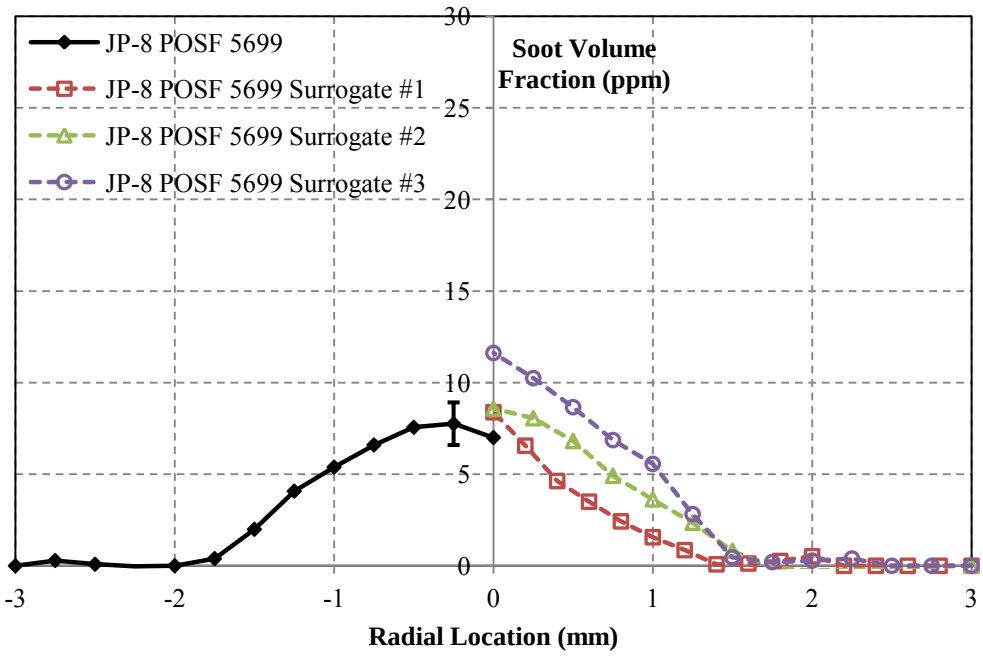

Figure 5.17(e) z = 0.8

Figure 5.17 Radial soot profiles for JP-8 POSF 5699 (left) and the solvent-based surrogates (right) at matching z locations.

The extinction data along the centerline were used to compare the line-of-sight soot volume fractions for the four fuels. The visible flame widths at each axial location were measured using a digital photograph of the flame. These widths were used as the extinction path lengths for the soot volume fraction calculations. The line-of-sight soot volume fractions are plotted against the normalized axial co-ordinate in **Figure 5.18**. At the smoke-point, no soot leaves the flames; therefore, the soot volume fraction is zero at the flame tip. The volume fraction reaches a maximum at a normalized coordinate of z ~ 0.5 for all fuels. The error bar in the figure corresponds to ± 15% uncertainty in the soot volume fractions. Within experimental uncertainty, the profiles for all the three surrogates agree well with JP-8 POSF 5699 as would be expected given how well the radial profiles match.

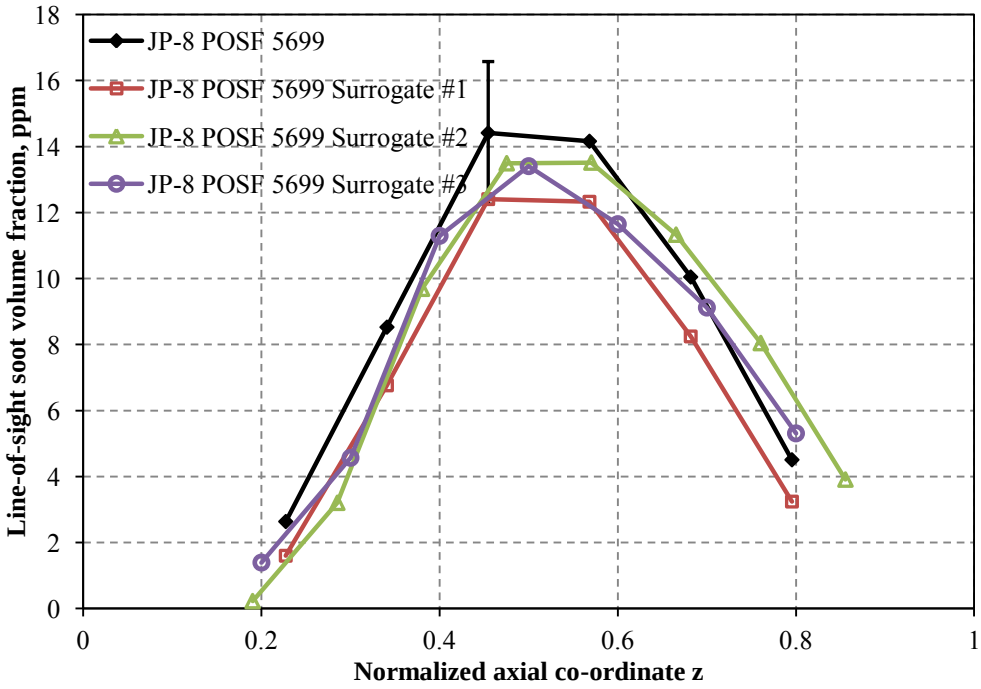

Figure 5.18 Line of sight soot volume fractions for JP-8 POSF 5699 and the solvent based surrogates.

5.4.4. Conclusions

The radial soot profiles for Jet A POSF 4658 and the 2nd generation surrogate on the wick burner showed good agreement in terms of the peak soot volume fractions, location of the peak volume fraction, and centerline volume fraction, within the uncertainty of ± 15%. The radial soot profiles for JP-8 POSF 5699 and the solvent-based surrogates on the wick burner showed good agreement within ± 15%. The line-of-sight soot volume fractions of the solvent-based surrogates also agreed well with JP-8 POSF 5699. Therefore, the Threshold Soot Index works well in estimating the soot fields in the wick burner.

5.5. Modular Gas Turbine Combustor (MGTC) Soot Laser Extinction Comparisons

5.5.1. Experimental apparatus and methodology

A detailed description of the model gas turbine combustor and laser extinction system for measuring soot volume fractions can be found in Refs. [27–29].

5.5.2. Experimental conditions

The experimental conditions for the model gas turbine combustor tests are shown in **Table 5.11**. The inlet air temperature was held constant for all tests by maintaining a temperature of 510 ± 10 K upstream of the critical venturi. An exit nozzle of 0.4 inches diameter was used to choke the exhaust and obtain a mean pressure of operation of 0.51 MPa. The air flow rate was set to 32 g/s and the equivalence ratio was varied by varying the fuel flow rate. Soot measurements were obtained as a function of equivalence ratio. The equivalence ratio was varied from $\varphi = 0.8$ to $\varphi = 1.8$ with intervals of 0.1. The equivalence ratios are not local values but average values determined by the flow rate of the air and the fuel.

Table 5.11 Summary of experimental conditions for the model gas turbine combustor tests.

Air flow rate	32 g/s
Inlet air temperature (upstream of venturi)	510 ± 10 K
Injector	MP, 12 holes, 0.005” diameter
Swirl angle	45°
Chamber pressure	0.51MPa
Chamber Length	307 mm

5.5.3. Results

Figure 5.19 shows the line-of-sight averaged soot volume fraction data obtained for JP-8 POSF 5699 near the exit of the model gas turbine combustor (measurement location 248 mm downstream of the dump plane). Mean soot volume fraction in parts per million are shown on the ordinate and the equivalence ratios are shown on the abscissa. Data from tests on two different days are presented to provide insight into the reproducibility of the results. Each test was comprised of one or more traverses of the equivalence ratio range, where each traverse included one set of “UP” and “DOWN” points. “UP” and “DOWN” refer to increasing and decreasing equivalence ratio, respectively. It can be seen that the soot produced by JP-8 POSF 5699 is very low below $\varphi = 1.2$ and the concentrations increase considerably above this equivalence ratio. A maximum soot volume fraction of 4.5 ppm is observed for JP-8 POSF 5699.

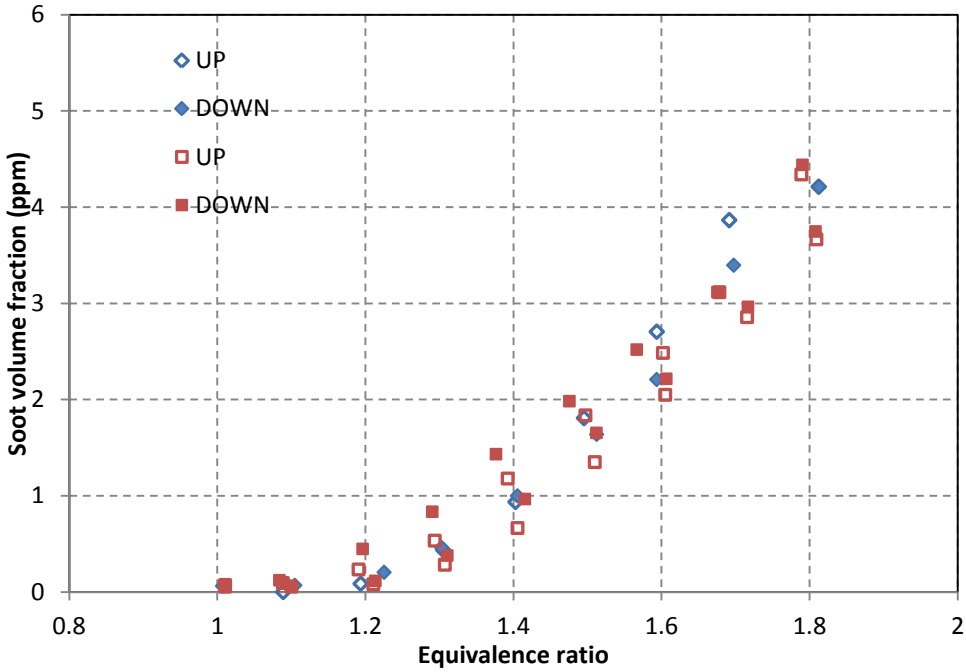

Figure 5.19 Line-of-sight soot volume fraction data for JP-8 POSF 5699 as a function of equivalence ratio. Two runs presented together shown with different symbols.

The presence of large number of data points in **Figure 5.19** makes it hard to discern the trends. For clarity, a least squares second-order polynomial curve is fit to the JP-8 POSF 5699 data points as illustrated in **Figure 5.20**. The data are shown by symbols and the fit is shown as a solid line. A coefficient of determination of $R^2 = 0.96$ is obtained for the fit. The error bars shown are based on a ± 2.6% uncertainty in the equivalence ratio and a ± 15% uncertainty in the extinction measurements.

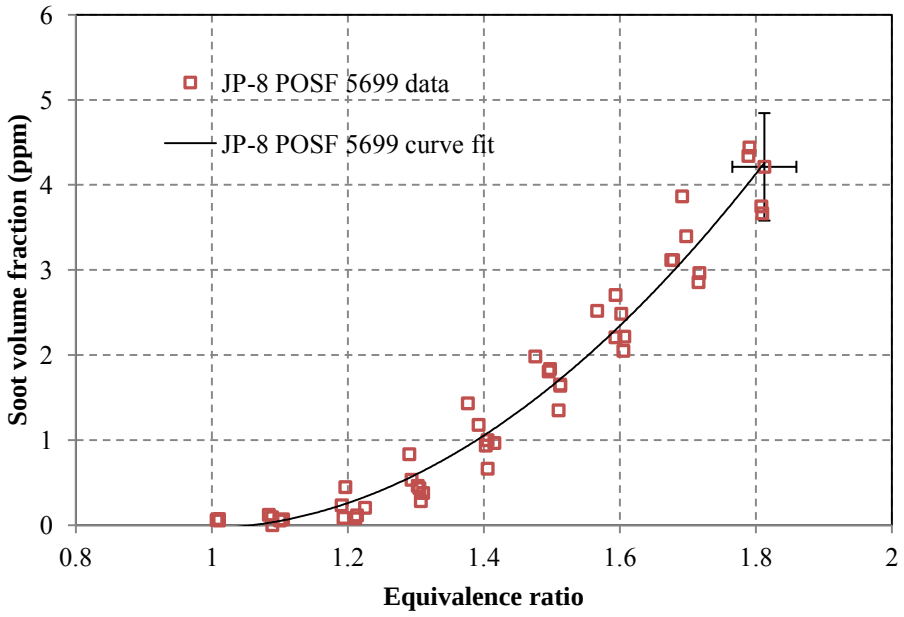

Figure 5.20 Polynomial fit for JP-8 POSF 5699 data.

Plots of the measured line-of-sight soot volume fraction as a function of equivalence ratio for JP-8 POSF 5699 and its three solvent-based surrogates are shown in **Figure 5.21a-d**. The trend of the data for the surrogates is similar to JP-8 POSF 5699 with negligible soot concentrations below φ = 1.2 and increasing values thereon. As seen from **Figure 5.21a** JP-8 POSF 5699 Surrogate #1 produced lower soot volume fractions than JP-8 POSF 5699 for equivalence ratios in the range of ~ 1.3 and 1.7. The mean soot volume fractions measured for JP-8 POSF 5699 Surrogate #2 had the very good agreement with JP-8 POSF 5699 for the entire range of equivalence ratios as seen in **Figure 5.21b.** JP-8 POSF 5699 Surrogate #3 in **Figure 5.21c** showed higher soot volume fractions at equivalence ratios of 1.7 and 1.8. A comparison between JP-8 POSF 5699 Surrogates #1, #2, #3, and JP-8 POSF 5699 in **Figure 5.21d** shows that Surrogate #3 produced slightly higher soot volume fractions at between φ = 1.7 to 1.8 even though they had the same TSI. It is possible that DCN and TSI may have some independent effects on sooting; however, fuels with larger variations in DCN need to be tested to corroborate this possibility [17]. Within experimental uncertainty, overall there was good agreement in mean soot volume fractions between JP-8 POSF 5699 and its solvent-based surrogates at all equivalence ratios tested. The effect of differences in physical properties of the solvent fuels was not evaluated in this study.

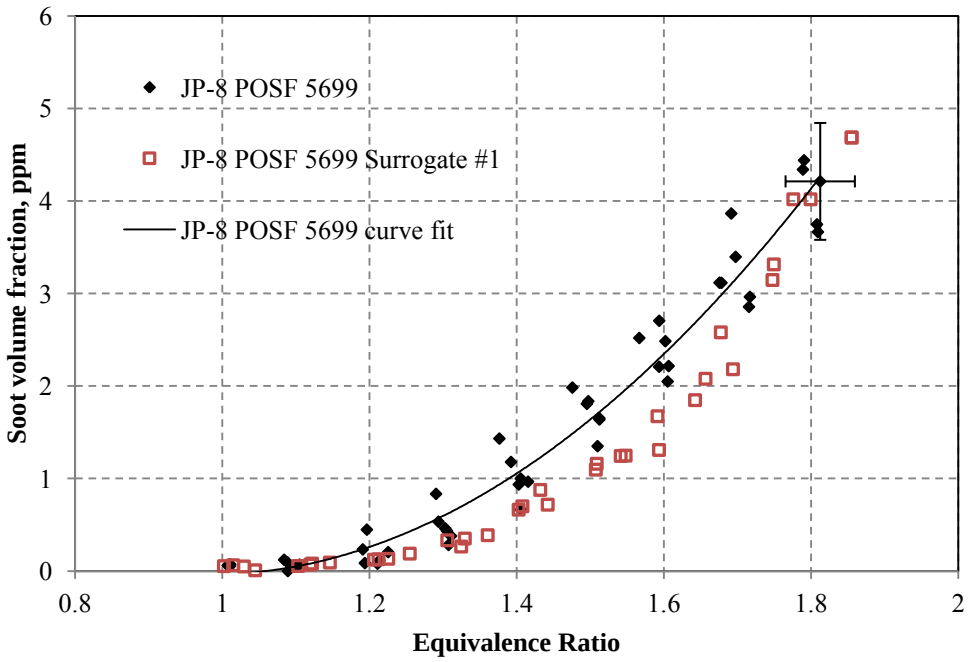

Figure 5.21(a) JP-8 POSF 5699 and JP-8 POSF 5699 surrogate #1

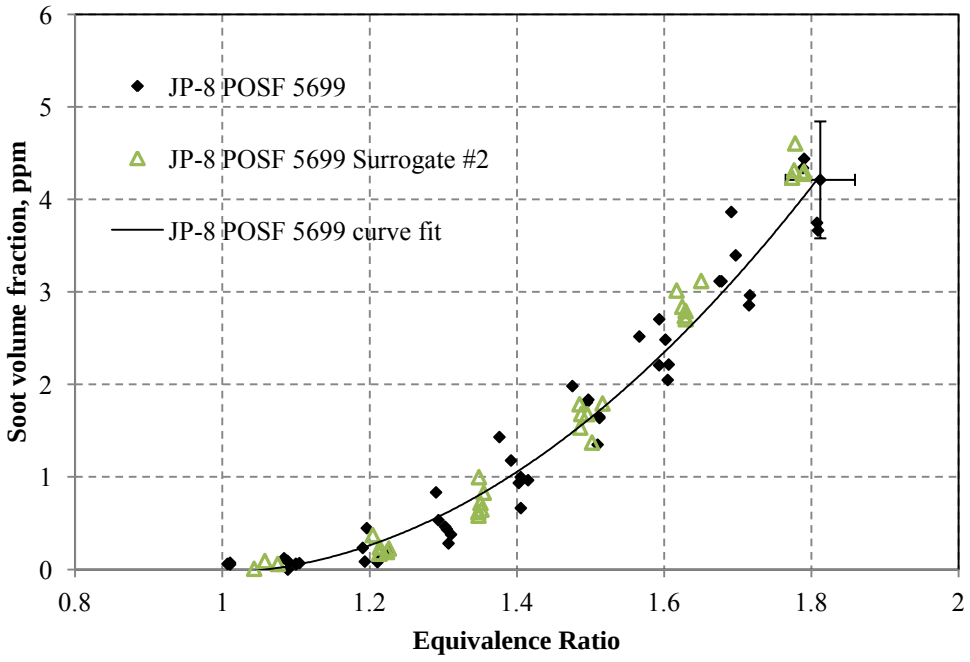

Figure 5.21(b) JP-8 POSF 5699 and JP-8 POSF 5699 surrogate #2

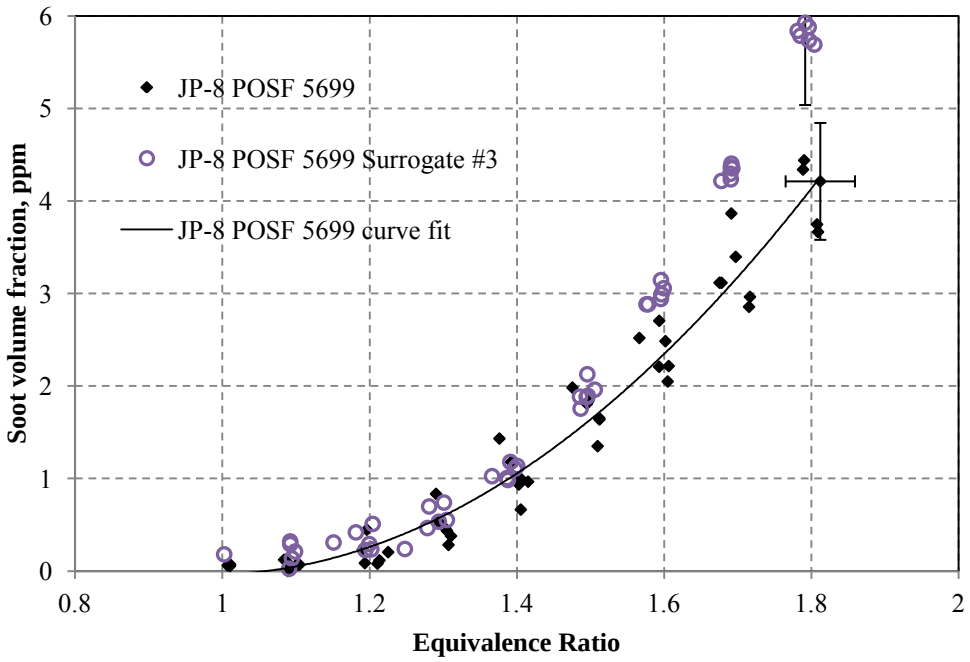

Figure 5.21(c) JP-8 POSF 5699 and JP-8 POSF 5699 surrogate #3

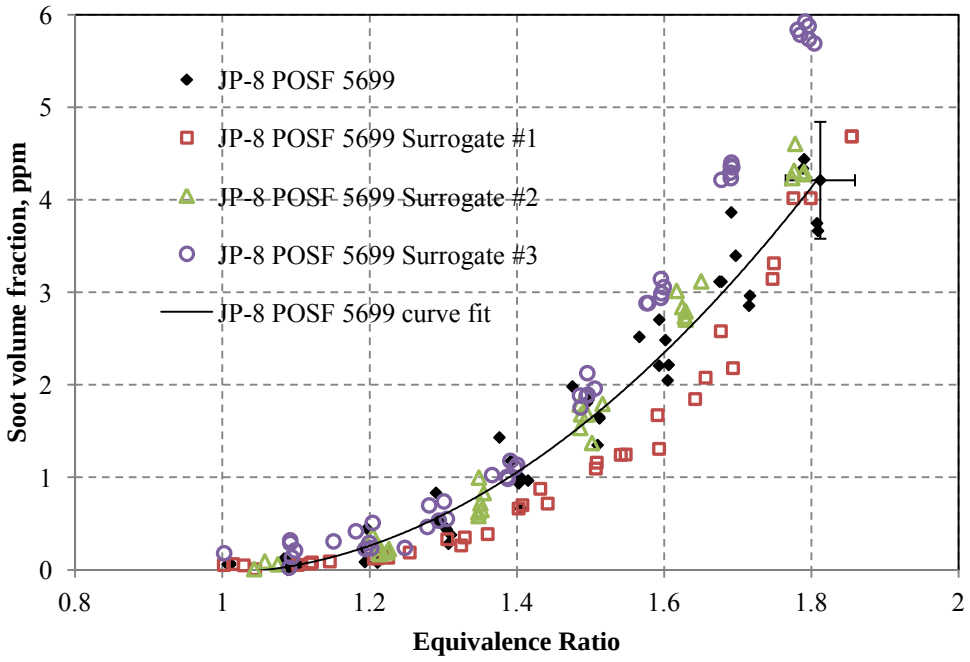

Figure 5.21(d) JP-8 POSF 5699 and JP-8 POSF 5699 surrogates #1, #2, #3

Figure 5.21 Line-of-sight soot volume fraction data for JP-8 POSF 5699 and the solvent-based surrogates as a function of equivalence ratio on the model gas turbine combustor.

5.5.4. Conclusions

The mean soot volume fractions on the model gas turbine combustor for the solvent-based surrogates matched the values of JP-8 POSF 5699 within the uncertainty of ± 15%. The results show that the Threshold Soot Index is a reasonably good indicator of the sooting characteristics in the model gas turbine combustor for JP-8 POSF 5699 and solvent-based surrogate fuels having the same TSI as JP-8 POSF 5699.

5.6. Experimental Apparatus and Methodology

5.6.1. Overview of the High-Pressure Flow Reactor Facility

Figure 5.22 shows a schematic of the high pressure flow reactor facility. The flow reactor is capable of operating at pressure of up to 30 atm, temperatures up to approximately 850 K, and is run with either gaseous or vaporized fuel. The oxidizer flow, composed mainly of air for this study, with some added oxygen, is supplied from two large tanks that are filled and pressurized to 700 psi by a compressor. The oxidizer is then heated to experimental temperatures in a large heater and flows through insulated lines where it then enters the main flow reactor tube. Liquid fuel is vaporized by a preburner and is then injected into the oxidizer where they undergo rapid mixing. A choked nozzle at the end of the tube maintains constant velocity and pressure during a test. Thermocouples and pressure transducers are used to detect a rapid rise in temperature and pressure associated with an autoignition event.

The experimental setup was designed to allow independent control over a variety of parameters as shown in **Table 5.12**. A choked nozzle fixes the velocity and, therefore, also the residence time (autoignition delay time) of the experiment. With the velocity set by the choked nozzle, pressure can then be varied by changing the mass flow rate. All gas mass flow rates were measured using critical orifices, while the liquid fuel mass flow rate was measured by a cavitating venturi. Changes in the mean temperature of the gas flowing in the flow reactor tube are achieved by varying the air heater temperature.

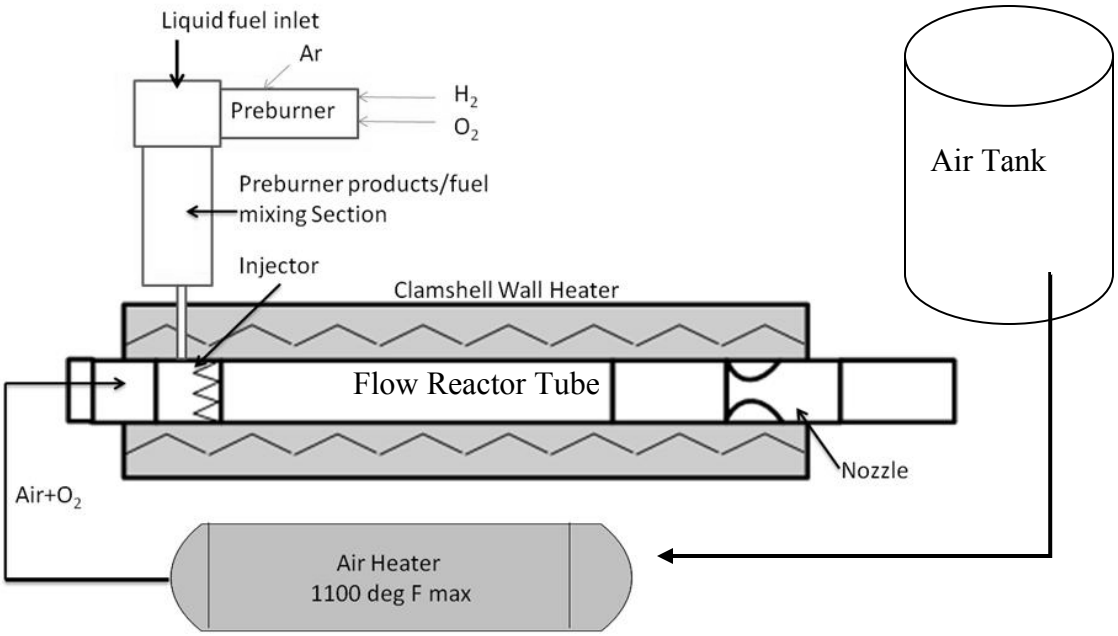

Figure 5.22 General layout of the high pressure flow reactor facility

Table 5.12 Flow reactor experiment parameter variability

Parameter	Set By
velocity/residence time	nozzle size
Pressure	Flow rate
Temperature	air heater
equivalence ratio	fuel flow rate

5.6.1.1. Flow Reactor Tube/Test Section

The flow reactor tube shown in Figure 5.23 is made of 310 stainless steel tubing with a 4.57 cm inner diameter and flanges at both ends. Rather than one continuous tube, sections of 0.305, 0.610, and 0.915 m were fabricated and can be assembled in various arrangements, allowing the overall flow reactor length to be altered between 0.305 m and 2.2 m in order to achieve a range of autoignition delay times. For the current work, the total flow reactor tube length between the injector and nozzle was constant at 2.2 m. The flow reactor tube walls are maintained at a constant temperature, set to match the air temperature using a 10 kW Split Tube Furnace (Series 3210), referred to as the clamshell heater, manufactured by Applied Test Systems, Inc.

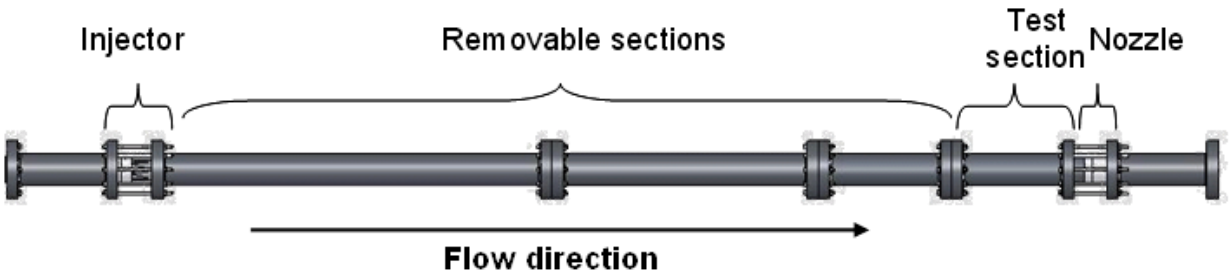

Figure 5.23 Sample flow reactor tube configuration: schematic

Thirteen thermocouples are distributed along the length of the test section Figure 5.24, with the first six distributed across the first 1.5 m and the remaining seven concentrated in the last 0.7 m section where autoignition is expected to occur. Additionally, three pressure transducers are located along the length of the flow reactor tube, one at the entrance, one in the middle, and one at the exit of the reactor. Both high speed and low speed data acquisition systems recorded data. The high speed system operated at 5000 Hz and detected an autoignition event and location, aborting a test if an experimental temperature of 1200 K or higher was reached. The low speed system (10 Hz) was used to measure pressures and temperatures needed to determine mass flow rates and initial conditions.

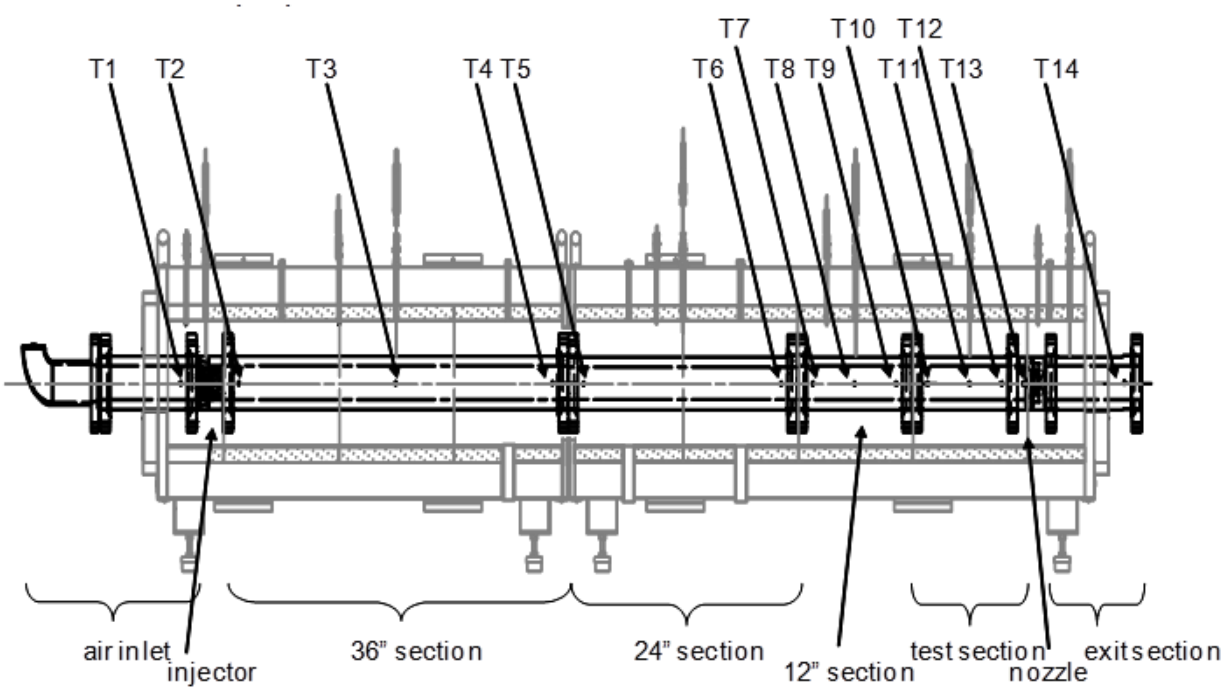

Figure 5.24 A schematic of the flow reactor tube identifying the array of thermocouples located 5 mm from the wall, providing for detection of the autoignition event when it occurs in the flow reactor tube

5.6.1.2. *Fuel Delivery and Preburner*

The fuel delivery system is a vaporizer composed of a preburner, a liquid fuel injector attached to a coupling adapter, followed by a mixing section as shown in Figure 5.25. The preburner, burning a hydrogen, oxygen, argon propellant mixture was used to provide heat for the vaporization of iso-octane used in this study. The preburner was fabricated from inconel, while the coupling adapter and mixing section were fabricated from stainless steel. The internal diameter of the preburner was 2.54 cm and the length is 17.78 cm. At the exit of the preburner, a transition piece is used to increase the diameter of the preburner from 2.54 cm to 4.064 cm to match the diameter of the coupling adapter where the liquid fuel injector is attached. This coupling adapter has a 90-degree bend, with the liquid fuel being injected along the centerline. The vaporized liquid and preburner products then mix in the 25.4 cm long, 4.064 cm diameter mixing section. At the outlet of this section, a nozzled section adapts to a 0.9525 cm inner diameter tube, connected to the fuel manifold on the flow reactor injector.

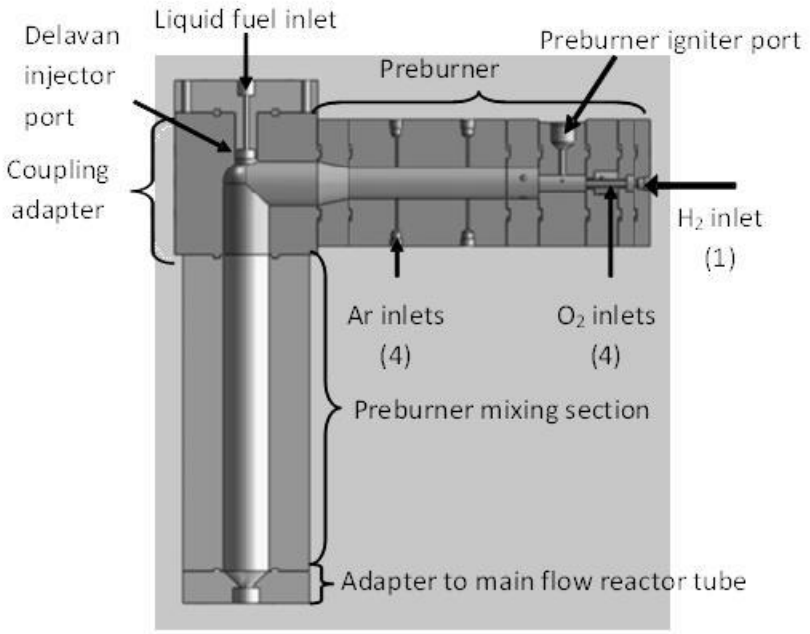

Figure 5.25 Drawing of the preburner, coupling adapter, and preburner mixing section layout

A stoichiometric mixture of hydrogen and oxygen was introduced into the preburner combustion chamber that when burned had only water (H_2O) as the combustion product. Using a stoichiometric mixture (O/F = 8) ensured no excess hydrogen or oxygen was present in the combustion products. Ignition of the preburner was initiated using a spark-ignited torch igniter flowing a mixture of hydrogen and oxygen at a mass flow rate of oxygen to hydrogen (O/F) of 4.5. The adiabatic flame temperature for this mixture is approximately 3500 K [30], much hotter than needed to vaporize the iso-octane. Argon was added downstream of the hydrogen and oxygen to reduce the preburner product temperature such that the temperature of the water vapor

mixed with argon and vaporized iso-octane would not reach temperatures above 800 K. The high combustion temperatures in the preburner limit the run times to short duration (less than 7 s) in order to avoid damage to the hardware.

Argon was chosen as the inert gas instead of nitrogen due to concerns that NO could form in the preburner, and catalyze autoignition at lower temperatures. It has been shown that as little as 20 ppm can have significant effect on the onset of autoignition [31,32]. Oxygen was added to air in the oxidizer stream to maintain a ratio of 21/79 by mole of oxygen to inert gases. The overall water vapor concentration ranged from approximately 1-2 mole percent throughout this series of experiments. This concentration is relatively low and in a previous study of vitiated JP-8 in an atmospheric flow reactor, it was shown that water concentration had very little effect on autoignition delay times [33].

Once all preburner flows were established, the liquid fuel was injected into the preburner products. The liquid iso-octane was supplied from a pressurized tank (up to 123 atm). Flow was controlled by setting the pressure in the tank to achieve the desired flow rate, which was measured by a cavitating venturi. The fuel was then directed through a single Delavan oil burner nozzle that sprays into the preburner mixing section before entering the main flow reactor injector manifold.

5.6.1.3. Main Autoignition Tube Injector

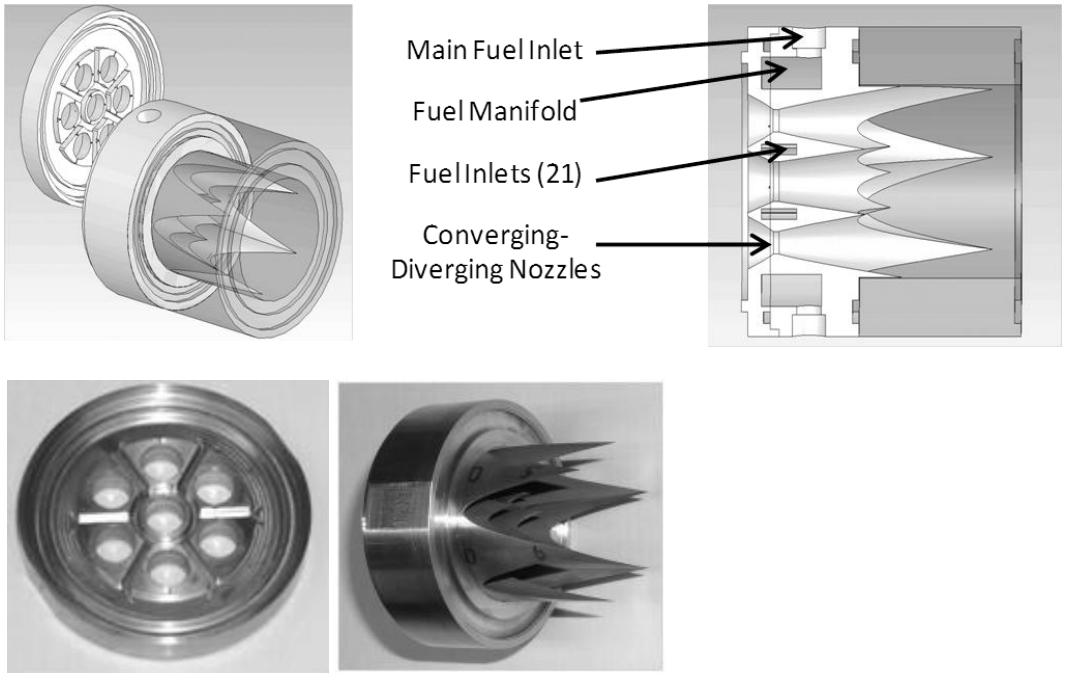

Figure 5.26 Drawings and photos of the main flow reactor tube injector

The injector is based on that used in work by Spadaccini [34] and was designed in order to promote rapid mixing of the fuel and air while minimizing the possibility of recirculation zones

within the flow reactor tube. A drawing of the injector is shown in Figure 5.26. Air enters through seven converging-diverging nozzles (one at the center, and six distributed concentrically), each having a 0.503 cm throat diameter. Fuel enters the injector body from one side of the nozzle and is distributed by a manifold where it is introduced into the air flow through three small holes at the throat of the converging-diverging nozzles. To promote proper mixing over a variety of flow conditions, several fuel injector plates were fabricated with varying areas to maintain appropriate pressure drops (5-25 psi) and momentum flux ratios of fuel to air (8-20). In the work presented here, the total fuel inlet areas ranged from approximately 0.2-0.4 cm^2.

5.6.1.4. Experimental Procedure

A novel experimental methodology was developed in which the threshold equivalence ratio for a given pressure, temperature, and residence time was targeted. The autoignition time, equal to the residence time, is equal to the length of the flow reactor tube divided by the velocity in the tube. This autoignition time is therefore set for a series of experiments. The pressure and temperature are then set at an equivalence ratio below the minimum where autoignition is expected. The test is run and if no autoignition occurs, the equivalence ratio is increased by a small increment. This procedure is repeated as shown in Figure 5.27 until an autoignition event is observed. A new temperature is then set, along with a low equivalence ratio and the process is repeated.

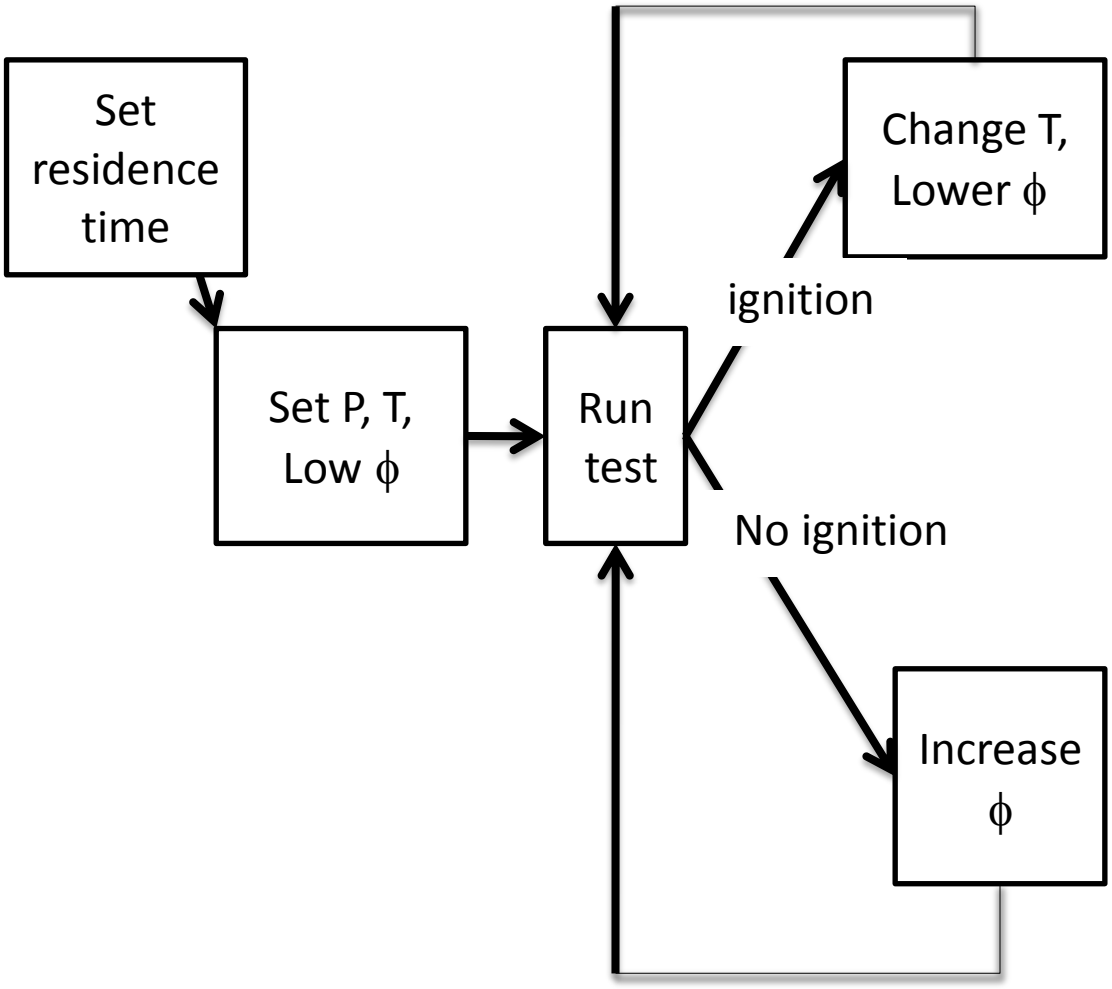

Figure 5.27 Experimental procedure flow diagram

5.6.2. Experimental Conditions

Experiments were conducted for pressures of 15, 17.5, 20, and 22.5 atm, temperatures ranging from approximately 625-850 K, equivalence ratios of approximately 0.244-0.8, and residence times of approximately 70, 100, 125, 155, and 175 ms. To achieve these conditions, flowrates of air ranged from 0.128-0.428 kg/s, while iso-octane flow rates ranged from 0.35-1.5 L/min. A summary of the range of equivalence ratios investigated as well as the mass flow rates of air, added oxygen, preburner hydrogen, preburner oxygen, preburner argon, and iso-octane for each pressure and residence time condition is shown in Table 5.13.

Table 5.13 Summary of equivalence ratios and average mass flow rates for each pressure and residence time condition

P	τ	ϕ	$\dot{m}_{air}$	$\dot{m}_{O2,add}$	$\dot{m}_{PB,H2}$	$\dot{m}_{PB,O2}$	$\dot{m}_{PB,Ar}$	$\dot{m}_{iC8H18}$
15	70	0.705-0.797	0.304	0.00735	3.12E-04	0.00251	0.0411	0.0167
	100	0.599-0.746	0.237	0.00600	2.08E-04	0.00166	0.0270	0.0116
	125	0.545-0.643	0.192	0.00481	1.46E-04	0.00116	0.0218	0.0083
	155	0.371-0.544	0.156	0.00393	1.61E-04	0.00128	0.0179	0.0055
	175	0.442-0.523	0.137	0.00370	1.33E-04	0.00106	0.0169	0.0048
17.5	100	0.461-0.562	0.280	0.00647	2.11E-04	0.00168	0.0299	0.0105
	125	0.348-0.494	0.227	0.00544	1.66E-04	0.00132	0.0250	0.0075
	155	0.351-0.481	0.186	0.00458	1.64E-04	0.00130	0.0212	0.0056
	175	0.408-0.442	0.160	0.00335	1.34E-04	0.00107	0.0155	0.0049
20	100	0.433-0.538	0.409	0.01288	4.18E-04	0.00332	0.0706	0.0151
	125	0.396-0.569	0.313	0.00764	2.11E-04	0.00169	0.0351	0.0103
	155	0.251-0.493	0.261	0.00479	1.62E-04	0.00129	0.0220	0.0072
	175	0.325-0.453	0.218	0.00521	1.61E-04	0.00128	0.0242	0.0061
22.5	100	0.275-0.437	0.356	0.00833	2.75E-04	0.00219	0.0387	0.0097
	125	0.244-0.468	0.303	0.00353	1.49E-04	0.00118	0.0161	0.0075
	155	0.309-0.441	0.251	0.00440	1.80E-04	0.00142	0.0200	0.0064

Experiments were conducted in the high pressure flow reactor facility at pressures of 15, 17.5, 20, and 22.5 atm, over a range of temperatures corresponding to 625-850 K. Experiments were run at a constant temperature with an equivalence ratio initially lower than required for autoignition. In subsequent experiments, the equivalence ratio was incrementally increased at a constant temperature until an autoignition event occurred at the fixed residence time.

Figure 5.28 plots typical data taken at 15 atm for a fixed autoignition delay time of 100 ms. The symbols show the equivalence ratio values where autoignition either did (solid symbols) or did not (open symbols) occur at the fixed residence time. As equivalence ratio was increased, the mixture temperature measured at the end of the autoignition tube also increased by a small amount due to low temperature, or first stage ignition, and increased by successively greater amounts until the test conditions permitted a strong autoignition event. For example at approximately 705 K, the initial equivalence ratio selected was approximately $\phi = 0.559$ and no autoignition was observed but a maximum temperature of 863 K was measured. Subsequent

increases to $\phi = 0.588$ and 0.615 also showed autoignition did not occur, but temperatures of 867 and 877 K were reached, respectively. However, at $\phi=0.644$ a strong autoignition event was observed. The four points discussed are enclosed in the ellipse. The ignition data presented in the remainder of this work are for equivalence ratios where the strong ignition occurred for a particular temperature, pressure, and residence time.

The experimental results for the first stage ignition (if present for a given set of conditions) will not be presented since the time response of the thermocouples and the variation of temperature along the length of the tube could not be captured with sufficient accuracy. This behavior will be discussed later in the model analysis section.

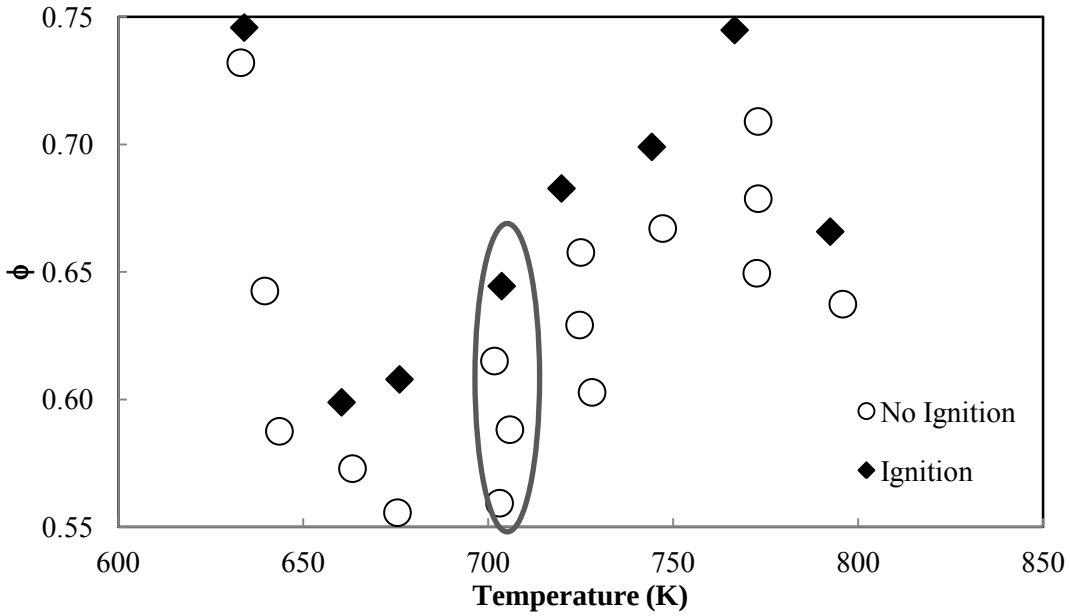

Figure 5.28. Experimental results for 15 atm, 100 ms residence time showing points where ignition did or did not occur

5.6.3. Chemical Kinetic Modeling

The Lawrence Livermore National Laboratory's Iso-Octane Mechanism, Version 3 (LLNL) [35] was chosen as the primary chemical kinetics mechanism for this study. This particular mechanism was chosen because it had been validated over temperatures of 550-1700 K, pressures of 1-45 atm, and equivalence ratios of 0.3-1.5 [36]. With the exception of equivalence ratios less than 0.3, the model covers the range of conditions of the present experimental study. Both ignition delay calculations and a temperature sensitivity analysis were performed using this model to provide a better understanding of the oxidation process. Reactions known to be important at both low-temperature and high-temperature conditions have been included in the

mechanism, with the low-temperature submechanism based on Lawrence Livermore National Laboratory's n-heptane mechanism [37]. The full iso-octane mechanism includes 3,600 elementary reactions and 860 chemical species. As this is currently the most comprehensive iso-octane mechanism, it has been compared with many experimental studies [38,39].

5.6.3.1. Chemical Reaction Engineering and Chemical Kinetics - Complete Hydrocarbon Mechanism (Low and High Temperature) version 1201

Another model, from the Chemical Reaction Engineering and Chemical Kinetics Group (CRECK) [40], was also utilized to compare with the experimental results of this study. The complete mechanism, updated in January 2012, contains 423 species and 13,139 reactions including the kinetics for C_1 to C_{16} hydrocarbons at low and high temperatures. It should be noted that as this is a reduced mechanism, the species are grouped resulting in a relatively smaller number of species to reactions than used in the LLNL mechanism. The full CRECK mechanism had very long computational times and, since alkanes larger than C_8 are not necessary for the current work, the model was further reduced by Frassoldati [41] to include only the relevant kinetics. The reduced mechanism included 256 species and 7,555 reactions. For iso-octane and n-heptane, this mechanism gives the same results as the complete mechanism and has been validated by various experimental studies [42–47]. As this is a reduced mechanism, which involves solving a series of algebraic equations within the model, the computation time is significantly longer than the LLNL mechanism. Therefore, only the 100 ms residence time for a pressure of 22.5 atm, as well as 70, 100, 125, 155, and 175 ms for 15 atm were studied with this mechanism. Again, due to the long computation times, a sensitivity analysis was not performed with the CRECK mechanism.

5.6.4. Experimental and Modeling Results of Ignition Delay Studies

5.6.4.1. Current Experimental Results Compared with Previous Experimental Results

Traditionally, autoignition data are presented on plots of autoignition time as a function of temperature, while parameters such as pressure or equivalence ratio are varied independently. Results from the current study along with data taken from the literature at pressures of 14-16 atm [48–52], normalized to 15 atm, are shown in Figure 5.29. The normalization was performed assuming a linear pressure dependence such that the normalized ignition delay time (τ_{norm}) was equal to the actual ignition delay time (τ_{act}) multiplied by the ratio of actual pressure (P_{act}) to the normalized pressure (P_{norm}) as shown in equation (6)

$$\tau_{norm} = \tau_{act}{}^{P_{act}}/_{P_{norm}} \tag{6}$$

These studies done by other research groups used either shock tubes or rapid compression machines. Note that temperature is represented as inverse temperature (1000/T), so temperature

is decreasing from left to right, and the ignition delay times are presented on a logarithmic scale. This figure clearly shows the operating temperature regimes of the different experimental apparatuses at this pressure. The shock tube results are all at temperatures greater than 1000 K with ignition delay times less than 2 ms. The rapid compression machine results are over a temperature range of approximately 675K to 1000 K with ignition delay times from 5-60 ms. Current results are at temperatures of 625-820 K with ignition delay times ranging from 70-185 ms. The current work overlaps the temperature range of the RCM studies performed by Van Hove et al. [48] and Minetti et al. [50], but is at lower equivalence ratio, and therefore, longer ignition delay times. The overlapping region of the RCM studies, which were both performed at equivalence ratios equal to one, shows the NTC behavior that was observed in the current study.

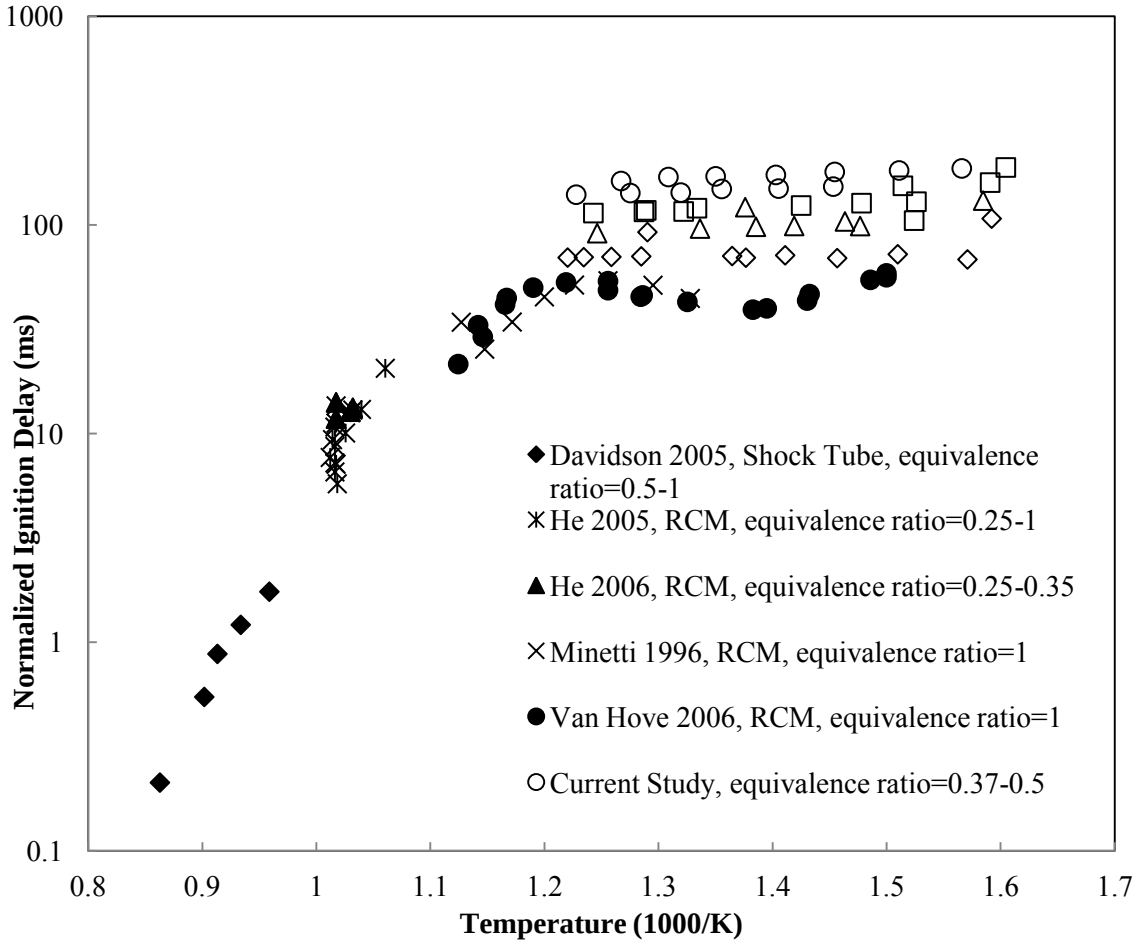

Figure 5.29 Iso-octane autoignition results from shock tubes [49], rapid compression machines [48,50–52], and the current flow reactor studies. All data points are from 14-16 atm and have been normalized to 15 atm

Figure 5.30 shows the literature data taken from 16.5-18.5 atm, normalized to 17.5 atm, along with the 17.5 atm results from the current study. Again note the shock tube results are measured for temperatures at approximately 1000 K or higher, with ignition delay times on the order of 1 ms. The RCM results for this pressure were taken at temperatures close to 980 K with ignition delay times on the order of 10 ms. There is very little overlapping data in the literature at the higher pressures of the current work (20 and 22.5 atm). Thus comparisons could not be made at the two higher pressures as was presented in Figure 5.29 and Figure 5.30. This clearly shows the importance

in results obtained in this ignition delay study. Shock tube and rapid compression machine ignition delay studies have been performed at lower and much higher pressures than the current work and were presented in the Literature Review chapter.

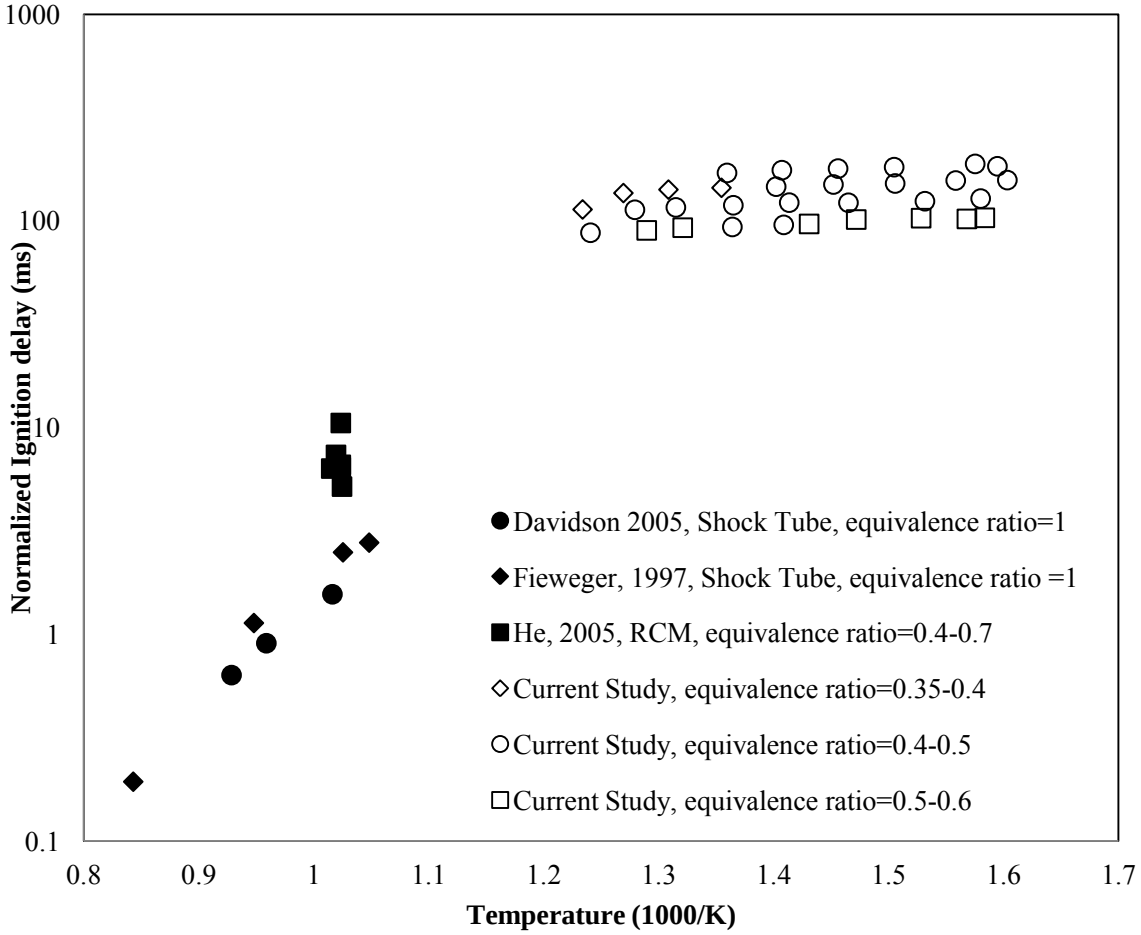

Figure 5.30 Iso-octane autoignition results from shock tubes [49,53], rapid compression machines [51], and the current flow reactor studies. All data points are from 16.5-18.5 atm and have been normalized to 17.5 atm

5.6.4.2. Comparisons between Experimental Results and Chemical Kinetics Model Predictions

In this work, the minimum equivalence ratio necessary for autoignition at the end of the flow reactor tube was obtained. For each of the five set residence times (70, 100, 125, 155, and 175 ms), the ignition delay time is equal to the residence time and was studied for pressures of 15, 17.5, 20, or 22.5 atm. Results corresponding to the minimum equivalence ratio required for autoignition, or the threshold equivalence ratio, are plotted as a function of temperature in Figure 5.31 through Figure 5.34. The LLNL [35] and CRECK [40] model predictions that correspond to the experiment is also included. Note as previously discussed, not all residence times could be studied for all pressures.

As described in the Experimental Setup and Methodology, an analysis to determine the precision uncertainty has been performed on the calculated values of equivalence ratio and mixture temperature, and is represented by the error bars on the experimental data points. Note that on figures showing multiple data sets, only one set of error bars is shown for each data set. Uncertainty on the equivalence ratio varied from 2-9.5%, while the uncertainty on the mixture temperature ranged from 2.5-7% of the absolute temperature. There is some overlap between temperature points within a set of pressures or residence times; however, there is little to no overlap across more than one adjacent data point. Additionally, the error bars overlap the model predictions in some regions, meaning that the model predicts the threshold equivalence ratio for ignition delay within the uncertainty limits of the experimental results.

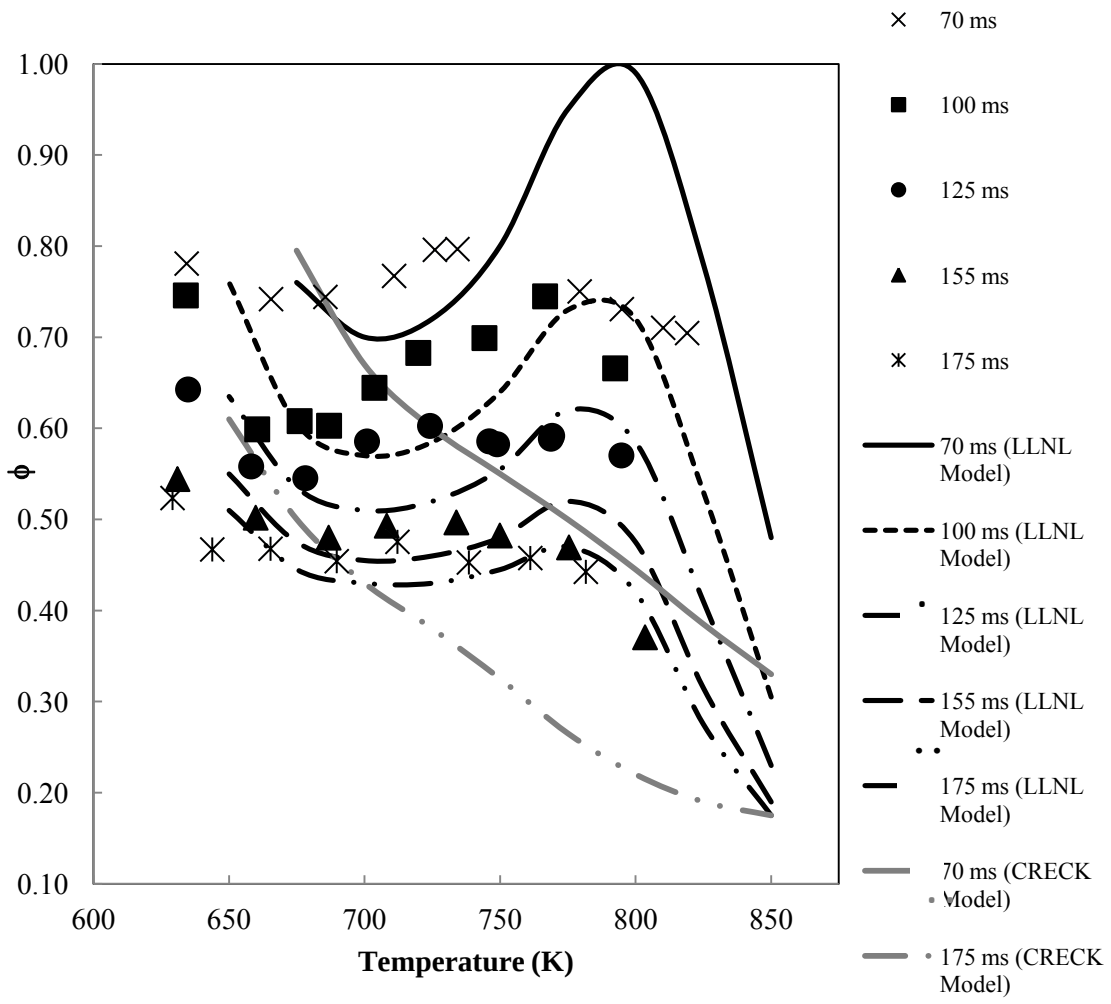

Figure 5.31 Experimental results and model predictions for the threshold equivalence ratio as a function of temperature at 15 atm. Symbols represent experimental results from the current study, black lines represent model results using the LLNL mechanism [35], and gray lines represent model results obtained using the CRECK mechanism [40].

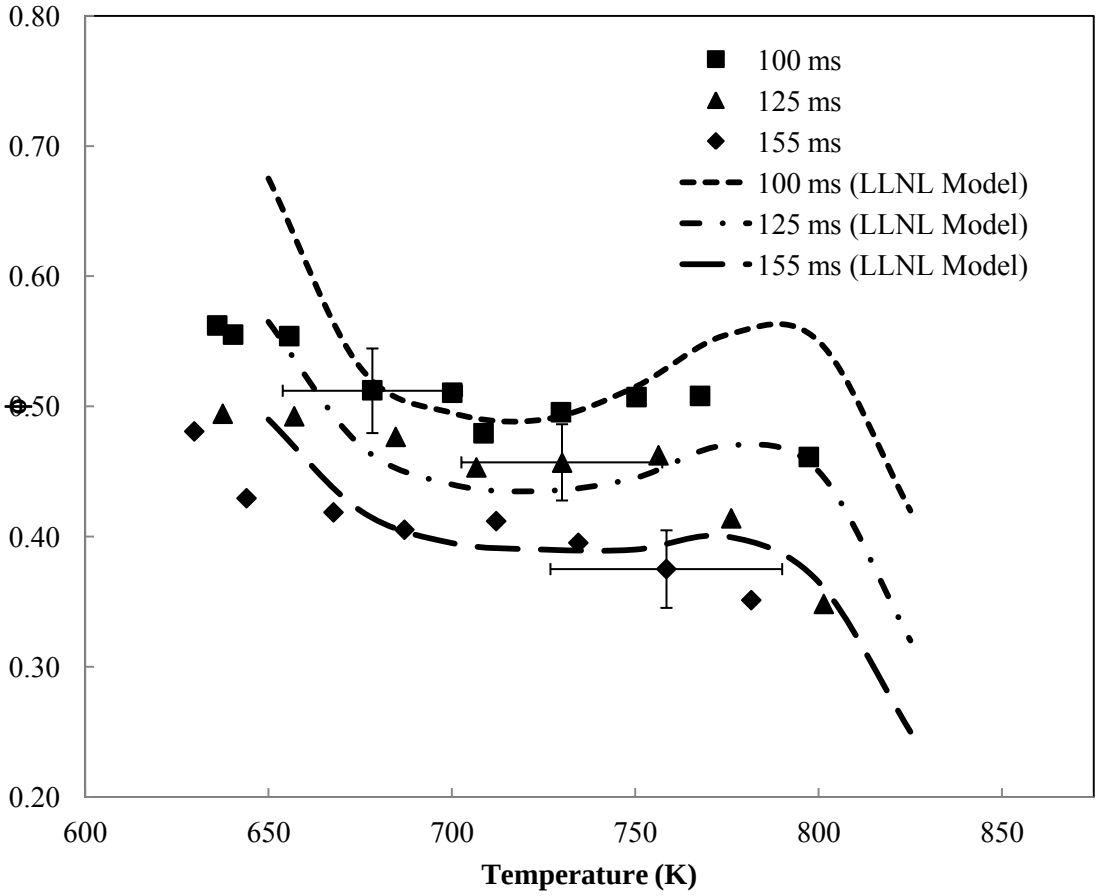

Figure 5.32 Experimental results and model predictions for the threshold equivalence ratio as a function of temperature at 17.5 atm. Symbols represent experimental results from the current study while lines represent model results using the LLNL mechanism [35].

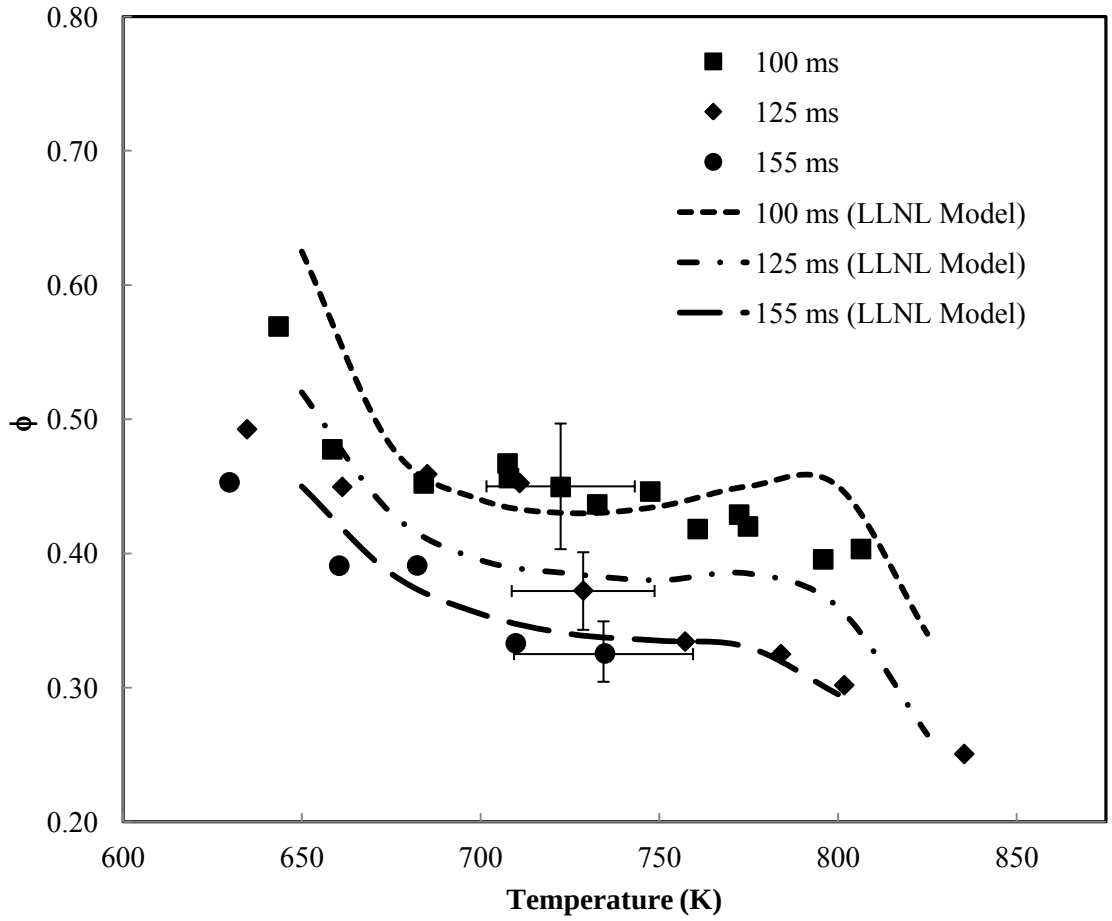

Figure 5.33 Experimental results and model predictions for the threshold equivalence as a function of temperature at 20 atm. Symbols represent experimental results from the current study while lines represent model results using the LLNL mechanism [35].

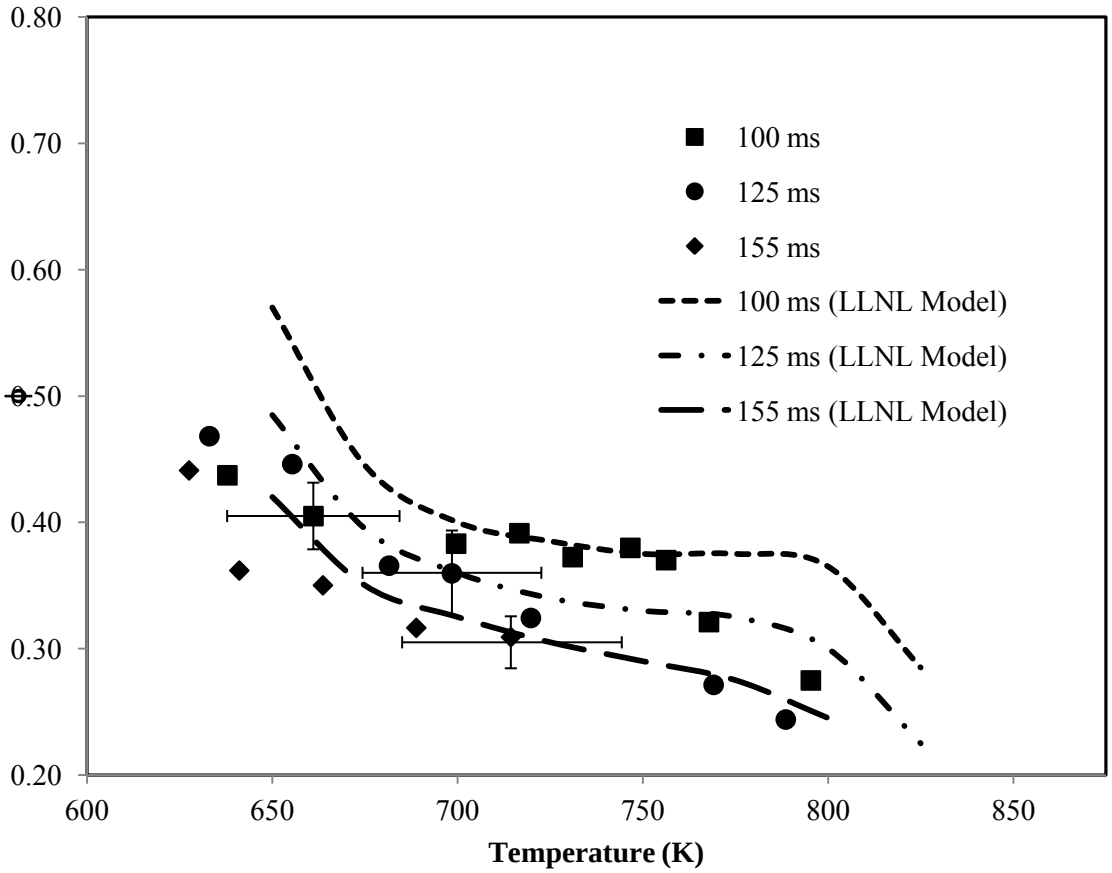

Figure 5.34 Experimental results and model predictions for the threshold equivalence ratio as a function of temperature at 22.5 atm. Symbols represent experimental results from the current study while lines represent model results using the LLNL mechanism [35].

Note that the equivalence ratio scale on the 15 atm plot ranges from 0.2 to 1.0 in order to include the model results at 70 ms. The remainder of the results have an equivalence ratio scale of 0.2-0.8. The same range of pressure, temperature, and equivalence ratio conditions could not be studied for each autoignition delay time. Shorter autoignition delay times required higher air flow rates, in some cases higher than the capabilities of the air heater to provide the required air temperatures. Additionally, for some of the longer autoignition delay times, as well as at some of the higher temperatures, the threshold equivalence ratios were lower than could be metered accurately with the cavitating venturi.

Trends from the experimental results show that the equivalence ratio at which ignition occurs decreases with increased autoignition delay time. For example, comparing results from 100 ms with 155 ms, the average equivalence ratios at which autoignition occurred for 155 ms were 24%, 39%, 24%, and 31% lower than at 100 ms for pressures of 15, 17.5, 20, and 22.5 atm, respectively. These average threshold equivalence ratios are for the results shown in Figure 5.31 through Figure 5.34. Additionally, the presence of the NTC region is shown to diminish with increasing pressure. The onset of autoignition in all cases is observed at approximately 640 K for

these experiments. The model did not predict autoignition at the residence times of this current work at temperatures below 650 K and in some cases, below 675 K.

In general, the LLNL model and experimental results are in good agreement in terms of the trends in the magnitude of equivalence ratio as a function of temperature. Predictions from the CRECK model show significant deviations from the experimental measurements, particularly the complete absence of the NTC region. For clarity, the individual conditions are plotted on separate graphs for 15 atm (Figure 5.35 through Figure 5.39), 17.5 atm (Figure 5.40 through Figure 5.42), 20 atm (Figure 5.43 through Figure 5.45), and 22.5 atm (Figure 5.46 through Figure 5.48) to allow a more detailed comparison of the experimental and model results. The results presented will be discussed for each condition.

At 15 atm for the 70 ms autoignition delay time (Figure 5.35), the magnitude of the peak of the NTC region is significantly over predicted by the LLNL model. Experimental results show a slight onset of the NTC region at approximately 700 K, where the equivalence ratio required for autoignition increases slightly and then begins to decrease after the point at 735 K. The LLNL model predicts onset of the NTC region at slightly higher temperature, just higher than 725 K, with a peak occurring at approximately 800 K at an equivalence ratio of 1.0. At temperatures above 800K the equivalence ratio required for autoignition rapidly decreases to 0.48 at 850 K. Both models predict the onset of autoignition at temperature of 675 K for the conditions of 15 atm and a residence time of 70 ms. At this low temperature, both models show good agreement with the experimental results.

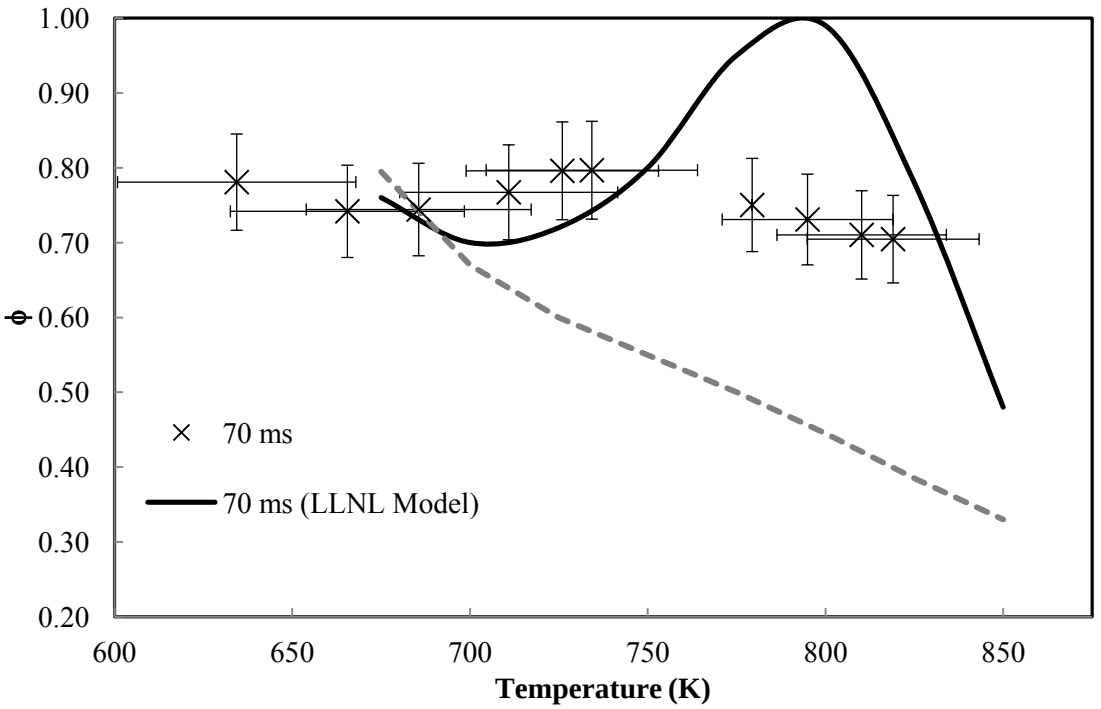

Figure 5.35 Experimental results and model predictions for the threshold equivalence ratio as a function of temperature at 15 atm and 70 ms autoignition delay times. Symbols represent experimental results from the current

study, solid lines represent model results using the LLNL mechanism [35], and dashed lines represent model results obtained using the CRECK mechanism [40].

For the remaining autoignition delay times of 100, 125, 155, and 175 ms at 15 atm (Figure 5.36 through Figure 5.39), exceptional agreement is shown between the LLNL model and experimental results. The NTC region for both the experimental results and model predictions occur over a temperature interval of 75 K. In experimental results, the NTC regions occurs at slightly lower temperatures than is predicted by the LLNL model, particularly for the 100 ms autoignition delay time (Figure 5.36). Again, the CRECK model predicts autoignition conditions within the uncertainty of the experimental results at temperatures below 675 K, but then shows at higher temperatures a rapid decrease in the equivalence ratio required for autoignition with no presence of the NTC region.

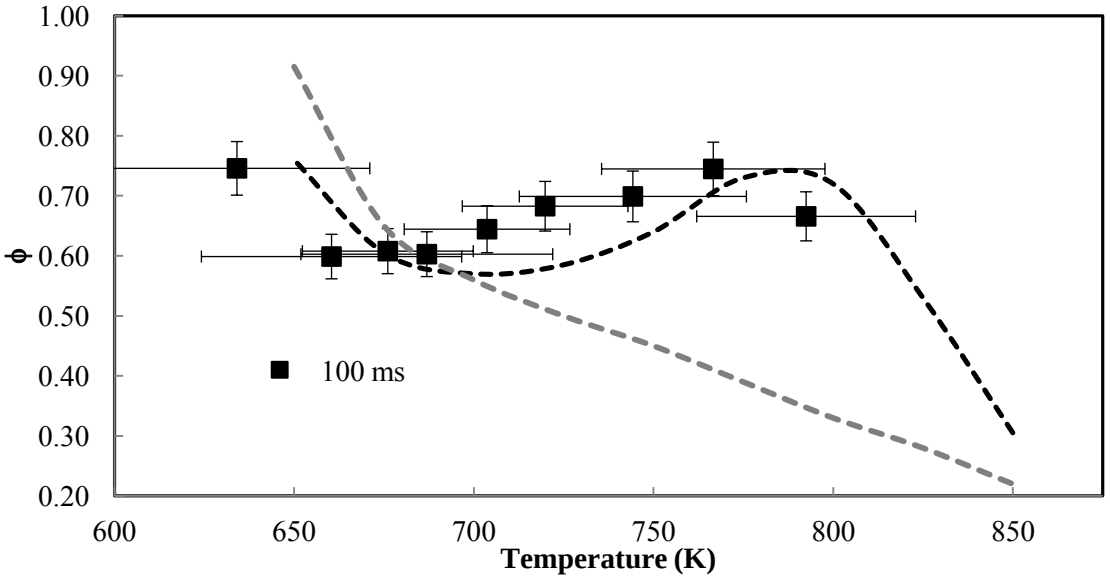

Figure 5.36 Experimental results and model predictions for the threshold equivalence ratio as a function of temperature at 15 atm and 100 ms autoignition delay times. Symbols represent experimental results from the current study, solid lines represent model results using the LLNL mechanism [35], and dashed lines represent model results obtained using the CRECK mechanism [40].

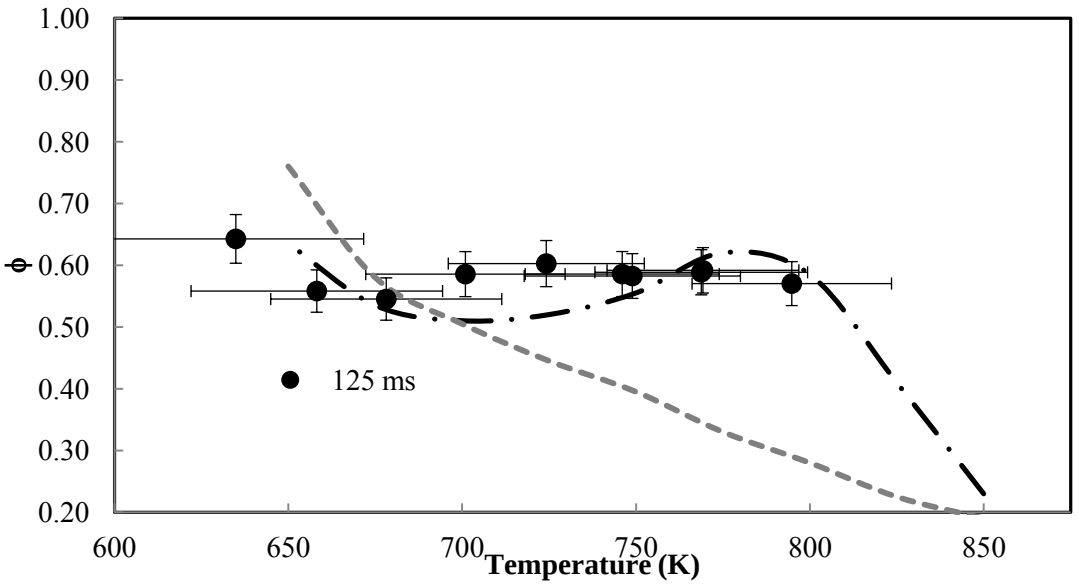

Figure 5.37 Experimental results and model predictions for the threshold equivalence ratio as a function of temperature at 15 atm and 125 ms autoignition delay times. Symbols represent experimental results from the current study, solid lines represent model results using the LLNL mechanism [35], and dashed lines represent model results obtained using the CRECK mechanism [40].

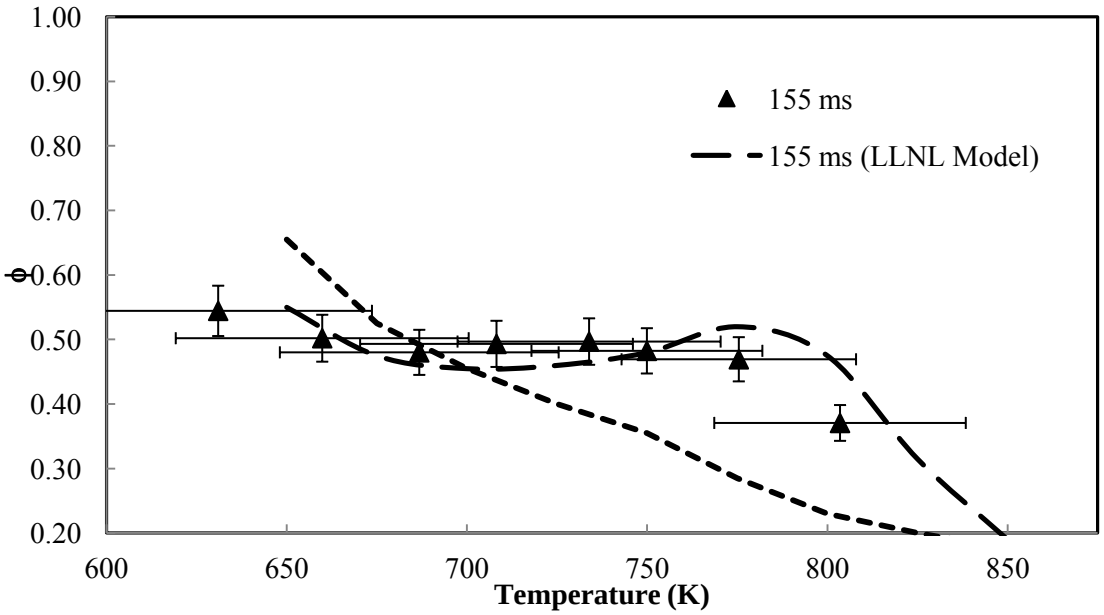

Figure 5.38 Experimental results and model predictions for the threshold equivalence ratio as a function of temperature at 15 atm and 155 ms autoignition delay times. Symbols represent experimental results from the current study, solid lines represent model results using the LLNL mechanism [35], and dashed lines represent model results obtained using the CRECK mechanism [40].

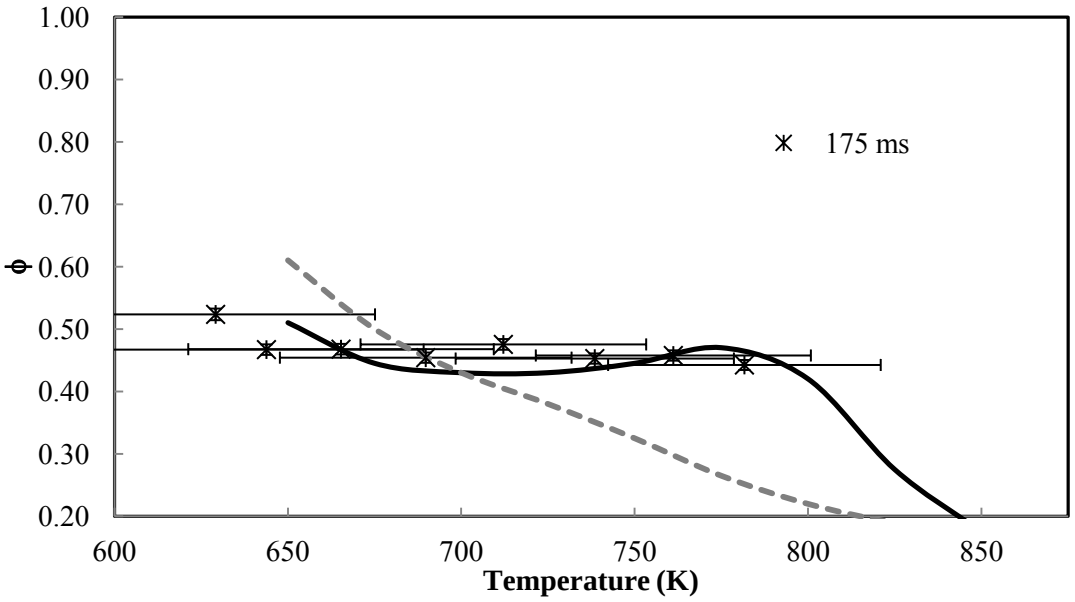

Figure 5.39 Experimental results and model predictions for the threshold equivalence ratio as a function of temperature at 15 atm and 175 ms autoignition delay times. Symbols represent experimental results from the current study, solid lines represent model results using the LLNL mechanism [35], and dashed lines represent model results obtained using the CRECK mechanism [40].

At 17.5 atm for the 100, 125, and 155 ms autoignition delay times (Figure 5.40 - Figure 5.42), very good agreement between the experiment and LLNL model is again shown. The main discrepancy is at the lower temperatures. For all three ignition delay times the model does not predict ignition for less than 650 K, while experimental results showed ignition occurring for temperatures as low as 630 K. Additionally, at the onset of autoignition, the model results predict a much higher required equivalence ratio. Similar to the 15 atm results, the model predicts a greater dependence on equivalence ratio in the NTC region than is shown by the experimental results. For the 100 ms ignition delay (Figure 5.40), the equivalence ratio required for ignition did not increase noticeably, however, the drop in equivalence ratio associated with the high temperature chemistry does not occur until 768 K. For the 125 ms (Figure 5.41) and 155 ms (Figure 5.42) conditions, the threshold equivalence ratio begins dropping slowly at approximately 750 K, about 25 K earlier than the model predicts.

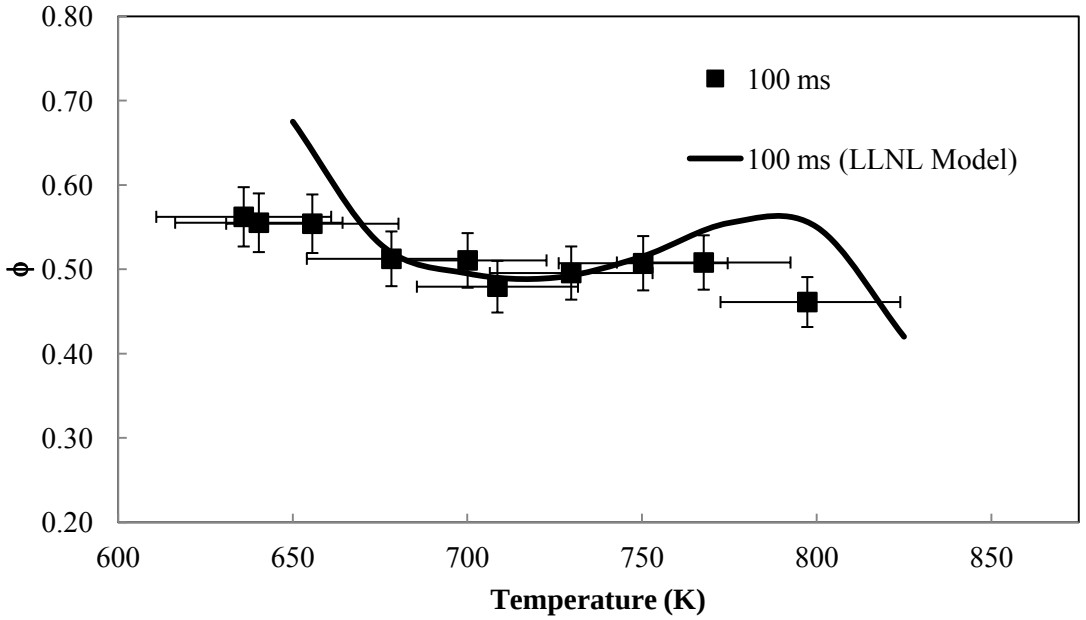

Figure 5.40 Experimental results and model predictions for the threshold equivalence ratio as a function of temperature at 17.5 atm and 100 ms autoignition delay times. Symbols represent experimental results from the current study and black lines represent model results using the LLNL mechanism [35].

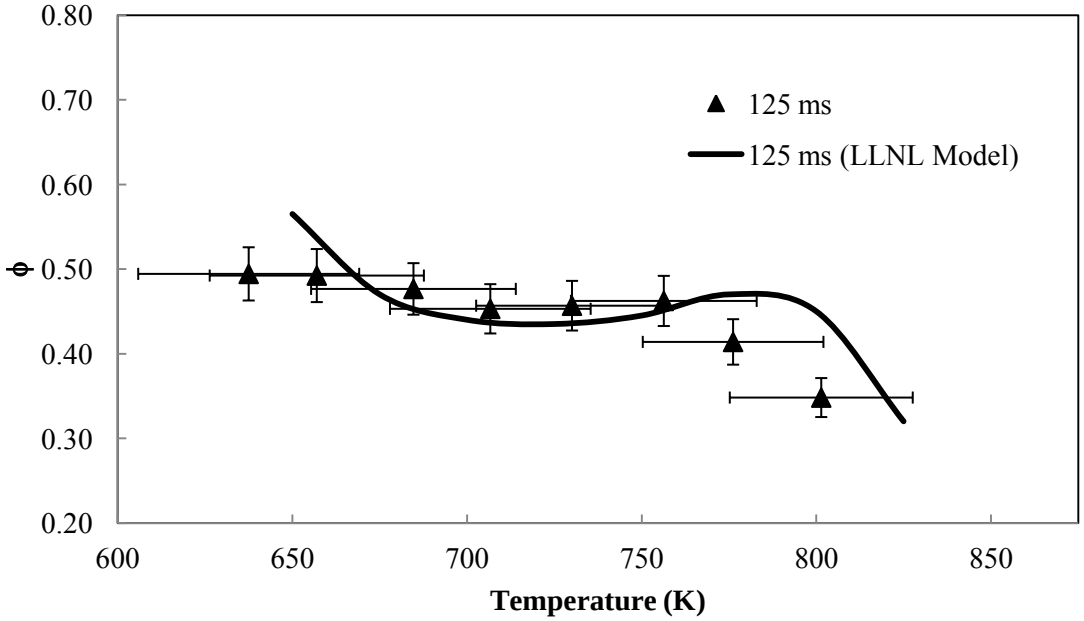

Figure 5.41 Experimental results and model predictions for the threshold equivalence ratio as a function of temperature at 17.5 atm and 125 ms autoignition delay times. Symbols represent experimental results from the current study and black lines represent model results using the LLNL mechanism [35].

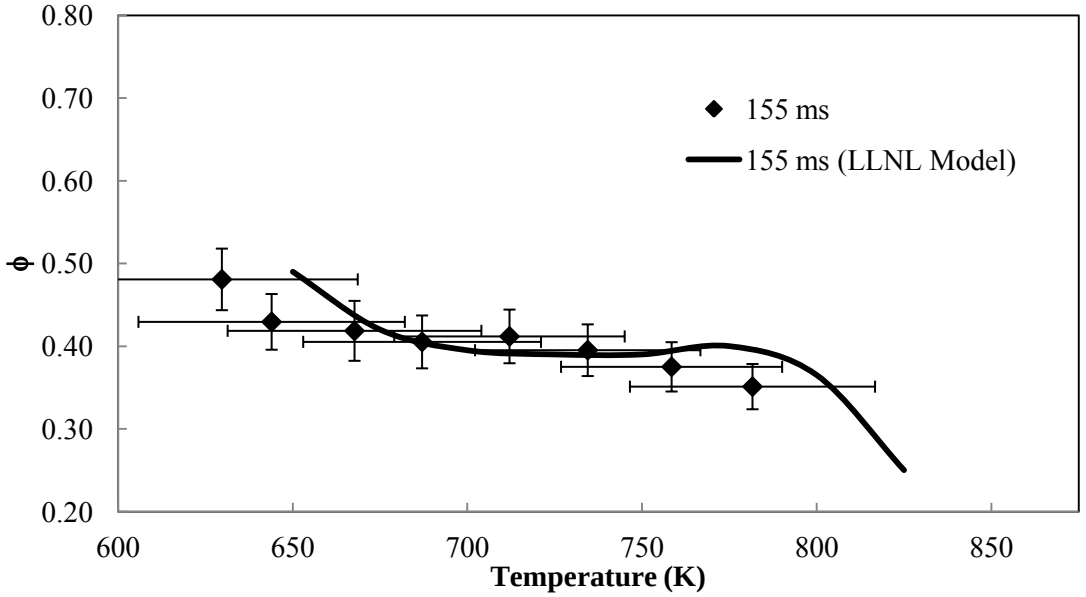

Figure 5.42 Experimental results and model predictions for the threshold equivalence ratio as a function of temperature at 17.5 atm and 155 ms autoignition delay times. Symbols represent experimental results from the current study and black lines represent model results using the LLNL mechanism [35].

At 20 atm, ignition delay times of 100, 125, and 155 ms were investigated. For 100 ms (Figure 5.43), the experimental and model results were quite similar. The main differences are at the lowest temperature where autoignition was observed. Experimental results show ignition starting at 643 K and from this point until around 675 K, the model predicts a similar dependence of ignition delay on threshold equivalence ratio but at 25 K higher in temperature. From 675 K to 750 K, results showed very good agreement. The model however, predicts a small NTC region from 725 K to just under 800 K, while the experimental results show a slight decrease in the dependence of equivalence ratio on temperature required for autoignition, always within experimental uncertainty.

At 125 ms (Figure 5.44), the model predicted very little rise in equivalence ratio required for autoignition, appearing more as a plateau than a rise in the NTC region. For the model prediction at 125 ms, the plateau associated with the NTC region occurs for an equivalence ratio of approximately 0.38 from temperatures of 725 K to 775 K. This plateau was observed at lower temperatures in the experimental results, from 660-710 K, and also at a higher equivalence ratio equal to 0.45, approximately 18% higher than the model prediction. The dependence of threshold equivalence ratio on temperature above 775 K for the model and 710 K for the experiment is similar, but the experimental results are shifted to lower temperature. The 155 ms results (Figure 5.45) are similar, shifted to lower temperature and about a 15% higher equivalence ratio.

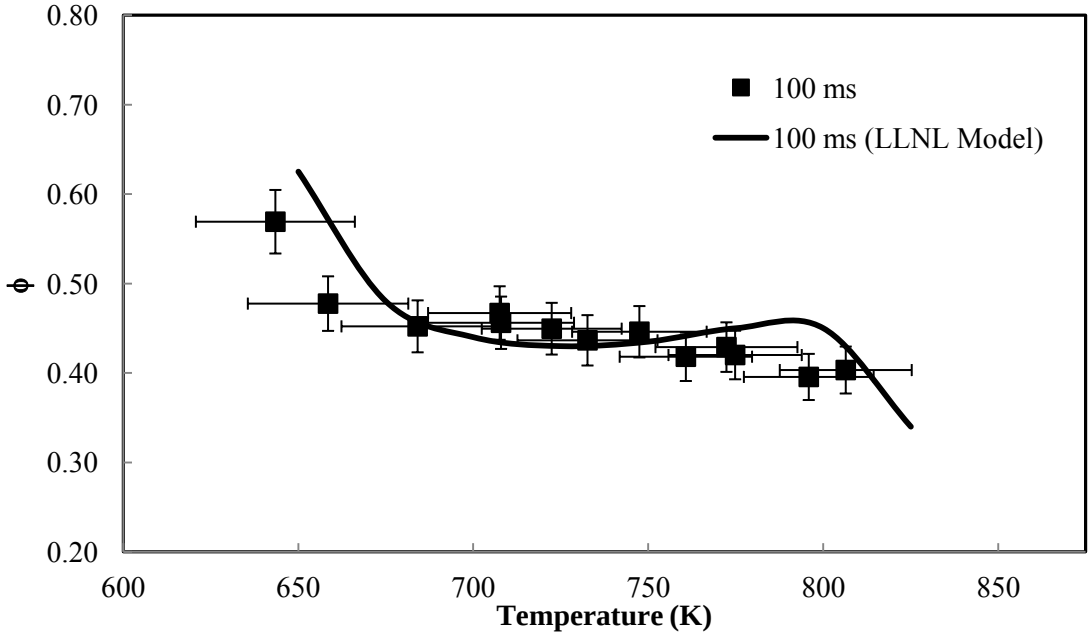

Figure 5.43 Experimental results and model predictions for the threshold equivalence ratio as a function of temperature at 20 atm and 100 ms autoignition delay times. Symbols represent experimental results from the current study and black lines represent model results using the LLNL mechanism [35].

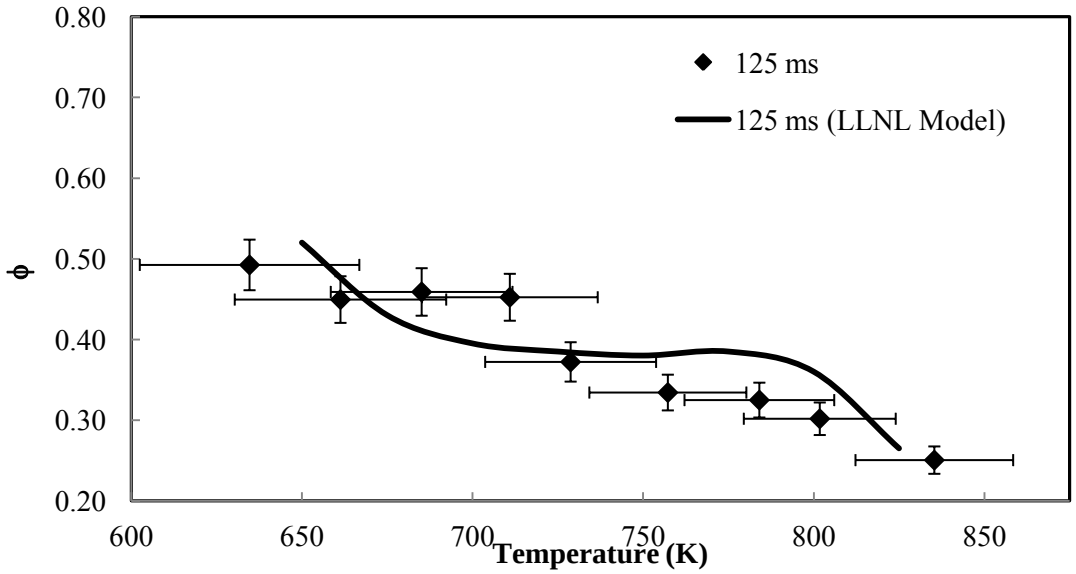

Figure 5.44 Experimental results and model predictions for the threshold equivalence ratio as a function of temperature at 20 atm and 125 ms autoignition delay times. Symbols represent experimental results from the current study and black lines represent model results using the LLNL mechanism [35].

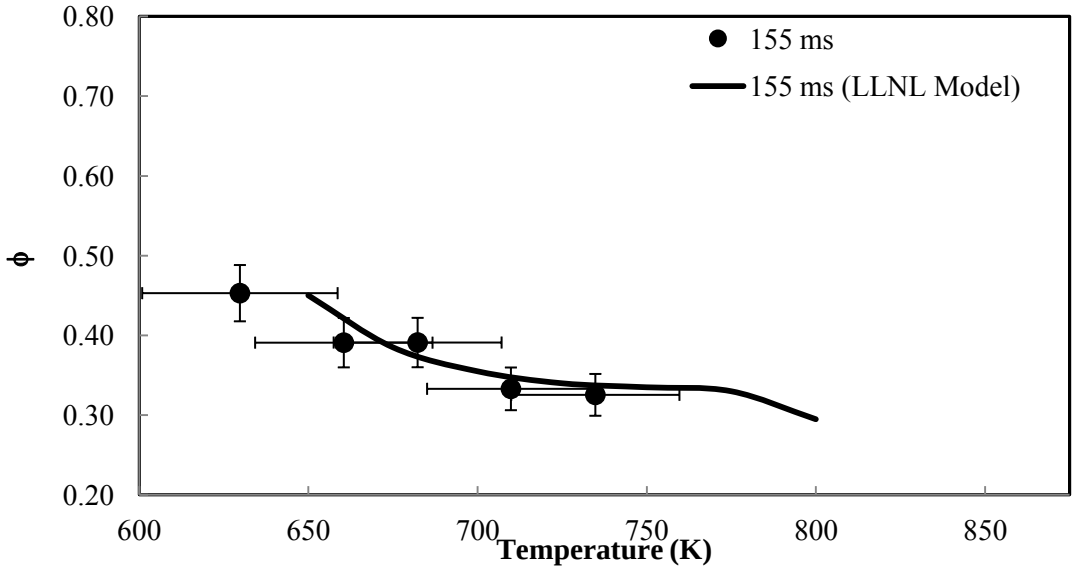

Figure 5.45 Experimental results and model predictions for the threshold equivalence ratio as a function of temperature at 20 atm and 155 ms autoignition delay times. Symbols represent experimental results from the current study and black lines represent model results using the LLNL mechanism [35].

Experimental results for 22.5 atm were obtained at 100, 125, and 155 ms. Model predictions are consistently shifted to higher temperatures. The plateau region associated with NTC behavior showed excellent agreement in terms of the threshold equivalence ratio. Figure 5.46 shows this plateau region for both the experimental results and model predictions occurring at an equivalence ratio equal to 0.375. For the experimental results, this plateau appears over the temperature range of 675-750 K, while the model predicts the plateau region shifted to approximately 50 K higher temperatures, from 725-800 K. The plateau region is significantly diminished at 125 ms (Figure 5.47), occurring over the temperature range of 675-700 K in the experimental results and 725-775 K in the model predictions. At 155 ms (Figure 5.48), this plateau is nearly nonexistent.

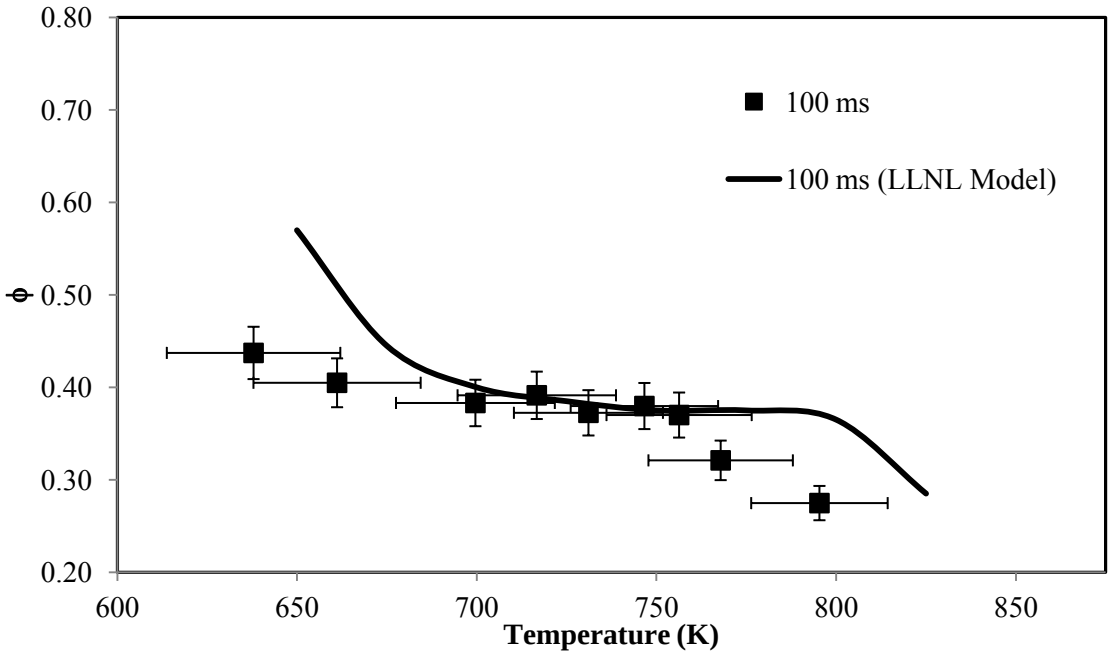

Figure 5.46 Experimental results and model predictions for the threshold equivalence ratio as a function of temperature at 22.5 atm and 100 ms autoignition delay times. Symbols represent experimental results from the current study and black lines represent model results using the LLNL mechanism [35].

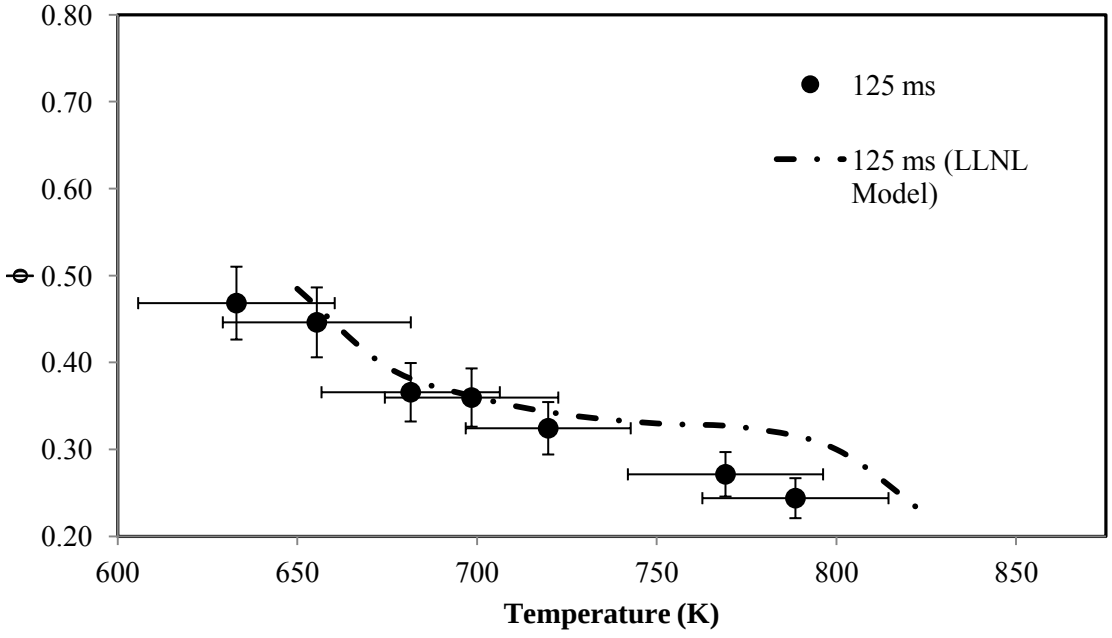

Figure 5.47 Experimental results and model predictions for the threshold equivalence ratio as a function of temperature at 22.5 atm and 125 ms autoignition delay times. Symbols represent experimental results from the current study and black lines represent model results using the LLNL mechanism [35].

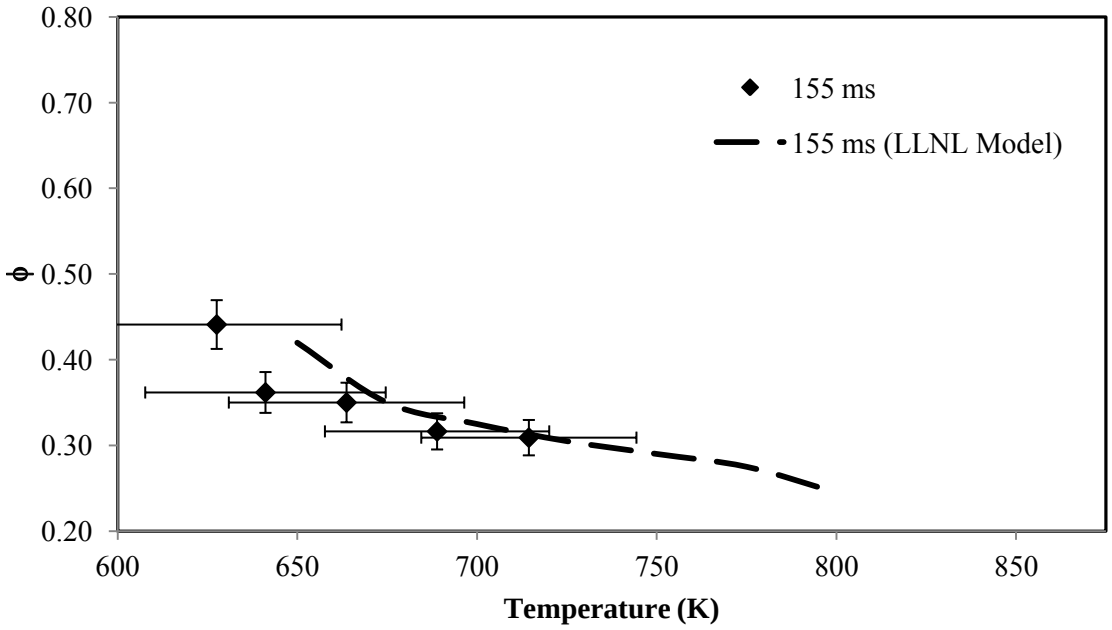

Figure 5.48 Experimental results and model predictions for the threshold equivalence ratio as a function of temperature at 22.5 atm and 155 ms autoignition delay times. Symbols represent experimental results from the current study and black lines represent model results using the LLNL mechanism [35].

Figure 5.49 through Figure 5.51 plot the same results shown previously, now the effect of pressure on the threshold equivalence ratio as a function of temperature, for a fixed autoignition delay time is compared. In general, the model predicts the experimental results quite well with the exception of the 17.5 atm results at 100 ms and 15 atm at 125 ms. For the experimental results at these conditions, the NTC region was broader than the model predictions. Nonetheless, there is remarkable agreement between the experiment and model results.

These figures (Figure 5.49 through Figure 5.51) more clearly show that the NTC region diminishes with increasing pressure for every autoignition delay time. Additionally, as the autoignition delay time increases the NTC region is less pronounced. In general, the equivalence ratio at which autoignition occurs decreases with increased pressure. For example, comparing results at 725 K from 15 atm to 22.5 atm, the equivalence ratio at which autoignition occurred were 64%, 80%, and 62% lower at autoignition delay times of 100, 125, and 155 ms, respectively. The difference for the 100 ms results is likely due to the more significant NTC region at this autoignition delay time. Additionally, at 15 atm and 640 K, the lowest temperature where an autoignition event was observed, it is shown that the equivalence ratio necessary for autoignition decreases with increasing autoignition delay time. For example, comparing 100 ms to 155 ms, the threshold equivalence ratio decreased from $\phi = 0.75$ to 0.44. However, at 22.5 atm at 640 K, the equivalence ratio is approximately constant at $\phi = 0.44$.

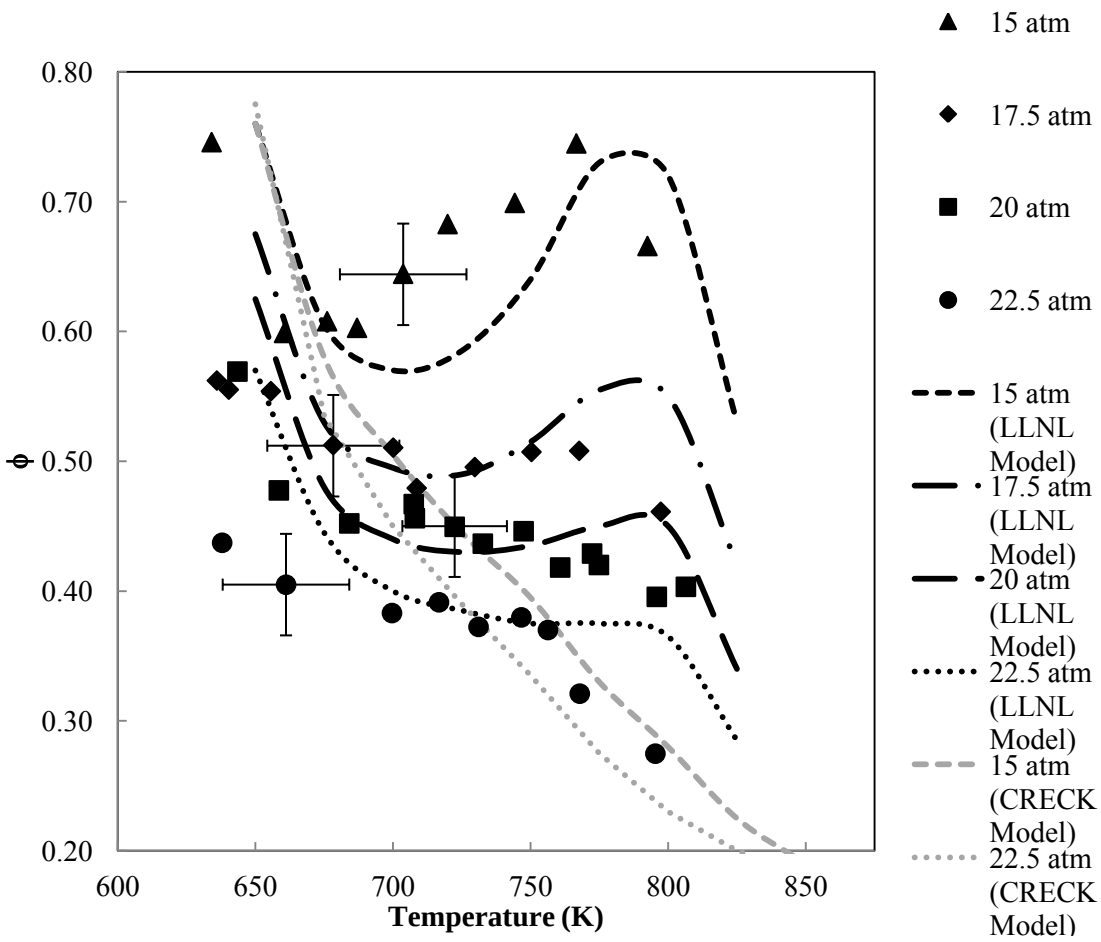

Figure 5.49 Experimental results and model predictions for the threshold equivalence ratio as a function of temperature at a residence time of 100 ms. Symbols represent experimental results from the current study, black lines represent model results using the LLNL mechanism [35], and gray lines represent model results obtained using the CRECK mechanism [40].

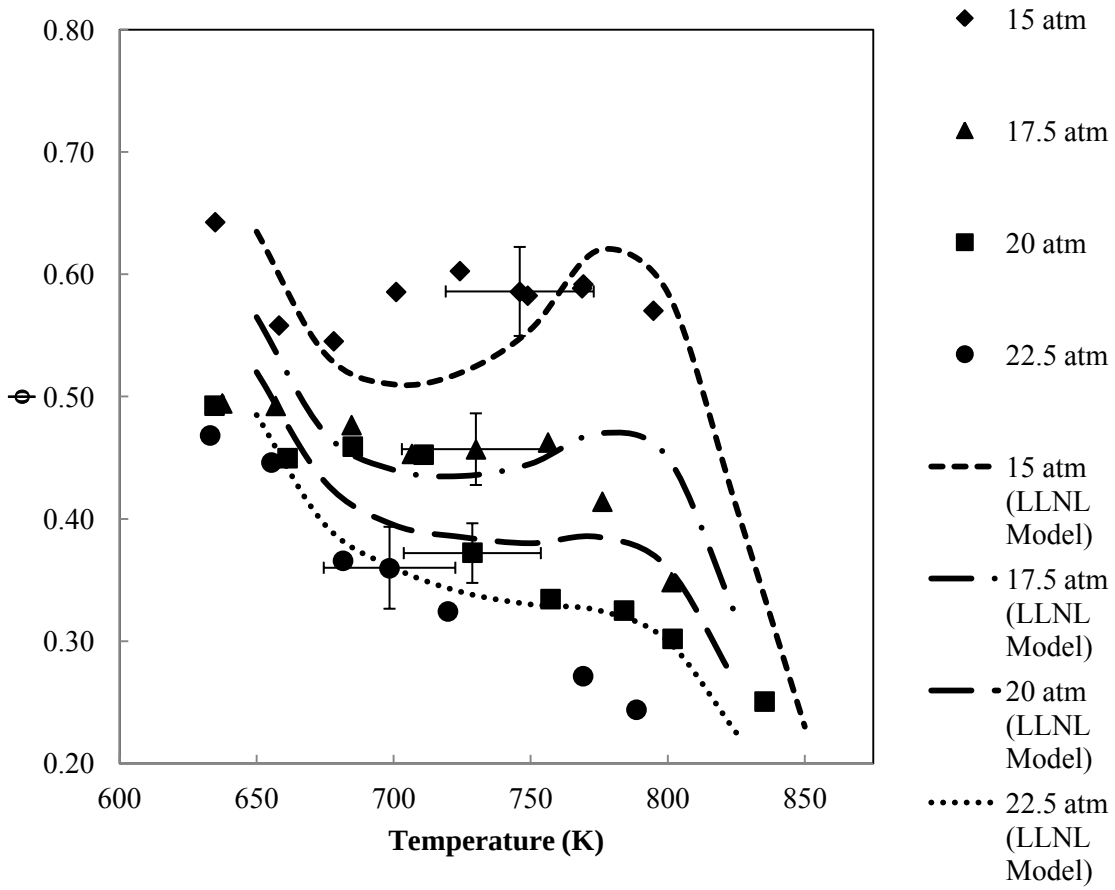

Figure 5.50 Experimental results and model predictions for the threshold equivalence ratio as a function of temperature at a residence time of 125 ms. Symbols represent experimental results from the current study and black lines represent model results using the LLNL mechanism [35].

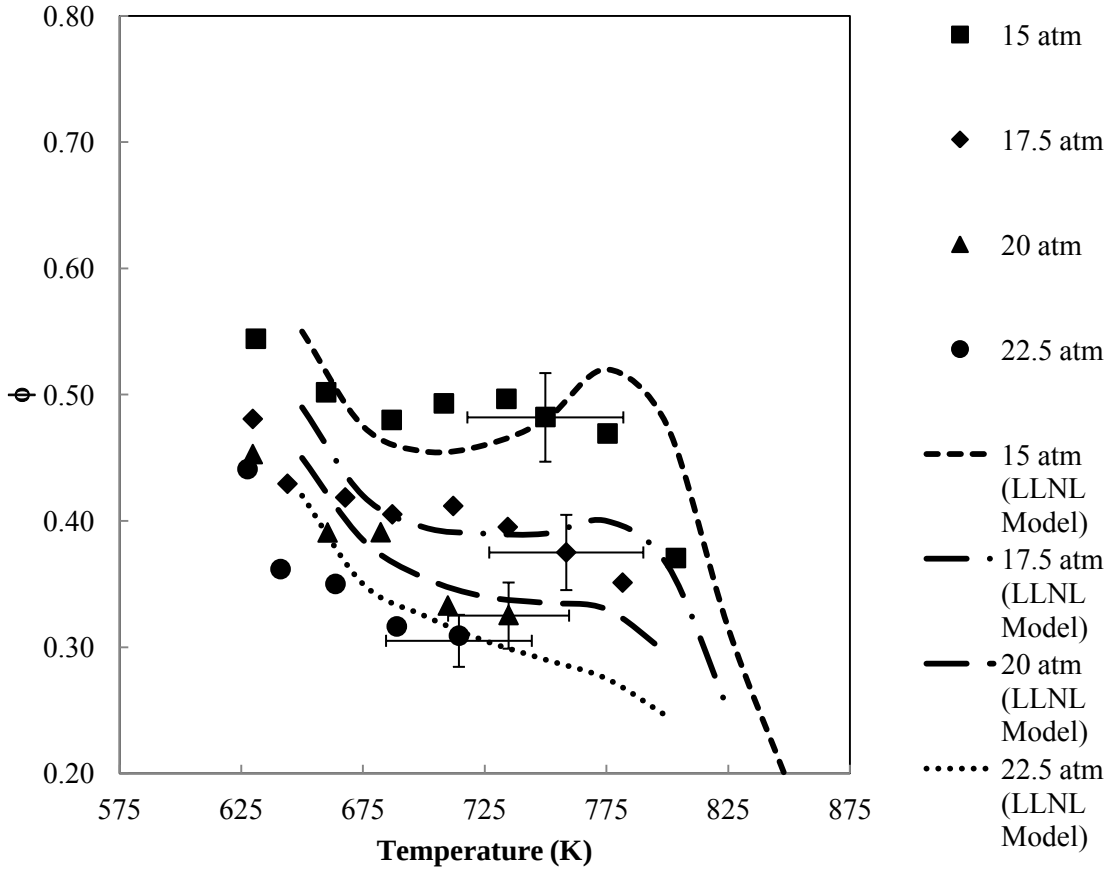

Figure 5.51 Experimental results and model predictions for the threshold equivalence ratio as a function of temperature at a residence time of 155 ms. Symbols represent experimental results from the current study and black lines represent model results using the LLNL mechanism [35].

5.6.5. Conclusions

A novel methodology for studying autoignition time in a high-pressure flow reactor with pre-vaporized iso-octane has been demonstrated. This new methodology allowed a careful study of the effect of equivalence ratio on autoignition time across varying temperatures and pressures. This experiment provided a dataset for conditions not previously studied in other apparatuses including pressures ranging from 15-22.5 atm, temperatures of approximately 650-850 K, and equivalence ratios ranging from approximately 0.3-0.8. The resulting ignition delay times for these conditions were 70-175 ms. Several trends were noticed by varying individual parameters. Additionally, a comparison with two chemical kinetics models was made and the results of one model were analyzed for temperature sensitivity of reactions as well as speciation results for oxidation.

5.6.6. Effect of Varying Conditions

(1) The temperature of onset of ignition for all pressures was around 640 K. As temperature increased reactivity increased and, as a result, the equivalence ratio necessary for autoignition decreased.
(2) A distinct NTC region, where slowed reactivity required higher equivalence ratio for autoignition, was also observed and was shown to start around 700-725 K and persisted until around 775 K. At temperatures above 775 K, reactivity again increased, and the resulting equivalence ratio required for autoignition also decreased.
(3) With increasing pressure, results showed an overall decrease in the equivalence ratio necessary for autoignition. Additionally, the presence of the NTC region was much more pronounced at lower pressures, appearing merely as a plateau at the highest pressure of 22.5 atm.

5.6.7. Comparison of Experimental Results with Chemical Kinetics Models

(1) A comparison to Lawrence Livermore National Laboratory's Iso-octane, version 3, chemical kinetics model showed good agreement across many conditions. The general ignition trends were captured nicely by the model; however, calculations tended to overpredict the equivalence ratio necessary for autoignition in the NTC region. Despite this discrepancy, overall remarkable agreement for an ignition study was shown.
(2) The Chemical Reaction Engineering and Chemical Kinetics Hydrocarbon chemical kinetics model showed fair agreement at the very lowest temperatures of 650 K, but did not exhibit any of the NTC behavior found in the experimental results or the LLNL model results.

5.7. References

[1] Maurice L. Q., Lander H., Edwards T., and Harrison W. E., 2001, "Advanced aviation fuels: a look ahead via a historical perspective," Fuel, **80**(5), pp. 747–756.

[2] Edwards T., Harrison B., and Maurice L. Q., 2001, "Properties and Usage of Air Force Fuel : JP-8," Proceedings of the AIAA Aerospace Sciences Meeting & Exhibit, **39**, pp. 1–11.

[3] Calcote H. F., and Manos D. M., 1983, "Effect of Molecular Structure on Incipient Soot Formation," Combustion and Flame, **49**, pp. 289–304.

[4] Gill R. J., and Olson D. B., 1984, "Estimation of Soot Thresholds for Fuel Mixtures," Combustion Science and Technology, **40**, pp. 307–315.

[5] 2000, "Standard Test Method for Smoke Point of Kerosine and Aviation Turbine Fuel," Annual Book of ASTM Standards.

[6] Hunt R. A. J., 1953, "Relation of Smoke Point to Molecular Structure," Industrial and Engineering Chemistry, **45**(3), pp. 602–606.

[7] McEnally C. S., and Pfefferle L. D., 2007, "Improved sooting tendency measurements for aromatic hydrocarbons and their implications for naphthalene formation pathways," Combustion and Flame, **148**, pp. 210–222.

[8] Mcenally C. S., and Pfefferle L. D., 2008, "Decomposition and hydrocarbon growth processes for hexadienes in nonpremixed flames," Combustion and Flame, **152**, pp. 469–481.

[9] Olson D. B., Pickens J. C., and Gill R. J., 1985, "The Effects of Molecular Structure on Soot Formation II. Diffusion Flames," Combustion and Flame, **62**, pp. 43–60.

[10] Minchin S. T., 1931, "Luminous Stationary Flames: the Quantitative Relationship between Flame Dimensions at the Sooting Point and Chemical Composition, with special Reference to Petroleum Hydrocarbons," Journal of the Institute of Petroleum Technologists, **17**, pp. 102–120.

[11] Clarke A. E., Hunter T. G., and Garner F. H., 1946, "The Tendency to Smoke of Organic Substances on Burning," Journal of the Institute of Petroleum, **32**, pp. 627–642.

[12] Schalla R. L., and McDonald G. E., 1953, "Variation in Smoking Tendency," Industrial and Engineering Chemistry, **53**(7), pp. 1497–1500.

[13] Yan S., Eddings E. G., Palotas A. B., Pugmire R. J., and Sarofim A. F., 2005, "Prediction of Sooting Tendency for Hydrocarbon Liquids in Diffusion Flames," Energy & Fuels, **19**(6), pp. 2408–2415.

[14] 2006, Petroleum Quality Information System Report, Ft. Belvoir, VA.

[15] Santoro R. J., Semerjian H. G., and Dobbins R. A., 1983, “Soot Particle Measurements in Diffusion Flames,” Combustion and Flame, **51**, pp. 203–218.

[16] Iyer V., Iyer S. S., Linevsky M. J., Litzinger T. A., and Santoro R. J., 2009, “Development of a wick-fed diffusion flame burner for liquid hydrocarbon fuels,” Proceedings of the Fall Technical Meeting of the Eastern States Section of the Combustion Institute.

[17] Iyer V. R., Iyer S. S., Litzinger T. A., and Santoro R. J., “Emulating the Sooting Propensity of JP-8 with Surrogate Fuels from Solvent Mixtures,” pp. 1–14.

[18] Iyer V., 2012, “Effect Of Aromatic Components In Surrogate Fuels On Soot In Co-Flow Flames And A Model Gas Turbine Combustor,” The Pennsylvania State University.

[19] Dasch C. J., 1992, “One-dimensional tomography: A comparison of Abel, onion-peeling, and filtered backprojection methods,” Applied Optics, **31**(8), pp. 1146–1152.

[20] Mensch A., Santoro R. J. J., Litzinger T. A. A., and Lee S. Y.-Y., 2010, “Sooting characteristics of surrogates for jet fuels,” Combustion and Flame, **157**(6), pp. 1097–1105.

[21] Dooley S., Won S. H., Chaos M., Heyne J., Ju Y., Dryer F. L., Kumar K., Sung C.-J., Wang H., Oehlschlaeger M. A., Santoro R. J., and Litzinger T. A., 2010, “A jet fuel surrogate formulated by real fuel properties,” Combustion and Flame, **157**(12), pp. 2333–2339.

[22] Dooley S., Won S. H., Heyne J., Farouk T. I., Ju Y., Dryer F. L., Kumar K., Hui X., Sung C.-J., Wang H., Oehlschlaeger M. a., Iyer V., Iyer S., Litzinger T. a., Santoro R. J., Malewicki T., and Brezinsky K., 2012, “The experimental evaluation of a methodology for surrogate fuel formulation to emulate gas phase combustion kinetic phenomena,” Combustion and Flame, **159**(4), pp. 1444–1466.

[23] Ladommatos N., Runbenstein P., and Bennett P., 1996, “Some effects of molecular structure of single hydrocarbons on sooting tendency,” Fuel, **75**(3), pp. 114–124.

[24] Hunt R. A., Rakowsky F. W., and Hunt R. A. J., 1956, “Variables in lamp Design That Affect Smoke Point,” Analytical Chemistry, **28**(10), pp. 1583–1586.

[25] Roper F. G., 1977, “The Prediction of Laminar Jet Diffusion Flame Sizes: Part I. Theoretical Model,” Combustion and Flame, **29**, pp. 219–226.

[26] Puri R., Richardson T., Santoro R., and Dobbins R. A., 1993, “Aerosol dynamic processes of soot aggregates in a laminar ethene diffusion flame,” Combustion and flame, **92**, pp. 320–333.

[27] Mordaunt C. J., Lee S. Y., Kalaskar V. B., Mensch A., Santoro R. J., and Schobert H. H., 2009, “Further Studies of Alternative Jet Fuels,” Proceedings of the ASME 2009 International Mechanical Engineering Congress and Exposition, ASME, Lake Buena Vista, Florida, pp. 1–10.

[28] Mordaunt C. J., 2005, "Dual Fuel Issues Related to Performance, Emissions, and Combustion Instability in Lean Premixed Gas Turbine Systems," Ph.D. Thesis, The Pennsylvania State University.

[29] Kalaskar V., 2009, "Emission Characteristics of JP-8, JP-900, Fischer-Tropsch(FT) and JP-8/FT Blends in a Model Gas Turbine Combustor," M.S. Thesis, The Pennsylvania State University.

[30] McBride B. J., and Gordon S., 1996, Computer Program for Calculation of Complex Chemical Equilibrium Compositions and Applications, Cleveland, OH.

[31] Faravelli T., Frassoldati A., and Ranzi E., 2003, "Kinetic Modeling of the Interactions Between NO and Hydrocarbons in the Oxidation of Hydrocarbons at Low Temperatures," Combustion and Flame, **132**, pp. 188–207.

[32] Frassoldati A., Faravelli T., and Ranzi E., 2003, "Kinetic Modeling of the Interactions Between NO and Hydrocarbons at High Temperature," Combustion and Flame, **135**, pp. 97–112.

[33] Fuller C. C., Gokulakrishnan P., Klassen M. S., Roby R. J., and Kiel B. V., 2008, "Investigation of the Effects of Vitiated Conditions on the Autoignition of JP-8," 45th AIAA/ASME/SAE/ASEE Joint Propulsion Conference and Exhibit., Denver, CO.

[34] Spadaccini L. J., and Tevelde J. A., 1986, "Autoignition Characteristics of Aircraft-Type Fuels," Combustion and Flame, **46**, pp. 283–300.

[35] "No Title," iso-Octane, Version 3. Available from: https://www-pls.llnl.gov/?url=science_and_technology-chemistry-combustion-iso_octane_version_3.

[36] Curran H. J., Gaffuri P., Pitz W. J., and Westbrook C. K., 2002, "A Comprehensive Modeling Study of Iso-octane Oxidation," Combustion and Flame, **129**(3), pp. 253–280.

[37] Curran H. J., Pitz W. J., Westbrook C. K., Callahan G. V., and Dryer F. L., 1998, "Oxidation of automotive primary reference fuels at elevated pressures," Symposium (International) on Combustion, **27**(1), pp. 379–387.

[38] Mehl M., Curran H. J., Pitz W. J., and Westbrook C. K., 2009, "Chemical Kinetic Modeling of Component Mixtures Relevant to Gasoline," European Combustion Meeting, Vienna, Austria.

[39] Mehl M., Curran H. J., Pitz W. J., and Westbrook C. K., 2009, "Detailed Kinetic Modeling of Low- Temperature Heat Release for PRF Fuels in an HCCI Engine," Powertrains, Fuels and Lubricants Meeting, Florence, Italy.

[40] "No Title," Gas phase combustion schemes - Kinetic Mechanism version 1201. Available from: creckmodeling.chem.polimi.it/kinetic.html.

[41] Frassoldati A., 2012, "Personal Communication."

[42] Faravelli T., Gaffuri P., Ranzi E., and Griffiths J. F., 1998, “Detailed thermokinetic modelling of alkane autoignition as a tool for the optimization of performance of internal combustion engines,” Fuel, **77**(3), pp. 147–155.

[43] Humer S., Frassoldati A., Granata S., Faravelli T., Ranzi E., Seiser R., and Seshadri K., 2007, “Experimental and kinetic modeling study of combustion of JP-8, its surrogates and reference components in laminar nonpremixed flows,” Proceedings of the Combustion Institute, **31**(1), pp. 393–400.

[44] Ranzi E., Dente M., Goldaniga A., Bozzano G., and Faravelli T., 2001, “Lumping procedures in detailed kinetic modeling of gasification, pyrolysis, partial oxidation and combustion of hydrocarbon mixtures,” Progress in Energy and Combustion Science, **27**(1), pp. 99–139.

[45] Ranzi E., Frassoldati, A.Granata S., and Faravelli T., 2004, “Wide-Range Kinetic Modeling Study of the Pyrolysis, Partial Oxidation, and Combustion of Heavy n-Alkanes,” Industrial & engineering chemistry research, **44**(14), pp. 5170–5183.

[46] Cooke J., Bellucci M., Smooke M. D., Gomez A., Violi A., Faravelli T., and Ranzi E., 2005, “Computational and experimental study of JP-8, a surrogate, and its components in counterflow diffusion flames,” Proceedings of the Combustion Institute, **30**(1), pp. 439–446.

[47] Bieleveld T., Frassoldati A., Cuoci A., Faravelli T., Ranzi E., Niemann U., and Seshadri K., 2009, “Experimental and kinetic modeling study of combustion of gasoline, its surrogates and components in laminar non-premixed flows,” Proceedings of the Combustion Institute, **32**(1), pp. 493–500.

[48] Vanhove G., Petit G., and Minetti R., 2006, “Experimental Study of the Kinetic Interactions in the Low-Temperature Autoignition of Hydrocarbon Binary Mixtures and a Surrogate Fuel,” Combustion and Flame, **145**(3), pp. 521–532.

[49] Davidson D. F., Gauthier B. M., and Hanson R. ., 2005, “Shock Tube Ignition Measurements of Iso-Octane/Air and Toluene/Air at High Pressures,” Proceedings of the Combustion Institute, **30**(1), pp. 1175–1182.

[50] Minetti R., Ribaucour M., Carlier M., and Sochet L. R., 1996, “Autoignition Delays of a Series of Linear and Branched Chain Alkanes in the Intermediate Range of Temperature,” Combustion Science and Technology, **113**(1), pp. 179–192.

[51] He X., Donovan M. T., Zigler B. T., Palmer T. R., Walton S. M., Wooldridge M. S., and Atreya A., 2005, “An Experimental and Modeling Study of Iso-Octane Ignition Delay Times Under Homogeneous Charge Compression Ignition Conditions,” Combustion and Flame, **142**(3), pp. 266–275.

[52] He X., Zigler, B.T.Walton S. M., Wooldridge M. S., and Atreya A., 2006, “A Rapid Compression Facility Study of OH Time Histories During Iso-octane Ignition,” Combustion and Flame, **145**(3), pp. 552–570.

[53] Fieweger K., Blumenthal R., and Adomeit G., 1997, "Self-Ignition of S.I. Engine Model Fuels: A Shock Tube Investigation at High Pressure," Combustion and Flame, **109**(4), pp. 599–619.

5.8. Archival Publications

A. Mensch, R. J. Santoro, T. A. Litzinger, S.-Y. Lee. Sooting Characteristics Of Surrogates For Jet Fuels, *Combust Flame* (2010) 157:1097-1105.

S. Dooley , S-H. Won , M. Chaos, J. Heyne, Y. Ju, F. L. Dryer, K. Kumar, C-J. Sung, H. Wang, M. A. Oehlschlaeger, R.J., Santoro, T. A. Litzinger. A Jet Fuel Surrogate Formulated by Real Fuel Properties, *Combust Flame* (2010) 157:2333-2339.

S. Dooley, S.H. Won, J. Heyne, T.I. Farouk, Y. Ju, F.L. Dryer, K. Kumar, X. Hui, C-J. Sung, H. Wang, M. A. Oehlschlaeger, V. Iyer, S. Iyer, T.A. Litzinger, R.J. Santoro, T. Malewecki, K. Brezinsky. The Experimental Evaluation of a Methodology for Surrogate Fuel Formulation to Emulate Gas Phase Combustion Kinetic Phenomena, *Combust Flame* (2012) 159: 1444-4466.

S. Jahangirian, S. Dooley, F.L. Dryer, V. Iyer, T.A. Litzinger, R.J. Santoro. Emulating the Combustion Behavior of Real Jet Aviation Fuels by Surrogate Mixtures from Solvent Blends, To be submitted to *Energy and Fuels* Oct, 2012.

5.9. Abstracts and Preprints

A. Mensch, R.J. Santoro, T.A. Litzinger, S-Y Lee. Sooting Characteristics of Surrogates for Jet Fuels, *47th AIAA Aerospace Sciences Meeting*, Orlando, FL, January 2009. AIAA paper 2009-1525.

V. Iyer, S. Iyer, S. Dooley, M. Linevsky, T. Litzinger, C. Mordaunt, R. Santoro, F. L. Dryer. Comparison of Sooting Propensity of JP-8 with its Surrogates in a Wick Burner and a Model Gas Turbine Combustor, Fall Technical Meeting of the Eastern States Section of the Combustion Institute Hosted by the University of Connecticut, Storrs, CT Oct. 9-12, 2011.

S. Jahangirian, S. Dooley, F.L. Dryer, V. Iyer, T.A. Litzinger, R.J. Santoro. Emulating the Combustion Behavior of Real Jet Aviation Fuels by Surrogate Mixtures from Solvent Blends, Fall Technical Meeting of the Eastern States Section of the Combustion Institute Hosted by the University of Connecticut, Storrs, CT Oct. 9-12, 2011.

M.K. Christensen, S. Pal, R.D. Woodward, and R.J. Santoro. Flow Reactor Autoignition Studies of Iso-octane at High Pressures and Low to Intermediate Temperatures, 50th AIAA Aerospace Sciences Meeting, 9-12 January 2012, Nashville TN.

V.R. Iyer, S.S. Iyer, T.A. Litzinger, R.J. Santoro, S. Dooley, F.L. Dryer, C.J. Mordaunt. Emulating the Sooting Propensity of JP-8 with Surrogate Fuels from Solvent Mixtures, 50th AIAA Aerospace Sciences Meeting, 9-12 January 2012, Nashville TN.

5.10. Presentations

V. Iyer, S. Iyer, M.J. Linevsky, T.A. Litzinger, R.J. Santoro, Development of a Wick-fed Diffusion Flame Burner for Liquid Hydrocarbon Fuels, Proceedings of the Fall Technical

Meeting of the Eastern States Section of The Combustion Institute, College Park, MD, October 18-21, 2009, 6 pp.

A. Mensch, R.J. Santoro, T.A. Litzinger, S-Y Lee. Sooting Characteristics of Surrogates for Jet Fuels, 32nd Symp. (Int'l.) on Combustion, Montreal, Canada (2008).

5.11. Graduate Theses

Amy Mensch. A Study On The Sooting Tendency Of Jet Fuel Surrogates Using the Threshold Soot Index, M.S. Thesis, The Pennsylvania State University, May 2009.

Michelle Christensen. Flow Reactor Autoignition Studies of Iso-octane at High Pressures and Low-To-Intermediate Temperatures, Ph.D. Thesis, The Pennsylvania State University, May 2012.

Venkatesh Iyer. Effect Of Aromatic Components In Surrogate Fuels On Soot In Co-Flow Flames And A Model Gas Turbine Combustor, Ph.D. Thesis, The Pennsylvania State University, August 2012.

5.12. Appendix A. *SP* and TSI Data for Binary Mixtures

Mole Fractions		*MW* (g/mol)	*SP* (mm)	TSI measured	TSI calculated
iso-cetane	1,2,4 TMB				
0.11	0.89	131.48	8.1	61	59
0.24	0.76	145.76	10.2	53	53
0.42	0.58	164.36	11.9	52	46
0.53	0.47	176.39	14.2	46	41
0.66	0.34	190.00	18.5	37	36
0.81	0.19	206.30	24.5	30	30
iso-octane	toluene				
0.10	0.90	94.39	8.4	41	37
0.24	0.76	97.35	10.2	34	32
0.39	0.61	100.79	12.3	29	27
0.49	0.51	102.99	14.5	24	24
0.66	0.34	106.69	20.0	17	19
0.72	0.28	108.05	21.7	15	17
0.78	0.22	109.48	24.6	13	15
0.85	0.15	110.98	29.4	11	12
0.92	0.08	112.56	35.0	8.3	10
m-xylene	n-dodecane				
0.17	0.83	159.35	36.9	13	14
0.33	0.67	149.43	26.8	18	20
0.34	0.66	148.43	26.4	18	21
0.36	0.64	147.49	23.9	20	21

0.37	0.63	146.52	24.0	20	22
0.39	0.61	145.61	23.0	21	22
0.50	0.50	138.31	19.5	24	27
0.65	0.35	128.57	14.1	32	33
0.78	0.22	120.58	11.9	36	38
0.88	0.12	113.68	9.8	43	42
1,2,4 TMB	1-MN				
0.75	0.25	125.64	6.9	69	71
0.60	0.40	128.92	6.2	80	76
0.40	0.60	133.32	6.2	83	84
0.25	0.75	136.64	6.2	85	90

Mole Fractions		*MW* (g/mol)	*SP* (mm)	TSI measured	TSI calculated
decalin	1-MN				
0.95	0.05	138.47	20.0	23	26
0.89	0.11	138.69	17.4	28	31
0.78	0.22	139.12	13.3	38	39
0.68	0.32	139.53	11.3	46	47
0.52	0.48	140.15	9.2	57	59
0.32	0.68	140.94	7.2	75	75
0.13	0.87	141.67	6.1	89	90
MCH	1-MN				
0.98	0.02	99.20	29.9	8.7	8.6
0.95	0.05	100.24	23.7	12	11

0.91	0.09	102.31	18.9	17	15
0.81	0.19	106.39	14.7	25	24
0.72	0.28	110.54	11.5	34	33
0.62	0.38	114.82	10.5	40	42
0.42	0.58	123.83	7.3	64	61
0.21	0.79	132.85	6.3	81	80

6. University of Illinois, Chicago (UIC) – K. Brezinsky

6.1. Abstract

A high temperature n-dodecane/iso-octane/n-propylbenzene/1,3,5-trimethylbenzene (2nd Generation Surrogate) surrogate kinetic model was developed and validated against high pressure shock tube speciation data. Shock tube experiments were conducted on the individual components in the surrogate, as well as n-decane and toluene, surrogate mixtures and the target real fuel, Jet A POSF 4658. The shock tube speciation data was first used to develop and validate individual kinetic models of the surrogate components and additional validation of the models using flow reactor speciation data and shock tube ignition delay times found in literature and conducted for the MURI program. The experimental work on the individual components and mixtures were performed in a heated high pressure single pulse shock tube at equivalence ratios of 0.46-2.35 and ∞, a temperature range of 835-1757 K, a pressure range of 16-74 atm, and reaction times from 1.11-4.05 ms. The mole fractions of the stable species were determined using gas chromatography and mass spectroscopy where the measured hydrocarbons species ranged from CH_4 to four-ring aromatics. Comparing the Jet A and the 2nd generation surrogate experiments showed that the surrogate fuel emulates the decay of O_2, and the formation of CO, CO_2, and C_1-C_3 intermediate species within experimental errors thus validating the methodology in the formulation of the Jet A surrogate. Additionally, the modeling results of the 2nd generation surrogate model compared against the experimental data showed good agreement with the mole fractions of CO, CO_2, C_1-C_3 intermediate species and the consumption of oxygen and the surrogate fuel components.

6.2. Introduction

The fundamental hypothesis underlying the experimental shock tube work was that the chemical behavior of real fuels could be predicted by characterizing the chemistry of individual representatives (surrogate species) and their mixtures (surrogate fuels) at the conditions pertinent to military aircraft engine operation. The secondary hypothesis was that the interactive chemistry of the components, i.e. the chemistry of the surrogate fuels and their intermediates, contained all the information necessary to predict performance related characteristics such as sooting and ignition times of real fuels. To test these hypotheses a series of experiments were planned in the unique UIC high pressure single pulse shock tube in which the combustion chemistry was characterized, by species, for the saturated alkanes iso-octane n-decane, and n-dodecane, and the three alkylated aromatics toluene, n-propyl benzene, and 1,3,5 trimethyl benzene as well as their mixtures. The conditions for the experiments were those encountered in practical military combustors, viz. temperatures ~ 1000-2000 K, pressures from 10 - 100 atm and variable fuel stoichiometries. The stable species data for the individual fuels and their mixtures were correctly anticipated to be the basis for validation and prediction via the development of detailed chemical kinetic models.

6.3. Summary of Research Findings

6.3.1. Iso-octane

High pressure iso-octane shock tube experiments were conducted to assist in the development of a Jet A surrogate kinetic model. Jet A is a kerosene based jet fuel composed of hundreds of hydrocarbons consisting of paraffins, olefins, aromatics and naphthenes. In the formulation of the surrogate mixture, iso-octane represents the branched paraffin class of hydrocarbons present in aviation fuels like Jet A. The experimental work on iso-octane was performed in a heated high pressure single pulse shock tube, **Figure 6.1**. The mole fractions of the stable species were determined using gas chromatography and mass spectroscopy and species profiles as a function of temperature were obtained for C_1-C_7 hydrocarbons. Experimental data on iso-octane oxidation and pyrolysis were obtained for temperatures from 835 to 1757 K, pressures from 21 to 65 atm, reactions times from 1.11 to 3.66 ms, and equivalence ratios from 0.52 to 1.68, and ∞. Iso-octane oxidation showed that the fuel decays through thermally driven oxygen free decomposition at conditions studied. This observation prompted an experimental and modeling study of iso-octane pyrolysis using an iso-octane sub-model taken from a recently published n-decane/iso-octane/toluene (1st Generation) surrogate model [1].

Figure 6.1 The heated high-pressure single-pulse shock tube; performance range 15-1000 atm, 900 to 2500K, 0.5 to 3 msec.

The 1st Generation Surrogate model was revised with additional reactions added and reaction rates taken from literature. The revised iso-octane sub-model showed improvements in predicting intermediate species profiles from pyrolytic experiments and oxidation experiments. The reactivity of iso-octane is well reproduced by all models used for comparison to the experimental data. Even though the revised 1st Generation Surrogate model is able to simulate with greater accuracy the formation of major species when compared to the unmodified 1st Generation Surrogate model and the iso-Octane model by Mehl et al. [2], the models still do not reproduce accurately the reactivity of oxygen and the formation of CO and CO_2 during oxidation and the formation of CH_4 and C_2H_2 during pyrolysis of iso-octane. However, when compared to the other two models used for comparison, the revised 1st Generation Surrogate model [3] is able to better reproduce the intermediate species profiles from a flow reactor and shock tube ignition delay times at temperature above 1000 K at both 10 and 50 atm.

The full description of the iso-octane experiments and associated modeling is presented in a recent publication from the 34th International Symposium on Combustion [3].

6.3.2. n-Decane and n-Dodecane

High pressure n-decane and n-dodecane shock tube experiments were conducted to assist in the development of a Jet A surrogate kinetic model. In the formulation of the surrogate mixture, n-decane or n-dodecane represent the normal paraffin class of hydrocarbons present in aviation fuels like Jet A. The experimental work on both n-alkanes was performed in the heated high pressure single pulse shock tube. The mole fractions of the stable species were determined using gas chromatography and mass spectroscopy. Experimental data on both n-decane and n-dodecane oxidation and pyrolysis were obtained for temperatures from 867 to 1739 K, pressures from 19 to 74 atm, reaction times from 1.15 to 3.47 ms, and equivalence ratios from 0.46 to 2.05, and 1.

Both n-decane and n-dodecane oxidation showed that the fuel decays through thermally driven oxygen free decomposition at the conditions studied. This observation prompted an experimental and modeling study of n-decane and n-dodecane pyrolysis using a recently revised n-decane/iso-octane/toluene (1st Generation) surrogate model [1]. The surrogate model was extended to n-dodecane in order to facilitate the study of the 1-olefin species quantified during the pyrolysis of n-dodecane and n-decane with additional reactions and reaction rate constants modified with rate constants taken from literature. When compared against a recently published generalized C_8-C_{16} n-alkane model [4] and the original and revised surrogate models [5], the revised (based on our experimental work) and extended surrogate model showed improvements in predicting 1-olefin species profiles from pyrolytic and oxidative n-decane and n-dodecane experiments. Even though the revisions made in this study focused on the lower concentration species detected during experimental work, the improved accuracy of prediction of these species by the model improved the prediction of the formation of the much higher concentrations of CO and CO_2 and the decay of O_2. The revised and extended model when compared to the published generalized n-alkane and surrogate models also showed improvements in predicting species profiles from flow reactor n-decane oxidation experiments, but similarly predicted n-decane and n-dodecane ignition delay times.

The full description of the n-decane and n-dodecane experiments and associated modeling is presented in a recent publication from the 34th International Symposium on Combustion [5].

6.3.3. n-Propylbenzene Oxidation

The high pressure and temperature kinetics of n-propylbenzene oxidation were investigated in the heated high pressure single pulse shock tube. Experiments were performed at nominal reflected shock pressures of 25 and 50 atm, with the temperatures ranging from 838 to 1669 K and for an equivalence ratio of 0.5–1.9. A variety of stable species ranging from aliphatic hydrocarbons to single ring and polycyclic aromatic hydrocarbons were sampled from the shock tube and analyzed using standard gas chromatographic techniques. Species concentrations of small hydrocarbons, mono-aromatic and multi-ringed aromatic species were obtained as a function of temperature. Within the range of this experimental study, the fuel decay was seen to be insensitive to the changes in pressure. The formation of the intermediates from the fuel were influenced by the concentration of the oxidizer. A detailed chemical kinetic model [6] was

developed to simulate the stable species profiles and to describe the decay of n-propylbenzene as obtained from the high pressure oxidation experiments. The model provides a satisfactory fit for the consumption of the fuel, oxidizer and the formation of the major aliphatic, mono-aromatic and polycyclic aromatic hydrocarbons.

The fuel decay pathways depended on the temperature. At low temperatures the majority of the fuel decayed by hydrogen abstraction reactions from the n-propyl side chain. At high temperatures the majority of the fuel is consumed primarily by the homolysis route. A direct pathway from the fuel was identified to be responsible for minor amounts of indene being formed. The model simulates the fuel decay and formation of most of the intermediates accurately for all the experimental data sets. The model has also been validated against the flow reactor oxidation data and jet stirred reactor oxidation data available in literature.

The full description of the n-propylbenzene experiments and the modeling is available in our recent publication in Combustion and Flame [6].

6.3.4. n-Propylbenzene Pyrolysis

The high pressure and high temperature kinetics of n-propylbenzene pyrolysis were investigated in the heated high pressure single pulse shock tube. Experiments were performed at a nominal pressure of 50 atm, with the temperatures ranging from 1027 to 1678 K. A variety of stable species ranging from aliphatic hydrocarbons to single ring and polycyclic aromatic hydrocarbons were sampled from the shock tube and analyzed using standard gas chromatographic techniques. A detailed chemical kinetic model [7] was developed to simulate the stable species profiles as obtained from the high pressure pyrolysis experiments. The model provides a satisfactory fit for the consumption of the fuel and the formation of the major aliphatic, monoaromatic and polycyclic aromatic hydrocarbons.

The subset of pyrolysis reactions in the UIC n-Propylbenzene Oxidation Model was utilized as a basis to model the formation of these stable intermediates. This model was further modified to include and update reactions for predicting the formation of polycyclic aromatic hydrocarbons, with greater agreement. From the final pyrolysis model, it was found that the fuel decays primarily by a homolysis pathway which has been seen to be the dominant pathway, irrespective of the temperature range of the decay of the fuel. The formation pathways of indene were dependent on temperature. At low temperatures, indene formation was influenced by the presence of C_9H_9 radicals. At high temperatures, indene was formed through the recombination pathway of benzyl radical and acetylene. Benzyl radical, cyclopentadienyl radical and propargyl radicals influenced the formation of other polycyclic aromatic hydrocarbons like naphthalene, anthracene and acenaphthylene.

The full description of the n-propylbenzene oxidation experiments and associated modeling is presented in a recent publication from the 34th International Symposium on Combustion [7].

6.3.5. 1,3,5-Trimethylbenzne

The high pressure and high temperature kinetics of the 1,3,5-trimethylbenzene oxidation were investigated in the heated high pressure single pulse shock tube. Experiments were performed at nominal reflected shock pressures of 20 and 50 atm, for a temperature range of 1017–1645 K,

and at equivalence ratios of 0.51, 0.95 and 1.86. A variety of stable species ranging from aliphatic hydrocarbons to single ring and polycyclic aromatic hydrocarbons were sampled from the shock tube and analyzed using standard gas chromatographic techniques. A 1,3,5-trimethylbenzene oxidation model [8] was developed to predict the decay of the fuel and the formation of aliphatic and single ringed aromatic hydrocarbons, as measured from our experiments. The model shows satisfactory predictions for the formation and consumption of most of the major intermediates.

Through reaction path analysis it was identified that the pathways involving oxidation of the 1,3,5-trimethylbenzyl and dimethylphenyl radical play an important role in the formation of the major intermediates such as benzene, toluene and 3,5-dimethylbenzaldehdye. Polycyclic aromatic hydrocarbon species such as anthracene and methylanthracene were formed through a sequence of steps, following the reaction of 1,3,5-trimethylbenzyl radical with benzene. The oxidation of 1,3,5-trimethylbenzene seems to have additional complications beyond our simple hypothesis of oxidation by simultaneous oxidation and abstraction of the methyl side chains.

The full description of the 1,3,5-trimethylbenzene experiments and the modeling is available in our recent publication in Combustion and Flame [8].

6.3.6. n-Decane/iso-Octane/Toluene (1st Generation Surrogate)

High pressure toluene and n-decane/iso-octane/toluene shock tube oxidation experiments were conducted to verify a recent Jet A surrogate model and the included toluene sub-model [9]. The experimental work on both the Jet A surrogate and toluene were performed in a heated high pressure single pulse shock tube at stoichiometric conditions. The mole fractions of the stable species were determined using gas chromatography and mass spectroscopy. Experimental data for the n-decane/ iso-octane/toluene and toluene oxidations were obtained over the temperature range 939- 1749 K, pressure range 22-59 atm, and reaction times from 1.19-2.81 ms.

Comparing toluene decay during both toluene and n-decane/iso-octane/toluene oxidation experiments showed that n-decane and iso-octane species are responsible for toluene to decay at a lower temperature in the surrogate mixture. Rate of production analysis completed for the revised model revealed the H atom reactions were responsible for the decay of toluene at approximately 1260K during the surrogate oxidation, where the H production was associated with the pyrolytic decomposition of n-decane and iso-octane. The radical buildup (mostly H atoms) through the decay of n-decane and iso-octane during n-decane/iso-octane/toluene oxidation initiates toluene decay at the lower temperatures. From a comparison of the original surrogate model to the revised model, the revised surrogate model showed improvements in predicting the formation of major intermediates such as toluene and also oxygen decay. Additionally, simulation of pure toluene oxidation revealed that the toluene sub-model is unable to predict intermediate species of the pure toluene oxidation with as good as agreement as when compared against the prediction of the same intermediates during n-decane/ iso-octane/toluene oxidation. These results indicate that missing pathways and/or less than optimal reaction rate constants might be responsible for the poorer prediction of fuel, oxygen, and intermediates during the simulation of toluene oxidation experiments. The revised and the original surrogate models showed similar predictions of flow reactor and ignition delay times.

The experimental work and the associated modeling, although not available in archival publications, is publically available in the PhD thesis of Tom Malewicki [9].

6.3.7. n-Dodecane/iso-Octane/n-Propylbenzene/1,3,5-Trimethylbenzene (2nd Generation Surrogate) and Jet A POSF 4658

Jet A POSF 4658 and n-dodecane/iso-octane/n-propylbenzene/1,3,5-trimethylbenzene (2nd Generation Surrogate) oxidation experiments were conducted in the heated shock tube at high pressures and at fuel lean and rich conditions to verify if the formulated surrogate fuel emulates the combustion characteristics of the jet fuel. A model [10] was developed for the 2nd generation surrogate using an existing 1st Generation Surrogate model [1] (n-decane/iso-octane/toluene) as the base model and sub-models for n-propylbenzene [6] and 1,3,5-trimethylbenzene [8] were included from the literature. The experimental work on both the Jet A and 2nd Generation Surrogate was performed in a heated high pressure single pulse shock tube at equivalence ratios of 0.46-1.86. Experimental data were obtained over the temperature range of 879-1760 K, a pressure range of 16-36 atm, and reaction times from 1.21-3.53 ms. The mole fractions of the stable species were determined using gas chromatography and mass spectroscopy. Comparing the Jet A and the 2nd Generation Surrogate experiments showed that the surrogate fuel emulates the decay of O_2, and the formation of CO, CO_2, and C_1-C_3 intermediate species within experimental errors.

Comparison of the modeling results for O_2 decay to the 2nd Generation Surrogate experiments and pure 1,3,5-trimethylbenzene oxidation experiments revealed that the surrogate fuel model is capable of predicting O_2 decay with a greater degree of accuracy in the 2nd Generation Surrogate experiments than in that of pure 1,3,5-trimethylbenzene experiments. This suggests that the radical pool formed due to the non-aromatics species during the consumption of 2nd Generation Surrogate fuel components prior to the formation of CO and CO_2 could contribute to the initial decay of O_2 at lower temperatures and thereby results in better prediction by the model, which includes both non-aromatics and aromatics chemistry, of O_2 decay and formation of CO and CO_2. Flow reactor simulations of the 2nd Generation Surrogate fuel experiments showed the surrogate model captures the overall trends of the decay of O_2 and the formation of CO, CO_2, and H_2O. Additionally, simulated shock tube ignition delay times above 750 K were within a factor of two when compared to experimental ignition delay times.

The full description of the Jet A POSF 4658 and n-dodecane/iso-octane/n-propylbenzene/1,3,5-trimethylbenzene (2nd Generation Surrogate) oxidation experiments and the modeling is available in publication currently in press for Combustion and Flame [10].

The methodology developed by Dooley et al. [11] for the formulation of surrogate fuel mixtures was validated using shock tube speciation data at $\Phi = 0.47$. It is theorized that if the surrogate fuel reproduces the formation of C_1-C_4 intermediate species as those of the real fuel, the radical pool buildup will also be reproduced and as a consequence the surrogate fuel will be able to reproduce the combustion kinetic behavior of the real fuel [11-14]. This reproducibility of the C_1-C_4 species by the surrogate fuel mixture (n-dodecane/iso-octane/n-propylbenzene/1,3,5-trimethylbenzene) represented by closed symbols to that of the real fuel, Jet A POSF 4658 (open symbols), is seen in **Figure 6.2**. The surrogate fuel not only emulates the reactivity of the real fuel, formation /consumption of O_2, CO and CO_2, but also closely, within experimental errors,

the formation/consumption of acetylene (C_2H_2), ethylene (C_2H_4), and ethane (C_2H_6) shown in **Figure 6.2b**, and methane (CH_4), propylene (C_3H_6), allene (aC_3H_4), and propyne (pC_3H_4) shown in **Figure 6.2c**, and 1-butene ($1\text{-}C_4H_8$) show in Figure 2d. As described by Dooley et al. [11], the disparities in measurement for higher molecular weight species are due to the propensity of the fuel components to form some intermediate species that are particular to that individual fuel component. This is especially true for the 2nd generation surrogate as it is composed of only four fuel components. For example, iso-butene is measured higher for the 2nd generation surrogate as it is the predominant intermediate species formed during the oxidation of the surrogate component iso-butene.

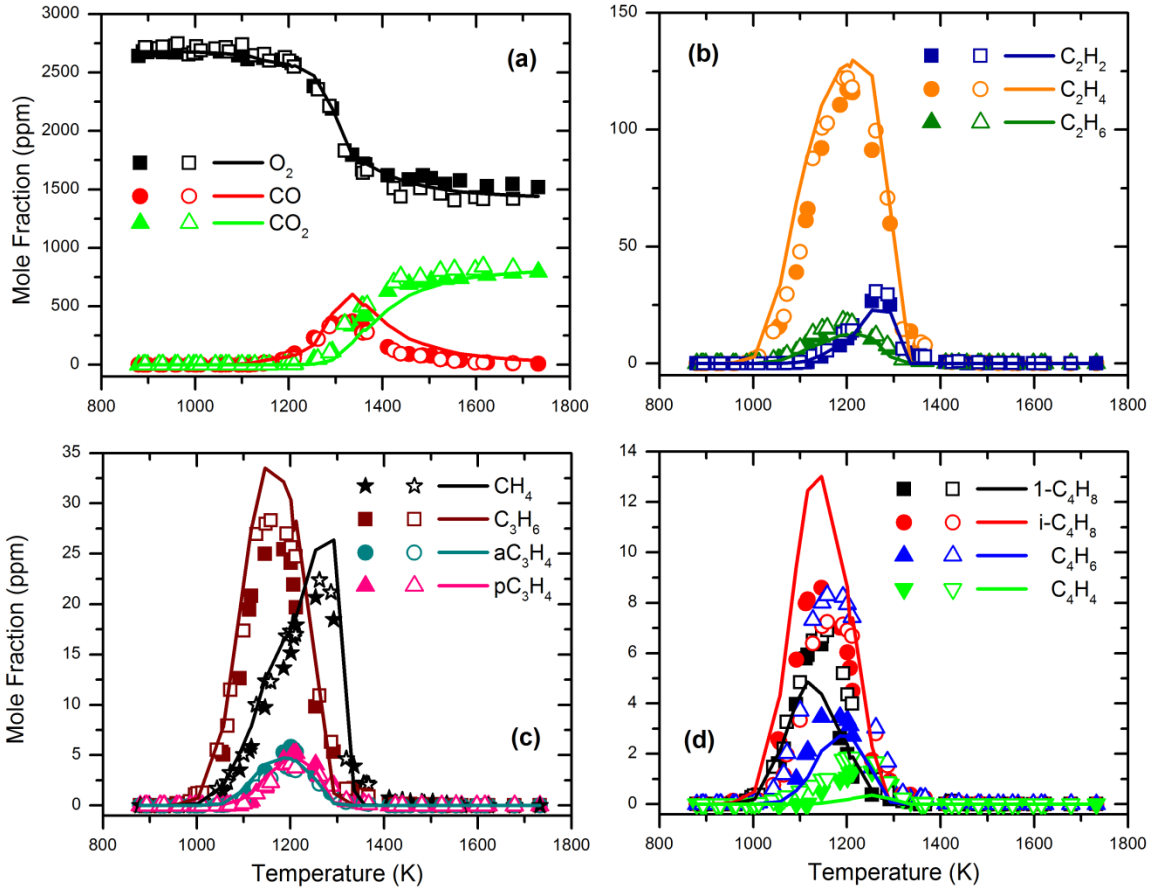

Figure 6.2. Comparison of CO, CO_2, O_2 and C_1-C_4 species between (closed symbols) n-dodecane/iso-octane/n-propylbenzene/1,3,5-trimethylbenzene (2nd Generation Surrogate, 34.23/24.31/19.9/6.24 ppm in Argon, 2676.5 ppm of O_2) shock tube oxidation experiments having a carbon total of 840.5, Φ = 0.47, P = 16-26 atm, and t = 1.3-3.4 ms, (open symbols) Jet A POSF 4658 (2724.6 ppm of O_2) shock tube oxidation experiments having a carbon total of 840.8, Φ = 0.46, P = 18-27 atm, and t = 1.3-3.2 ms, and (lines) 2nd Generation Surrogate model simulated using the 2nd Generation Surrogate experimental reaction temperature, time, and pressure.

As shown in **Figure 6.2**, the developed 2nd Generation Surrogate model represented by solid lines is also validated against experimental data. The model not only is able to capture the overall reactivity (consumption/formation of O_2, CO, and CO_2) but it is also capable of predicting the formation/consumption of C_1-C_3 species to that of the surrogate fuel (closed

symbols) within experimental errors. The surrogate model as shown in **Figure 6.3** is capable to predict the consumption of the fuel components in the surrogate fuel well within experimental errors.

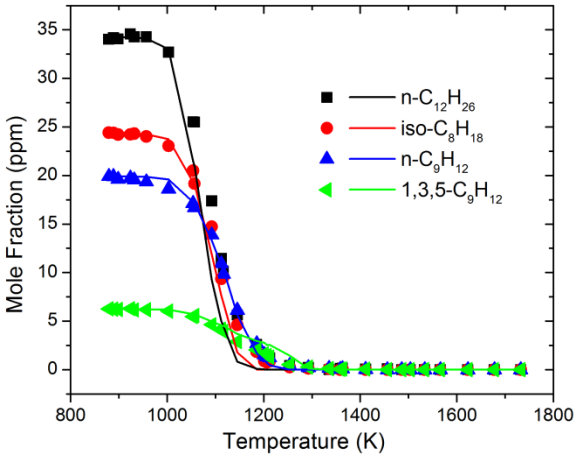

Figure 6.3. Consumption of fuel components during (closed symbols) n-dodecane/iso-octane/n-propylbenzene/1,3,5-trimethylbenzene (2nd Generation Surrogate, 34.23/24.31/19.9/6.24 ppm in Argon, 2676.5 ppm of O_2) shock tube oxidation experiments having a carbon total of 840.5, Φ = 0.47, P = 16-26 atm, and t = 1.3-3.4 ms, and (lines) 2nd Generation Surrogate model simulated using the 2nd Generation Surrogate experimental reaction temperature, time, and pressure.

The two figures shown above, **Figures 6.2 and 6.3**, and the discussion of them are completely new data, and the modeling results have not been reported elsewhere than in this report.

6.3.8 Connection with Soot Modeling

Soot formation in combustion systems is associated with the chemical formation of polynuclear aromatic species (PAH's). These soot related species were formed in our studies of the rich oxidation of 1,3,5-trimethylbenzene and n-propylbenzene. Representative examples are fluorene, indene, anthracene and naphthalene. The chemical routes to the formation of most of the PAH's are included in our models for the oxidation and pyrolysis of the two aromatic fuels. When these two aromatics were combined with iso-octane and n-dodecane to make up the 2nd Generation Surrogate and the surrogate subsequently oxidized, the PAH concentrations were very significantly reduced! It can be hypothesized that the interactive chemistry between the alkanes, their fragments and the radicals produced with the aromatics and their intermediates, inhibits PAH formation. To be sure if our observations are the result of interactive chemistry, it would first be necessary to perform a series of high concentration rich oxidation experiments to force more PAH formation if it were to occur. Nevertheless, in the absence of those experiments, our current models contain enough information for future studies that would hypothesize and test interactive chemistry that could lead to a reduction in PAH formation and by implication, soot. However, actual soot formation from any PAH formation from the surrogate fuel and/or its individual components could only be deduced from the coupling of the 2nd Generation Surrogate model to a well validated soot formation model. That coupling was beyond the scope of the MURI project but would be a very worthwhile future endeavor.

6.4. Summary of Project Outcomes

- Provided high pressure shock tube species data for the second generation surrogate
- Collaborated with the MURI group to produce the joint Combustion and Flame paper
- Completed the acquisition of species profiles for the pyrolysis and oxidation of n-propylbenzene
- Completed the modeling of the pyrolysis and oxidation of n-propylbenzene and published results
- Completed the acquisition of 1,3,5-trimethylbenzene oxidation species, modeled them and published results
- Completed the acquisition of species data from the pyrolysis and oxidation of iso-octane, modeled them and published the results
- Completed the acquisition of species data from the oxidation and pyrolysis of n-decane and n-dodecane, modeled the species and published the results.
- Completed the acquisition of species data for the oxidation of Jet A and 2nd generation surrogate modeled them and the publication is in press.

6.5. References

[1] S. Dooley, S.H. Won, M. Chaos, J. Heyne, Y. Ju, F.L. Dryer, K. Kumar, C.-J. Sung, H. Wang, M.A. Oehlschlaeger, R.J. Santoro, T.A. Litzinger, *Combust. Flame* (2010) 157: 2333–2339.

[2] M. Mehl, H.J. Curran, W.J. Pitz, C.K. Westbrook, in: European Combustion Meeting, Vienna, Austria, 2009.

[3] T. Malewicki, K. Brezinsky. Experimental and Modeling Study on the Pyrolysis and Oxidation of Iso-Octane, *Proc. Combust. Inst.*, (2012) 34: xxx-xxx. dx.doi.org/10.1016/j.proci.2012.06.137

[4] Westbrook, C. K., W. J. Pitz, O. Herbinet, H. J. Curran, and E. J. Silke, *Combust. Flame* 156 (1) (2009) 181-199, LLNL-JRNL-401196

[5] T. Malewicki, K. Brezinsky. Experimental and Modeling Study on the Pyrolysis and Oxidation of n-Decane and n-Dodecane, *Proc. Combust. Inst.*, (2012) 34: xxx-xxx. dx.doi.org/10.1016/j.proci.2012.06.156

[6] S. Gudiyella, K. Brezinsky. High Pressure Study of n-Propylbenzene Oxidation", *Combust Flame*, (2012) 159:940-958.

[7] S. Gudiyella, K. Brezinsky. The High Pressure Study of n-Propylbenzene Pyrolysis, *Proc. Combust. Inst.*, (2012) 34: xxx-xxx. dx.doi.org/10.1016/j.proci.2012.05.007

[8] S. Gudiyella, K. Brezinsky. High Pressure Study of 1,3,5-Trimethylbenzene Oxidation, *Combust Flame* (2012) 159:3264-3285.

[9] Tom Malewicki, Development of a Jet A Chemical Surrogate Model Using High Pressure Shock Tube Speciation Data. PhD Thesis, University of Illinois Chicago (2012).

[10] T. Malewicki, S. Gudiyella, K. Brezinsky. Experimental and Modeling Study on the Oxidation of Jet A and the n-Dodecane/iso-Octane/n-Propylbenzene/1,3,5-Trimethylbenzene Surrogate Fuel, *Combust Flame* (In Press).
[11] S. Dooley, S.H. Won, J. Heyne, T. Farouk, F.L. Dryer, Y. Ju, K. Kumar, X. Hui, C.-J. Sung, H. Wang; M. Oehlschlaeger, R. Santoro, T. Litzinger, V. Iyer, T. Malewicki, K. Brezinsky. The Experimental Evaluation of a Methodology to Surrogate Fuel Formulation for the Emulation of Gas Phase Combustion Kinetic Phenomena by a Theory of Real Fuel Oxidation, *Combust Flame* (2012) 159:1444-1466.
[12] F. Battin-Leclerc, *Prog. Energ. Combust. Sci.* (2008) 34 (4):440-498
[13] F. Battin-Leclerc, E. Blurock, R. Bounaceur, R. Fournet, P.A. Glaude, O. Herbinet, B. Sirjean, V. Warth, *Chem. Soc. Rev.* (2011) 40 (9):4762-4782
[14] J.M. Simmie, *Prog. Energ. Combust. Sci.*(2003) 29 (6): 599-634

6.6. Archival Publications

S. Dooley, S.H. Won, J. Heyne, T. Farouk, F.L. Dryer, Y. Ju, K. Kumar, X. Hui, C.-J. Sung, H. Wang; M. Oehlschlaeger, R. Santoro, T. Litzinger, V. Iyer, T. Malewicki, K. Brezinsky. The Experimental Evaluation of a Methodology to Surrogate Fuel Formulation for the Emulation of Gas Phase Combustion Kinetic Phenomena by a Theory of Real Fuel Oxidation, *Combust Flame* (2012), 159:1444-1466.

S. Gudiyella, K. Brezinsky. The High Pressure Study of n-Propylbenzene Pyrolysis, *Proc. Combust. Inst.*, (2012) 34: xxx-xxx. http://dx.doi.org/10.1016/j.proci.2012.05.007

S. Gudiyella, K. Brezinsky. High Pressure Study of n-Propylbenzene Oxidation", *Combust Flame*, (2012) 159:940-958.

S. Gudiyella, K. Brezinsky. High Pressure Study of 1,3,5-Trimethylbenzene Oxidation, *Combust Flame* (2012) 159:3264-3285.

T. Malewicki, K. Brezinsky. Experimental and Modeling Study on the Pyrolysis and Oxidation of Iso-Octane, *Proc. Combust. Inst.*, (2012) 34: xxx-xxx. http://dx.doi.org/10.1016/j.proci.2012.06.137

T. Malewicki, K. Brezinsky. Experimental and Modeling Study on the Pyrolysis and Oxidation of n-Decane and n-Dodecane, *Proc. Combust. Inst.*, (2012) 34: xxx-xxx. http://dx.doi.org/10.1016/j.proci.2012.06.156

T. Malewicki, S. Gudiyella, K. Brezinsky. Experimental and Modeling Study on the Oxidation of Jet A and the n-Dodecane/iso-Octane/n-Propylbenzene/1,3,5-Trimethylbenzene Surrogate Fuel, *Combust Flame* (In Press).

6.7. Abstracts and Preprints

S. Gudiyella, T. Malewicki, K. Brezinsky. High Pressure Study of n-Propylbenzene Oxidation, 7th U.S. National Combustion Meeting, Georgia Institute of Technology, Atlanta, GA, March 20-23, 2011.

S. Gudiyella, K. Brezinsky. High Pressure Study of 1,3,5-Trimethylbenzene Oxidation, Fall Technical Meeting of the Eastern States Section of the Combustion Institute Hosted by the University of Connecticut, Storrs, CT, Oct 9-12, 2011.

6.8. Presentations

T. Malewicki, A. Comandini, K. Brezinsky, "Experimental and Modeling Study on the Pyrolysis and Oxidation of Iso-Octane", 34th International Symposium on Combustion, Warsaw, Poland, July 29 - August 3, 2012

T. Malewicki, K. Brezinsky, "Experimental and Modeling Study on the Pyrolysis and Oxidation of n-Decane and n-Dodecane", 34th International Symposium on Combustion, Warsaw, Poland, July 29 - August 3, 2012

S. Gudiyella, K. Brezinsky, "The High Pressure Study of n-Propylbenzene Pyrolysis", 34th International Symposium on Combustion, Warsaw, Poland, July 29 - August 3, 2012

T. Malewicki, S. Gudiyella, K. Brezinsky, "Detailed Studies on the Oxidation of Surrogate Fuel Components, Surrogate Mixtures and Real Fuels", Multi-Agency Co-ordination Committee for Combustion Research (MACCCR), Fuels Research Review, Chicago, United States, September 2011

T. Malewicki, K. Brezinsky, "High Pressure Shock Tube Study on the Oxidation and Pyrolysis of iso-Octane", International Conference on Chemical Kinetics, Boston, United States, July 2011

S. Gudiyella, K. Brezinsky, "High Pressure Study of n-Propylbenzene Oxidation", International Conference on Chemical Kinetics, Boston, United States, July 2011

S. Gudiyella, K. Brezinsky, "High Pressure Study of n-Propylbenzene Pyrolysis", International Conference on Chemical Kinetics, Boston, United States, July 2011

S. Gudiyella, K. Brezinsky, "Oxidation of Aromatic Surrogate Fuel Components of Jet Fuels", UIC Student Research Forum, Chicago, United States, Apr 2011

T. Malewicki, S. Gudiyella, K. Brezinsky, "Detailed Studies on the Surrogate Fuel Components of JP-8", Multi-Agency Co-ordination Committee for Combustion Research (MACCCR), Fuels Research Review, Princeton, United States, September 2010

T. Malewicki, K. Brezinsky, "High Pressure Study of Oxidation and Pyrolysis of n-Decane", Work in Progress Poster, 33rd International Symposium on Combustion Institute, Beijing, China, August 1-6, 2010

S. Gudiyella, T. Malewicki, K. Brezinsky, "High Pressure Study of n-Propylbenzene Oxidation", Work in Progress Poster, 33rd International Symposium on Combustion, Beijing, China, August 2010

T. Malewicki, S. Gudiyella, K. Brezinsky, "Oxidation of Potential Surrogate Fuel Components of JP-8", Multi-Agency Co-ordination Committee for Combustion Research (MACCCR), Fuels Research Review, Los Angeles, United States, September 2009

S. Gudiyella, T. Malewicki, K. Brezinsky, "Oxidation of Potential Surrogate Fuel Components of JP-8", Poster Presentation, UIC Chemistry Department, Chicago, United States, September 2008

T. Malewicki, S. Gudiyella, K. Brezinsky, "Oxidation of Potential Surrogate Fuel Components of JP-8", Multi-Agency Co-ordination Committee for Combustion Research (MACCCR), Fuels Research Review, Gaithersburg, United States, September 2008

T. Malewicki, S. Gudiyella, K. Brezinsky, "Oxidation of Potential Surrogate Fuel Components of JP-8", Work in Progress Poster, 32nd International Symposium on Combustion, Montreal, Canada, August 2008

6.9. Graduate Theses

Soumya Gudiyella, An Experimental and Modeling Study of the Combustion of Aromatic Surrogate Jet Fuel Components, PhD Thesis, University of Illinois Chicago (2012).

Tom Malewicki, Development of a Jet A Chemical Surrogate Model Using High Pressure Shock Tube Speciation Data. PhD Thesis, University of Illinois Chicago (2012).

6.10. Personnel

Dr. Soumya Gudiyella

Dr. Tom Malewicki